On the mechanisms of sulfur isotope fractionation during microbial sulfate reduction

On the mechanisms of sulfur isotope fractionation during microbial sulfate reduction

A DISSERTATION PRESENTED

BY

WILLIAM DAVIE LEAVITT

TO

THE DEPARTMENT OF EARTH AND PLANETARY SCIENCES

IN PARTIAL FULFILLMENT OF THE REQUIREMENTS

FOR THE DEGREE OF

DOCTOR OF PHILOSOPHY

IN THE SUBJECT OF

EARTH AND PLANETARY SCIENCES

HARVARD UNIVERSITY

CAMBRIDGE, MASSACHUSETTS

MARCH 2014

Dissertation Advisor
David T. Johnston

Author
William Davie Leavitt

On the mechanisms of sulfur isotope fractionation during microbial sulfate reduction

ABSTRACT

Underlying all applications of sulfur isotope analyses is our understanding of isotope systematics. This dissertation tests some fundamental assumptions and assertions, drawn from equilibrium theory and a diverse body of empirical work on biochemical kinetics, as applied to the multiple sulfur isotope systematics of microbial sulfate reduction. I take a reductionist approach, both in the questions addressed and experimental approaches employed. This allows for a mechanistic, physically consistent interpretation of geological and biological sulfur isotope records. The goal of my work here is to allow interpreters a more biologically, chemically and physically parsimonious framework to decipher the signals coded in modern and ancient sulfur isotope records.

The key findings of these individual studies can be summed up as follows. As the rate of microbially catalyzed sulfate reduction slows, the kinetic isotope fractionations accrued during sulfate reduction approach the theoretical equilibrium exchange values (large isotope effects). As the rate increases, the kinetic values approach a biochemical minimum set by the slowest enzymatic step (assuming sulfate is not limiting or co-limiting). This step reflects the value we measure for DsrAB, 15.3‰. The actual value set by DsrAB, or any enzyme, is itself a combination of all the intermediary steps during enzymatic binding of substrate and the making or breaking of chemical bonds. This cannot be determined directly from first principles using present calculation techniques. This highlights the necessity of empirical work, such as that in chapter 4. Furthermore, the previously proposed biological threshold of 200 micromolar sulfate, below which closed system effects take over and fractionation is not expressed, is not universal, differing for microbes with different physiological abilities and evolutionary histories (chapter 3). These observations require a revisiting of the numerous geological studies where this assumption has been applied. Furthermore, our approach to understanding the intracellular dynamics of sulfate reduction through targeted genetic manipulations of the pathway further our experimental tools with which to investigate S isotope fractionation during microbial sulfate reduction (chapter 5).

Though more work is needed before metabolic, diagenetic, and indeed global biogeochemical box models of the sulfur cycle can become predictive, the path forward is clear. Through constrained experiments, such as those detailed below, we may eventually come to understand the local and global biogeochemical cycling of light stable isotopes such as sulfur.

CONTENTS

ACKNOWLEDGEMENTS

It is undoubtedly true that 'it takes a village', both to raise a kid, and in raising a new PhD. This is particularly true in both cases with a subject as stubborn as myself. As such there are many to thank, too many to name here, but I'll try…

Thanks to my committee: David Johnston, Ann Pearson, Colleen Hansel, Colleen Cavanaugh, Alex Bradley, and Ines Pereira. With their leadership and scholarship I have begun to transition from a bumbling in the dark scientist to one with a little bit more light. It is early still, but you've all set me on a good path. To Dave, for taking me on when I was ready to leave science, you've taught me much, through thick and thin. To Ann, for giving me a shot in the first place as a technician, starting in the fall of 2006. To Alex, for beating stable isotope notation and making me derive the Rayleigh equation from first principles and helping me understand the significance of crystal structures, and of course obsessions with *R*. To C^2, for getting me into MBL in 2008, supporting the seemingly hair-brained enzyme work from the begging and beyond. To Colleen H., you are colleague, friend and family; what more could I possibly ask… maybe you'll let me drive the car again one day? To Inês, for welcoming me into your lab and teaching me more biochemistry than I could every have hoped for, and keep me on track in understanding the incredible nuance and complexity of microbial sulfate reduction.

My time at EPS and Harvard has been made much easier by the great administrative staff in the department. Particular thanks goes to Sarah Colgan, Chenoweth Moffatt, and indeed Paul Kelly. An especial thanks to Sabinna Cappo for ensuring all my trips aboard went smoothly. Lab mates in the U.S. and abroad, from all the various labs I've haunted over the last 7 years of my Masters and PhD, both through OEB, SEAS, and EPS at Harvard, as well as the ITQB in Portugal. In particular Scott Wankel, Julie Robidart, Helen White, Erik Cordes, Roxie Beinhardt, John Sanders, Ben Gill, Adiari Rodriguez-Vasquez, Chris Lentini, Deric Lerman, Cara Santelli, Renata Cummings, Emily Estes, Erin Beirne, Andy Masterson, Emma Bertran, Viv Cumming and Erik Sperling. From my time at the ITQB, so much could not have been done without the biochemical expertise of Sofia Venceslau, Andre Santo, Raquel Ramos and Fabian Grein. To friends in EPS and poor office-mates that have

tolerated my odd hours: Scott, Hilary, Itay, John, Suni, Meytal, Katie, Emma, Lauren, Andy, Sierra, Joe, Kristian, Erik S., Erik M., Eric C., Carling, Natalia, Kate, Glenn, Crowley, JC, Ben K., Rowan, Strauss, Sarah, Roderick, and those I've forgotten… you made EPS, the labs and the offices a special brewery for thought, discovery, and a productive environment in which to get Science done. In particular Andy, without you, who the heck knows what I would have done in the lab. To the Hampshire College and Montana State folks that got me into Science in the first place: Jason Tor and Lynn Miller, Gill Geesey and Eric Boyd, respectively. Who knows what farm or brewery I'd be working in otherwise? To Friends in Cambridge: The 92 Myrtle Crew (Allie, Jake, Suen, Jason, Archie, and the chickens). To Allie and Jake, you've been my grad school parents/brother/sister/best friends I am so lucky and undeserving to have. To LeeAnn, I'm glad we finally got to live together, even if for only a short while… there will be many more fried pickles to come. To the cast and crew of Top of the Two's: Liza, Fenna, Maude (and earlier A&J), what raucous and amazing place: To the Bashio! To the crews of Dimick and Ibbetson: Sarah, Justin (& honorary members Elana, and Shooby), Rooney and Hannah: you guys have been most excellent friends through the peaks and the valleys… you are and will be lifelong friends and colleagues. And to all those who kept me out of doors, both in the mountains: Potter, Davey, Petey, EZ, Allie, Anderson, Raph, Nina, Allie, and others; and to those who kempt me climbing running Ultimate'ing and snow-shoe racing: Dr. Mancini & Chewy, Susie Buckets & Evs, Katie Pesce, Esther, Tor, Justin, Elana, Erik, Sean and Madeline. To close friends far flung across the globe who've supported me throughout: James in Dresden, Maga and cousins Jessie, Jesse and baby Ingraham in Amsterdam/The Hague, Mari all over Europe and Africa, Dinah in Chicago: for hosting and feeding me on the long trips across the Atlantic. And to David F. and Itay, for taking me in and involving me in a new and exciting project. To Claire, 'it's been about a week,' right? I can't wait for the next, and the next and the next! And of course, where would I be with out an amazing family: Mom and Dad (Ellie & Jim), Jenny, Julia, Rossi. Your love and support over all these years has gotten me through. I hope I can give you a little back in the end. Too all my family and friends: first beers are on me. *Science!*

For my grandmothers,

Marjorie James Leavitt & Ellen Ingraham Torrence

CHAPTER 1.

INTRODUCTION

Context for this dissertation

Sulfur plays a major role in the redox balance of Earth's atmosphere and oceans and has done so throughout Earth history (Canfield 2001b; Holland 1973; JORGENSEN 1982; Johnston 2005; J. Farquhar, Johnston, et al. 2007a; Sim, Ono, et al. 2011c; Sim, Bosak & Ono 2011a; Leavitt et al. 2013). The availability of gaseous O_2 as a terminal oxidant to aerobic life forms is underlain by the operation and evolution of the sulfur cycle, and sulfur is a primary agent in transferring electrochemical energy between the major redox active elements, namely carbon and iron (Herbert et al. 1956; Johnston et al. 2007; Monod 1950; Hayes & Waldbauer 2006). A key means to tracking the evolution of global sulfur cycling over million to billion year times-scales is to develop an accurate accounting scheme for how much sulfur enters, remains in, or leaves the surface system – oceans, atmospheres, and mineral reservoirs – per a given time interval. This requires knowing the inputs and outputs, their average redox state, and the mechanisms that transfer mass between pools (e.g. sulfate reduction to sulfide). This approach is rendered quantitative by building accounting ('box') models to include isotopic information on the pools and fractionation factors associated with transformations (Habicht et al. 2002; Holland 1973; GARRELS & LERMAN 1981). Sedimentary rock forming sulfate and sulfide minerals provide the oxidized and reduced end-members of the geologic sulfur isotope record, respectively. To interpret these records the following must be established: i) high temporal resolution records of the geologically stable pools, their masses and isotopic compositions; ii) the mechanisms of exchange between reservoirs; and iii) the mechanisms of isotope fractionation during the exchange reactions. Taken together, these smaller scale fractionation models are integrated into larger geochemical models, solved for fluxes – with the final aim being a better estimate for the history of oxygen on Earth (Lyn A Chambers et al. 1975; R. Berner 2001; Kaplan & Rittenberg 1964; Bergman & Lenton 2004; Sim, Ono, et al. 2011c; Kump 2008; Habicht & Canfield 1997). The models themselves have evolved over the last few decades (Horita et al. 2002; Holland 1973; R. A. Berner & Canfield 1989; R. Berner 2001; R. A. Berner 2006; R. A. Berner 2009; Holland 2009), as have the geological sulfur isotope records (see compilations in (Ingvorsen et al. 1984; Canfield & J. Farquhar 2009; Wu et al. 2010; J. Farquhar et al. 2010)). While inroads have been made into targets i) (Herbert et al. 1956; Canfield & J. Farquhar 2009; Wu et al. 2010; J.

Farquhar et al. 2010) and ii) (Lyn A Chambers et al. 1975; Johnston 2011; Herbert et al. 1956; Whitehill et al. 2013; Halevy 2013), target iii) has remained largely unaddressed in the primary literature. Therefore, what remains open is our fundamental lack of understanding for the mechanisms of sulfur isotope fractionation in the global sulfur cycle.

The major aqueous reservoir of sulfur on Earth today are the oceans (Lyn A Chambers et al. 1975; Hayes & Waldbauer 2006; Davidson et al. 2009; Stam et al. 2010). The primary mechanism to naturally reduce sulfate to sulfide under most Earth surface conditions (<100°C, pH 5-9) is microbial sulfate reduction (MSR), with some minor influence from thermochemical sulfate reduction (TSR) (Ohmoto & Lasaga 1982; Lyn A Chambers et al. 1975; Goldhaber & Kaplan 1975). This is also the first critical linkage to the carbon cycle, as those eight electrons are most often sourced from organic carbon in sediments. This remineralization reaction releases dissolved inorganic carbon, and alters alkalinity locally (Boudreau & Westrich 1984; Stumm & Morgan 2012; DE 1991; Canfield et al. 1993). Following the eight-electron reduction of sulfate to sulfide, any number of fates may befall the sulfide. Sulfide may be partially or completely reoxidized at the expense of environmental oxidants, such as iron or manganese oxides, nitrate or dissolved oxygen itself, directly coupling the major elemental redox cycles. Sulfide and intermediate valence sulfur species (e.g. sulfite, elemental sulfur, thionates, polysulfides) can also be oxidized by microorganisms as part of their energy metabolisms. If the sulfide or intermediates are generated in the photic zone, anoxygenic photosynthetic chemoautotrophic bacteria often take advantage of the reducing power in those S-compounds, along with light-energy, and fix carbon dioxide into biomass (Heidelberg et al. 2004; Frigaard & Dahl 2009; Keller & Wall 2011). Furthermore, the intermediate valence compounds themselves can be re-reduced to sulfide, oxidized completely back to sulfate, or through a combination of the two, *disproportionated* (Bak & Cypionka 1987). Disproportionation is essentially an inorganic fermentation, where one S intermediate acts as the electron donor and the other the electron acceptor (Bak & Cypionka 1987; Bak & Pfennig 1987; Thamdrup et al. 1993) . Finally, sulfur is lost from the marine cycle when it is precipitated as a base-metal sulfide (e.g. FeS, FeS_2) or due to sulfate mineral formation as either barite ($BaSO_4$), gypsum or anhydrite ($CaSO_4$) (Martinez-Ruiz & Eagle 2004). Central to this entire marine sulfur cycle (Fig. 1.1) is the

simple fact that without MSR, all downstream reactions cannot occur in typical marine or lacustrine conditions. MSR both initiates and maintains todays marine sulfur cycle.

In addition to being the largest soluble (mobile) sulfur reservoir in Earths surface environment, sulfate is the most stable and least amenable to isotopic exchange at lower temperatures (< 150°C) (Ames & Willard 1951; Ohmoto & Lasaga 1982). As such, biochemical systems come into play, and particularly because so little of the Earths oceans might experience TSR. Early in the evolution of S isotope (bio)geochemistry it was demonstrated that life, in particular MSR, participates in generating secular variation in the modern and ancient sulfur isotope records (Szabo et al. 1950; Thode et al. 1953). The field then honed in on determining which microbial metabolisms contribute fractionation signals (Harrison & Thode 1958; Kaplan & Rittenberg 1964; Nakai & Jensen 1964; Kemp & THODE 1968; Lyn A Chambers et al. 1975; Detmers et al. 2001; Habicht et al. 2005; Johnston et al. 2007; Zerkle et al. 2009; Sim, Ono, et al. 2011c; Sim, Bosak & Ono 2011a; Johnston 2005), both in terms of magnitude and directionality. This approach appears to have guided the literature for the last 60 years up through the present, with much headway made since that earliest study (Thode et al. 1951). Fundamental to this pursuit is the early recognition (Szabo et al. 1950; Thode et al. 1953) that tracking sulfur isotope fractionations provide us more than just a geochemical tracer, but a metric of *bio*geochemical activity, particularly where other metrics may not be available, e.g. ancient sedimentary record.

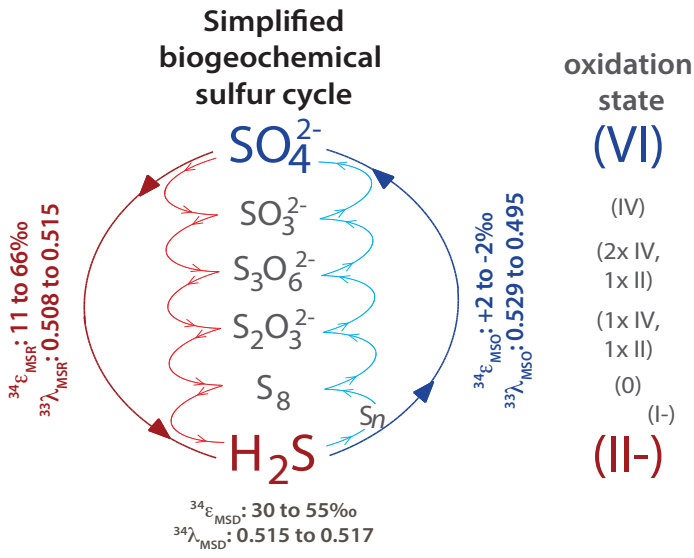

Figure 1.1. The global biogeochemical sulfur cycle and the generalized MSR DSR pathway. A simplified sulfur cycle, accounting for the reductive branches in red, with complete MSR in bold, the oxidative branches in blue, and variable disproportionation variable combinations of the thinner red and blue arrows. The range of major and minor isotope fractionations are presented from studies where both $^{34}\varepsilon$ and $^{33}\lambda$ data are available. References appear in the text.

With the advent of high precision multiple sulfur isotope (^{32}S, ^{33}S, ^{34}S, & ^{36}S) measurement methods (c.f. (J. Farquhar et al. 2000)), it soon became clear that minor isotope systematics (e.g. $^{33}S/^{32}S$) may help differentiate the variable influenced of the three major geomicrobial sulfur cycle processes (Canfield 2001a). These being: sulfate reduction (J. Farquhar et al. 2003), sulfide and sulfur oxidation (Zerkle et al. 2009), and intermediate valence S-compound disproportionation (Johnston 2005). Since, a wide array of claims for which S-based metabolism(s) dominated the sulfur cycle at different periods in Earths history have surfaced (Johnston et al. 2005; Philippot et al. 2007; J. Farquhar, M. Peters, et al. 2007b; Sim, Bosak & Ono 2011a; Shen et al. 2001). Though early days still, our understanding of each mechanism improves, and as the geological records fill out, so might our understanding for when – or even if – these metabolisms were active participants in the sulfur cycle, particularly during critical intervals of evolutionary history. For example, following the collapse in the mass independent atmospheric chemistry signal, following the 'Great Oxidation Event/Interval' (J. Farquhar et al. 2000; Lyons et al. 2014) (with the onset of oxygenic photosynthesis and the accumulation of O_2 and O_3 in the atmosphere, the style of multiple sulfur isotope fractionation preserved in geological records transitioned from primarily atmospheric, mass-independent effects in the Archean, to predominantly mass-dependent microbial effects thereafter).

Biological fractionations dominate the geological sulfur isotope record from at least the earliest Proterozoic to and through the modern (J. Farquhar et al. 2000; Canfield & J. Farquhar 2009; Johnston 2011). To understand and interpret these records, constructing a detailed understanding for the mechanisms of fractionation is paramount. This approach has and continues to be an integral approach in understanding both modern and ancient carbon and nitrogen cycles (Park & Epstein 1960; Hayes 1993; Hayes 2001; Mariotti et al. 1981; Casciotti et al. 2010; Santoro et al. 2011; Higgins et al. 2012). To-date, we know much about the magnitude of MSR sulfur isotope fractionations, but little about the mechanisms of isotopic discrimination. If metabolic isotope models (Rees 1973; Brunner & Bernasconi 2005; Johnston et al. 2007; J. Farquhar, Johnston, et al. 2007a; Bradley et al. 2011) are to become predictive, and if it is reasonable to even use as a tool to better understand ancient environments. Presently these models are at best descriptive. Moreover, the collective push

needs to focus on *how* isotope fractionations are generated and whether these are reflective of environmental conditions. That is, we now seek to understand the mechanisms of sulfur isotope fractionation and the internal (biological) and external (physicochemical) forcings that constrain them.

Roadmap of this dissertation

In this work I set out to 1) determine the primary environmental controls on the magnitude of sulfur isotope fractionations, 2) determine what enzymatic steps impart isotopic discrimination and the magnitude of fractionation during microbial sulfate reduction, and 3) determine how the environmental parameters interact with and ultimately drive intracellular effects to express themselves differently under specific environmental regimes. In combining observations from in vivo and in vitro experimental approaches I aim to construct a mechanistically grounded interpretive framework for the isotopic compositions of sulfur species in modern marine and freshwater environments. The hope is this will aid us in deriving a better understanding of extant biogeochemical processes as we work to reconstruct ancient Earth environments.

In Chapters 2 and 3 we systematically test the influence two critical environmental parameters on the magnitude of MSR isotope fractionation – reductant or oxidant availability. Each section allows for a significant reinterpretation of the Phanerozoic (Chapter 2) and Archean (Chapter 3) sulfur isotope records, respectively. Together these studies put in place facies testable hypothesis we hope geologists, geochemists, and historical geobiologists alike will carry with them in the field, and in interpreting secular trends in the geological sulfur isotope record going forward. In Chapter 4, the multiple sulfur isotope fractionation factors of key MSR enzyme, DsrAB, are determined. These are the first such boundary conditions for any metabolic fractionation models in the sulfur cycle. These values also allow us to reinterpret the last sixty years worth of experimental MSR sulfur isotope fractionation work (Chapter 4, Fig. 4.2a), and help to uncover patterns in the modern sedimentary records not previously recognized (Chapter 4, Fig. 4.2a). These simple experiments also offer deeper insight into the mass-dependent fractionation component of geological sulfur isotope records (J. Farquhar et al. 2010; Johnston 2011); in particular that of the Neoarchean (2.8 to 2.5 Ga) (J. Farquhar et al. 2013).

In the back of this dissertation are three appendices. In Appendix A, we review and up-date the metabolic sulfur isotope fractionation model for MSR. This up-date reflects recent advances in the biochemistry of MSR, notably the inclusion of multiple branching reactions off of sulfite, and focuses our attention on the possibility for different operational modes of the MSR pathway in response to environmental and/or intracellular forcings. We also include parameterizations for minor isotope fractionations (Johnston et al. 2007; J. Farquhar, Johnston, et al. 2007a). Perhaps most valuable is the publically available mathematical MSR model derived and built by Alex Bradley, coded in ***R***, such that is open-source. Appendix B is a stand-alone study that originated as the undergraduate thesis of Renata Cummins, designed by Dave and myself, and carried further by Dave, research fellow Marian Schmidt, Alex Bradley and myself. The results of these closed-bottle sulfite and thiosulfate reduction experiments, again using well-characterized strains of MSRs, yielded striking results, particularly for site-specific multiple sulfur isotope fractionations. The observed isotope fractionations open up a slew of new questions regarding intracellular thionate cycling, and whose implications likely extend to natural marine sediments, where thiosulfate in particular plays an important role in redox cycles (Jorgensen 1990). In Appendix C I note, in some detail, the follies foibles and stumbles I encountered during this dissertation work. For what is the value of mistakes if we do not learn from them, share them, and prevent the next generation from making them again? I have and will continue to make errors, blunders, and missteps along the way. I relish the chance to do so, and to learn from them. Any in the work presented here are mine alone.

In the final chapter I offer general conclusions and a synthesis of the key findings. I then sketch out a detailed, albeit incomplete, roadmap of my on-going and some intended future studies that will continue this vein of inquiry. This trajectory reflects my biases as a scientist: I strive to understand the underlying mechanisms of microbiologically driven processes, to reveal how microorganisms alter their environment, and how the environment, in turn, constrains microbial activity adaptation and evolution.

CHAPTER 2.

THE INFLUENCE OF SULFATE REDUCTION RATES ON THE PHANEROZOIC SULFUR ISOTOPE RECORD

A version of this chapter is published as:

Leavitt, W.D., I. Halevy, A. Bradley, and D.T. Johnston. 2013. Influence of sulfate reduction rates on the Phanerozoic sulfur isotope record. *Proceedings Of The National Academy Of Sciences Of The United States Of America*, 110(28), pp.11244–11249.

ABSTRACT

Phanerozoic levels of atmospheric oxygen relate to the burial histories of organic carbon and pyrite sulfur. The sulfur cycle remains poorly constrained, however, leading to concomitant uncertainties in O_2 budgets. Here we present experiments linking the magnitude of fractionations of the multiple sulfur isotopes to the rate of microbial sulfate reduction. The data demonstrate that such fractionations are controlled by the availability of electron donor (organic matter), rather than by the concentration of electron acceptor (sulfate), an environmental constraint that varies among sedimentary burial environments. By coupling these results with a sediment biogeochemical model of pyrite burial, we find a strong relationship between observed sulfur isotope fractionations over the last 200 million years and the areal extent of shallow seafloor environments. We interpret this as a global dependency of the rate of microbial sulfate reduction on the availability of organic-rich sea floor settings. However, fractionation during the early/mid-Paleozoic fails to correlate with shelf area. We suggest that this decoupling reflects a shallower paleo-redox boundary, primarily confined to the water column in the early Phanerozoic. The transition between these two states begins during the Carboniferous and concludes approximately around the Triassic-Jurassic boundary, indicating a prolonged response to a Carboniferous rise in O_2. Together, these results lay the foundation for decoupling changes in sulfate reduction rates from the global average record of pyrite burial, highlighting how the local nature of sedimentary processes affects global records. This distinction greatly refines our understanding of the S cycle and its relationship to the history of atmospheric oxygen.

INTRODUCTION

The marine sedimentary sulfur isotope record encodes information on the chemical and biological composition of Earth's ancient oceans and atmosphere (Canfield 2004b; J. Farquhar et al. 2000). However, our interpretation of the isotopic composition of S-bearing minerals is only as robust as our understanding of the mechanisms that impart a fractionation. Fortunately, decades of research identify microbial sulfate reduction – MSR – as the key catalyst of the marine S cycle, both setting the S cycle in motion and dominating the mass-

dependent fractionation preserved within the geological record (Canfield 2004b; Strauss 1997; Johnston 2011). Despite the large range of S-isotope variability observed in biological studies (Johnston 2011; Detmers et al. 2001; Johnston 2010), attempts to calibrate the fractionations associated with MSR are less mechanistically definitive (Habicht et al. 2002; Canfield 2001b) than analogous processes influencing the carbon cycle (Park & Epstein 1960; Laws et al. 1995). What is required is a means to predict S isotope signatures as a function of the physiological response to environmental conditions (e.g., reduction-oxidation potential).

Microbial sulfate reduction couples the oxidation of organic matter or molecular hydrogen to the production of sulfide, setting in motion a cascade of reactions that come to define the biogeochemical S-cycle. In modern marine sediments, sulfide is most commonly shuttled back toward sulfate through oxidation reactions (biotic and abiotic) or scavenged by iron and buried as pyrite (Canfield 2001a). It is the balance of oxidation reactions and pyrite burial that influences geological isotope records, which in turn carry historical information on the oxidation state of Earth's biosphere. Such records generally are thought to indicate that oxidant availability has increased with each passing geologic Eon (Holland 2006). Although playing prominent roles in sedimentary redox cycles (Canfield & J. Farquhar 2009), oxidation reactions carry only modest S isotopic fractionations (*see* Section 2.4, Notation) (Gest & Hayes 1984; Zerkle et al. 2009). In typical modern marine sediments, the oxidative region of aerobic organic carbon remineralization is separated from the zone of sulfate reduction (where MSR takes place) by an intermediate layer in which both sulfide oxidation and sulfur disproportionation occur (Canfield 2006; Canfield & Thamdrup 2005). Despite sulfur recycling across that boundary layer, the sulfur that is eventually buried as pyrite predominately reflects the isotopic fractionation associated with MSR (Jorgensen 1979).

Numerous studies show a correlation between microbial sulfate reduction rate (mSRR) and the expressed magnitudes of the MSR S isotopic fractionations (Lyn A Chambers et al. 1975; Kaplan & Rittenberg 1964; Harrison & Thode 1958; Goldhaber & Kaplan 1975). The mSRR depends on a suite of physiological controls (i.e., metabolic enzymes) (Peck et al. 1982) having variable efficiencies in response to environmental conditions (e.g., nutrient availability, redox potential, etc. (Canfield 2001b; JORGENSEN 1982)). Such

reactions can be presumed to be first-order with respect to a limiting reactant (Herbert et al. 1956; Monod 1950). In the case of MSR, either the electron acceptor (sulfate (Habicht et al. 2002)) or the electron donor (generally organic carbon: OC (Lyn A Chambers et al. 1975; Kaplan & Rittenberg 1964; Sim, Ono, et al. 2011c; Habicht & Canfield 1997)) plays this role. It has been hypothesized that since the Archean – Proterozoic boundary, sulfate (oxidant) limitation has not occurred in the water column, but rather has been restricted to significantly below the sediment-water interface. This is consistent with estimates through the Proterozoic and Phanerozoic Eons (Horita et al. 2002), which suggest seawater sulfate concentrations in excess of the physiologically-inferred minimum threshold for MSR (Ingvorsen et al. 1984). It thus follows that the quantity and quality of organic carbon delivery to the zone of sulfate reduction should most often dictate sulfate reduction rates where sulfate is abundant, and consequently, play the larger role in determining the sulfur isotope record.

The most direct experimental means of studying the metabolic rate of a bacterial population is to maintain the culture in a chemostat. In a chemostat, the input concentration of the limiting substrate (e.g., micronutrient, electron donor or electron acceptor) dictates the biomass yield (i.e., new biomass per mass substrate utilized), while turnover time of the reactor (dilution rate: D, time^{-1}) dictates growth rate ((Herbert et al. 1956)). It follows that the mSRR (specifically, the rate of reduction per unit biomass) scales with the availability of the limiting nutrient, and thus with D (Lyn A Chambers et al. 1975; Herbert et al. 1956). Limited previous experimental work with open and semi-open experimental systems hints that mSRR inversely correlates with fractionation of the major S isotopes ($^{34}S/^{32}S$) (Lyn A Chambers et al. 1975; Davidson et al. 2009; Stam et al. 2010) – a prediction that is reinforced by measurement of the same relationship in modern marine sediments (Harrison & Thode 1958; Lyn A Chambers et al. 1975; Kaplan & Rittenberg 1964; Goldhaber & Kaplan 1975; Nakai & Jensen 1964; Kemp & THODE 1968; Detmers et al. 2001; Habicht et al. 2005; Johnston et al. 2007; Zerkle et al. 2009; Sim, Ono, et al. 2011c; Sim, Bosak & Ono 2011a; Johnston 2005). However, the limited range of mSRRs previously explored does not adequately capture the vast range of rates inferred from marine sediments (Thode et al. 1951; Boudreau & Westrich 1984; DE 1991; Canfield et al. 1993). In this work we present an empirical calibration of a ~50-fold change in mSRR, nearly doubling the previous experimental ranges. We also

target the minor isotope, ^{33}S, in addition to targeting ^{34}S fractionations; this supplies a new dimension for interpreting the geologic record. We then apply this calibration to Phanerozoic isotope records to reveal how secular changes in S isotopic fractionation reflect a temporal history of paleo-redox conditions. This enables us to reassess the burial of pyrite and associated changes in environmental conditions across the Phanerozoic Eon.

RESULTS AND DISCUSSION

We conducted a suite of continuous culture experiments with the model sulfate reducing bacterial strain *Desulfovibrio vulgaris* Hildenborough (DvH). Strain DvH is among the most well studied sulfate reducers and is genetically tractable (Szabo et al. 1950; Heidelberg et al. 2004; Thode et al. 1953; Keller & Wall 2011). Though DvH is nominally a non-marine strain, the concentration of sulfate in the chemostat was always near modern marine levels (28mM) and well above known sulfate affinity constants (Tarpgaard et al. 2011). The sole electron donor (lactate) was always the limiting nutrient in these experiments and was provided at a stoichiometric 1:2 or 1:20 ratio with sulfate (experimental details in the *Methods*).

These experiments show that MSR isotope fractionation is strongly inversely dependent on electron donor concentration (Fig. 2.1). In detail, mSRR follows a 1st-order nonlinear relationship to D (Fig. 2.1) – as we decrease D, lactate availability and mSRR decline, while $^{34}\varepsilon_{MSR}$ increases. The values of $^{34}\varepsilon_{MSR}$ and $^{33}\lambda_{MSR}$ refer to the isotopic differences between the sulfate and sulfide from chemostat experiments, whereas $^{34}\varepsilon_{GEO}$ and $^{33}\lambda_{GEO}$ refer to those differences calculated from sulfate and pyrite sedimentary records as time-binned averages (Dataset S1, Table 2.S2, Eqn 2.S4-2.S7). These open-system experiments allow for the direct calculation of fractionation factors from the isotopic composition of output sulfate and sulfide (Hayes 2001), without having to apply Rayleigh distillation models addressing closed system (batch) dynamics (Johnston et al. 2007). We demonstrated conservation of elemental and isotopic mass balance throughout the entire experiment (Dataset S1) via the direct measurement of SO_4^{2-}, H_2S/HS^-, $S_2O_3^{2-}$, and $S_3O_6^{2-}$ – the latter two of which were always below detection (2.5 mM), but have been previously detected in semi-open system experiments (Davidson et al. 2009).

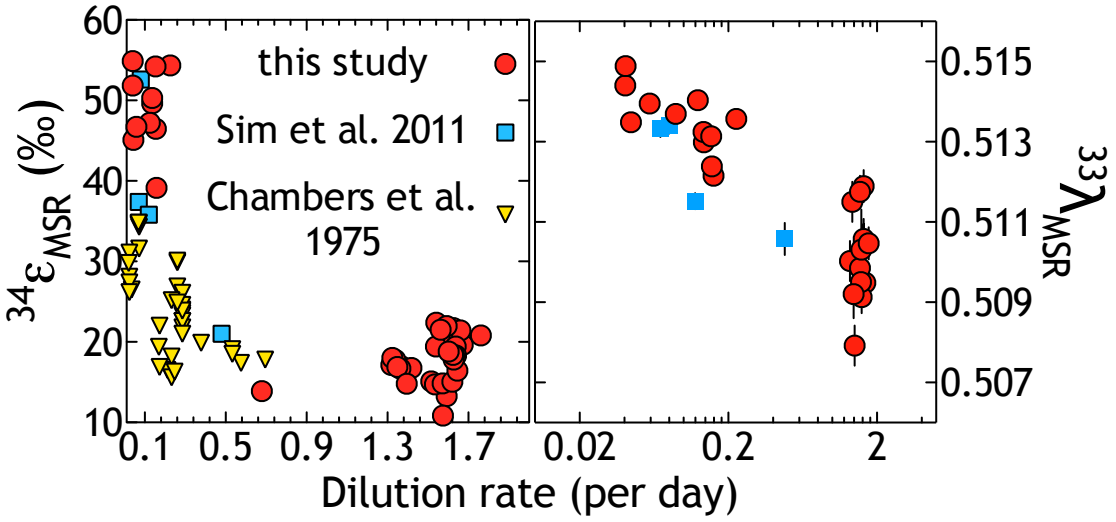

Figure 2.1. **Multiple sulfur isotope fractionations as a function of dilution or sulfate reduction rate in chemostat experiments.** In these experiments, growth and sulfate reduction rates scale inversely with organic carbon (lactate) delivery rate, expressed here as dilution rate (D, hr^{-1}, see SI for further definitions). This rate dictates the magnitude of major (A) and minor (B) isotope fractionation between sulfate and sulfide. Error bars in (A) are smaller than the symbols (2σ = 0.3‰), while vertical error bars in s are 2σ standard deviations.

Our data complement and significantly extend previous open system experiments (Canfield 2001b; Lyn A Chambers et al. 1975; Sim, Ono, et al. 2011c; J. Farquhar et al. 2008; Stam et al. 2011). Over a ~50-fold change in mSRR (Fig. 2.1), $^{34}\varepsilon_{MSR}$ ranged from 10.9 to 54.9‰ (Fig. 2.1a), while $^{33}\lambda_{MSR}$ varied from 0.5079 to 0.5144 (Fig. 2.1b). In addition to aiding in our understanding of environmental/geological records (*see below*), these data allow for an empirically derived fractionation limit for DvH under conditions of maximal electron donor limitation. We apply a nonlinear regression model (Motulsky & Ransnas 1987) based on a pseudo-first order rate expression, appropriate for a reaction where rate depends on the concentration of a single reactant (Eqn. S8-S9) (Monod 1950; Habicht et al. 2005). The results of the model illustrate the capacity of MSR to exceed the classic 47‰ limit for $^{34}\varepsilon_{MSR}$ (Fig. 2.2 (Rees 1973)), here suggesting an upper limit of 56.5 ± 2.6‰. The same nonlinear

regression model (Eqn. S9) predicts a minor isotope limit (in $^{33}\lambda$) at 0.5143 ± 0.0004. Given that our experiments were performed with an axenic population of sulfate reducers, we can definitively rule out contributions from intermediate S-oxidizing or disproportionating organisms (Sim, Bosak & Ono 2011a). However, although the magnitudes of these fractionations exceed the canonical MSR limits ($^{34}\varepsilon$ = 47‰), they do not reach the low-temperature equilibrium predictions between sulfate and sulfide in $^{34}\varepsilon$ (at 20°C, $^{34}\varepsilon$ = 71.3‰ (Johnston et al. 2007)).

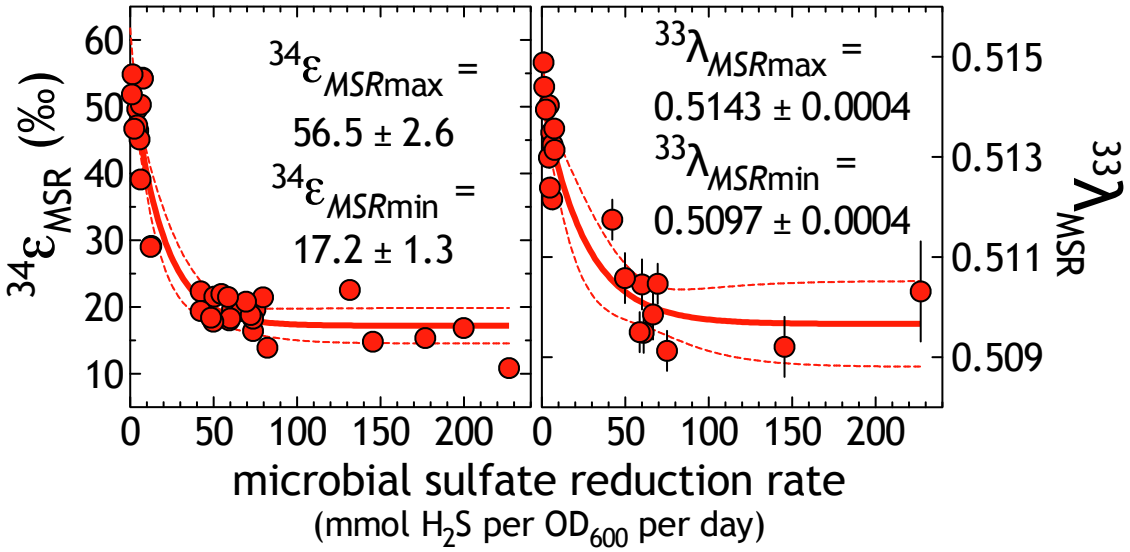

Figure 2.2. **Demonstration of new fractionation limits under electron-donor limitation**. A non-linear regression model (eqn. S8-S9) was used to calculate the empirical fractionation limit in (A) $^{34}\varepsilon_{MSR}$ (r^2 = 0.9151) and (B) $^{33}\lambda_{MSR}$ (r^2 = 0.8905), as a function of mSRR. Bold lines indicate the best-fit estimates with 95% confidence intervals as the thin dashed lines ($^{34}\varepsilon_{MSR}$: 51-62‰; $^{33}\lambda_{MSR}$: 0.5135-5151). Inset values are the calculated fitting parameters (along with k_{MSR_ε} = 0.054 ± 0.012 and k_{MSR_λ} = 0.0395 ± 0.0158) with standard errors used in calculations for 95% CI.

Decoupling the isotopic effects of sulfate reduction rates from pyrite burial records

In modern marine sediments, OC availability is strongly tied to sedimentation rate (Westrich & R. A. Berner 1984; LaRowe & Van Cappellen 2011; Middelburg 1989). Faster sedimentation (such as in river deltas or on continental shelves) generally leads to more efficient delivery of OC below the depth of oxygen penetration, into the zone of sulfate reduction – extreme sedimentation rates, of course, deviate from this prediction and can lead to OC dilution. The absolute flux of OC also scales directly with primary production. The balance of these processes dictates where sulfate reduction occurs with respect to the sediment-water interface, as well as how much sulfate ultimately is reduced (Hartnett et al. 1998). Because some fraction of the resulting sulfide will be buried as pyrite – with concomitant release of oxidant to the ocean-atmosphere system – it is critical to determine how the mSRR-dependent isotope fractionation ($^{34}\varepsilon_{MSR}$ and $^{33}\lambda_{MSR}$) influence the S-isotopic records of pyrite relative to coeval sulfate ($^{34}\varepsilon_{GEO}$ and $^{33}\lambda_{GEO}$).

Analogous to the influence of lactate on mSRR in our experimental system, the availability of greater quantities of more highly labile OC to the sulfate reduction zone in modern sediments translates to an increase in sulfate reduction rates, with a corresponding decrease in the magnitude of $^{34}\varepsilon_{MSR}$ (JORGENSEN 1982; Canfield et al. 1993; Canfield 1994). Conversely, decreases in sulfate reduction rates down a sediment column due to the modeled loss of OC quality and quantity are consistent with observations that $^{34}\varepsilon_{MSR}$ increases (Westrich & R. A. Berner 1984; Goldhaber & Kaplan 1975; Goldhaber et al. 1977). Together these ideas describe the concept of *net* sedimentary sulfate reduction rate (sedSRR; mol S per square meter per year). The sedSRR, because it integrates the depth-dependent rate through the entire zone of sulfate reduction, must encompass a depth-weighted average of the variable $^{34}\varepsilon_{MSR}$ as well as be tightly linked to the initial OC delivery to the sediment-water interface. Data from the modern seafloor (Jorgensen 1979; Goldhaber & Kaplan 1975; Aharon & Fu 2000) confirm the expected inverse relation between bulk *in situ* sedSRR and the magnitude of the net sedimentary S isotope fractionation ($^{34}\varepsilon_{GEO}$).

The concept of sedSRR also contains another important distinction from mSRR. In most environments, measures of microbial population density are lacking, as are measures of the metabolically available organic

carbon compounds. Our experimental system quantifies these parameters and enables direct calculation of mSRR. However, in the environment, the useful metrics are the bulk sedSRR and the global sulfate reduction rate (gSRR: mol S per year). The sedSRR is converted to gSRR through an areal normalization and a reoxidation coefficient (Canfield 2004b; Canfield & Thamdrup 2005); further details are presented in Table S1. It is gSRR that is necessary for determining long-term oxidant budgets and global pyrite burial.

We propose that it is possible to decouple the isotopic effects caused by variable sedSRR from the ultimate sedimentary record of S isotopes. For example, under iron-replete conditions, net pyrite burial may increase as a result of more sulfide production and/or an increased sulfide scavenging efficiency by iron (i.e. less oxidation), but at a constant sedSRR. Alternatively, pyrite burial could increase in response to a higher sedSRR, if it were driven by a higher flux of metabolizable organic carbon to the sedimentary zone of sulfate reduction. This comparison can also be extended to include the roles for weathering and changes in the abundance of shallow water environments (shelf area). We posit that it is possible to differentiate between these scenarios and determine the ultimate control (tectonics vs. OC) on pyrite burial at the global scale: The first case would maintain a constant $^{34}\varepsilon_{GEO}$ and $^{33}\lambda_{GEO}$, whereas varying sedSRR would be recorded by a change in the fractionation patterns.

Interpreting Phanerozoic records

Phanerozoic compilations provide a context for evaluating the potential variability in sedSRR through time. Records of $^{34}\varepsilon_{GEO}$ and $^{33}\lambda_{GEO}$ from Phanerozoic sedimentary basins provide a time series approximation of the mean isotopic difference between coeval sulfates and sulfides (Fig. 2.3, Table 2.S2) (Canfield & J. Farquhar 2009; Wu et al. 2010). In parallel, we utilize recent estimates for the areal extent of continental shelf and abyssal ocean across Phanerozoic time (Table S2 (HALEVY et al. 2012; Hannisdal & S. E. Peters 2011)). Assuming that the physical processes dictating OC delivery to sediments today hold throughout the Phanerozoic, shelf environments are generally expected to be OC-rich and support higher sulfate reduction rates than deep-water settings (Canfield & Thamdrup 2005; Goldhaber & Kaplan 1975). This is reinforced by modern observations,

where in shallow water sediments (<1000 m deep), the area-weighted average sedSRR is 96 μmol SO_4^{2-} cm^{-2} yr^{-1}, whereas in deep-water sediments (>1000 m deep) it is approximately 1 μmol SO_4^{2-} cm^{-2} yr^{-1}.

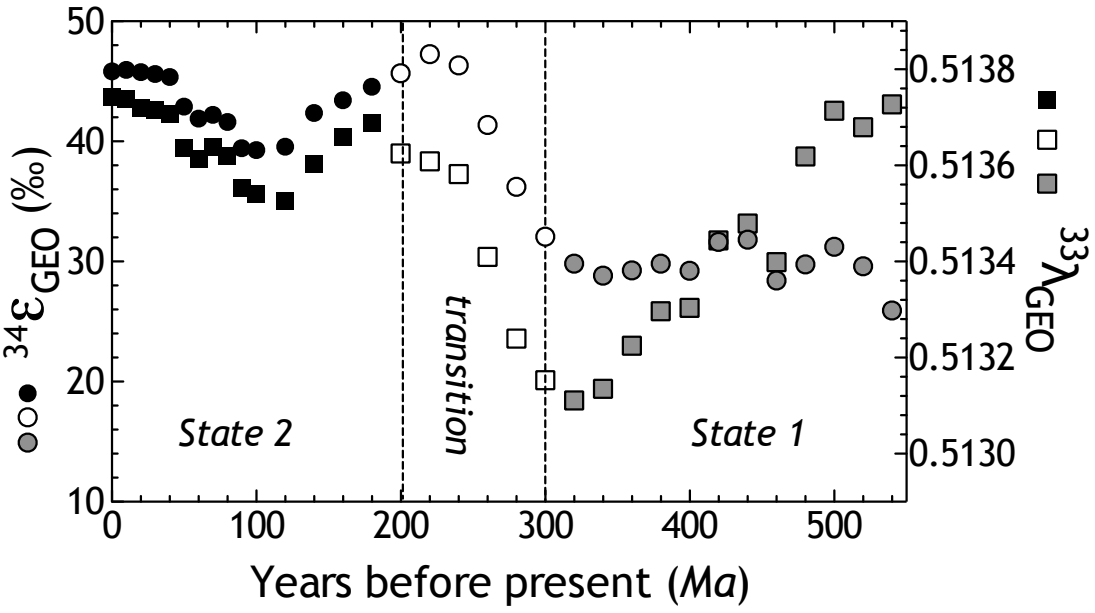

Figure 2.3. The Phanerozoic sulfur isotope record. See *Detailed Methods* for compilation, binning strategy and data handling.

It has long been appreciated that the $^{34}\varepsilon_{GEO}$ record through the Phanerozoic carries a definitive structure (Canfield & J. Farquhar 2009; GARRELS & LERMAN 1981; R. A. Berner 2004) – the earliest Paleozoic has mean fractionations of ~30‰ and transitions through the Permian and Triassic to a Meso-Cenozoic average near ~45‰ (Fig. 2.3). This temporal distinction also exists for estimates of $^{33}\lambda_{GEO}$ (Fig. 2.3) (Wu et al. 2010). Interestingly, by comparing both isotope metrics ($^{34}\varepsilon_{GEO}$ and $^{33}\lambda_{GEO}$) with estimates of shelf area, we are able to resolve temporal patterns (Fig. 2.4, 2.S4). From our analysis of the compiled datasets, we find that as shelf area increases, both $^{34}\varepsilon_{GEO}$ and $^{33}\lambda_{GEO}$ tend to decrease (Fig. 2.4, 2.S4). Closer examination of these data illustrate, however, that the statistical significance of these correlations rests largely on the tightly coupled behavior in the Meso-Cenozoic. In contrast, the Paleozoic has a less coherent relationship (Fig. 2.4, 2.S4). We thus interpret the

multiple S isotope record as being divisible into two states offset by a transition. The first state is the early Paleozoic (540-300 Ma), where $^{34}\varepsilon_{GEO}$ is lower, shelf areas are larger and $^{33}\lambda_{GEO}$ is highly variable; the second state is the Meso-Cenozoic (200-0 Ma), where $^{34}\varepsilon_{GEO}$ and $^{33}\lambda_{GEO}$ are larger and associated with less shelf area. The transition spans at least the Permian and the Triassic (ca. 300-200 Ma).

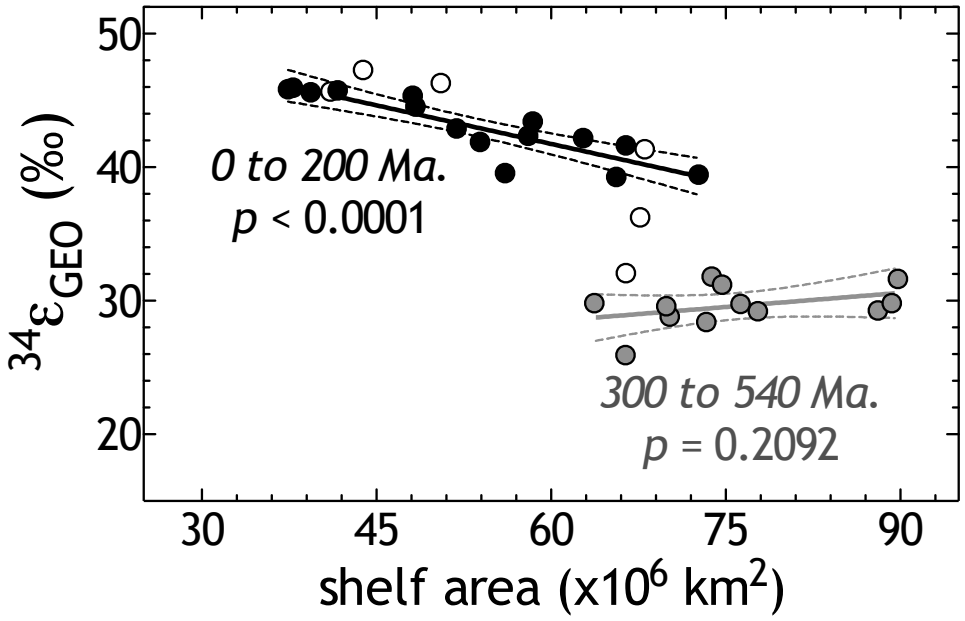

Figure 2.4. Relating Phanerozoic shelf area estimates to isotopic records. Data are binned and color-coded as in Fig. 2.3, with the Permian-Triassic in white to highlight this transition. The *p*-values are for the 0 to 200 and 300 to 540 Ma intervals. Significant covariance ($p < 0.0001$) between shelf area and both isotope metrics only exist in the last 200 Ma. A similar relationship exists for $^{33}\lambda_{GEO}$ relative to shelf area (Fig. 2.S4). A more robust interpretation of ^{33}S records will require a larger geologic database than is currently available.

Although there is relatively less sulfur isotopic variability in the Meso-Cenozoic compared to the Paleozoic, the interval from the Cretaceous to the present (ca. 100-0 Ma) shows increases in $^{34}\varepsilon_{GEO}$ and $^{33}\lambda_{GEO}$ of 7‰ and ~0.0002, respectively (Fig. 2.3). The opposite trends, and by analogy the converse arguments, apply to

the Mesozoic interval from 200-100 Ma (Fig. 2.3). In our conceptual framework, this may represent a constant sedSRR with a decreasing shelf area (thereby decreasing both gSRR and pyrite burial); or it may represent a decrease in sedSRR with concomitant decline in shelf area. We first consider the case of constant sedSRR: Here, a ~10% decrease in pyrite burial is required to accommodate the 7‰ increase in $^{34}\varepsilon_{GEO}$. Such a fluctuation in pyrite burial is reasonable. However, changes in pyrite burial cannot affect $^{33}\lambda_{GEO}$, and as such, the observed variance in $^{33}\lambda_{GEO}$ means that a change in shelf area alone (as it relates to gSRR) cannot explain the Meso-Cenozoic S isotope record, *i.e.*, sedSRR also must have changed.

As an alternative to a change only in shelf area, our experimental data provide a means to test the second hypothesis: variable sedSRR. The sediment data for $^{33}\lambda_{GEO}$ versus $^{34}\varepsilon_{GEO}$ through the Meso-Cenozoic are statistically within the relationship extracted from our chemostat data ($^{33}\lambda_{MSR}$ vs. $^{34}\varepsilon_{MSR}$; Fig. 2.S5). This suggests that the dominant control on fractionation is sulfate reduction, and that the geologic data can be interpreted in the context of where they fall on the slope-rate relationship of MSR (Fig. 2.S5). The isotopic record of the Meso-Cenozoic corresponds to an estimated mean 83^{105}_{70}% variation in sedSRR if based on our experimentally determined $^{34}\varepsilon_{MSR}$—rate relation, or a mean 43^{119}_{27}% variation in sedSRR if based on the $^{33}\lambda_{MSR}$—rate relation (Fig. 2.5 and 2.S4; $^{34}\varepsilon_{MSR}$- or $^{33}\lambda_{MSR}$-derived mSRR is converted to sedSRR by using the Plio-Pleistocene as a reference and assuming that the scaling relationship is constant over time).

We postulate that synergistic changes in sedSRR and shelf area work together to explain the Meso-Cenozoic sulfur isotope record. The pattern of change in sedSRR between 200-0 Ma is also significantly correlated to the variability in shelf area over that same interval (Fig. 2.5, Fig. 2.S4). This implies that sedSRR and shelf area are at least partially inseparable variables, although the underlying coupling between them is not immediately clear. Importantly, an increase in sedSRR is not simply an increase in the molar flux of sulfate reduction, proportional to increased shelf area. An increase in sedSRR requires a change in the local mSRR integrated in a local sediment column. This must signal a response to availability of the limiting reactant – in this case OC – either via its quantity or quality delivered to the sedimentary zone of sulfate reduction. We hypothesize

that changes in the absolute flux of nutrients (Canfield 1989) to shelf environments is influencing the location and intensity of primary productivity, changing the delivery of OC to the sediments, and influencing the sedSRR. In this way, sedSRR joins the many other sedimentary biogeochemical processes known to respond to varying nutrient regimes (Tsandev et al. 2008). Further refining the structure of the Meso-Cenozoic record may provide critical insight into what processes are playing a prominent role in setting sedSRR, and we consider the consequences of this prediction below. However, we first consider the different patterns apparent in the Paleozoic records.

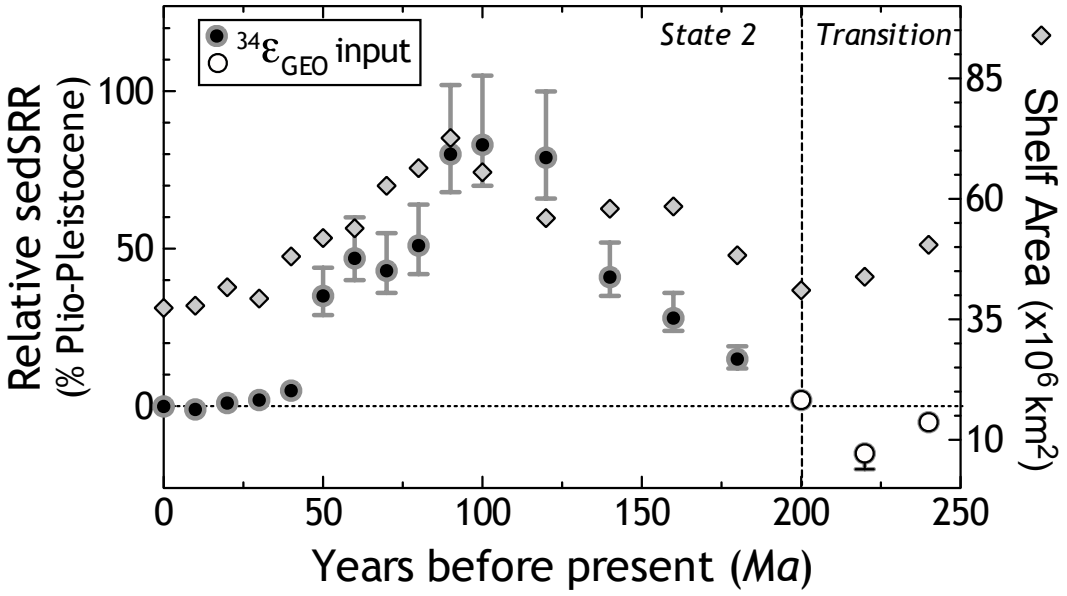

Figure 2.5. Calculated changes in sedimentary sulfate reduction rates over the Meso-Cenozoic. There is a statistically significant relationship between the calculated relative change in sulfate reduction rate and shelf area over the last 200 Ma, with a Cretaceous maximum nearly 40 to 80 times higher than the Plio-Pleistocene average. Prior to 200 Ma, rate predictions from $^{34}\varepsilon_{GEO}$ and $^{33}\lambda_{GEO}$ are not always convergent or statistically robust (Fig. 2.S4). The sedSRR calculated using the $^{33}\lambda_{GEO}$ as input is presented in (Fig. 2.S4), but should be interpreted with care given the modestly sized dataset underpinning Phanerozoic predictions (Wu et al. 2010).

Our mechanistic understanding of the S-isotope record of the last 200 Ma does not explain the $^{33}\lambda_{GEO}$–$^{34}\varepsilon_{GEO}$ relationship of the Paleozoic. When compared to the Mid-Cenozoic, the early-mid Paleozoic (540-300 Ma) records a similar variance in $^{34}\varepsilon_{GEO}$ values (~6‰ around an Era mean of ~30‰), but three times the variability in $^{33}\lambda_{GEO}$ (a continuous decrease of ~0.0008, Fig. 2.3). This results in a significant departure of the Paleozoic from the ^{33}S to ^{34}S slope-rate relationship that defines the last 200 Ma (Fig. 2.4, 2.S5). The lower overall $^{34}\varepsilon_{GEO}$ during the Paleozoic (~30‰), if paired with the lowest Paleozoic $^{33}\lambda_{GEO}$ from that same interval (Pennsylvanian; Fig. 2.S4), may indeed relate to an elevated sedSRR and greater areal extent of shallower sea floor (Fig. 2.4). However, the failure of the Paleozoic data to plot on the $^{33}\lambda_{MSR}$ vs. $^{34}\varepsilon_{MSR}$ line (Fig. 2.S5) not only undermines any confidence in applying our experimental calibration to this earlier interval, it also is consistent with the observed weak relationship between the $^{34}\varepsilon_{GEO}$ and $^{33}\lambda_{GEO}$ data to shelf area (Fig. 2.4). This suggests that the general decoupling of $^{34}\varepsilon_{GEO}$ from $^{33}\lambda_{GEO}$ within the Paleozoic is not readily attributable only to changes in sedSRR. The breakdown of the observed relationships that applied in the Meso-Cenozoic suggests that, for the Paleozoic, a conceptual model that ascribes changes in $^{34}\varepsilon_{GEO}$ and $^{33}\lambda_{GEO}$ to a codependent relationship between sedSRR and shelf area is insufficient. Because fluctuations in $^{33}\lambda_{GEO}$ for the Paleozoic are largely independent of changes in $^{34}\varepsilon_{GEO}$, there must be additional forcings.

Modeling studies illustrate how such an isotopic decoupling can be produced, either through an increase in re-oxidative fluxes and associated processes (Johnston et al. 2005), or through non-steady state behavior (Wortmann & Paytan 2012). The former may seem unlikely given lower estimated pO_2 during the first two thirds of the Paleozoic (Bergman & Lenton 2004). However, lower pO_2 also implies a sulfate reduction zone closer to the sediment–water interface, or perhaps within the water column. Under these conditions, the delivery of oxidant to the sulfate reduction zone is no longer diffusion limited, and as a result, re-oxidation reactions may be fractionally more important despite lower overall pO_2. This includes both classic sulfide oxidation (at the expense of oxygen, nitrate, manganese (IV) oxides, and iron (III) oxide-hydroxides) as well as disproportionation reactions. Both have been tentatively shown to produce a negative slope of the $^{33}\lambda_{A\text{-}B}$ vs. $^{34}\varepsilon_{A\text{-}B}$ isotope relationship (Zerkle et al. 2009; Johnston et al. 2005). The shallow slope of the Paleozoic $^{33}\lambda_{GEO}$ vs. $^{34}\varepsilon_{GEO}$ data suggests that

this opposite isotopic directionality partially is expressed and preserved (Johnston 2005). A change in the location and flux through re-oxidation reactions is also dependent on the proximity to iron (water column vs. sediment), given that pyrite formation is a terminal sink (i.e., re-oxidation inhibitor) for aqueous sulfide (Poulton & Canfield 2011). Non-steady state behavior of the Paleozoic S cycle is also possible and necessarily relates to seawater sulfate concentrations; however, current estimates suggest Paleozoic sulfate was abundant enough to circumvent such direct, first-order microbial control on fractionation (Horita et al. 2002). We therefore favor the explanation that a fundamentally different zonation of the paleo-redox boundary in the Paleozoic decoupled the controls on S-isotopes from sedimentary processes (sedSRR) and shelf area effects. Although speculative, this idea is testable using modern environments with strong redox gradients.

Equally as intriguing as the difference between the early Paleozoic and the last 200 million years is the isotopic transition captured during the Permian and Triassic (Fig. 2.3 and 2.S4). The generally weak correlations between $^{34}\varepsilon_{GEO}$ and $^{33}\lambda_{GEO}$ within the Paleozoic are followed by a 15‰ increase in average $^{34}\varepsilon_{GEO}$ and a 0.0005 increase in $^{33}\lambda_{GEO}$. This implies a major state change to the global biogeochemical S-cycle across 100 Ma spanning the Permo-Triassic boundary. Complementary geochemical metrics ($\delta^{13}C$, $\delta^{18}O$, $^{87}Sr/^{86}Sr$) also record major changes as Earth transitioned from the later Paleozoic to late Triassic (Prokoph et al. 2008). A recent statistical treatment elegantly points to the assembly and breakup of Pangaea as the explanation for this state change (Hannisdal & S. E. Peters 2011). Pangaea formed during the end Paleozoic and began to rift during the Triassic (Torsvik & Voo 2002). This, of course, relates to shelf area (HALEVY et al. 2012), but also affects primary production (OC) through the effect of continental weathering on nutrient budgets (Cárdenas & Harries 2010). Although this transition in the S cycle encapsulates the Permo-Triassic boundary, it began tens of millions of years before the P/T extinction. Such a protracted timescale for the isotopic transition (from 300 to 200 Ma) may implicate the possible cause as a change in the ratio of S to Fe from rivers (Poulton & Canfield 2011) associated with a Carboniferous increase in pO_2 (Bergman & Lenton 2004).

CONCLUSIONS

We propose that changes in sulfate reduction rates in marine sediments, rather than global pyrite burial, dictated S-isotope records over the last 200 million years. The post-Triassic geological record suggests that sedSRR increased to a mid-Cretaceous apex, and then slowed again over the last 100 Ma. (Fig. 2.5). What then controlled sedSRR? During this interval our estimates of sedSRR correlate strongly with estimates for shelf area (Fig. 2.S4b). To the degree that global shelves capture weathering fluxes and modulate nutrient delivery to primary producers, they may not only dictate the quantity and quality of organic matter reaching the zone of sulfate reduction, but they also help dictate the position of this zone with respect to the sediment-water interface. Thus, if the combination of organic carbon delivery and sedimentation rate controls sedSRR, marine sedimentary S isotope compositions may reflect a combination of Meso-Cenozoic productivity and shelf area. For this relationship to hold, i.e., to maintain the direct connection to shelf area, it requires that pO_2 be elevated in the Meso-Cenozoic relative to the early/mid-Paleozoic (Bergman & Lenton 2004), because it must relegate the locus of sulfate reduction to be (on average) below the sediment-water interface. Encouragingly, this provides a facies testable hypothesis, applicable to high-resolution datasets from Phanerozoic sections where multiple biogeochemical isotope proxies are measurable and interpretable.

The Paleozoic $^{33}\lambda_{GEO}$ versus $^{34}\varepsilon_{GEO}$ relationship requires significant contribution from processes other than changing OC delivery rates or total shelf area. As such, building a quantitative understanding of the Paleozoic sulfur cycle remains difficult. The disagreement between Paleozoic sedimentary data and our experimental calibration leaves room for other S metabolisms to contribute significantly to the observed S fractionations (biotic and abiotic sulfide oxidation, as well as disproportionation). Indeed, if a major difference between the Paleozoic and Meso-Cenozoic is the locality and magnitude of sulfide re-oxidation – the water column in the Paleozoic, vs. the sediments in the Meso-Cenozoic – then the delivery of reactive iron to the zone of sulfate reduction (HALEVY et al. 2012; Raiswell 2011) will determine whether most iron sulfides are syngenetic or diagenetic. This in turn influences the net pyrite burial flux and the balance of global oxidants. Further measurements and modeling are required to define these fluxes over both Eras. Still, we can state with

some confidence that recent multiple sulfur isotope records do not require changes in pyrite burial over the last 200 Ma. Recent sediments carry a detailed and rich repository of small-scale microbial activities, while the magnitude of overall S fractionations likely reflects global oxidant budgets working in tandem with major tectonic changes.

Ultimately it is the reduction potential trapped in pyrite and organic matter—rather than the rate of sedimentary sulfate reduction—that influences Earth's surface oxidant budget on billion year time scales. Our hypotheses suggest that pyrite burial flux (and by extension its contribution to pO_2) has not changed dramatically in recent times. Conversely, changes in pyrite burial flux remain a potentially critical control on the oxidant budget during the first half of the Phanerozoic. Continued measurements of geological materials (marine pyrites, sulfates, and terrestrial deposits), coupled with additional microbial experimentation and biogeochemical modeling, promise to yield further insight into the behavior of the sulfur cycle over Earth's history.

MATERIALS & METHODS SUMMARY

An experiment with DvH in a custom-built chemostat was run with lactate as the sole electron donor and rate-limiting nutrient for sulfate reduction. The dilution rate was varied over 43-fold ($D \propto$ mSRR), with measurements of the following biological, geochemical, and isotopic parameters on all samples (Dataset S1): temperature, pH, dilution rate, cell density, sulfide production rate (the sole detectable sulfate reduction product), acetate production rate, $^{33}\alpha$ and $^{34}\alpha$ of sulfate and sulfide and cell density. By measuring the difference between the S-isotope compositions of sulfate and sulfide, and because S-mass balance is closes with these two pools alone (i.e., no thionates detected), we may directly calculate the ${}^{3x}\alpha_{A-B}$ and ${}^{33}\lambda_{A-B}$. Specific growth rate is calculated by measuring the dilution rate and the rate of change in optical density between time-points (Dataset S1 in the original manuscript (Leavitt et al. 2013)). The non-linear regression models (based on pseudo-first order kinetics) are applied to the experimental data—$^{34}\varepsilon_{MSR}$ or $^{33}\lambda_{MSR}$ versus mSRR—allowing us to calculate theoretical $^{34}\varepsilon_{MSRmax}$ and $^{33}\lambda_{MSRmax}$, along with corresponding fitting parameters, standard errors, and $CI_{95\%}$ (Fig. 2.2). We compare between models by examining the goodness of fit from each model (Fig. 2.S3). The resultant expressions relate a measured isotopic fractionation (Eqns. S8-S9) to mSRR and the fitted kinetic constant (k) in order to extract fractionation limits (e.g., $^{34}\varepsilon_{MSRmax}$ and $^{34}\varepsilon_{MSRmin}$). Relative sedSRR are calculated with Eqns. S12-14. Phanerozoic data compilations and isotope mass-balance models are detailed in *Section 2.5*.

Multiple Sulfur Isotope Notation

Variability in ^{3x}S of a measured pool, y, is tracked through $\delta^{3x}S_y$: $\delta^{3x}S_y = \left[\left({}^{3x}S/{}^{32}S\right)_{sample}\right]/\left[\left({}^{3x}S/{}^{32}S\right)_{standard} - 1\right] \times 1000$, where x = 3, 4, or 6, and Y is a distinct S-bearing species or operationally defined pool. The difference between two pools (y = A or B, e.g., sulfate and sulfide or sedimentary sulfate and pyrite) is calculated rigorously (i.e., not a simple arithmetic difference), as must be done in studies tracking both major and minor isotope variability: ${}^{3x}\varepsilon_{A-B} = \left({}^{3x}\alpha_{A-B} - 1\right) \times 1000$, where ${}^{3x}\alpha_{A-B} = \left[\left({}^{3x}S/{}^{32}S\right)_A/\left({}^{3x}S/{}^{32}S\right)_B\right]$. Variability in ^{33}S is tracked through

$^{33}\lambda$: $^{33}\lambda_{A-B} = [\ln\left(1+\frac{\delta^{33}S_A}{1000}\right) - \ln\left(1+\frac{\delta^{33}S_B}{1000}\right)]/[\ln\left(1+\frac{\delta^{34}S_A}{1000}\right) - \ln\left(1+\frac{\delta^{34}S_B}{1000}\right)]$. Qualitatively, $^{33}\lambda$ describes the slope of a line connecting to points on a $\delta^{33}S$ vs. $\delta^{34}S$ plot.

DETAILED MATERIALS AND METHODS

Microbial sulfate reduction (MSR) is the principle mechanism to partition sulfur isotopes between oxidized and reduced reservoirs, and subsequently between mineral phases within geological reservoirs (Canfield 2001a; THODE et al. 1961; Kaplan & Rittenberg 1964). Further, the degree to which sulfur isotopes are segregated between sedimentary sulfates and sulfides is used to track changes in Earth's surface redox state (R. A. Berner & Canfield 1989; Canfield 2004b). These models are predicated upon our understanding of prokaryotic dissimilatory sulfate reduction – encompassing all Bacteria and Archaea that perform this metabolism (Canfield & Raiswell 1999) – and the physicochemical controls on the associated sulfur isotope fractionation (Bradley et al. 2011). Previous work has demonstrated that the magnitude to which sulfate reduction partitions isotopes between sulfate and sulfide is a function of physiology, which in turn is a reflection of environment (Harrison & Thode 1958; Kaplan 1975; Kaplan et al. 1963; Lyn A Chambers et al. 1975; Habicht et al. 2005; HOEK et al. 2006; Canfield 2001b; Canfield et al. 2006; Johnston et al. 2007; Sim, Ono, et al. 2011c). Coupling quantitative measures of the cardinal geochemical environmental parameters (i.e. E_h, pH, temperature) to the physiological state of MSR and isotope fractionation is the ultimate calibration required for full interpretation of the geological record. From previous and on-going work it appears that there are four major environmental parameters that control the observable MSR isotope fractionation. These are:

(i) electron donor (organic carbon or H_2) delivery and/or availability to MSR when oxidant (sulfate) is non-limiting (this study; (Lyn A Chambers et al. 1975; Sim, Ono, et al. 2011c))

(ii) sulfate availability, when reductant is non-limiting,

(iii) co-limitation, such as of sulfate and reductant (Habicht et al. 2002; Habicht et al. 2005), and

(iv) oxidative stress (Mangalo et al. 2008; Einsiedl 2009).

In this work we explicitly test the effect of electron donor availability on the magnitude of MSR sulfur isotope fractionation (parameter *i*). For Phanerozoic and likely Proterozoic studies, targeting electron donor limitation is postulated to be the primary variable controlling MSR (Habicht et al. 2002; Horita et al. 2002). We conducted experiments in a continuous gas and liquid-flow chemostat under both steady and non-steady state delivery regimes (Laws et al. 1995), greatly expanding the range of growth rates previously assayed (Lyn A Chambers et al. 1975; Sim, Ono, et al. 2011c). We also extend previous treatments through quantifying these responses in $^{33}\lambda_{MSR}$. In a chemostat, growth rate is directly proportional to the turnover time of the reactor volume (dilution rate: *D*, in volume per time per reactor volume, such that reported units are: $time^{-1}$), assuming the limiting constituent is introduced in the aqueous phase, as is the case in this study. For our experiments, organic carbon flux (in the form of lactate) tracked the liquid flux, pinning the specific growth rate and microbial sulfate reduction rate (mSRR) to *D*. Relating *D* and mSRR to fractionation is not new to our study (Lyn A Chambers et al. 1975); however, we expand the range of *D* and mSRR tested. This provides added perspective on the rate vs. fractionation relationship. We adopted this approach to understanding MSR effects from classic experiments aimed at characterizing the kinetic isotope effect associated with carbon fixation (Laws et al. 1995; Hayes et al. 1999). Inspired by such works, we move forward with an open-system experimental design to investigate the biologically catalyzed carbon remineralization pathway of sulfate reduction and its associate kinetic isotope effects.

Culture medium and batch (closed system) conditions

Batch cultivation of *Dv*H was performed with a modified freshwater MSR medium (*23*), designated KA-medium and composed as follows: $NaC_3H_5O_3$ 60% *w/w* syrup, 0.4375 or 4.375 mL^{-1} (2.8 or 28 mM, respectively); KH_2PO_4, 0.5 g L^{-1} (3.67 mM); NH_4Cl, 1.0 g L^{-1} (18.35 mM); $CaCl_2$, 0.06 g L^{-1} (0.41 mM); $MgSO_4*7H_2O$, 2.0 g L^{-1} (8.12 mM); Na_2SO_4, 2.825 g L^{-1} (19.89 mM), and $NaHCO_3$, 1.5 g $liter^{-1}$ (17.86 mM); trace element, vitamin, and amino acid solutions were provided for standard freshwater MSR media (Rabus et al. 2006). The final sulfate concentration was always 28mM, while was lactate the sole electron donor provided at either 2.8 or 28 mM. Deoxygenated and autoclaved or filter sterilized (0.22μm sterile syringe filters) media

components were combined aseptically and anoxically under O_2 free N_2:CO_2 (90:10), and titrated to a final pH of 7.00±0.02 with deoxygenated sterile HCl or NaOH. *Dv*H was regularly transferred into 100mL of fresh 25°C medium in 160mL serum bottles at 1% dilutions. Growth rate was determined by optical density readings (OD_{600}; Genesys 10S UV-Vis, Thermo Scientific) calibrated to microscopic cell counts, performed on an Olympus BX60 fluorescence microscope, at 400x magnification on DAPI stained cells, previously fixed in 2% glutaraldehyde.

Chemostat (open-system) setup, operation, sampling, and calculations

Open system experiments were performed in a chemostat ('chemical environment in static'; Fig. 2.S1). Critically, all surfaces in contact with sulfide (gas or liquid) were glass, PEEK ('polyether ether ketone'), or PTFE ('polytetrafluoroethylene') to avoid re-oxidation of the biogenic sulfide. Prior to all chemostat runs the reactor vessel (6-port 3L working volume vessel, BellcoGlass, part no. 1964-06660) is filled with 1.5 liters of KA medium, containing 28 mM of both lactate and sulfate. The medium is then autoclave-sterilized, degassed with high purity O_2-free N_2:CO_2 (90:10), and titrated to pH 7.0±0.02 via the pH-probe activated titration pump (Etatron, DLX pH-RX/MBB metering pump)—dosing in either 1M HCl or 1M NaOH, both previously degassed with N_2 and autoclave sterilized. Following these preparations, the vessel is inoculated with 100mL of a mid-exponential *Dv*H culture, cultivated in batch as above, previously transferred >7 times (>50 generations) to ensure adaptation to the minimal medium. The organism-specific growth rate (based on OD_{600} measurements and cell counts with time) was determined in batch prior to inoculation of the vessel so that appropriate flow rates can be calculated. That is, the organism's maximum specific growth-rate (μ_{max}; (Herbert et al. 1956)) estimated from batch work is a critical value to know in advance of chemostat inoculation, as the dilution rate (D) must be less than or equal to μ_{max} in order to avoid a washout of the biomass (Herbert et al. 1956). For our preparation, the inoculated reactor is allowed to grow under gas flux only (i.e. as a closed system to liquid flux, but open to gas flux) for 5.5 days to an initial operating cell density (OD_{600}=0.383), equivalent to late log-phase on the same media in batch. At this point, inflow and outflow pumps (Ismatec 4-channel Reglo analog peristaltic pump with Tygon HC F-4040-A tubing, minimum flow rates are achieved by using tubing of different internal diameter's: 0.25mm, 0.51mm, and

0.64mm) were activated at the high flow-rate and high lactate concentration condition (*Dataset S1*). After 9 days, the influent media was changed to an identical matrix of KA medium, but 2.8mM lactate instead of 28mM (previous run). Three further media bottle changes were performed at 18, 26, and 51 days respectively, but no further changes to influent lactate or sulfate concentrations were made for the remainder of the experiment. The influent-effluent rate was slowed from the 'fast' condition to the 'slower' condition at 29 day, diminished further from 'slower' to 'slowest' at 45 days, but finally reinvigorated to the 'fast' flow rate at 58 days. The experiment was terminated after 62 days. Specific values for all conditions are available in *Dataset S1*.

Over the course of the chemostat run we sampled the gas (G), liquid effluent (L), and reactor solution proper (R) to quantify all sulfur and carbon species during each sampling interval, and to measure the major and minor isotope compositions of all S-species (see *Analytical Procedures* below and *Dataset S1*). Steady state is defined when OD_{600} and cell density remained constant between consecutive samplings (*Dataset S1*). This means that the population is growing and metabolizing at a constant rate. Further investigation might consider quantifying protein concentrations and instantaneous sulfate reduction rates in sub-samples of the reactor volume (c.f. (Jørgensen 1978)). Microbe-specific sulfate reduction rate (mSRR), turnover time, and fractionation relationships for all turnover times are visualized in Fig. 2.S2. Clear and coherent relationships emerge between the fast, slower, and slowest flow rate conditions in metrics of SRR (mSRR and csSRR) and fractionation ($^{34}\varepsilon_{MSR}$ and $^{33}\lambda_{MSR}$), presented in Fig.'s 2.1 to 2.2 and 2.S2.

G, L, and R samples were preserved at each time point, along with 1mL samples for cell counts and optical density readings. Gas samples were collected over the course of a sampling interval by bubbling N_2:CO_2 (90:10) through two traps in series containing zinc acetate (20% w/v) buffered with glacial acetic acid (60mL L^{-1}) to pH 4.5. The pH homeostasis of the zinc acetate capture solution is critical to ensuring no sulfur isotope fractionation occurs upon continuous sample collection. Prior to initiating the chemostat experiment we determined that the pH of un-buffered 20% zinc acetate trapping solution becomes acidic within 12 hours of sulfide flux under the high lactate:sulfate condition, resulting in incomplete sulfide capture. As such, the zinc acetate was always buffered at a pH >4.25 with acetic acid, and was monitored daily by checking the zinc trap with

a calibrated pH probe (Mettler-Toledo, 405-DPAP-SC-K8S/325mm).

The theory behind chemostat operation as related to pseudo-first order biochemical kinetics in a continuous culture (*i.e.,* partial Monod kinetics) is reviewed in detail elsewhere (Herbert et al. 1956). The dilution rate (D) of the chemostat reactor volume is calculated as:

$$D = \frac{liquid\ flux}{reactor\ liquid\ volume} = \frac{liters/day}{liter} = \frac{1}{day} \qquad (S1)$$

To compare our experimental cell-specific sulfate reduction rates (csSRR), we calibrated the OD_{600} to cell number via cell counts, and derive the following relationship for csSRR in an open system (for csSRR in a closed system see (Detmers et al. 2001)):

$$csSRR = \frac{mol\ sulfide\ produced}{(\#cells/volume)\times(reactor\ volume)\times(collection\ interval)}$$

$$= \frac{mol\ sulfide}{(\#\ of\ cells)\times day} \qquad (S2)$$

For comparison to previously published closed-system datasets (Kaplan & Rittenberg 1964; Habicht et al. 2005; Canfield 2001b; Detmers et al. 2001), we convert to *f*mols per cell per day. In all experiments, mass balance is closed such that sulfate flux values may be substituted into the above equation. Finally, for non-linear regression calculations it is critical to minimize error in the independent-variable (x-axis (Motulsky & Ransnas 1987)). Therefore, we calculate the microbial sulfate reduction rates (mSRR), taking advantage of the minimal variance in replicate OD_{600} measurements over different flux-states (i.e. flow rates, equivalent to differential D):

$$mSRR = \frac{mol\ sulfide\ produced}{\left(\frac{OD_{600}}{reactor\ volume}\right)\times(collection\ interval)\times(collection\ volume)}$$

$$= \frac{mol\ sulfide}{OD_{600}\times day} \qquad (S3)$$

Thus, the mSRR is offset from csSRR values by the OD_{600} to cell count calibration. Implicit to our use of OD_{600} measurements in place of cell counts is the reasonable assumption that the integrated variance in cell volume is

significantly less than error associated with all the steps in preservation, staining, and microscopic counting of individual cells. In future work it will be important to normalize biomass-specific geochemical fluxes to a more universal metric, such as protein concentrations (or rRNA copy number). Protein-normalized rates will be more directly comparable to sediment and natural system SRR, where protein concentrations are readily quantifiable where accurate cell counts are difficult (e.g., sediments, mineral surfaces, biofilms).

Analytical procedures

Sulfate, lactate, and acetate concentrations in fresh and spent used medium from both R and L samples were determined on (0.45μm) filtered sampled by suppressed anion chromatography with conductivity detection (Dionex ICS-2000, AS11 column). An eluent gradient method was employed: running first 1mM KOH isocratically for 6 minutes, followed by a linear ramp to 30mM KOH over 8 minutes, then a linear ramp to 60mM KOH over 4 minutes, followed by 5 minutes re-equilibration at 1mM KOH between samples (duplicate analysis S.D. ±5%; detection limit 1μM). Sulfide concentrations were measured by the methylene blue method (Cline 1969) modified to work on 96-well plates, with OD_{670} readings taken at the Harvard University Center for Systems Biology (UV-Vis Spectramax Plus 384 plate reader, Molecular Devices, Sunnyvale, CA) (8-replicate S.D. ±2-7%; detection limit 5μM). We also measure thiosulfate ($S_2O_3^{2-}$) and trithionate ($S_3O_6^{2-}$) on reactor (R) and effluent (L) samples by cyanolysis (Don P Kelly & Wood 1994; Sörbo 1957). Here, all samples were below a detection limit of 50μM.

Sulfate (L & R) or product sulfide (G+L+R) samples were first prepared for major isotope analysis ($\delta^{34}S$) as $BaSO_4$ or Ag_2S, respectively (Johnston 2005). All samples for sulfur isotope analysis (as SF_6 or SO/SO_2) were first treated as such: gas samples (*G*) collected as ZnS were treated with excess $AgNO_3$ to generate Ag_2S and incubated overnight in the dark followed by centrifugation to concentrate the precipitate along with wash, re-suspension by vortex, and re-concentration steps performed in the following order (35-40mL of each): 1M CH_3COOH 2x, DI water 3x, 1M NH_4OH 1x, water 2x, and dried at 50°C prior to weighing for fluorination. Reactor (*R*) and liquid (*L*) sulfate samples were quantitatively reduced to Ag_2S by the method of Thode

(THODE et al. 1961; Forrest & Newman 1977), and washed with NH_4OH and water as above. Samples were converted to SO_2 by combustion at 1040°C in the presence of excess V_2O_5 (Elemental Analyzer, Costech ECS 4010) and analyzed by continuous flow isotope ratio mass spectrometry (1σ of ±0.3‰; Thermo-Finnegan DELTA V Plus). All samples as Ag_2S were fluorinated under 10X excess F_2 to produce SF_6, which is then purified cryogenically (distilled at -107°C) and chromatographically (on a 6' molecular sieve 5Å inline with a 6' HayeSep Q 1/8"-stainless steel column, detected by TCD). Purified SF_6 was measured as SF_5^+ (m/z of 127, 128, 129, and 131) on a Thermo Scientific MAT 253 (1σ: $\delta^{34}S$ ±0.2, $\Delta^{33}S$ ±0.006‰, $\Delta^{36}S$ ±0.15‰). All isotope ratios are reported in parts per thousand (‰) as experimentally paired sulfates and sulfides measured. Long-term running averages and standard deviations for IAEA standards: S1, S2, S3 for sulfides, or NBS-127, SO5, SO6 for sulfates. Isotope calculations and notation are detailed below. Isotope ratios are presented as paired sulfate-sulfide measurements.

Isotope ratio and fractionation calculations

Sulfur has four stable isotopes: ^{33}S, ^{34}S, ^{36}S, and ^{32}S in relative abundance 0.76%, 4.29%, 0.02%, and 94.93%, respectively (Coplen et al. 2002). Isotope ratios ($^{3x}R = {}^{3x}r/{}^{32}r = [({}^{3x}S/{}^{32}S)_A/({}^{3x}S/{}^{32}S)_B]$) are used to determine the fractionation factor (α) between two pools (A and B; x = 3, 4, or 6, & y = 3 or 6:

$$ {}^{3x}\alpha_{A-B} = \left[\left({}^{3x}S/{}^{32}S\right)_A/\left({}^{3x}S/{}^{32}S\right)_B\right] \qquad (S4.1) $$

$$ {}^{3x}\varepsilon_{A-B} = \left({}^{3x}\alpha - 1\right)\times 1000 \qquad (S4.2) $$

$$ \delta^{3x}S_A = \left[\left({}^{3x}S/{}^{32}S\right)_{sample}\right]/\left[\left({}^{3x}S/{}^{32}S\right)_{standard} - 1\right]\times 1000 \qquad (S5) $$

$$ \Delta^{3y}S = \delta^{3y}S - 1000\times\left[\left(1 + {}^{\delta^{34}S}/_{1000}\right)^{0.515} - 1\right] \qquad (S6) $$

where 0.515 defines the mass-dependent relationship and is assigned a value of 0.515 for y = 3. Last, in determining the isotopic fractionation associated with a specific process—even if that process is constituted by a number of steps—lambda is defined, differing from that used above in the definition of $\Delta^{3x}S$.

$$^{33}\lambda_{A-B} = \left[ln\left(1+\frac{\delta^{33}S_A}{1000}\right) - ln\left(1+\frac{\delta^{33}S_B}{1000}\right)\right] / \left[ln\left(1+\frac{\delta^{34}S_A}{1000}\right) - ln\left(1+\frac{\delta^{34}S_B}{1000}\right)\right] \qquad (S7)$$

This definition is specific for a pair of samples (e.g. sulfate sulfide), but may also be applied through a field of data defined by a common mechanism or process. Qualitatively, $^{33}\lambda$ describes the slope of a line connecting data on a plot of $\delta^{33}S$ vs. $\delta^{34}S$. All fractionations presented in the main text and used as input in deriving the fractionation limit and rate calculations are between the G and L pools. The L and R were almost always identical in $\delta^{34}S$ value, except during significantly non-steady state conditions in the flow through system.

Calculating empirical fractionation limits for DvH

To determine the empirical limits of *Dv*H S-isotope fractionation we applied multiple non-linear regression models to our experimental data and calculate the *first ever organism-specific maximum and minimum fractionations factors* for both major and minor S-isotope metrics (i.e., $^{34}\varepsilon_{MSRmax}$, $^{34}\varepsilon_{MSRmin}$, $^{33}\lambda_{MSRmax}$, and $^{33}\lambda_{MSRmin}$). The best-fit model of those tested (Fig. 2.S3) is a simple one-phase decay model (Eqn. S8-S11). Another rigorously examined model is based on the partial-Monod equation, and uses the inverse of our rate measure ($mSRR^{-1}$). In both models the fitted rate constant is first order with respect to a single reactant—organic carbon (herein, lactate). This assumption is valid in our system because the chemostat grown culture of *Dv*H was limited with respect to electron donor while sulfate was always present in excess. The measured sulfate reduction rates used in these calculations is parameterized as the mSRR (moles of sulfide produced per day per unit biomass), where this biomass normalized metric of sulfide flux (mSRR or csSRR) is a direct measure of the biomass specific sulfate reduction rate, constrained by a specific dilution rate (D, $days^{-1}$):

$$mSRR = \frac{ln\left(\frac{^{34}\varepsilon_{MSRobs} - {}^{34}\varepsilon_{MSRmin}}{^{34}\varepsilon_{MSRmax} - {}^{34}\varepsilon_{MSRmin}}\right)}{-k_{\varepsilon_{MSR}}} \quad (S8)$$

$$mSRR = \frac{ln\left(\frac{^{33}\lambda_{MSRobs} - {}^{33}\lambda_{MSRmin}}{^{33}\lambda_{MSRmax} - {}^{33}\lambda_{MSRmin}}\right)}{-k_{\lambda_{MSR}}} \quad (S9)$$

$$mSRR^{-1} = \frac{k'_{\varepsilon_{MSR}}}{\left(^{34}\varepsilon_{MSRmax}/{}^{34}\varepsilon_{MSRobs}\right) - 1} \quad (S10)$$

$$mSRR^{-1} = \frac{k'_{\lambda_{MSR}}}{(^{33}\lambda_{MSRmax}/\ \ {}^{33}\lambda_{MSRobs}) - 1} \quad (S11)$$

Data inputs are the measured (observed) $^{34}\varepsilon_{MSRobs}$ or $^{33}\lambda_{MSRobs}$ for a given dilution rate (D) and the corresponding mSRR. Fitting parameters are as follows: k, a pseudo-first order rate constant specific to each non-linear regression (k_ε, k_λ, k'_ε, and k'_λ); $^{34}\varepsilon_{MSRmax}$ (or $^{33}\lambda_{MSRmax}$), the theoretical maximum fractionation as $mSRR^{-1}$ approaches infinity (which physically corresponds to a D approaching zero), and in the case of the one-phase decay model (Eqn. S8-S9) the $^{34}\varepsilon_{MSRmin}$ (or $^{33}\lambda_{MSRmin}$) corresponds to classically defined 'plateau', where the minimum value corresponds to the rate-limiting step in sulfate reduction when our organism (*D*vH) is growing and metabolizing at its μ_{max}. Here mSRR is also normalized to OD_{600} to account for minor variance due to differences in cell density (i.e., biomass yield will vary as a function of D and electron donor:acceptor ratio). Cell densities (OD_{600}) were used as a normalization factor rather than cell counts due to the lower-order variance in the OD_{600} measurements, as it is critical to minimize error in the x-value inputs to non-linear regression models (Motulsky & Ransnas 1987). Results of the main two model fits and standard error estimates, fitting parameters and their standard errors, and the 95% confidence intervals (dashed lines) are presented in Fig. 2.S3. The one-phase decay model makes no assumptions about mechanism, whereas the partial Monod has some mechanistic underpinning to an pseudo-first order enzymatic system, as we might predict is broadly the case in our chemostat.

Phanerozoic compilation and modeling analyses

Sedimentary sulfur isotope compilations stem from table A1 in (Wu et al. 2010) and are binned and recalculated in Table S2. Shelf area estimates are from (HALEVY et al. 2012). Data from (Wu et al. 2010) was first averaged over the time bin of interest. The $\delta^{33}S$ was then calculated from the $\Delta^{33}S$ provided, which then serves as an input in the ensuing calculation of $^{33}\lambda$ (Eqn. S7). From this compilation, isotope mass balance allows for the calculation of the classic metric of pyrite burial: f_{py} (Canfield 2004b). Using this definition, we provide a sensitivity test in the text to better understand what change in f_{py} would accompany an 8‰ change in the range of fractionation observed between sulfate and sulfide (e in the f_{py} equation).

Estimates of absolute Phanerozoic sedSRR rates are calculated by inputting geological isotope data from Table S2 (time binned averages) into equations S8 and S9. Importantly, the fitting parameters derived from the empirical (chemostat) calibration were incorporated in this exercise. To estimate a standard error range in given our calibration output from the non-linear models (Eqn. S8 and S9), we recalculate the sedSRR's using the same geological inputs (Table S2), but utilize the maximum, median, or minimum standard error estimates for each fitting parameter (these standard error values are presented in Fig. 2.3 as the inset text; these differ from the dashed lines in Fig. 2.S3 are 95% CI). These yield the most conservative estimates in both directions on our scale. While the Phanerozoic sedSRR calculated from $^{34}\varepsilon_{GEO}$ or $^{33}\lambda_{GEO}$ time bin inputs (along with fitted constants: $mSRR_{MSRmax}$, $mSRR_{MSRmin}$, and k from either $^{34}\varepsilon_{MSR}$ or $^{33}\lambda_{MSR}$ non-linear regression, Eqn. S12 or S13, respectively) vary in their absolute magnitude (from Eqn. S8 and S9 versus shelf area), and we assume mSRR relate to sedSRR by a scalar of biomass per unit sediment—a values we do not need to know when comparing relative sedSRR—the *relative* change over the Meso-Cenozoic scales consistently (converted using Eqn. S12 relative to Plio-Plisotocene estimates of sedSRR), and correlates strongly with shelf area (Fig. 2.4 and 2.S4). This relationship is weak in the Paleozoic, and we present the entire Phanerozoic sedSRR predictions in Fig. 2.S4c to simply highlight the disagreement in sedSRR estimates from major and minor isotope inputs. Interestingly, the sedSRR disagree most strongly when poorly correlated with shelf area (Fig. 2.S4). We do not further interpret calculated sedSRR

prior to 200 Ma. This supports our hypothesis that changes in microbial sulfate reduction rates scale with sedimentary sulfate reductions rates, and where both scale with shelf area.

$$sedSRR = \frac{ln\left(\frac{^{34}\varepsilon_{\mathrm{GEO}} - {}^{34}\varepsilon_{\mathrm{MSRmin}}}{^{34}\varepsilon_{\mathrm{MSRmax}} - {}^{34}\varepsilon_{\mathrm{MSRmin}}}\right)}{-k_{\varepsilon_{MSR}}} \quad (S12)$$

$$sedSRR = \frac{ln\left(\frac{^{33}\lambda_{GEO} - {}^{33}\lambda_{MSRmin}}{^{33}\lambda_{MSRmax} - {}^{33}\lambda_{MSRmin}}\right)}{-k_{\lambda_{MSR}}} \quad (S13)$$

Time bin ('geo bin n') sedSRR calculated from geological isotope data (Table S2), relative to Plio-Pleistocene.

$$\%\ sedSRR\ (rel.to\ Plio-Pleistocene) = \left(\frac{mSRR_{geo\ bin\ n}}{mSRR_{Plio-Pleistocene\ bin}} - 1\right) \times 10^2. \ (S14).$$

Detailed Materials and Methods Figures

Table 2.S1. We employ various definitions of reduction rates that all have small, but critical differences. The acronyms and their definitions (and units) are listed below.

Acronym	*Definition*	*Units*	*Notes*
MSR	microbial sulfate reducer	n/a	Used in reference to all Bacterial and Archeal sulfate reducers, in lieu of the more restrictive BSR (Bacterial sulfate reducers
mSRR	microbial sulfate reduction rate	mol S per OD_{600} per day	The specific rate of sulfate reduction accounting for biomass (here optical density), liquid flux, and time. This is similar to csSRR.
csSRR (appears in SI only)	cell specific sulfate reduction rate	mol S per cell per day	Same as mSRR only normalized to cell numbers rather than OD. The calibration of cell density carries a large error, and as such, the error in this measure is much larger than in mSRR.
sedSRR	sedimentary sulfate reduction rate	mol S per cm^2 per year	The literal rate at which sulfate is being reduced at the pore-water scale within a sediment package. This metric differs from mSRR (and csSRR) in that it lacks a biomass normalization (e.g cell#, protein content, mRNA copy# of MSR).
gSRR	global sulfate reduction rate	mol S per year	The rate of sulfate reduced integrated at the global scale. This is independent from the actual rate of reduction in sediments, or the spatial area over which that reduction is occurring. This would relate to classic measures of pyrite burial through a re-oxidation coefficient.

Table 2.S2. Phanerozoic multiple S isotope records. The Phanerozoic multiple S-isotope compilation and calculations, derived from (Wu et al. 2010), but re-binned herein, with calculations of $\Delta^{33}S_{GEO}$ and $^{33}\lambda_{GEO}$ changed to Eqn. S6 and S7, respectively. Shelf area estimates from (HALEVY et al. 2012).

Age bin (Ma)	Shelf area ($x10^6$ km^2)	$\delta^{34}S_{sulfate}$ (‰)	$\delta^{34}S_{pyrite}$ (‰)	$D^{33}S_{sulfate}$ (‰)	$D^{33}S_{pyrite}$ (‰)	$^{34}\varepsilon_{GEO}$ (‰)	$^{33}\lambda_{GEO}$ (n.a.)
0	37.41	21.85	-24.00	0.042	0.098	45.85	0.513743
10	37.84	22.03	-23.93	0.042	0.098	45.97	0.513739
20	41.67	21.90	-23.87	0.042	0.099	45.77	0.513719
30	39.35	21.87	-23.77	0.042	0.099	45.63	0.513715
40	48.11	21.70	-23.67	0.042	0.099	45.37	0.513708
50	51.90	19.33	-23.57	0.042	0.099	42.90	0.513636
60	53.91	18.43	-23.47	0.042	0.099	41.90	0.513613
70	62.76	18.83	-23.37	0.042	0.098	42.20	0.513638
80	66.44	18.50	-23.13	0.042	0.098	41.63	0.513620
90	72.66	18.35	-21.10	0.042	0.098	39.45	0.513554
100	65.60	16.88	-22.40	0.042	0.098	39.28	0.513540
120	56.04	16.44	-23.12	0.042	0.099	39.56	0.513525
140	58.03	17.00	-25.36	0.042	0.100	42.36	0.513602
160	58.44	17.06	-26.36	0.042	0.099	43.42	0.513659
180	48.34	17.56	-27.00	0.041	0.098	44.56	0.513688
200	41.04	17.94	-27.74	0.035	0.096	45.68	0.513625
220	43.84	19.34	-27.94	0.029	0.093	47.28	0.513609
240	50.52	20.08	-26.24	0.025	0.089	46.32	0.513582
260	68.06	16.52	-24.84	0.020	0.084	41.36	0.513410
280	67.65	13.38	-22.86	0.015	0.078	36.24	0.513242
300	66.43	13.50	-18.56	0.012	0.071	32.06	0.513153
320	63.72	14.62	-15.22	0.010	0.066	29.84	0.513111
340	70.18	15.74	-13.08	0.008	0.061	28.82	0.513135
360	88.08	19.06	-10.22	0.006	0.057	29.28	0.513225
380	89.27	20.90	-8.92	0.004	0.054	29.82	0.513297
400	77.76	21.84	-7.38	0.002	0.051	29.22	0.513304
420	89.79	26.04	-5.60	0.000	0.048	31.64	0.513444
440	73.80	27.06	-4.76	-0.003	0.045	31.82	0.513479
460	73.32	25.90	-2.52	-0.005	0.040	28.42	0.513399
480	76.29	30.48	0.72	-0.007	0.034	29.76	0.513619
500	74.69	35.30	4.08	-0.009	0.030	31.22	0.513714
520	69.89	33.36	3.76	-0.010	0.029	29.60	0.513680
540	66.39	30.18	4.25	-0.007	0.026	25.93	0.513727

Figure 2.S1 (following page). Anoxic Chemostat, The main reaction chamber is a 3-liter short glass vessel with 1x140mm and 6x45mm diameter ports, where the 45mm ports housed the following: (i) liquid in/out flow from the media reservoir and out to the 5% zinc chloride (at initiation) containing liquid trap; (ii) in/out flow of the pre-reduced and hydrated N_2:CO_2 (90:10), plumbed into the media reservoir, then into reaction chamber, and finally out into the primary and secondary 20% zinc acetate trapping solution—trapping solutions are changes upon sampling; (iii) a dedicated port houses the pH probe, which controls the titrant delivery pump (input through port (iv)), set to deliver 1M HCl upon pH rise as H_2S is swept out, thus maintaining a pH of 7.00+/- 0.02. Ports (v-vi) were primarily unused during this experiment, but are available for a custom built liquid level controller that controls a second peristaltic pump, which will remove liquid to counter balance additional liquid over the desired volume, as introduced by the pH titrant pump; if a second delivery solution is desired, or if non constant out-flow/in-flow is desired. Through port (iv) one of the four sub-ports is dedicated to a static sampling valve, which is sealed by a PEEK ¼-28 ball valve when not in use. All continuous liquid (L) and gas (G) samples have a matching reactor (R) sample collected at the end of each sampling interval. (R samples were taken for OD_{600}, sulfate, sulfide, lactate and acetate concentration measurements, and major isotope measurements (on both sulfate and sulfide).

Figure 2.S1 (continued).

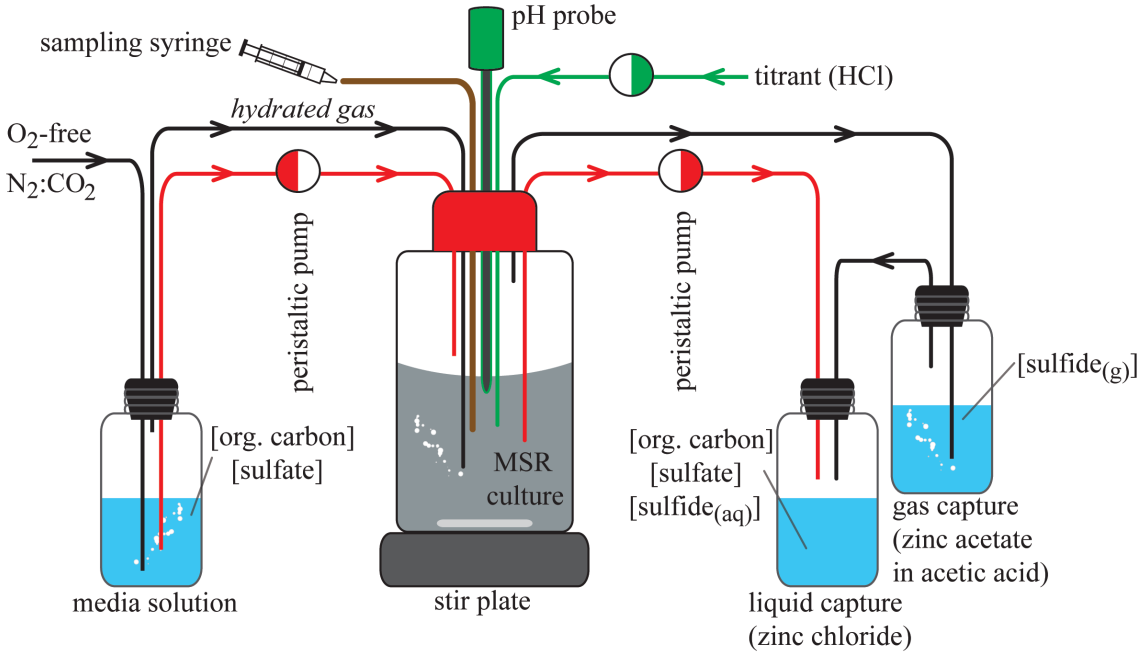

Figure 2.S3 (on the following page). Chemostat data. All dilution rate (*D*), mSRR, csSRR, $^{34}\varepsilon_{MSR}$ and $^{33}\lambda_{MSR}$ data from the *Dv*H chemostat experiments, including steady state and transition conditions (changes to the influent electron donor concentration or liquid flux). The values in A are equivalent to B, plotted on log or linear x-axes, respectively; this holds for panels C and D. Interestingly, the different electron donor flux where *D* is the same (i.e., 28mM versus 2.8mM input lactate at the highest dilution rate) yields a slightly different baseline in $^{34}\varepsilon_{MSR}$ or $^{33}\lambda_{MSR}$ (panels E & F). The data in panels E and F are all major and minor isotope measures from chemostat experiments with axenic cultures.

Figure 2.S2. (continued)

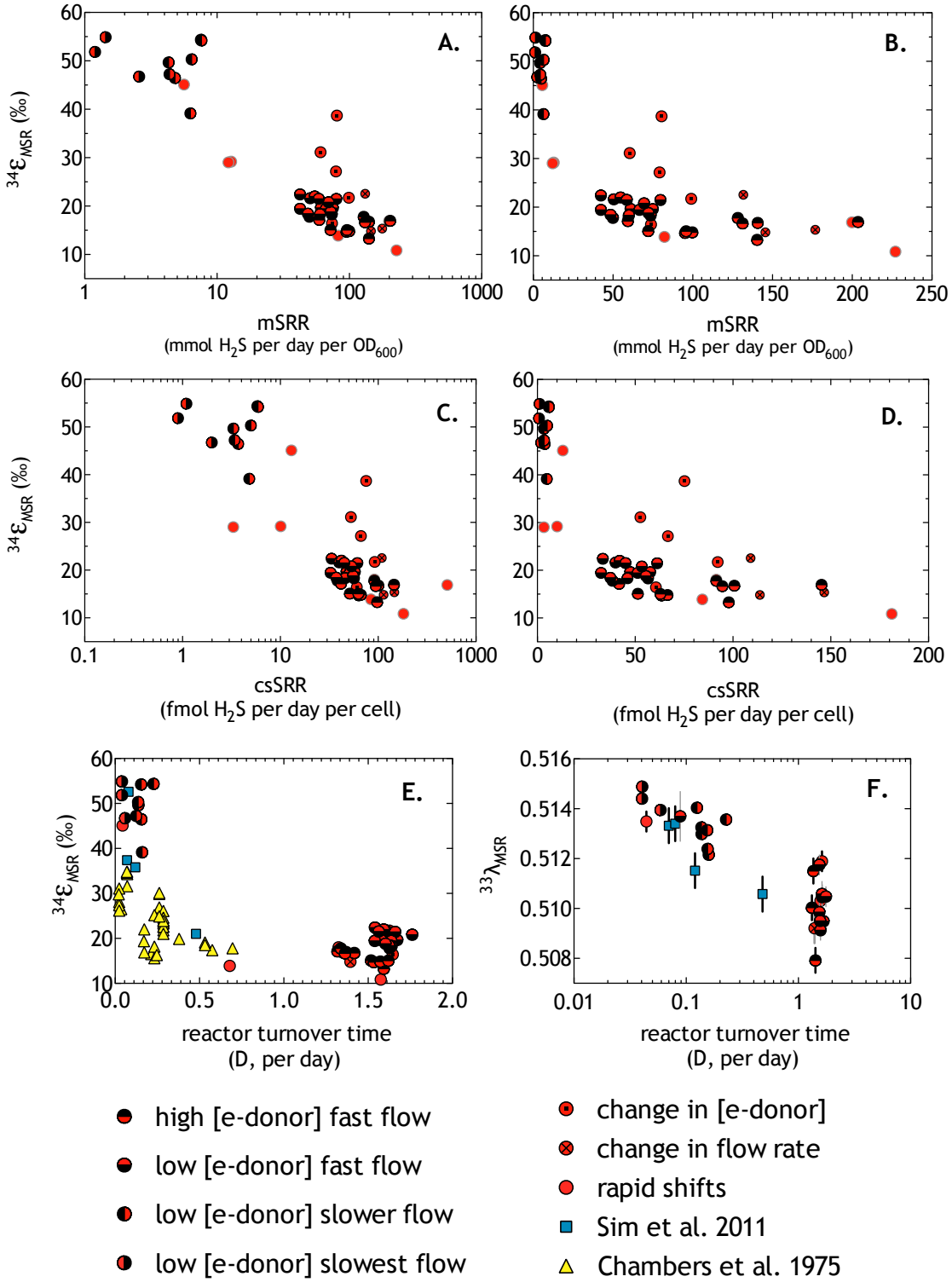

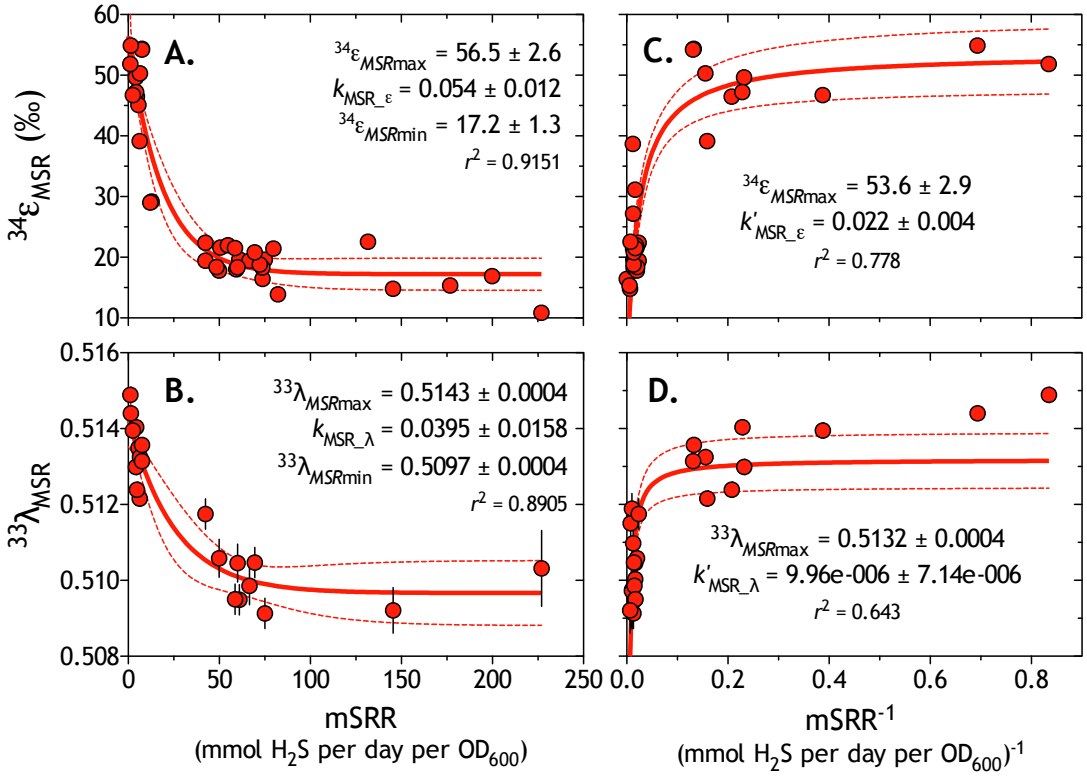

Figure 2.S3. Non-linear regression model fits to chemostat major and minor isotope measurements. In all panels, paired sulfate-sulfide major ($^{34}\varepsilon_{MSR}$) or minor ($^{33}\lambda_{MSR}$) observed fractionation factors are plotted against the mSRR, with the non-linear regression fit (thick line), 95% confidence intervals (dashed lines), and fitting parameters with standard error estimates (r^2 = coefficient of determination). All data are from only the 2.8:28mM lactate:sulfate conditions. Panels A and B are the one-phase decay model fits (Eqn. S8-S9), C and D are the modified partial-Monod model fits (Eqn. S10-S11). Both models allow for the calculation of empirical fractionation limits in $^{34}\varepsilon_{MSR}$ and $^{33}\lambda_{MSR}$, and both provide similar estimates of $^{34}\varepsilon_{MSRmax}$ and $^{33}\lambda_{MSRmax}$. The one-phase decay model, however, (A and B) yield better fits in both measures of fractionation (*see* r^2 in A vs. C, B vs. D).

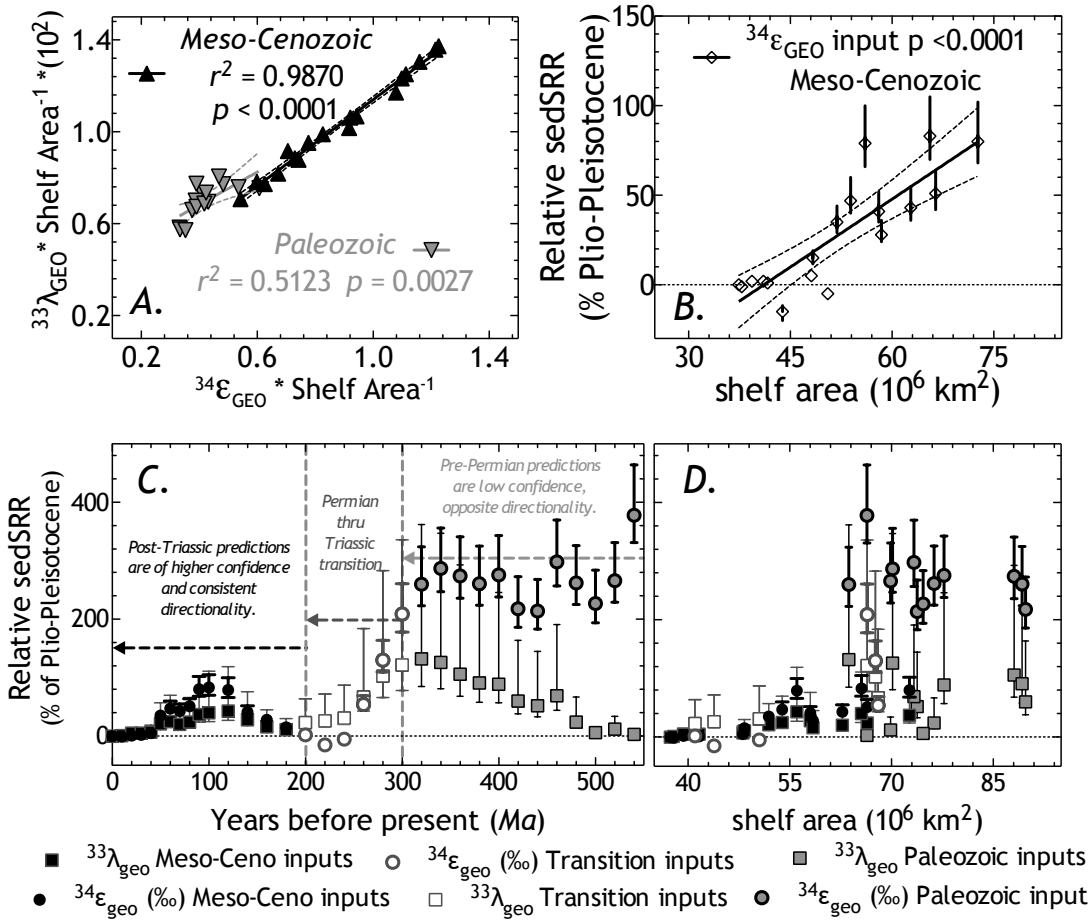

Figure 2.S4. Shelf area and relative change (%) in mSRR predicted from isotopic record inputs. (A) Comparison of the geological isotope records normalized to shelf area demonstrates a strong correlation of isotope records as a function of shelf area over the Meso-Cenozoic, but a weaker correlation over the Paleozoic. Using equations S9, S10, and normalizing to rates calculated from the Plio-Pleistocene (most recent time bin) (B-C, Eqn. S12). Broad agreements in changes to sulfate reduction rates from the major and minor isotope record $^{34}\varepsilon_{GEO}$ or $^{33}\lambda_{GEO}$ inputs are apparent over the last 200 Ma (B), but not before (also see, Fig. 2.5). (C) This biphasic trend (Meso-Cenozoic versus Paleozoic) in correlations appears to be a function of shelf-area, though other factors must have contributed to isotopic signals during the Paleozoic.

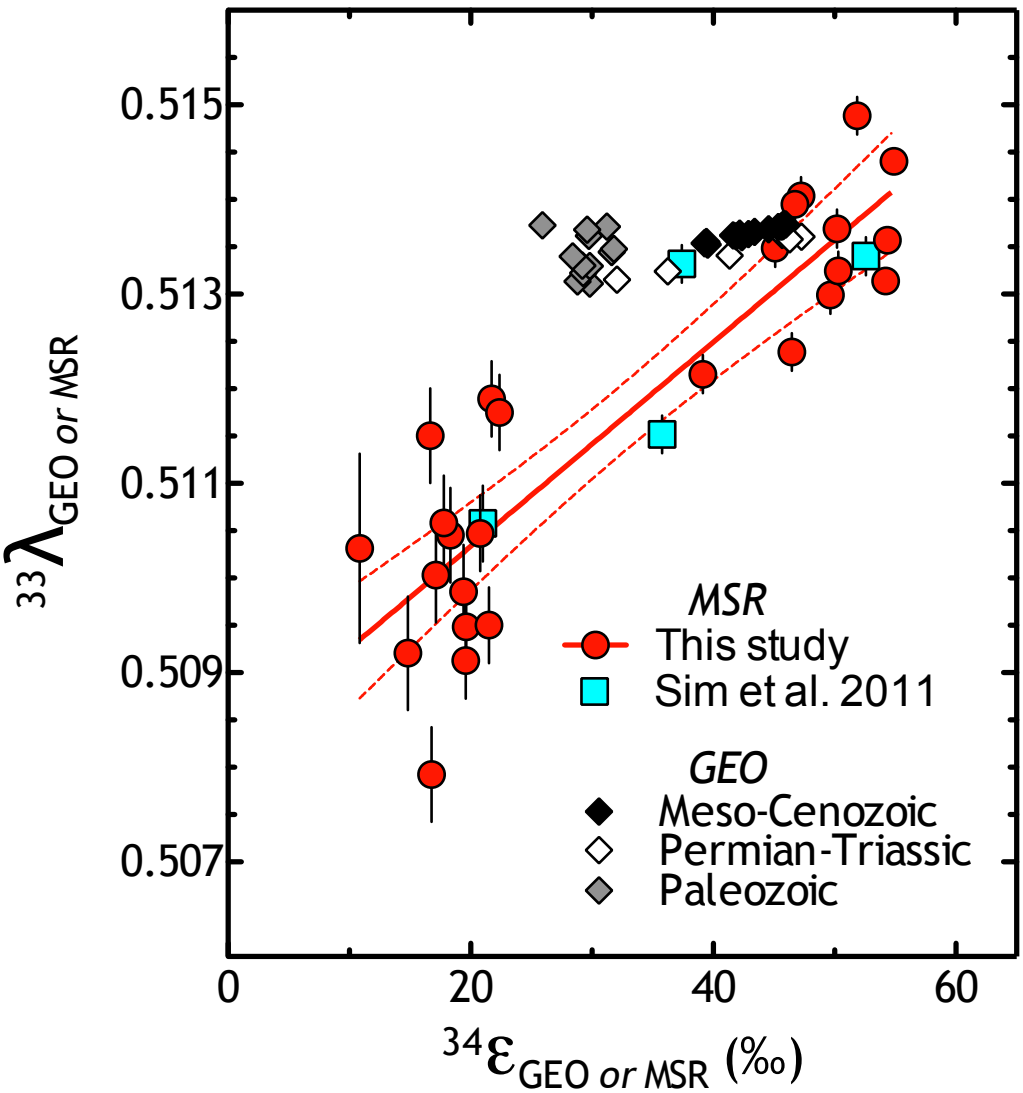

Figure 2.S5. Multiple sulfur isotope fractionations from our chemostat experiments plotted along side the Phanerozoic compilations (Table S2). Mean values from the last 200 million years are fall within the 95% CI of our MSR chemostat calibration. Mean isotope values from the earlier Paleozoic and parts of the Permian-Triassic transition are well out of our experimental calibration, indicating fractionating processes other than MSR contribute to the mean isotope signals of each time bin.

ACKNOWLEGDEMENTS: We thank A. Pearson for detailed comments that greatly improved this manuscript. Comments from C. Cavanaugh, C. Hansel, T. Laakso, and JC Creveling helped along earlier versions of this manuscript, and Tim Lyons and an anonymous reviewer for thoughtful commentary. A. Masterson, E. Beirne and M. Schmidt provided expert analytical assistance. The NSF-GRFP (WDL), Microbial Sciences Initiative at Harvard (WDL, DTJ), NASA-NAI, NSF-EAR-IF, NSF-CAREER program and Harvard University (DTJ) supported this work.

CHAPTER 3.

PATTERNS OF MICROBIAL SULFUR ISOTOPE FRACTIONATION AT LOW SULFATE CONCENTRATIONS

A version of this chapter is in review at *Geobiology* with co-authors:

Alexander S. Bradley[†], Marian Schmidt, Andrew H. Knoll, Peter R. Girguis, and David T. Johnston. [†]Authors contributed equally.

ABSTRACT

Studies of microbial sulfate reduction have suggested that the magnitude of sulfur isotope fractionation varies as a step function of ambient sulfate concentration, with a critical threshold at roughly two hundred micromolar (Habicht et al. 2002; Habicht et al. 2005). This threshold concentration has been interpreted as an upper bound on the sulfate concentration in Archean seawater, given low sulfur isotope fractionations preserved in sedimentary rocks of this age (Habicht et al. 2002). Here we examined S-isotope fractionation in two strains of sulfate-reducing bacteria grown under continuous culture conditions between 0.1 and 6 mM sulfate. The relationship between S-isotopic fractionation and sulfate abundance was observed to be strain-specific and highly variable. *Desulfovibrio vulgaris* str. Hildenborough cultures showed a large and relatively constant isotope fractionation (~25‰) between sulfate and sulfide over the aforementioned sulfate concentrations, whereas *Desulfovibrio alaskensis* G20 exhibited fractionations ranging from 2‰ to 15‰, correlating linearly with sulfate concentration. Together these data reveal that fractionation can vary as a function of concentration for some strains, even at sulfate concentrations well above thresholds typical of cellular half-saturation (K_s) constants. While the ratio of sulfate concentration to K_s is likely to be an important factor in determining sulfur isotope fractionation, these data suggest that the realized fractionation can be significantly influenced by other physiological factors such as sulfate uptake mechanism(s) or the chemical species of electron donor, which must also be considered when interpreting environmental sulfur isotope ratios.

INTRODUCTION

Evolution of the marine sulfate reservoir is a key parameter in modeling Earth's surface oxidation state through time (R. A. Berner & Canfield 1989; Canfield 2004b). Today, seawater sulfate represents an oxidant reservoir ten times the size of atmospheric O_2 (Hayes & Waldbauer 2006). One of the most powerful tools for understanding the paleo-record of this reservoir is the ratio of stable sulfur isotopes in minerals such as pyrite and sulfate evaporites found in marine sedimentary rocks. Marine sulfate concentrations are linked to geological

isotope records largely via microbial metabolism – most notably microbial sulfate reduction (MSR), a metabolic process that couples organic carbon or hydrogen oxidation to sulfate reduction. Details of the isotopic record may permit the quantification of seawater sulfate through Earth history, but such efforts must be predicated on a fundamental understanding of the broad suite of factors that influence the fractionation of sulfur isotopes during MSR.

MSR can yield a large mass-dependent fractionation between sulfate and sulfide (Harrison & Thode 1958; Lyn A Chambers et al. 1975; Sim, Bosak & Ono 2011a; Leavitt et al. 2013). The product sulfide is depleted in heavy isotopes, thereby enriching residual sulfate. Both environmental and physiological factors contribute to the expressed fractionation. For example, it has been suggested that $^{34}S/^{32}S$ fractionations greater than 5‰ are expressed only when ambient sulfate concentration exceeds 200 micromolar (Habicht et al. 2002) - approximately one percent of the sulfate concentration in modern seawater. This concentration threshold is similar in magnitude to the sulfate half-saturation concentrations (K_s) of many sulfate-reducing strains (Pallud & Van Cappellen 2006; Tarpgaard et al. 2011). When paired with Precambrian sedimentary sulfur isotope record, this fractionation threshold value was taken to imply an increase in seawater sulfate concentrations near the Archean – Proterozoic boundary, where a dramatic expansion of S-isotope fractionation is preserved (Habicht et al. 2002). This, in turn, may suggest a strong physiological control on the geological isotope record (Habicht et al. 2002; Habicht et al. 2005).

Microbial physiology provides a context for evaluating how low sulfate concentrations limit sulfur isotope fractionation. Extensive work on the sulfate uptake half-saturation constant (K_s) demonstrates a range of sulfate affinities, observed in natural communities and pure cultures alike (see compilations in (Tarpgaard et al. 2011; Pallud & Van Cappellen 2006)). For instance, it was originally intuited that microbes adapted to lacustrine environments with low ambient sulfate concentrations should have high sulfate uptake affinities, with the opposite posited for marine strains (Bak & Pfennig 1991; Holmer & Storkholm 2001). However, surveys of K_s show no clear relationship with salinity, presenting similar K_S ranges (0.001 mM to 3 mM $[SO_4^{2-}]$) for both marine and freshwater organisms (see review in (Tarpgaard et al. 2011)). Furthermore, genomic analyses predict that

individual microbial strains may carry multiple sulfate transporters (Tarpgaard et al. 2011), possibly of varying sulfate affinity. Such physiological complexity suggests that the relationship between S isotope fractionation and sulfate abundance may be more complex than a simple and universal step function.

Experiments with natural populations of sulfate reducers provide one approach to understanding how environmental variables like sulfate concentration might affect bulk sulfur isotope fractionation (Canfield 2001b). Such experiments have the advantage of including the ecological complexity found in natural environments. However, laboratory studies of mixed communities can introduce biases that favor the activity of select members of the microbial community. Given the inherent complexity, it is challenging to constrain this effect and its subsequent influence on isotope geochemistry. As a complement to mixed community studies, experiments on single strains provide constraints on the extent to which physiological and biochemical factors influence the relationship between sulfate concentration and S isotope fractionation. By judiciously selecting the appropriate strains, one can test specific hypotheses (e.g., the nature of sulfate acquisition by freshwater vs. marine sulfate reducers) and ultimately provide the constraints necessary to more rigorously interpret the results of mixed community studies. Such reductionist approaches can provide a foundational perspective for understanding natural systems.

We report results from two sets of chemostat experiments, each employing an axenic culture of a sulfate-reducing bacterium. In each set of experiments, the bacterial population was grown over a range of sulfate concentrations, to assay the relationship between sulfate concentration and isotope fractionation. *Desulfovibrio vulgaris* str. Hildenborough (DvH), a freshwater strain, and *Desulfovibrio alaskensis* str. G20 (G20), a marine strain, were selected because they are among the most well studied sulfate reducers (Hansen 1994; Wall et al. 1993; I. A. C. Pereira et al. 2011). Both have fully sequenced genomes (Hauser et al. 2011; Heidelberg et al. 2004), and both have been established as genetically tractable, making them good candidates for future research targeting the molecular basis of sulfur isotope fractionation. Notably, previous physiological work suggests a sulfate K_s for DvH at 0.032 mM (Ingvorsen et al. 1984). Based on analyses of closely related strains, the value for G20 is likely in the range of 0.005 to > 0.250 mM (Okabe et al. 2004; Dalsgaard & Bak 1994; Fukui & Takii

1994). Here we present our experimental design and results, consider potential physiological and environmental factors that might explain the observed differences, and discuss the ramifications of these data on previous and future studies.

MATERIALS AND METHODS

Each strain (G20 and DvH) was grown in stirred continuous culture vessels held at room temperature for roughly 40 days. We employed a continuous flow bioreactor to avoid the complexities of closed-system Rayleigh effects incurred during growth in batch culture. In continuous culture at steady state, substrate concentration remains invariant; growth rate (μ: day^{-1}) is also constant and equal to the dilution rate (D: day^{-1}). This design also allowed us to match DvH and G20 growth rates at 0.037 ± 0.003 and 0.034 ± 0.001 ($days^{-1}$), respectively. Any variability recorded in these experiments should, thus, primarily reflect the isotopic response to changing sulfate concentrations. We modulated growth rate and biomass yield with lactate availability, keeping this constant in each experiment. Having sulfate as the limiting nutrient is not advantageous, as the stoichiometric conversion of sulfate to sulfide produces no measurable isotope effect. Our approach allows us to measure the fractionation behavior of MSR over a range of sulfate concentrations (0.1 to 6.1 mM). The ratio of sulfate (e^- acceptor) to lactate (e^- donor) was held invariant in the media supplying the bioreactors, with equimolar ranges from 0.5 to 10 mM. The reactor vessel was continuously purged with a pre-conditioned (O_2-free and hydrated) anaerobic gas mixture (N_2:CO_2, 90:10), which also served to carry gas phase sulfide out of the reactor to a series of zinc acetate traps. Reactor pH was maintained at 7.0±0.02 via a pH-probe activated titration pump, which dosed either 1M HCl or 1M NaOH as appropriate (N_2-degassed and autoclave-sterilized). From the effluent, concentrations of lactate/acetate and sulfate/sulfide were measured daily along with optical density and all (gas and liquid) flow rates. Steady-state sulfate concentrations were measured directly from the bioreactor medium, and represent the concentration available to the population (lower than the concentration of the inlet media). The fractionations of interest ($^{34}\varepsilon$ and $^{33}\lambda$) are thus between reactant sulfate and product sulfide. For isotopic analysis, all samples were

measured for $\delta^{34}S$ via SO_2 and select samples were fluorinated to SF_6 and measured for high precision $\delta^{33}S$ analysis. We use standard isotope notation, where $\delta^{3x}S$ is the ratio of ^{3x}S to ^{32}S in a sample relative to a standard. We use $^{34}\varepsilon$ to capture the isotopic difference between sulfate and sulfide ($=[^{34}\alpha - 1]\ 1000$). Minor isotope notation includes $\Delta^{33}S$ ($=^{33}S + 1000[^{34}S/1000 + 1]^{0.515} - 1$), which relates a composition to a theoretical reference line, and $^{33}\lambda$ ($=\ln[^{33}\alpha]/\ln[^{34}\alpha]$), which is the slope of a line on a plot of $\Delta^{33}S$ vs. $\delta^{34}S$. Elemental flux balances (i.e. inputs = outputs) were always satisfied to within 2%. Growth rate was determined given growth data (cells/mL) with respect to the dilution rate (D: L/day), and only samples satisfying a steady-state flow regime were included in the final analysis. All chemical, biological, and isotopic methods are described in the supplemental materials.

Bacterial strains

In this study, we grew two strains of sulfate-reducing δ-Proteobacteria in a chemostat at room temperature under lactate-limited conditions with feedstock media containing equimolar concentrations varying between 0.5 mM, 1 mM, 2 mM, and 5 mM. The strains in this study were *Desulfovibrio vulgaris* strain Hildenborough (hereafter: DvH) and *Desulfovibrio alaskensis* strain G20 (G20), both of which are available from the Deutsche Sammlung von Mikroorganisms und Zellkulturen, Braunschweig, Germany (DSMZ 644 and DSMZ 16109, respectively).

Culture conditions

DvH cultures were supplied with anaerobic carbonate buffered freshwater medium supplemented with lactate as the electron donor and carbon source. The medium was a modified Postgate C medium and per liter of water contained: 0.07 g KH_2PO_4, 1.5 g $NaHCO_3$, 0.6 g NaOH, 0.06 g $CaCl_2{\cdot}2H_2O$, 0.1 g NH_4Cl, 0.189 mg Na_2SeO_3, 10 mL of sterile trace elements solution (containing in one liter: 1.5 g nitrilotriacetic acid at pH 8.3, 2.1 g $Mg(CH_3COO)_2$, 0.452 g $Mn(NO_3)_2$, 0.1g $FeCl_2{\cdot}4H_2O$, 0.1 g $CaCl_2{\cdot}2H_2O$, 0.1 g $CoCl_2{\cdot}6H_2O$, 0.13 g $ZnCl_2$, 0.01 g $CuCl_2{\cdot}2H_2O$, 0.01 g $AlCl_3{\cdot}6H_2O$, 0.01 g H_3BO_3, 0.03 g $Na_2MoO_4{\cdot}2H_2O$, 0.025 g $NiCl_2{\cdot}6H_2O$, 0.025 g $Na_2WO_4{\cdot}2H_2O$), and 1 mL of sterile vitamin solution (including in one liter of water at pH 7.0: 0.02 g biotin, 0.02

g folic acid, 0.1 pyridoxine HCl, 0.05 g riboflavin, 0.05 g thiamine-HCl, 0.05 g nicotinic acid, 0.05 g pantothenic acid, 0.001 g vitamin B_{12}, 0.05 g p-aminobenzoic acid, 0.05 g thioctic acid, 2 g L-arginine, 2 g L-serine, 2 g L-glutamic acid). Sulfate ($MgSO_4$) and sodium lactate ($NaC_3H_5O_3$) were added to final concentrations of 0.5 mM, 1 mM, 2 mM, and 5 mM. Sodium ascorbate ($NaC_6H_7O_6$; 1.5 g per liter) was added as a reducing agent. The medium was autoclaved and cooled to room temperature while it was gassed with N_2/CO_2 (90/10). Once cooled, calcium chloride, ammonium chloride, sodium selenite, trace metals, vitamins, sodium lactate and magnesium sulfate were added from sterile (autoclaved or 0.22 μm filter sterilized), anaerobic stock solutions. The final pH of the medium was adjusted to 7.0 ± 0.1.

G20 was supplied with anaerobic carbonate buffered salt-water media with lactate as the electron donor and carbon source. Per liter of water the medium contained: 20 g NaCl, 0.3 g KH_2PO_4, 1.5 g $NaHCO_3$, 0.6 g NaOH, 0.14 g $CaCl_2{\cdot}2H_2O$, 0.1 g NH_4Cl, 0.189 mg Na_2SeO_3, 0.82 g $MgCl_2{\cdot}6H_2O$, 10 mL of sterile trace element solution (described above), and 1 mL of vitamin solution (see above). As with the D*v*H experiment, sulfate ($MgSO_4$) and lactate ($NaC_3H_5O_3$) were added to final concentrations of 0.5 mM, 1 mM, 2 mM, and 5 mM and sodium ascorbate ($NaC_6H_7O_6$; 1.5 g per liter) was added as a reducing agent. The medium was autoclaved and cooled to room temperature while it was gassed with N_2/CO_2 (90/10). Once cooled, calcium chloride, ammonium chloride, sodium selenite, magnesium chloride, trace metals, vitamins, sodium lactate and magnesium sulfate were added from sterile (autoclaved or 0.22 μm filter sterilized), anaerobic stock solutions. The final pH was 7.0 ± 0.1.

Chemostat setup

Both D*v*H and G20 were grown in a custom-made glass chemostat or continuous culture (BellcoGlass, Part no. 1964-06660; total volume of 5 L) containing about 2.0 L of medium. The chemostat was fitted with 6 ports with autoclavable sulfide-resistant PTFE caps (Western Analytical). All connections consisted of 1/16" PEEK tubing (McMaster-Carr) fitted with ¼-28 PEEK nuts and ferrules (Cole-ParmerThe pH was sustained at 7.0±0.1 with an autoclavable pH electrode (Mettler-Toledo, model 405-DPAS-SC-K8S/325) connected to a

conductivity controlled dosing pump (Etatron, DLX pH-RX/MBB) that titrated with a sterile solution of 1M HCl to the bioreactor. The medium was pumped in and out of the bioreactor with the use of a peristaltic pump (Ismatec 4-channel Reglo-Analog MS-4/8 fitted with Tygon HC F-4040-A tubing) from a N_2:CO_2 (90:10) pressurized 10 liter reservoir bottle with an average dilution rate of 0.703 L/day (D*v*H) and 0.631 L/day (G20). The chemostat was continuously stirred with a Teflon-coated magnetic stir bar and constantly gassed with O_2-scrubbed N_2:CO_2 (90:10) at an average flow rate of 173 mL/min (D*v*H) and 78 mL/min (G20) to keep the culture anoxic and to enable sulfide collection. The chemostat was kept at room Each experiment, consisting of a given set of lactate and sulfate concentrations, was performed for several days, during which growth was monitored by daily measurement of optical density. during a steady state in each growth condition, which was generally achieved after two days.

We sampled the gas trap (G), liquid effluent (L), and reactor solution (R) in order to quantify all sulfur and carbon species and to measure the major and minor isotope compositions of all sulfur species. Daily samples were withdrawn from the chemostat in four ways: First, a 1 mL sample was taken from the bioreactor for optical density measurements (OD_{600}; Genesys 10S UV-Vis, Thermo Scientific). Second, a 10 mL sample of medium from the bioreactor was taken from a sample port and combined with 1 mL of 5% zinc chloride ($ZnCl_2$) to measure the reactor sulfide and sulfate concentrations (R). Third, H_2S produced through sulfate reduction in the bioreactor was carried out of the vessel with the N_2:CO_2 purge gas and trapped in two consecutive traps of 50 mL of 20% (w/v) zinc acetate buffered with glacial acetic acid (60mL L^{-1}) to pH 4.5 (first trap was changed daily for samples). The first gas trap was used to measure the concentration and isotopic composition of sulfide (G). Fourth, the spent media from the bioreactor was pumped out to maintain a constant volume into a 2 L bottle with 100 mL of 5% $ZnCl_2$ (to cease metabolism and trap sulfide; changed daily). Sulfide concentration and sulfate isotope composition were measured from this liquid reservoir (L). The final volume of this reservoir was changed daily with the flow rate of the pump. All samples were stored frozen until further analysis.

Analytical procedures

Cell numbers were determined by optical density readings (OD_{600}; Genesys 10S UV-Vis, Thermo Scientific) calibrated to microscopic cell counts, performed on an Olympus BX60 fluorescence microscope, at 100x magnification on DAPI (4',6'-diamindino-2-phenylindole) stained cells, previously fixed in 2% glutaraldehyde.

Sulfate, lactate, and acetate concentrations in fresh and spent used medium from both R and L samples were determined on (0.45μm) filtered sampled by suppressed anion chromatography with conductivity detection (Dionex ICS-2000, AS11 column). An eluent gradient method was employed: running first 1mM KOH isocratically for 6 minutes, followed by a linear ramp to 30mM KOH over 8 minutes, then a linear ramp to 60mM KOH over 4 minutes, followed by 5 minutes re-equilibration at 1mM KOH between samples (duplicate analysis S.D. ±5%; detection limit 1μM). Sulfide concentrations were measured by the methylene blue method (*28*) at OD_{670} (3-replicate S.D. ±2-7%; detection limit 5μM). We also measure for thiosulfate ($S_2O_3^{2-}$) and trithionate ($S_3O_6^{2-}$) on reactor (R) and effluent (L) samples by cyanolysis (*29, 30*). All samples were below the thionate detection limit of 50nM.

Sulfate (L & R) or product sulfide (G+L+R) samples were first prepared for major isotope analysis ($\delta^{34}S$) as $BaSO_4$ or Ag_2S, respectively. All samples for sulfur isotope analysis (as SF_6 or SO/SO_2) were first treated as such: gas samples (*G*) collected as ZnS were treated with excess $AgNO_3$ to generate Ag_2S and incubated overnight in the dark followed by centrifugation to concentrate the precipitate along with wash, re-suspension by vortex, and re-concentration steps performed in the following order (35-40mL of each): 1M CH_3COOH 2x, DI water 3x, 1M NH_4OH 1x, water 2x, and dried at 50°C prior to weighing for fluorination. Reactor (*R*) and liquid (*L*) sulfate samples were quantitatively reduced to Ag_2S by the method of Thode (THODE et al. 1961; Forrest & Newman 1977), and washed with NH_4OH and water as above. Samples were converted to SO_2 by combustion at 1040°C in the presence of excess V_2O_5 (Elemental Analyzer, Costech ECS 4010) and analyzed by continuous flow isotope ratio mass spectrometry (1σ of ±0.3‰; Thermo-Finnegan DELTA V Plus). All samples as Ag_2S were fluorinated under 10X excess F_2 to produce SF_6, which is then purified cryogenically (distilled at -107°C) and

chromatographically (on a 6' molecular sieve 5Å inline with a 6' HayeSep Q 1/8"-stainless steel column, detected by TCD). Purified SF_6 was measured as SF_5^+ (m/z of 127, 128, 129, and 131) on a Thermo Scientific MAT 253 (1σ: $\delta^{34}S$ ±0.2, $\Delta^{33}S$ ±0.006‰, $\Delta^{36}S$ ±0.15‰). All isotope ratios are reported in parts per thousand (‰) as experimentally paired sulfates and sulfides measured. Long-term running averages and standard deviations for IAEA standards: S1, S2, S3 for sulfides, or NBS-127, SO5, SO6 for sulfates. Isotope calculations and notation are detailed below. Isotope ratios are presented as paired sulfate-sulfide measurements.

Isotope ratio and fractionation calculations

Sulfur has four stable isotopes: ^{33}S, ^{34}S, ^{36}S, and ^{32}S in relative abundance 0.76%, 4.29%, 0.02%, and 94.93%, respectively (Coplen et al. 2002). Isotope ratios ($^{3x}R = {}^{3x}r/{}^{32}r = [(^{3x}S/^{32}S)_A/(^{3x}S/^{32}S)_B]$) are used to determine the fractionation factor (α) between two pools (A and B; x = 3, 4, or 6, & y = 3 or 6:

$$^{3x}\alpha_{A-B} = \left[\left(^{3x}S/^{32}S\right)_A/\left(^{3x}S/^{32}S\right)_B\right] \quad (3.1)$$

$$^{3x}\varepsilon_{A-B} = \left(^{3x}\alpha - 1\right)\times 1000 \quad (3.2)$$

$$\delta^{3x}S_A = \left[\left(^{3x}S/^{32}S\right)_{sample}\right]/\left[\left(^{3x}S/^{32}S\right)_{standard} - 1\right]\times 1000 \quad (3.3)$$

$$\Delta^{3y}S = \delta^{3y}S - 1000\times\left[\left(1 + {}^{\delta^{34}S}/_{1000}\right)^{0.515} - 1\right] \quad (3.4)$$

where 0.515 defines the mass-dependent relationship and is assigned a value of 0.515 for y = 3. Last, in determining the isotopic fractionation associated with a specific process—even if that process is constituted by a number of steps—lambda is defined, differing from that used above in the definition of $\Delta^{3x}S$.

$$^{33}\lambda_{A-B} = \left[ln\left(1+\frac{\delta^{33}S_A}{1000}\right) - ln\left(1+\frac{\delta^{33}S_B}{1000}\right)\right]/\left[ln\left(1+\frac{\delta^{34}S_A}{1000}\right) - ln\left(1+\frac{\delta^{34}S_B}{1000}\right)\right] \quad (3.5)$$

This definition is specific for a pair of samples (e.g. sulfate sulfide), but may also be applied through a field of data defined by a common mechanism or process. Qualitatively, $^{33}\lambda$ describes the slope of a line connecting data on a plot of $\delta^{33}S$ vs. $\delta^{34}S$.

Sample selection

We imposed a requirement that cells selected for isotope analysis must be growing in steady state with respect to the chemostat. We determined the growth rate via the equation:

$$\mu = \frac{dC/dt}{C} + \frac{j_0}{V}, \qquad (3.6)$$

where μ is the specific growth rate, C is the concentrations of cells (inferred from optical density), j_0 is the media flux of into the chemostat and V is the chemostat volume. At steady state, dC/dt=0 and μ is equal to the dilution rate D = j_0/V. We calculated the growth rate and dilution rate for each sample, and imposed the requirement that the growth rate had to be within 10% of the dilution rate, or the sample was considered not sufficiently close to steady state, and not included in further analyses.

RESULTS AND DISCUSSION

Figure 3.1 plots the isotopic fractionation between sulfate and sulfide as a function of sulfate concentration for both DvH and G20. Experiments with *Dv*H yielded a range of $^{34}\varepsilon_{DvH}$, from 18.0 to 32.7‰, over the targeted sulfate concentrations. These data show no discernible covariance (p = 0.19) between sulfate concentration and fractionation; $^{34}\varepsilon_{DvH}$ does not preserve a first order dependence on sulfate concentration between roughly 0.1 and 5 mM. That noted, these experiments demonstrate the capacity for significant isotope fractionation ($^{34}\varepsilon_{DvH}$ > 25‰) at sulfate concentrations as low as 0.1 mM. In contrast, experiments with strain G20 produce a $^{34}\varepsilon_{G20}$ that varied systematically from near 0 to 13‰ as sulfate concentrations increased. These data are well fit by a linear regression model: $^{34}\varepsilon_{G20} = (2.2 \pm 0.12)\times[SO_4^{2-}] + (1.2 \pm 0.34)$, (p < 0.001), consistent with a first-order dependence of $^{34}\varepsilon_{G20}$ on sulfate concentration over the range tested (0.1 to 6.1 mM). Thus, our two experimental strains demonstrate strikingly different patterns in both the magnitude of $^{34}\varepsilon$ and its dependence on ambient sulfate concentration.

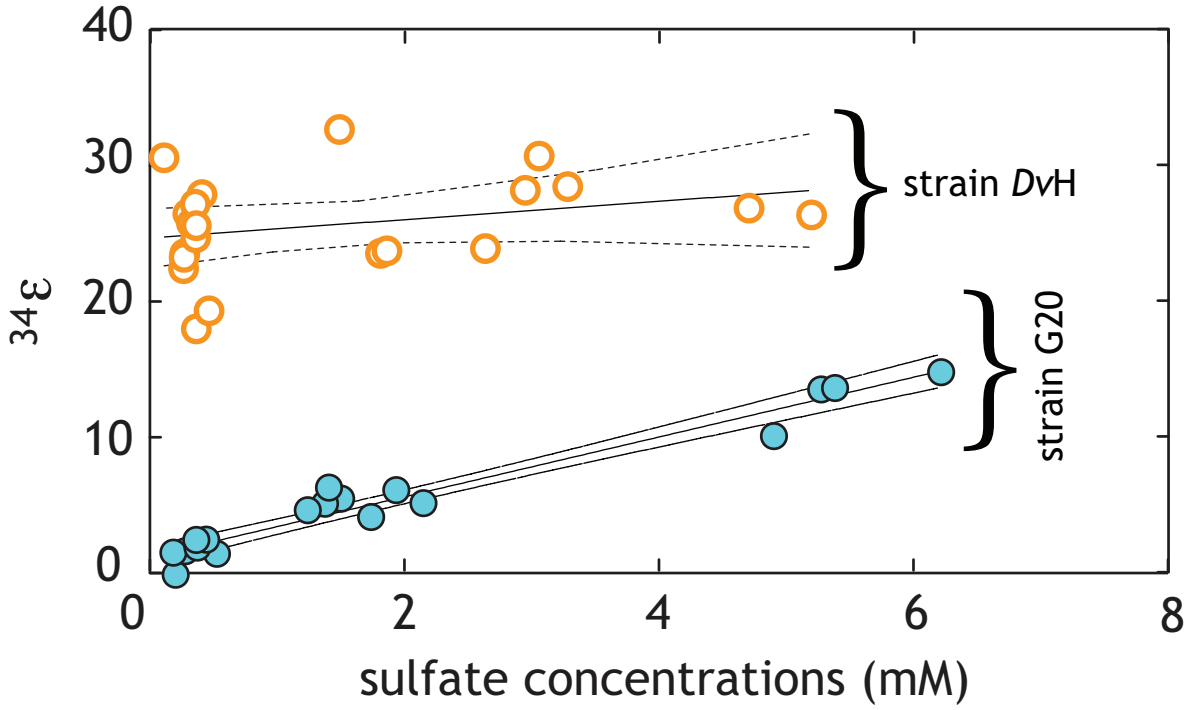

Figure 3.1. The relationship between sulfate concentration in chemostat experiments and the resulting $^{34}\varepsilon$ between sulfate and sulfide. Reported sulfate concentrations are from within the reactor, capturing the concentration actually experienced by the microorganisms and not that of the original medium. Strain *Desulfovibrio vulgaris* str. Hildenborough (DvH), in yellow, exhibits large isotope effects across the full range of sulfate concentrations, whereas strain *Desulfovibrio alaskensis* G20, in blue, shows a strong concentration dependence. Error envelopes are 95% confidence intervals.

The relationship between sulfate concentration and isotopic fractionation ($^{34}\varepsilon$) described above and elsewhere (Habicht et al. 2002; Habicht et al. 2005) can be extended to $^{33}\lambda$. These data are presented in Fig. 3.2 in the context of two complementary minor isotope notations: $^{33}\lambda$ and $\Delta^{33}S$ and. Here, $^{33}\lambda$ reflects the slope of a line spanning the point ($\delta^{34}S$, $\delta^{33}S$) and the origin, and describes a relationship between ^{33}S and ^{34}S contents. Thermodynamic equilibrium predicts $^{33}\lambda = 0.515$, while kkinetic processes have smaller slopes (Young et al. 2002). The $\Delta^{33}S$ is defined as the residual between the measured $\delta^{33}S$ and that predicted by the $\delta^{34}S$ with $^{33}\lambda = 0.515$. As both terms are widely used, we plot our data both ways.

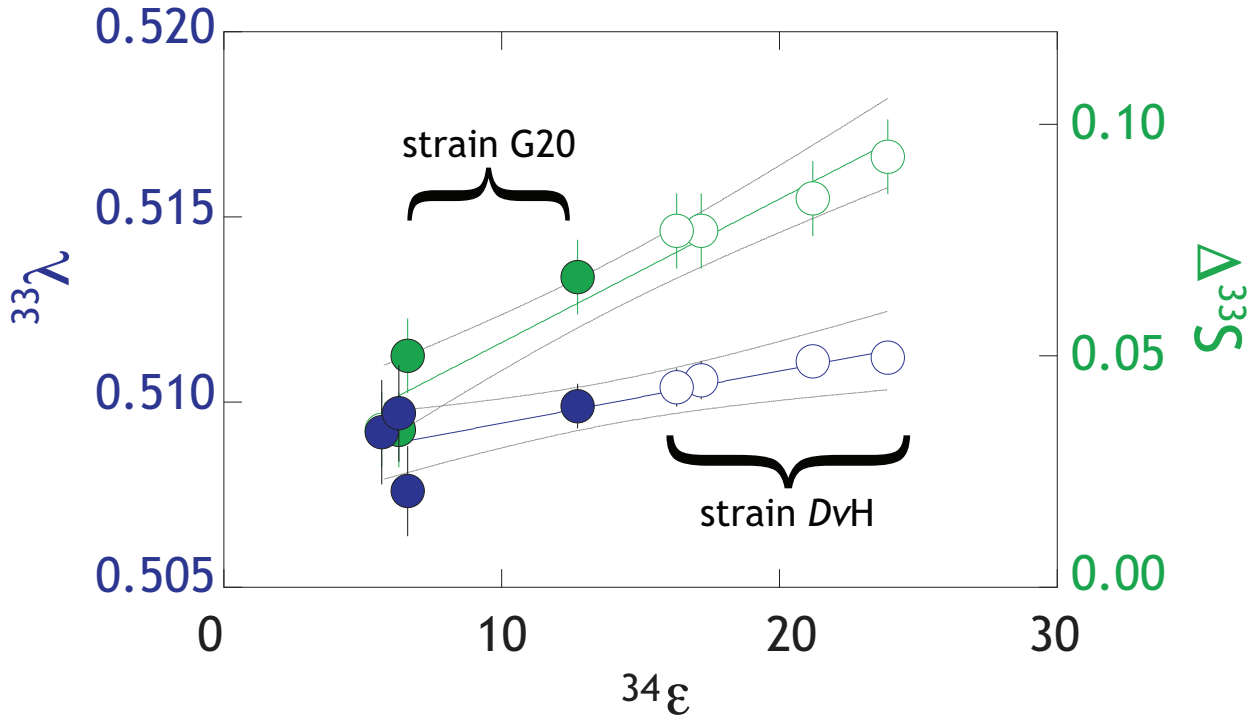

Figure 3.2. Triple isotope data for variable sulfate chemostat experiments. Right y-axis shows $\Delta^{33}S$, plotted against $^{34}\varepsilon$ for DvH (blue open circles) and G20 (blue closed circles). Left y-axis indicates $^{33}\lambda$, again plotted against $^{34}\varepsilon$ for DvH (green open circles) and G20 (green closed circles). Regressions and 95% confidence intervals represent strain independent and metabolism specific trends associated with MSR.

Previous studies targeting $^{33}\lambda$ in open-systems MSR experiments suggest that $^{33}\lambda$ varies linearly with $\delta^{34}S$ as a function of metabolic rate (Sim, Bosak & Ono 2011a; Leavitt et al. 2013). Because the slope is metabolism-specific, this relationship extends the biogeochemical utility of S isotopes, as $^{34}\varepsilon$ alone cannot always differentiate among different microbial processes. For example, the $^{34}\varepsilon_{G20}$ values (0-13‰) expressed in our experiments by strain G20 are not unique to MSR; it is the isotopic fractionation in ^{33}S that allows MSR to be distinguished from similar magnitude $^{34}\varepsilon$ effects produced by sulfide oxidation (Zerkle et al. 2009) or disproportionation (Johnston 2005). In our experiments, $\Delta^{33}S$ and $^{33}\lambda$ both show a strong relationship with $^{34}\varepsilon$ when we summed across experiments (Fig. 3.2) ($\Delta^{33}S = {}^{34}\varepsilon \times (-0.0031 \pm 0.0003) + (0.02 \pm 0.01$, $p < 0.0001$). While the

mechanism for these linear relationships cannot be identified definitively, the data are consistent with the activity of a reversible sulfate permease, with variable internal reversibility of the sulfur cycle (Bradley et al. 2011; Brunner & Bernasconi 2005; Rees 1973; J. Farquhar, Johnston, et al. 2007a; Johnston et al. 2007). The $^{33}\lambda - {}^{34}\varepsilon$ results for G20 and DvH fit within the context of previous work in which $^{33}\lambda_{MSR}$ spans a range from 0.508 to 0.514 (J. Farquhar et al. 2003; Johnston 2005; J. Farquhar, Johnston, et al. 2007a; Sim, Ono, et al. 2011c; Sim, Bosak & Ono 2011a; Leavitt et al. 2013; Johnston et al. 2007). In contrast, sulfide oxidation and sulfur disproportionation reactions result in $^{33}\lambda > 0.5145$ (Johnston 2005; Zerkle et al. 2009). These data, therefore, provide a robust indicator of physiology but do not clearly distinguish among variations associated with other experimental parameters (e.g., temperature, MSR strain, or sulfate concentration).

Evaluating sulfate affinity as a predictor of fractionation

These experiments demonstrate that different strains of sulfate reducing bacteria can show distinct relationships between sulfate concentration and isotope fractionation. The observed differences prompt a reexamination of previous data to search for similar patterns. Harrison and Thode (1958) demonstrated a relationship between sulfate concentration and sulfur isotope fractionation with *D. desulfuricans*. More recent work using modified flow-through reactors (Habicht et al. 2002) and chemostats (Habicht et al. 2005) shows a relationship in which $^{34}\varepsilon$ increases with sulfate concentration, asymptotically approaching a maximum value. This work targeted the archaeal sulfate reducer *Archaeoglobus fulgidus* and controlled for growth and SRR through organic carbon limitation. The authors modeled this asymptotic behavior with an equation identical in form to a Monod equation (Monod 1949). The half-saturation constant in this fractionation equation ($K_{m\text{-}frac}$) is the concentration of sulfate at which the modeled fractionation was one-half the maximum fractionation. The value of $K_{m\text{-}frac}$ for sulfate was similar in magnitude to the Monod constant K_s for sulfate-limited growth. This similarity in these constants inspired the proposition that $K_{m\text{-}frac}$ and K_s are related, implying that the half saturation constant carries an isotopic (and perhaps geologic) fingerprint (Habicht et al. 2002).

A Monod-like mathematical relationship correctly predicts the fractionation pattern displayed by DvH. Previous work indicates that K_s for sulfate in DvH is near 0.03 mM (Ingvorsen et al. 1984), well below the sulfate concentrations in our experiments. If $K_{m\text{-}frac}$ is of a similar magnitude, then at our minimum sulfate concentration of 0.1 mM, we expect to observe more than 90% of the maximum fractionation under the specific experimental conditions employed (Fig. 3.1). Only a modest increase in fractionation would accompany further increases in sulfate concentrations, consistent with our observations for DvH.

A Monod-like equation, however, does not adequately explain the experimental results for strain G20. We are unaware of any published sulfate K_s values from strain G20 specifically, although K_s values from related strains (*D. desulfuricans*) are consistently less than 0.5 mM (Tarpgaard et al. 2011). If we assume a sulfate K_s of similar magnitude for G20, then the increased fractionation observed up through ~6 mM sulfate would not be predicted. As specific growth rates (m) are constant across this range of sulfate concentrations, the source of variable fractionation is unclear. One possibility is that strain G20 strain has sulfate uptake mechanisms with low affinity, which may have been selected for during isolation (Wall et al. 1993) or evolved post-isolation. It is common to find such variations in phenotype among related microorganisms, so it would not be surprising to find that G20 differs from related strains. If it turns out that G20 has a sulfate K_s near or above 5 mM, then the relationship between K_s and $K_{m\text{-}frac}$ may hold. A sulfate K_s of this magnitude is within the upper limits of published K_s values for sulfate (Fukui & Takii 1994; Ingvorsen et al. 1984; Pallud & Van Cappellen 2006; Roychoudhury & Porter 2013). In either case, these results have implications for the interpretation of sulfur isotope compositions in the rock record (Fig. 3.3). Currently there is little understanding of how sulfate affinity (at a biochemical level) has evolved through Earth history, or among environments of differing sulfate concentration.

These new data highlight the fact that the relationship between enzymatic affinity for sulfate and isotope fractionation remains unclear, or is at a minimum heterogeneous. While K_s values for sulfate are directly related to the kinetics of growth under sulfate-limited conditions, experiments on the fractionation of sulfur isotopes are generally executed under electron donor limitation. Growth rates are therefore directly related to the K_s of electron donor. Sulfate K_s still pertains to the cellular affinity for sulfate and may affect fractionation, particularly

when sulfate is *not* growth limiting. For example, sulfate permeases are ATP-dependent active transporters that "pump" sulfate into the cell against a concentration gradient (Piłsyk & Paszewski 2009). Active transporters function by binding to the target molecule, and frequently result in isotopic fractionation as demonstrated for a wide range of elements and compounds (Nikaido & Saier 1992). Therefore, one plausible explanation for the apparently divergent patterns in Fig. 3.1 is that transport mechanisms differ between the two strains tested. For example, sulfate might be actively transported by DvH, allowing the internal "pool" of sulfate to remain elevated and resulting in an apparent fractionation that primarily reflects discrimination by the transporter(s). One could hypothesize that active sulfate transporters should be most common among freshwater strains, but sulfate transporters may be of value in marine systems as well, and may be expressed when sulfate reducers compete for sulfate in organic-rich sediments, where sulfate concentrations are rapidly depleted. Strains may also have evolved passive ion channels for sulfate acquisition, enabling the uptake of sulfate without the expenditure of cellular energy when appropriate (this requires that environmental sulfate concentrations be higher than those within the cell). While such ion channels have yet to be characterized among MSRs, organisms such as plants do have separate high and low affinity sulfate uptake mechanisms, some of which appear to be passive ion channels (Buchner 2004). Moreover, evidence from marine sediments suggests the presence of both high- and low-affinity mechanisms (Tarpgaard et al. 2011). While low-affinity ion channels often face challenges, such as the non-specific transport of other molecules (e.g., chloride), they are ubiquitous throughout the domains of life, and it is highly plausible they exist among MSRs. Indeed, a previously unknown hydrosulfide ion channel was reported recently (Czyzewski & Wang 2012), illustrating the possibility that other ion channels may still remain unidentified. All of these considerations are generally consistent with the lack of isotopic response to sulfate concentrations above the DvH K_s (a freshwater strain) as compared to the strong response in G20 (a marine strain).

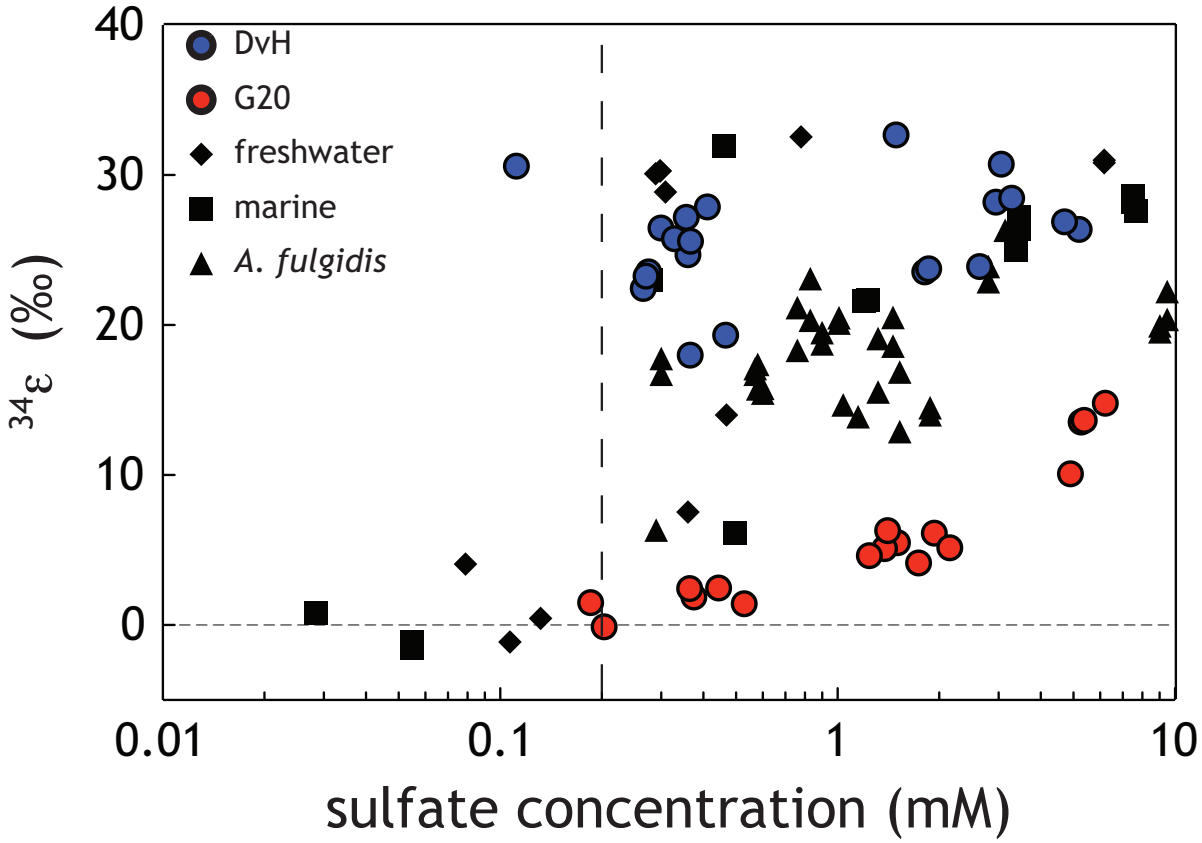

Figure 3.3. Comparison between our data, DvH in blue and G20 in red, and those generated in a chemostat-like continuous culture device by Habicht and colleagues (2002). Data from Habicht et al. (2002) include natural populations from freshwater (diamonds) and marine strains (squares), as well as pure culture studies on *Archaeoglobus fulgidis* (triangles). The vertical dashed line represent the two-hundred micromolar threshold proposed by Habicht and colleagues (Habicht et al. 2002).

Affinity regimes and evolution

We propose that controls on S isotopic fractionation can generally be divided into (at least) four regimes (Fig. 3.4). Within each regime, transport and physiological factors will also affect observed fractionation.

1.) Sulfate limitation: Where sulfate is near or below its K_s and electron donor concentrations are well above the respective K_s, sulfate availability may control isotopic fractionation. In this regime, sulfur isotope fractionation will be minimized as sulfate approaches quantitative reduction. To the extent that sulfate uptake is the rate-limiting step in this scenario, it may carry a small (even inverse) isotope effect (Harrison & Thode 1958),

but expressed fractionation is predicted to be small. It was within this regime that Habicht and colleagues looked to calibrate Archean seawater sulfate levels (Habicht et al. 2002).

2.) Electron donor limitation: sulfate concentration is well above its K_s; electron donor concentration limits growth and sulfate reduction rates, and in turn isotopic fractionation (Leavitt et al. 2013). In this regime, sulfate K_s will not likely play a role, as sulfate concentrations greatly exceed K_s. This assumes that the Monod equation can be amended to suit the isotopic approach of Habicht et al., 2002. This application and its appropriateness are robust given our current understanding, but is the target for future theoretical work. The experiments we have conducted here with DvH fall into this category, as sulfate is always well above the known K_s for DvH. In contrast, results from the G20 experiment indicate that sulfate concentration is still limiting the maximum expressed fractionation, even though the ambient $[SO_4^{2-}]$ probably exceeds the Ks. This may imply an as-yet unidentified factor affecting fractionation, such as a sulfate ion channel or active transporter.

3.) Substrate co-limitation: Concentrations of both sulfate and electron donor are near or below their respective K_s values. Growth rate in this case may be a second-order function that relates to the concentration and K_s of both substrates, or it may be the minimum growth rate predicted by either parameter (Liebig's law: (Saito et al. 2008)). Under these conditions, the expressed fractionation is likely to be a compound function of physiology and environment – fractionation is thus difficult to predict uniquely. If limitation of one constituent exerts ultimate control, then the system approaches regime 1 or 2.

4.) Nutrient limitation: The final condition we explore is where another nutrient such as nitrogen, iron, or phosphorous (Sim et al. 2012), some physical parameter (e.g. temperature, (Canfield 2001b)), or an intrinsic organismal factor (e.g., maximum genome duplication rate) limits growth rate and fractionation. The rate-fractionation relationship has been demonstrated for electron donor/acceptor (Leavitt et al. 2013; L A Chambers & Trudinger 1975; Habicht et al. 2005) and for nutrients (Sim et al. 2012), but may plausibly extend to other parameters. Where growth rates are controlled by factors intrinsic to the cell, expressed fractionations are likely to reflect rates of intracellular electron transport to electron-accepting sulfur intermediates (Bradley et al. 2011).

These regimes indicate that multiple interactions ultimately control the sulfur isotope fractionation expressed by any given organism in any particular environment. As mentioned above, one complexity not yet explored is the potential for organisms to carry multiple sulfate uptake machineries (with varying affinities). For example, as sulfate is consumed through a typical early diagenetic marine profile (Jorgensen 1979), the sulfate concentrations available for MSR vary from 28 to < 1 mM. High affinities for sulfate may confer a selective advantage at low sulfate concentrations, but would not be required at high concentrations, and the converse is also true. A recent study identified both high and low affinity uptake schemes through a sulfate-methane transition zone profile in marine sediments (Tarpgaard et al. 2011), showing that large differences in affinity are possible at least within microbial communities from a specific environment. This sort of physiological flexibility is also observed in other physiological processes, such as carbon fixation, wherein RuBisCO is optimized to intracellular CO_2/O_2 ratios (Tcherkez et al. 2006). The genome of DvH (http://www.ncbi.nlm.nih.gov) contains three annotated sulfate transport proteins, while the genome of G20 contains 10. This redundancy is consistent with a potential range of affinities, which could be further extended if unknown transport proteins are also present.

An apparent range in affinities of enzymatic machinery for sulfate sets in place a 'K_s continuum' at the organismal level. The K_s expressed under any set of conditions is physiologically dependent and may incorporate feedbacks sensitive to sulfate concentration. The presence of both high and low affinity uptake mechanisms, at the cellular and community scales, is relevant to interpretation of the geochemical record. Continuing research will need to identify the full genetic and enzymatic controls on sulfate K_s in a variety of organisms, as well as the selective pressures to which these controls respond. In the future, geochemical interpretations of sulfur isotopes might well include an understanding of how sulfate affinity has evolved in response to changing ocean redox conditions, and how this evolution has influenced the sulfur isotope record. A high affinity for sulfate would probably have been particularly advantageous early in Earth history, the requirement becoming more relaxed as the Earth's surface became more oxidizing and sulfate more plentiful. That is, natural selection has probably altered dominant patterns of sulfur isotope fractionation over the course of Earth history. A genomic memory of ancient high affinity machinery may still be present in modern lacustrine environments. As new genomes and

tools for analyzing molecular evolution become available, these questions become more tractable and applicable to the understanding of the geochemical record.

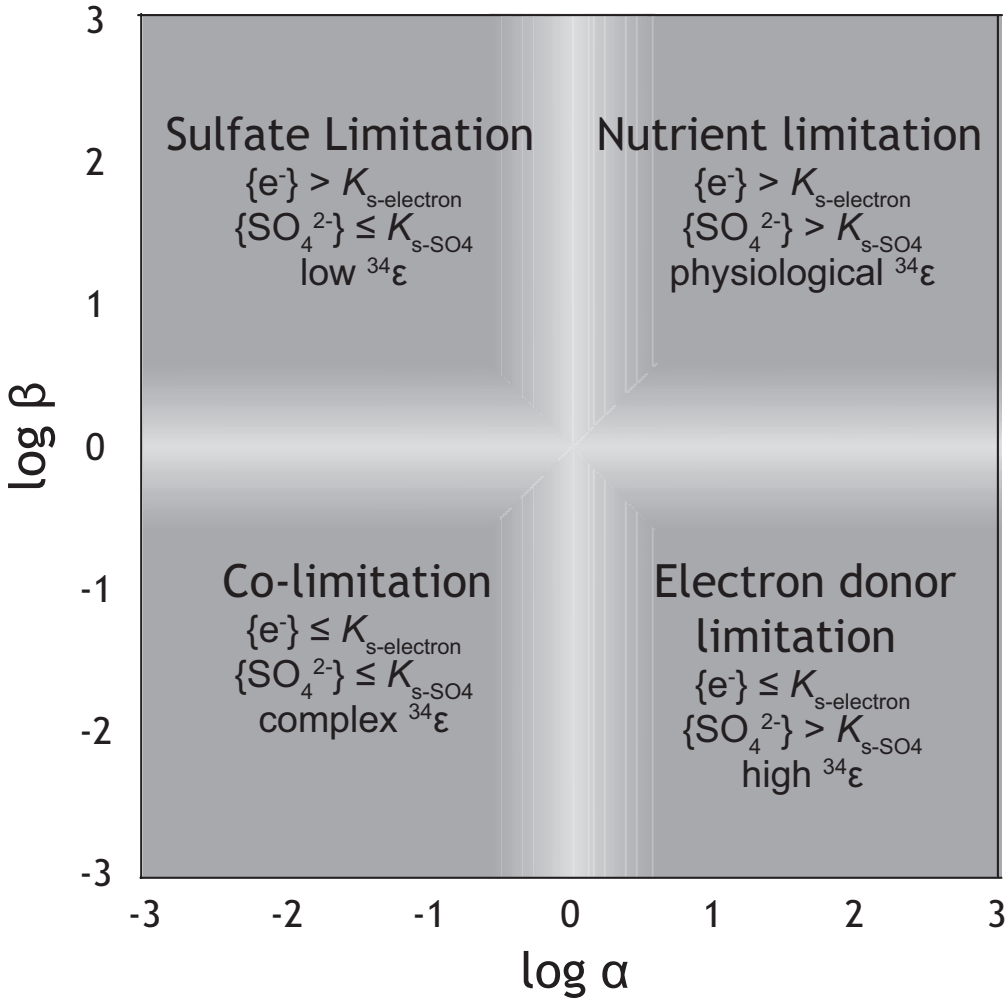

Figure 3.4. Four ecological regimes relevant to sulfur isotope fractionation. X-axis indicates the concentration of sulfate relative to K_s for sulfate for a given organism ($\alpha = [SO_4]/K_{s\text{-}SO4}$; log scale); y-axis indicates a similar relationship for electron donor (β = [electron donor]/$K_{s\text{-electron donor}}$; log scale). In growth under sulfate limitation electron donor is in excess and fractionation is low. In growth under electron donor limitation, high fractionation is expected, largely as a function of slow growth. Co-limitation of sulfate and electron donor is likely to produce a complex physiological pattern that is not well understood. Nutrient or other growth limitation (e.g. temperature) suggests that both sulfate and donor will be abundant (as is typical at the beginning of batch growth experiments); isotope fractionations are expected to be intermediate in magnitude. Boundaries between these regimes are fuzzy, but expected to fall near K_s.

CONCLUSIONS

Understanding the paleoenvironmental information encoded in sulfur isotopes during sulfate reduction requires an understanding of how growth and physiology effect fractionation (Bradley et al. 2011; Rees 1973). Deconvolving these effects becomes tractable through experiments and theoretical metrics such as K_s, which serves as a common means of comparing data from different strains. It is unlikely that a single threshold sulfate concentration turns the fractionation capacity of MSR (as a metabolism) on or off in all sulfate-reducing microorganisms. Thus, while sulfate concentrations were undoubtedly low in Archean oceans, they could have exceeded 200 μM, depending on both the availability of electron donors and the physiology of contemporaneous sulfate reducers. Importantly, the quantitative reduction of sulfate will always yield a small to negligible isotope effect regardless of the expression of an intrinsic of fractionation step. Future work on K_s values for sulfate reducers, especially G20, will serve to test the range of possible sulfate concentration dependencies on fractionation.

In addition to being driven by global scale sulfur cycling, microbial evolution and ecological community structure play a role in generating the isotopic record observed in sedimentary minerals. The identification of two strains that show different fractionation across the range of sulfate abundances likely to have characterized Proterozoic and early Paleozoic oceans opens new possibilities for interpreting the deep sedimentary record of sulfur isotopes. A more complete understanding of that record will rely on a better understanding of relevant enzymes, their expression in response to environmental variables, and their evolution over the course of Earth history.

ACKNOWLEDGMENTS

The authors acknowledge funding from NASA Exobiology Grant NNX07AV51G (to AHK, PRG and DTJ), NASA Astrobiology Institute (DTJ, AHK), the Microbial Sciences Initiative at Harvard (DTJ), and NSF EAR Instrument and Facilities as well as Low Temperature Geochemistry and Geobiology (to DTJ). ASB and WDL thank the Agouron Institute and NSF-GFRP for funding, respectively.

CHAPTER 4.

SULFUR ISOTOPE FRACTIONATION BY DISSIMILATORY SULFITE REDUCTASE

A version of this chapter is in review at *Nature* with co-authors:

Alexander S. Bradley†, André Santos, Inês A. C. Pereira, David T. Johnston.

†Authors contributed equally.

The biogeochemical sulfur cycle helps govern the oxidation state of Earth's surface. Microbial sulfate reduction (MSR) is central in this cycle. MSR couples the oxidation of organic matter to the reduction of sulfate, producing sulfide that is depleted in the heavier (^{33}S, ^{34}S, ^{36}S) relative to the lightest (^{32}S) stable sulfur isotope. This biological signal is captured in modern sedimentary pore-waters and authigenic minerals throughout geologic time. Therefore, precise interpretation of these isotopic records requires an understanding of the biochemical controls on sulfur isotope fractionation. Here we provide the first direct measurement of isotope fractionation imparted by a key enzyme of MSR – dissimilatory sulfite reductase. This enzyme-specific fractionation factor ($^{34}S/^{32}S$) is 15.3‰ in two different organisms across a range of temperatures. This result is 0.3 to 0.6 times the magnitude of previous indirect estimates (25 to 53‰)(Harrison & Thode 1958; Rees 1973; Brunner & Bernasconi 2005), and can explain a large proportion of the most frequent pure culture fractionation observations. Further, these data account for the lower fractionation limit approached at high sulfate reduction rates in modern marine sediments and laboratory experiments(Harrison & Thode 1958; Goldhaber & Kaplan 1975; Rees 1973; Brüchert et al. 2001; Leavitt et al. n.d.). Direct examination of fractionations imparted by individual enzymes is a fundamental step toward a biochemical foundation for reinterpreting the geobiological sulfur isotope record and, in turn, the oxidation of the Earth's surface(Holland 1973).

MSR provides a critical link between Earth's exogenic S, C, Fe, and O cycles, with decades of research suggesting it is the prevailing driver of mass-dependent variance in sedimentary S isotope records(Holland 1973; Thode et al. 1953; Canfield & J. Farquhar 2009). The magnitude of fractionation produced by MSR relates to environmental conditions, namely the availability of reductant (organic matter or hydrogen) relative to oxidant (sulfate). Whole cell (in vivo) experimental systems express a median isotope fractionation between sulfate and sulfide (herein MSR $^{34}\varepsilon$) near 17‰ (Fig. 4.1), with recent work(Canfield, Farquhar, et al. 2010a; Sim, Bosak & Ono 2011a) suggesting an upper limit approaching the theoretical low temperature equilibrium estimates of approximately 75‰(Tudge & Thode 1950). Experimental approaches aimed at understanding controls on

fractionation can guide interpretations of the wide range of MSR $^{34}\varepsilon$ in modern environments and the geologic record. In this work we seek to untangle the relationship between environment and preserved isotopic fractionation, analogous to studies on the relationship between isotopic fractionation and C-fixation by RuBisCO. Just as the measurement of isotope fractionation by RuBisCO allowed insight into carbon isotope records(Hayes 1993) targeting dissimilatory sulfite reductase in MSR serves to shed new light on Earth's modern and ancient sulfur cycle.

We determined sulfur isotope fractionations associated with sulfite reductase (DsrAB) purified from two model organisms: a bacterium (*Desulfovibrio vulgaris* strain Hildenborough) and an archaeon (*Archaeoglobus fulgidus* strain DSM 4304T). *In vitro*, sulfite reductase catalyzes the reduction of sulfite to two thionate products, trithionate and thiosulfate. We applied a novel closed system model developed to accurately depict the experimental system in order to calculate the fractionation associated with sulfite reductase ($^{34}\varepsilon$ and $^{33}\lambda$, *see* Supplementary Information). This resulted in a calculated $^{34}\varepsilon$ for sulfite reductase of 15.3±0.4‰ (Fig. 4.2), with a parallel $^{34}\varepsilon$ associated with sulfonate production of 2±0.3‰. The bacterial, and very limited archaeal sulfite reductase fractionations are consistent across the temperatures tested (20, 30, and 65°C) (Supplementary Information). That noted, we move to discuss the reductive fractionation step within the DvH sulfite reductases. We interpret the observed fractionation factors as representing the binding and reduction of sulfite by dissimilatory sulfite reductase. To our knowledge, this is the only *in vitro* measurement of the DsrAB fractionation factor utilizing purified enzyme.

Our direct constraint on the enzymatic sulfite reductase $^{34}\varepsilon$ indicates that the previous assignments of 25‰(Harrison & Thode 1958) and 53‰(Brunner & Bernasconi 2005) are over-estimates. This is perhaps not surprising given that previous appraisals were generated through various indirect approaches(Harrison & Thode 1958; Rees 1973; Brunner & Bernasconi 2005). Our measured $^{34}\varepsilon$ value for sulfite reduction (15.3±0.4‰) is large enough to account for a substantial portion of the more than sixty years of *in vivo* MSR experiments (mean of 17.9±0.4‰), as seen when our data is compared to a statistical analysis of the literature (Fig. 4.1). In more detail, recent *in vivo* work demonstrates that $^{34}\varepsilon$ between sulfate and sulfide scales inversely and non-linearly with

sulfate reduction rate(Harrison & Thode 1958; Leavitt et al. n.d.; Goldhaber & Kaplan 1975; Rees 1973; Brunner & Bernasconi 2005; Brüchert et al. 2001). In the lab as in nature, sulfate reduction rates scale as a function of organic carbon and sulfate (reductant to oxidant) availability at the locus of sulfate reduction(Goldhaber & Kaplan 1975; Holland 1973; Harrison & Thode 1958; Leavitt et al. n.d.; Brüchert et al. 2001; Kaplan & Rittenberg 1964; Rees 1973). As the net forward rate of MSR slows toward the bioenergetically allowable lower limit, larger and larger kinetic isotope fractionations are incurred and approach, but do not reach, the theoretical equilibrium values for sulfate—sulfide S isotope exchange(Holland 1973; Tudge & Thode 1950; Thode et al. 1953; J. Farquhar et al. 2003; Canfield & J. Farquhar 2009; Johnston et al. 2007) (Fig. 4.3). At elevated sulfate reduction rates, smaller $^{34}\varepsilon$ are observed, representing the isotopic expression of the single slowest (overall rate-limiting) step within MSR(Canfield, Farquhar, et al. 2010a; Rees 1973; Sim, Bosak & Ono 2011a). The closeness between the fractionation limit at high metabolic rates(Tudge & Thode 1950; Leavitt et al. n.d.) ($^{34}\varepsilon$ = 17.3±1.3‰) and our *in vitro* experiments (15.3±0.4‰) are consistent with the hypothesis that the rate-limiting step within MSR under these conditions is sulfite reduction (Fig. 4.3). Recent oxygen isotope incorporation studies(Hayes 1993; Mangalo et al. 2008), as well as classic biochemical work demonstrating that steps upstream of DsrAB in the MSR pathway are fully reversible(Harrison & Thode 1958; Peck 1962), support the interpretation that DsrAB is the rate-limiting step at elevated sulfate reduction rates. This interpretation is supported by modern sediment sulfur isotope data(Brunner & Bernasconi 2005; Goldhaber & Kaplan 1975), which also preserve a coherent fractionation minima of MSR $^{34}\varepsilon$ = 17.3±3.8‰ (1σ), statistically indistinguishable from that of sulfite reduction (Fig. 4.3).

Measuring minor S-isotope ($^{33}S/^{32}S$) fractionation provides unique information about the class of reaction mechanism associated with *in vitro* DsrAB activity. Lambda ($^{33}\lambda$) relates the fractionation of ^{34}S to that of ^{33}S (*see* Isotope Notation). In cases where $^{33}\lambda$ is 0.515, a purely equilibrium fractionation is inferred[15,16], whereas values <0.515 would imply a kinetic isotope fractionation[19,20,](Young et al. 2002). Dissimilatory sulfite reductase produces a minor isotope fractionation ($^{33}\lambda$) of 0.515±0.001 between sulfite and reduced sulfur sites and 0.510±0.001 between sulfite and sulfonate. Interpreting the fractionation associated with sulfite reductase in light

of previous suggestions would most directly suggest that *in vitro* aqueous sulfite is subject to an isotopic equilibrium reaction, whereas isotope fractionation during sulfonate formation is kinetic. However, the exponent (λ) relating fractionation in triple isotope systems (such as S and O) derives from the mass dependence of different aspects of partition functions for equilibrium versus kinetic processes. As such, there is nothing physically inherent behind the derivations of the equilibrium and kinetic λ's that requires convergence – i.e. values approaching 0.515 are not unique to equilibrium, though values less than 0.515 are likely diagnostic of disequilibrium. Thus, specific predictions for the sulfite reductase enzyme, for example, require more detailed modeling of the structure and function of the DsrAB enzymatic active site. This level of analysis – where inroads joining empirical work with theory are constructed – is present in analogous systems(Karsh et al. 2012)'(Guo et al. 2010) but not yet constrained for MSR. This leaves open the possibility that the sulfite reduction step, as captured in these experiments, is purely kinetic. Nonetheless, the work here provides the first triple-isotope constraints on enzyme-specific fractionation factors in both MSR and the global biogeochemical S cycle. Further, this approach can be applied to other enzymatic systems with multiple stable isotopes (e.g. O, Fe, Mg, Se, Zn, Mo).

Overall these results indicate that sulfite reductase can only be responsible for less than a quarter of the maximum MSR fractionation observed(Holland 1973; Sim, Bosak & Ono 2011a; Thode et al. 1953; Canfield, Farquhar, et al. 2010a; Canfield & J. Farquhar 2009) (Fig. 4.1). Together, the $^{34}\varepsilon$ and $^{33}\lambda$ measurements for sulfite reductase provide critical boundary conditions for the interpretation of all MSR isotope fractionations and models reliant on these values(Sim, Bosak & Ono 2011a; L A Chambers & Trudinger 1979; Tudge & Thode 1950; Bradley et al. 2011; Rees 1973; J. Farquhar et al. 2003; Canfield, Farquhar, et al. 2010a; Brunner & Bernasconi 2005; Johnston et al. 2007; J. Farquhar, Johnston, et al. 2007a; J. Farquhar et al. 2008). This requires that previous approaches, which arbitrarily distributed fractionation over the MSR metabolic pathway (with sums approaching 50‰(Tudge & Thode 1950; Rees 1973) or 73‰(G. D. Farquhar et al. 1982; Brunner & Bernasconi 2005; Johnston et al. 2007)), are no longer valid conceptual models. Larger and variable observed MSR $^{34}\varepsilon$ is due to changes in metabolic rate(Hayes 1993; Goldhaber & Kaplan 1975; Kaplan & Rittenberg 1964; Brüchert et al.

2001; Lyn A Chambers et al. 1975; Leavitt et al. n.d.; Sim, Bosak & Ono 2011a), which allows for reversibility in sulfate activation to APS and APS reduction to sulfite; both may yield additional fractionation(Harrison & Thode 1958; Rees 1973; Brunner & Bernasconi 2005; Johnston et al. 2007; Bradley et al. 2011). For instance, it is understood that *in vivo* MSR fractionations may reflect the aggregate of the sulfite reductase fractionation (this study), the enzymatic reduction of sulfate to sulfite(Brunner & Bernasconi 2005; Rees 1973; Bradley et al. 2011), and possibly the terminal production of sulfide by DsrC: the later step is the newly recognized terminal step in MSR(Harrison & Thode 1958; Oliveira, Vonrhein, Matias, Venceslau, P. M. Pereira, et al. 2008b; Rees 1973; Brunner & Bernasconi 2005). No direct enzymatic or theoretical estimates exist for either of these two additional electron transfer reactions. Loose estimates from crude cell extracts and resting cell studies (i.e. not purified enzymes) suggest a putative $^{34}\varepsilon$ for the cumulative sulfate activation and reduction to sulfite of 11±4‰ (n=37, Extended Data Tables 4.1 and 4.3), but when summed with the $^{34}\varepsilon$ of sulfite reductase, these two fractionations only accommodate a net $^{34}\varepsilon$ of 26±4‰. These value fall short of the maximal MSR $^{34}\varepsilon$ observed in some laboratory experiments(Leavitt et al. n.d.; Sim, Bosak & Ono 2011a) and a diverse array of natural environments – both marine and lacustrine sediments(Canfield, Farquhar, et al. 2010a; Goldhaber & Kaplan 1975), as well as the bulk of the Proterozoic geologic record(Rees 1973; Wu et al. 2010; Brunner & Bernasconi 2005; Canfield & J. Farquhar 2009).

Microbial sulfate reduction is the centerpiece of the sulfur cycle and is associated with the majority of the isotope signal in the geologic record(Kaplan & Rittenberg 1964; L A Chambers & Trudinger 1979). Determining the isotopic fingerprints of key enzymes in this pathway is critical to uncovering the environmental controls influencing these sedimentary records throughout Earth history. Dissimilatory sulfite reductase is one major component of this pathway, and the $^{34}\varepsilon$ reported herein explains the fractionation limits approached at high metabolic rates for MSR in continuous chemostat cultures and modern marine sediments (Fig. 4.3). High MSR rates result in a unidirectional flow path where DsrAB is the rate-limiting step, hence the expression of a fractionation of 15‰ when sulfate is not limiting. What remains unclear is how DsrC, as it participates with DsrAB and is subject to independent regulation, may contribute to isotope fractionation. Furthermore, these data

also demonstrate that isotope fractionation associated with DsrAB is significantly smaller than previously assumed. As such, the large sulfur isotope fractionation, which approach a low-temperature equilibrium value of 74 to 80‰(Tudge & Thode 1950), must be a consequence of both the net reaction rate, the relative reversibility within the reaction network, and the intrinsic isotope effects not catalogued here. Finally, the $^{33}\lambda$ data point to a complex, likely kinetic fractionation scheme and provides the basis for subsequent *ab initio* isotope calculations. Having direct constraints on a critical enzymatic isotope fractionation, when placed in context of laboratory(Leavitt et al. n.d.) and field observations(Canfield, Farquhar, et al. 2010a; Goldhaber & Kaplan 1975), represents a key step toward an improved understanding of how environmental factors come to control biochemical sulfur isotope fractionations in nature.

Isotope Notation

Variability in ^{3x}S of a measured pool is tracked through: $\delta^{3x}S_y = \left[\left({}^{3x}S/{}^{32}S\right)_{\text{sample}}\right]/\left[\left({}^{3x}S/{}^{32}S\right)_{\text{standard}} - 1\right] \times 1000$, where x = 3, 4, or 6, and y is a distinct S-bearing species or operationally defined pool. The difference between two pools (y = A or B, e.g., sulfite and reduced thionate S or sedimentary sulfate and pyrite) is calculated by: ${}^{3x}\varepsilon_{A-B} = \left({}^{3x}\alpha_{A-B} - 1\right) \times 1000$, where ${}^{3x}\alpha_{A-B} = \left[\left({}^{3x}S/{}^{32}S\right)_A/\left({}^{3x}S/{}^{32}S\right)_B\right]$. Variability in ^{33}S is tracked through:

$$^{33}\lambda_{A-B} = \left[\ln\left(1+\frac{\delta^{33}S_A}{1000}\right) - \ln\left(1+\frac{\delta^{33}S_B}{1000}\right)\right]/\left[\ln\left(1+\frac{\delta^{34}S_A}{1000}\right) - \ln\left(1+\frac{\delta^{34}S_B}{1000}\right)\right].$$

The $^{33}\lambda$ defines the slope of a line connecting to points on a $\delta^{33}S$ vs. $\delta^{34}S$ plot (see Extended Data Fig. 4.S4 and 4.S7). Expanded discussion of notation can be found in Young et al. (2002)(Young et al. 2002) and Johnston (2011)(Johnston 2011).

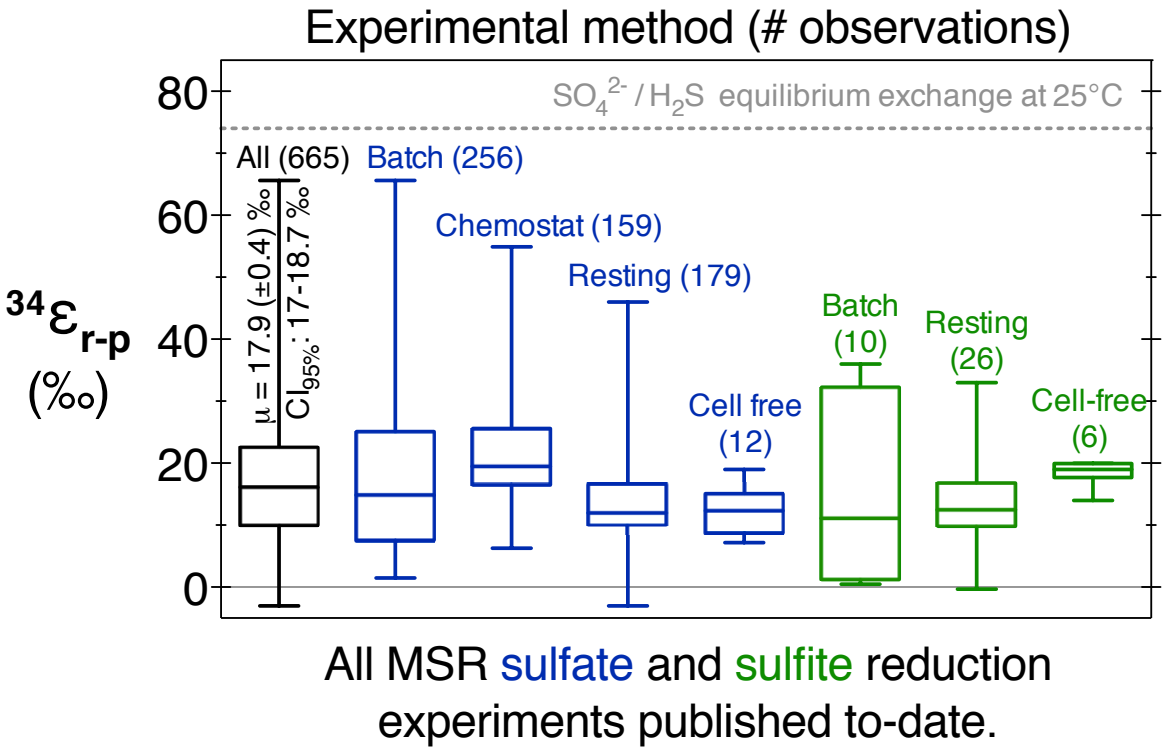

Figure 4.1. A compilation of S isotope fractionation ranges from all published pure cultures as of April 2014. A box-whisker plot of all published MSR pure-culture experiments (black), or separated by experimental method (e.g. batch, chemostat, etc. *see* Supplementary Information for details) and reactant/product pair (sulfate/sulfide in blue, sulfite/sulfide in green). Each box bounds the median (line) and 25th-75th percentiles (bottom-top), while the whiskers enclose the full range. The SO_4^{2-}/H_2S equilibrium fractionation (grey dashed line) is from(Tudge & Thode 1950). Each is expressed in $^{34}\varepsilon$ between reactant (r: sulfate or sulfite) and product (p: sulfide). Positive values signify enrichment of heavy isotopes in the reactant to simplify statistical analysis (Supplemental Information, Section 7).

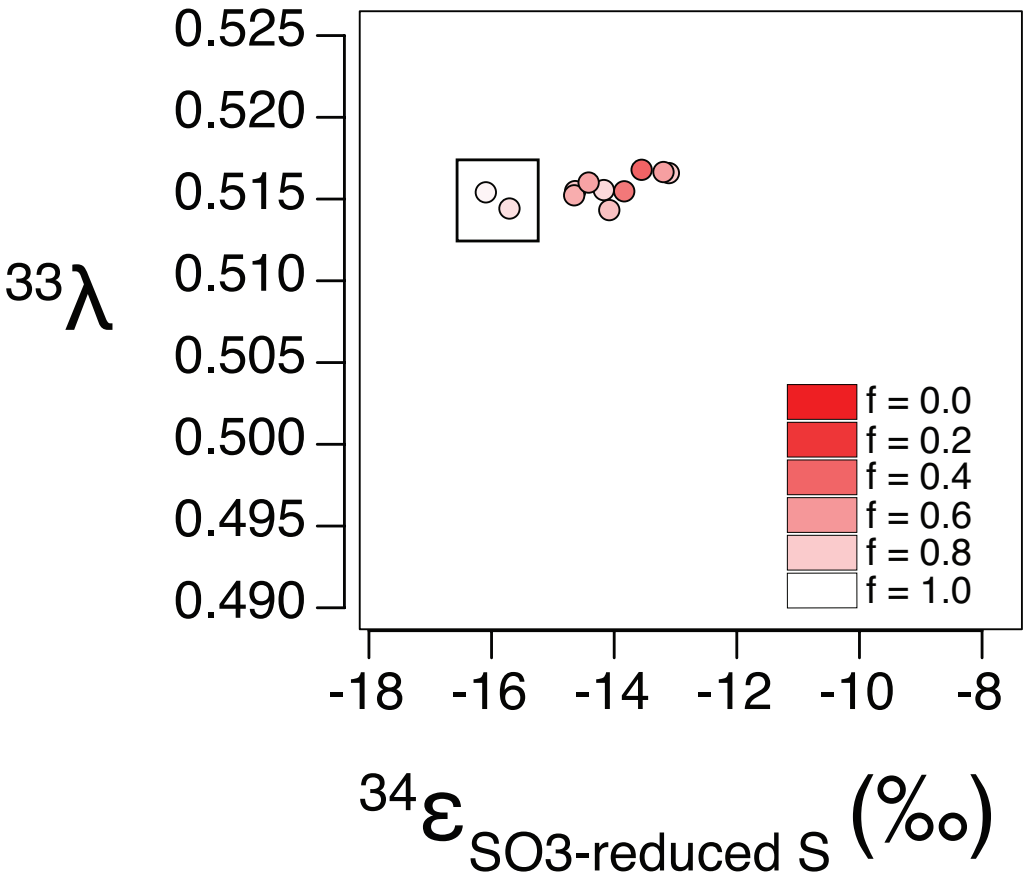

FIGURE 4.2. Sulfur isotope fractionation during sulfite reduction by bacterial DsrAB. (A) Fractionation between sulfite and the reduced sulfur moieties of trithionate and thiosulfate. Initial values of $^{34}\varepsilon$ are near 15.3‰ ($^{34}\alpha$ near 0.9847), and increase with decreasing *f* (*f* = fraction of reactant sulfite remaining). The exponent $^{33}\lambda$, relating ^{33}S and ^{34}S fractionation is stable near 0.515. The box indicates the two points with highest *f*. See the Supplemental Information for the details of the experiments (Section 2) measurements (Section 10) and modeling (Section 7). Expanded model treatments and fits of the sulfonate fractionations are presented in Extended Data Figure 4.S7.

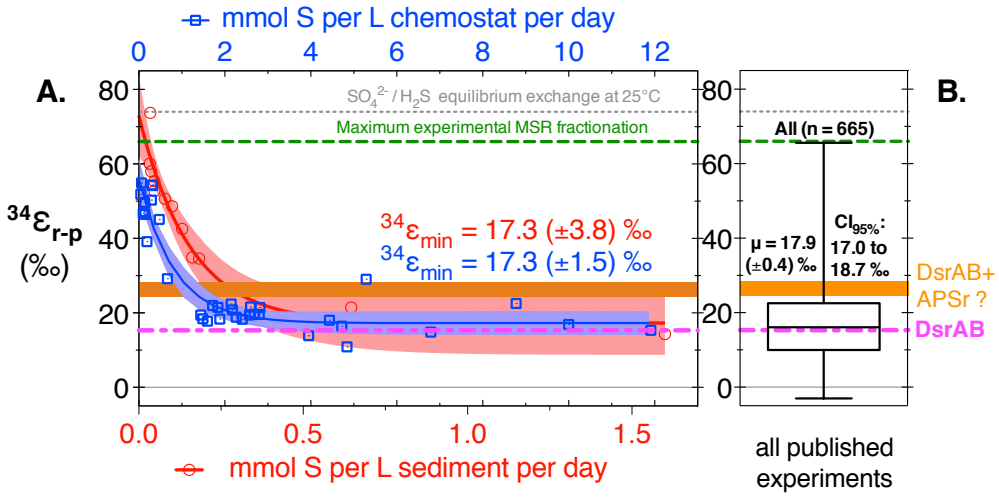

Figure 4.3. A compilation of S isotope fractionation ranges from pure cultures and modern sediments overlain by the now measured fractionation factor of DsrAB, and our best estimate for the sum of DsrAB and sulfate activation to sulfite (noted as APSr). Each panel is expressed in $^{34}\varepsilon$ between reactant (r: sulfate or sulfite) and product (p: sulfide). Positive values signify enrichment of heavy isotopes in the reactant, keeping all values > 0 to simplify statistical analysis (Supplemental Information, Section 7). (A) Fractionation as a function of sulfate reduction rate from pure-culture (blue squares(Leavitt et al. n.d.)) and modern marine sediments (red circles(Goldhaber & Kaplan 1975)) treated with a non-linear regression (solid line at the mean, shaded at CI_{95}). The estimated minimum fractionations (inset values $^{34}\varepsilon_{min}$) are statistically indistinguishable from one another or $^{34}\varepsilon$ of DsrAB. The SO_4^{2-}/H_2S equilibrium fractionation (grey dashed line) is from Tudge and Thode (1950)(Tudge & Thode 1950). DsrAB catalyzed sulfite reduction fractionation (this study) is indicated by the bold dashed pink line: $^{34}\varepsilon$ = 15.3‰, with the sum of DsrAB and our literature estimate for fractionation of sulfate activation and reduction to sulfite (11±4‰) represented by the orange band (Supplemental Information, Section 8). DsrAB accounts for a bulk of the fractionation at high rates and in experiments, while DsrAB and APSr together account for more than 75% of the experimental data, and a larger fraction of the sedimentary data. (B) The box-whisker treatment of all measured (n = 665) sulfate and sulfite reduction experimental $^{34}\varepsilon$, from Fig. 4.1, with the column statistics inset.

CHAPTER 4. SUPPLEMENTARY MATERIALS, METHODS AND FIGURES TO:

In any event, values assigned to the kinetic isotope effects [within MSR] must be viewed with reserve not only because they are derived in large measure indirectly, but also because assumptions have been made regarding the [microbial] sulfate-reduction pathway. At the present time these assumptions have not been entirely validated.

Chambers & Trudinger (1979)(L A Chambers & Trudinger 1979)

Section 4.1.

4.1.1 Dissimilatory MSR metabolic network in detail

In this study we tested the assumptions aptly summarized by Chambers & Trudinger(L A Chambers & Trudinger 1979). The fractionation factors we calculate for sulfite reduction by the central MSR enzyme DsrAB (a_2b_2 heterodimer 'dissimilatory sulfite reductase AB subunit') place the first direct empirical estimates of the key step in MSR (Extended Data Figure 4.S1 step *iv*), and highlight the prospects for the further studies necessary to constrain the steps whose S (and even O) isotope fractionation factors remain under or unconstrained, specifically at the *in vitro* scale. In particular, sulfate transport across the inner and outer membranes (Extended Data Figure 4.S1, step *i*), the reversible(Harry D Peck 1960) activation of sulfate to APS ('adenosine 5'-phosphosulfate') (Extended Data Figure 4.S1, step *ii*), the reversible(Peck 1962) two electron reduction of APS to sulfite (Extended Data Figure 4.S1, step *iii*), and the terminal two electron reduction of DsrAB-bound 'S^0' to H_2S by DsrC(Oliveira, Vonrhein, Matias, Venceslau, P. M. Pereira, et al. 2008b) (g_1 monomeric previously referred to as 'dissimilatory sulfite reductase C subunit') (Extended Data Figure 4.S1, step *vi*). This study has direct bearing on the updated MSR pathway architecture, recently incorporated into isotope models(Bradley et al. 2011), and begins a larger effort to constrain the magnitude of individual enzyme and abiotic fractionation factors, and their cumulative influence on the net MSR fractionation ($^{34}\varepsilon_{MSR}$) that is ultimately observed during

experiments. Knowing the subcellular fractionations is critical to untangling the controls over $^{34}\varepsilon_{MSR}$, particularly because recent work shows the observable may range widely (Figure 4.1(Kaplan & Rittenberg 1964; Lyn A Chambers et al. 1975; Leavitt et al. n.d.)). Fortunately, a physical basis for understanding environmental controls on this range in both modern and ancient aqueous and sedimentary environments is burgeoning(Goldhaber & Kaplan 1975; D. S. Jones & Fike 2013; Leavitt et al. n.d.; Gomes & Hurtgen 2013).

In Extended Data Figure 4.S1 we present the simplified in vivo microbial sulfate reduction pathway (redrawn after(Bradley et al. 2011)) and the known enzymes involved. There are potentially multiple operational modes, from completely linear (steps i thru vii excluding the branching and rejoining at step vi in Extended Data Figure 4.S1), to highly branched (all steps). In intact cells (in vivo) sulfate is (*i*) transported into the cytoplasm with the symport of $2H^{+}$ or $1Na^{2+}$ by a variety of permeases, then (*ii*) sulfate is activated to the high energy intermediate APS at the expense of an ATP and formation of pyrophosphate (PP*i*) by the enzyme, by sulfate-adenylyl transferase (Sat); (*iii*) APS is then reduced to sulfite through a two-electron transfer by active site of the soluble cytoplasmic enzyme APS reductase (AprBA, *a.k.a.* APSr), coupled to energy conservation by the membrane-bound complex QmoABC(R. Pires et al. 2003)—this step is highly reversible, depending on the solution conditions(Peck 1962). Next, (*iv*) sulfite is reduced stepwise by DsrAB to two sulfur intermediates (steps *1a* and *2a*), of which the second, zero-valent sulfur intermediate is converted to H_2S by the action of DsrC(Oliveira, Vonrhein, Matias, Venceslau, P. M. Pereira, et al. 2008b). When DsrC is available and efficiently recycled, (*vi*) H_2S is rapidly produced by the terminal reduction of DsrC-bound sulfur(Oliveira, Vonrhein, Matias, Venceslau, P. M. Pereira, et al. 2008b), where H_2S leaves the cell as the most common S-bearing product of MSR(Rabus et al. 2006). In a branching scenario, the absence or inactivity of DsrC is prevalent and depending on the solution conditions, e.g. high concentrations of sulfite)(H. E. Jones & Skyring 1975; H. E. Jones & Skyring 1974; Akagi et al. 1994), a number of thionate products are formed by further reaction of sulfite with the partially reduced intermediates. This produces trithionate (sub step *1b*) and thiosulfate (steps *2b* and 3). These products can also be reduced to sulfide (*vi*)(Parey et al. 2010), but in vitro the reaction will terminate before the production of H_2S under the conditions we select for our in vitro work. In vitro sulfite reduction reactions

performed in this study are captured by step (i*v*.), in particular constituent steps *1*-*3*. In (*1a*) sulfite binds to the siroheme-Fe in DsrAB and receives two electrons from the adjacent Fe-S clusters(Oliveira, Vonrhein, Matias, Venceslau, I. A. C. Pereira, et al. 2008a). At this point, if electron transfer is rapid and sulfite concentrations are in excess, steps 1a and *2a* and will proceed rapidly, and if DsrC is present and reduced, step *v* will proceed. However, if (*1a*) is more rapid than (*2a*), and/or (*2b*) more rapid than (*v*), then trithionate (*1b*) or thiosulfate (*2b*) is formed. Further, trithionate is known to be reduced by MSR cells and cell-free extracts(Drake & Akagi 1976; Drake & Akagi 1978; Kim & Akagi 1985), as is thiosulfate(Drake & Akagi 1977; Drake & Akagi 1976), yielding steps (3) and (*vi*.), respectively. Both compounds may are also be reduced by an Archeal form of *A. fulgidus* DsrAB(Parey et al. 2010), and we confirmed that *D. vulgaris* DsrAB can also perform such reductions: i.e. trithionate can be reduced to thiosulfate by DsrAB, releasing a sulfite(Drake & Akagi 1978). As such, we performed a series of closed system in vitro sulfite reduction experiments with DsrAB in isolation, sacrificing replicate bottles at numerous points along a reaction co-ordinate (*f*), track mass and isotope mass balance in each bottle, and apply a closed system isotope distillation model in order to calculate the major and minor S isotope fractionation factors associated with sulfite reduction. See the below sections for details of each step in our experimental, analytical, and data reduction approach.

1.2 Enzymes relevant S isotope fractionation in the MSR network

The reactions and constituent MSR enzymes of particular interest in S (and O) isotope fractionation are APS reductase (AprBA, *aka* APSr; Fig. 4.S1b. step *iii*) as this is the first redox transformation of S during MSR, has been predicted to be the pathway rate-limiting step in previous works(Harrison & Thode 1958; Rees 1973), and we now know APSr binds APS directly on through the S within to the FAD ('flavin adenine dinucleotide') cofactor center, as is apparent from the enzyme crystal structure(Fritz 2002). The recent work of Mangalo(MANGALO et al. 2007) and Einsiedl(Mangalo et al. 2008; Einsiedl 2009) and colleagues supports the reversibility of this step, as demonstrated by oxygen isotope exchange of sulfite with water, as do prior early works by Peck(Peck 1962). Sulfate adenylyltransferase (Sat, Extended Data Fig. 4.S1 step *ii*) may be of interest in

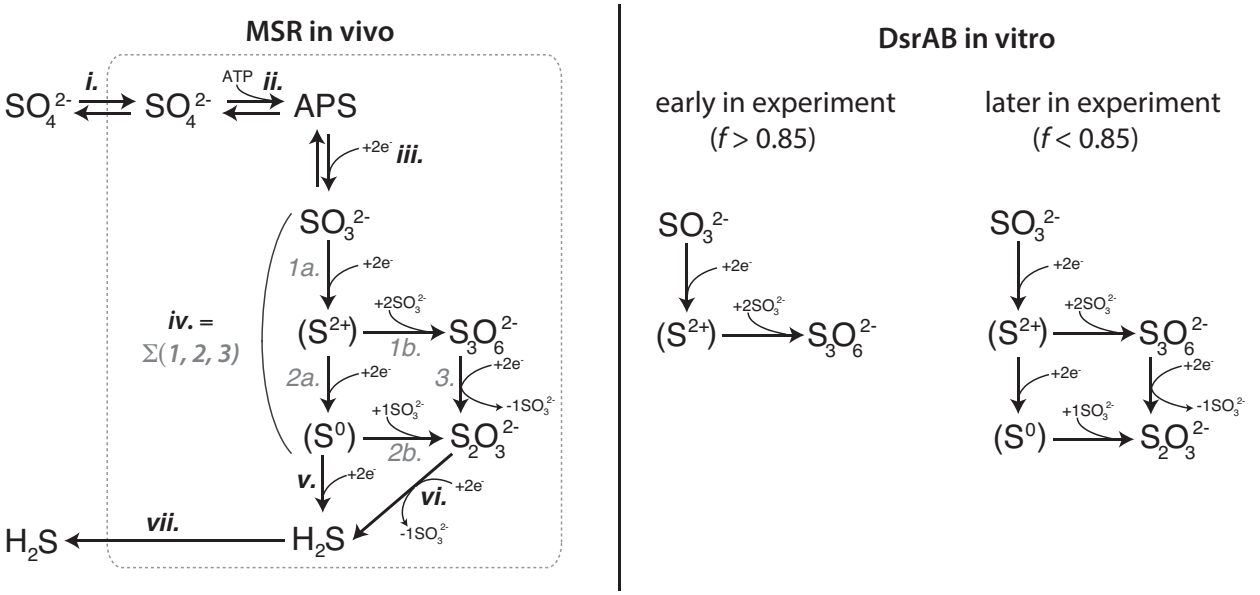

Extended Data Figure 4.S1. The dissimilatory component of the microbial sulfate reduction metabolic network in vivo (left) and in vitro (right). Early in the experiments ($f > 0.85$) the reaction stoichiometry is simpler, and only trithionate is detected, whereas after enough time and trithionate accumulation ($f < 0.85$) thiosulfate is produced. This is documented in both the concentration and isotope data (Extended Data Figures 4.S2 and 4.S3). The constituent steps relevant to S isotope fractionation are APS reduction to sulfite, sulfite reduction (the subject of this study), and potentially sulfide production. The pathway description, along with biochemical and crystallographic evidence for which steps most likely involve S isotope fractionation (and which do not) can be found in the supporting text.

understanding O isotope fractionations during MSR(Wankel et al. 2014; Müller et al. 2013; Kohl et al. 2012), as it binds the oxygen's of sulfate and forms a new O-S bond on the sulfate(Fritz 2002). Similarly, trans-membrane sulfate transporters (Extended Data Fig. 4.S1 step *i*) may have a direct influence of the oxygen isotopic composition of intracellular sulfate as they interact more directly with sulfate-oxygen(PFLUGRATH & QUIOCHO 1988), though they may also influence the isotopic composition of intracellular sulfate by mass-transport effects (i.e. a distillation effect) if membrane fluidity changes drastically due to environmental parameters such as lower temperatures(Furusaka 1961). Earlier predictions that heavier sulfate (^{34}S) would be favored by the active transport of sulfate across the membrane(Kaplan & Rittenberg 1964), due to the higher

bond stability of the heavier S atoms, are likely not correct if sulfate transporters only interact with bind the O's, as secondary isotope effects will be negligible. Still, more protein structures are needed before this can be ruled out entirely.

Section 4.2. DsrAB purification, activity tests, and in vitro fractionation experiments

4.2.1 DsrAB purification, quantification, and activity

DsrAB was purified from *Desulfovibrio vulgaris* Hildenborough (DSM 644) cells grown in a 300L batch culture in a modified lactate/sulfate medium(Le Gall et al. 1994) at iBET (www.ibet.pt). The soluble cell fraction was obtained as previously described (Le Gall et al. 1994). All the purification procedures were performed under atmosphere at 4°C using an AKTA FPLC (Amersham Biotech Pharmacia) with two buffers, (A) 20mM TrisHCl and (B) 50mM TrisHCl with 1M of NaCl (both pH 7.6 and containing 10% glycerol). Buffer (A) was used to equilibrate the columns and buffer (B) to generate the ionic strength gradient. The soluble cell fraction was loaded into a Q-Sepharose fast-flow (XK50/30) columns, and a stepwise salt gradient applied, with the DsrAB-containing fraction eluting with at 300 mM NaCl. The characteristic DsrAB ('desulfoviridin') absorption peak at 630 nm was used to track the protein, as previously described (Marritt & Hagen 1996; WOLFE et al. 1994). DsrAB-containing fractions were then loaded into Q-Sepharose fast-flow (26/10) columns and eluted in 250 mM NaCl. To verify enzyme purity, the final DsrAB-containing sample was analyzed by a 12% SDS-PAGE gel electrophoresis. DsrC is present in the DsrAB preparation, but remains functionally inactive during in vitro assays, as previously described (Oliveira, Vonrhein, Matias, Venceslau, P. M. Pereira, et al. 2008b), and in these assays specifically because the membrane complex (DsrMKJOP) required for DsrC recycling (R. H. Pires et al. 2006; Oliveira, Vonrhein, Matias, Venceslau, P. M. Pereira, et al. 2008b) is absent. Thus, we refer only to the 'DsrAB' fraction in the *D. vulgaris* experiments. In the *A. fulgidus* experiments, DsrAB is free of any DsrC. Protein is quantified by the method of Bradford (Bradford 1976). The *D. gigas* [NiFe] hydrogenase used in all assays was purified as described previously (Romão et al. 1997).

To ensure the activity of purified DsrAB was not strongly influenced by the high initial concentration of sulfite used during the fractionation experiments (10 or 15mM), we performed small-volume kinetic assays under the same conditions as the experiments performed for isotope measurements (*see* Section 6). The assays were performed with DsrAB fraction #14.5 or #14.8 (0.3μM enzyme f/c) at 31°C. Sulfite was measured by HPLC on monobromobimane (MBBr) derivatized samples(Newton et al. 1981). The HPLC assay was performed by mixing 10μL of reaction sample, 82μL of pH 8.0 HEPES, 4μL of 50mM MBBr (Invitrogen) and after 10 min in the dark the addiction of 4μL of 5M methanesulfonic acid (Sigma-Aldrich). The final volume loaded into HPLC vials was 200μL, with appropriately bracketing concentration standards. Once the sulfite concentrations for each initial and final (0 and 2 hours) time points were sampled, derivatized, measured and calculated, we applied a non-linear regression formulated from the standard Michaelis-Menten equation (Equn. S2.1), solving for the V_{max} and K_m (Fig. 4.S2), using *Prism5c*.

Equation S2.1. $$Y = \frac{V_{max} \times X}{K_M + X}$$

At both 10 and 15mM initial sulfite we are assured to be well above the DsrAB K_m for sulfite estimated herein (Fig. 4.S2), and no sulfite inhibition was observed at these concentrations. When the kinetic assay was performed for two hours, the K_m calculated from initial difference in sulfite concentration (relative to t_0 sulfite) is approximately 4.1 mM. This is likely due to the accumulation of trithionate and thiosulfate that can then, in principle, competitively bind at the active site and inhibit reaction rates with sulfite.

Extended Data Figure 4.S2. Small volume activity assays with 0.3μM purified DsrAB, fraction #14.5. The difference between initial and final concentration of sulfite at either two hours was then used to calculate a rate. The Michaelis-Menten equation (Equn. S2.1) was solved for K_m and V_{max}. The analytical error is less than the size of the symbols (1σ = 1μM). One unit (U) is defined as the quantity of enzyme that catalyzes the conversion of one micro mol of substrate per minute

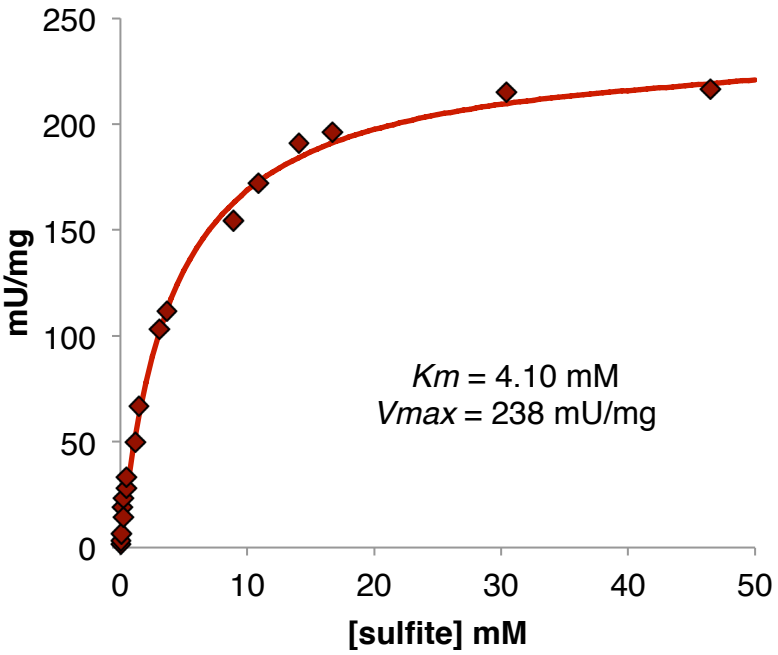

4.2.2 *D. vulgaris* DsrAB in vitro sulfite reduction S isotope fractionation experiments

To determine the DsrAB-specific fractionation factors we designed and executed a series of batch (closed-system) sulfite reduction experiments. The key considerations in experimental design are: (*i*) to provide enough sulfite at t_0 to ensure we generate significant enough quantities of all the product pools so we can measure, at high precision and accuracy, and at multiple [time] points on *f*, the multiple S isotopic composition of each pool (*i.e.*, 2μmols of S per pool per SF_6 measurement on the DI-IRMS, which means 2μmols per fluorination reaction, *see* Section 10.7 for details); (*ii*) to provide the proper reaction conditions to allow DsrAB optimal activity for goal *i* (pH = 7.1, T = 20 or 31°C), while also ensuring DsrAB activity is not diminished by the initial reaction conditions necessary to goal (*i*)—namely, that the 10 or 15mM t_0 sulfite used is not inhibitory, and it is not (Extended Data Figure 4.S2); (*iv*) to ensure hydrogenase activity is not inhibited by the pH chosen (optimum above pH 7.5, activity significantly depleted below pH 6.5, so we chose pH 7.1, to account for optima of both DsrAB and [NiFe]-Hydrogenase); and finally (*v*) to ensure the sulfite to hydrogen ratio favors sulfite over reductant capacity (i.e., pH_2 in the headspace relative to $[sulfite]_{t0}$), such that no more than 70% of t_0 sulfite is consumed to all products, and less than 50% to the reduced S. Finally, (*vi*) determining the sampling interval to

ensure proper distribution of points along *f*, such that applying a closed system distillation model is possible, and statistically robust (*see* Section 10).

In vitro reactions were carried out in 100mL acid-washed, autoclave-sterilized, borosilicate glass bottles sealed with butyl-rubber septa and aluminum crimps. Each bottle contained 50% reaction buffer and 50% gaseous headspace. The headspace gas was initially 95:5 N_2:H_2 during manipulations in the anaerobic chamber, replaced by deoxygenated 100% Ar upon removing the reaction mixture-filled bottles from the chamber, and later exchanged for 100% H_2, to initiate the experiments. Gasses are deoxygenated by passage over hot reduced copper filings as previously described (Rabus et al. 2006). Experimental buffer is 50mM phosphate buffer (KP*i*), initially prepared at pH 6.90±0.05, but final pH is 7.10±0.05 following the addition of the stock Na_2SO_3 solution. All reaction solutions contained the following: 50mM KP*i* buffer (final pH 7.1±0.05), 10 or 15 mM sodium sulfite (Part No. S0505, Sigma-Aldrich), 0.8325 mM methyl viologen (Part No. 856177, Sigma-Aldrich), 315nM fraction #14.5 or 242nM of #14.8 from *D. vulgaris* DsrAB, and 8.25nM [NiFe] hydrogenase (4459 U/mg). Experimental mixtures are prepared in previously boiled and N_2-degassed 18.2MΩ water.

On the bench (prior to working in the anaerobic chamber):

(Step 1) KP*i*: weigh out the KH_2PO_4 and K_2HPO_4 for 1.0L of 50mM KP_i at pH 6.9 (upon sulfite addition, pH 7.1);

(Step 2) weigh out Na_2SO_3 for 10mL of 1M, (KP*i* added in chamber); acid wash enough 100mL serum bottles, and butyl stoppers for 1 per reaction replicate, acquire Al-crimp seals, decrimper and crimper;

(Step 3) Prepare the 277.5mM MV with Hydrogenase (50uL per 100mL reaction), pre-reduce under 100% H_2, to do this: first add MV to a 10mL (acid-washed) serum vial, then add 18.2MΩ H_2O and dissolve, then add the Hase[NiFe] hydrogenase, and alternate H_2/vacuum until the mixture is a deep blue;

(Step 4) add 100uL DsrAB per replicate to a 10mL (acid-washed) serum vial, cap and crimp cap and flux under vacuum/H_2; maintain all enzymes on ice until incubation begins.

In the anaerobic chamber (95:5 N_2:H_2):

(Step 5) add 10mL of KP_i to the Na_2SO_3 in the volumetric flask by 5mL glass pipette (acid-washed), up to the 10mL line, shake until dissolved, add more KP_i until at 10mL, mix;

(Step 6) to the 100mL serum bottles, add 50mL of 50mM pH=6.9 KP_i by glass pipette;

(Step 7) Add to f/c 10 or 15mM Na_2SO_3 from the 1M solution;

(Step 8) add the methyl viologen Hydrogenase mixture to all bottles;

(Step 9) add DsrAB, 0.1mL, to appropriate bottles, mix well;

(Step 10) Remove 1.0mL for Fuschin assay, cyanolysis, and Cline from all bottles, and place samples into 1.5 or 2mL microcentrifuge tubes on ice;

(Step 11) cap and crimp all bottles, remove from chamber. *Back on the bench*:

(Step 12) flux all bottles under vacuum/H_2 on the bench; note the color becomes *blue*, after 3 fluxes as the hydrogenase reduced the methyl viologen, continue to 5-total flux cycles.

(Step 13) Place at 20 or 31°C, given the experiment, shaking at 150 r.p.m in a shaking water bath; except for the t_0 samples, which are immediately sacrificed and frozen.

(Step 14) At each successive time-point, samples are removed via-Ar degassed syringe/needle for Fuschin, cyanolysis, and Cline, then the entire reaction mixture (still in the original 100mL serum bottle) is flash frozen in dry-ice ethanol slurry to rapidly cease DsrAB and hydrogenase activity.

Notes: Each 50mL bottle is prepared/incubated/sampled, in duplicate, per time point, per condition set. Bottles are not allowed to rise above 0°C (kept in freezer at -20°C or on ice during later manipulations) until after the extraction procedure is initiated (see below). The sampling intervals were determined by running the experiments previously in single volumes (in triplicate) prior to the 'isotope' experiment, subsampling for the analytical assays.

4.2.3 Operational definitions of S moieties

In this study we measure the concentrations of three pools: sulfite, trithionate, and thiosulfate (see *Section 10* below), and attempted to measure sulfide (none found); we measure the major and minor sulfur

isotopic compositions of three operationally defined pools: 'reactant' sulfite (initial and residual), product 'sulfonate', and 'reduced product' S. What we refer to as the pooled product 'sulfonate' sulfurs are known in inorganic chemistry as sulfuryl groups ($O_2S\text{-}X_2$), where here one of the X's represents an O^-/OH and the other a S in oxidation state +2 or 0, meaning the outer sulfurly-S is in approximately oxidation state +4, the same as initial and residual reactant sulfite sulfur (SO_3^{2-}). The sulfonate S differs from sulfite S in that it is bound to either an approximately 0 valent sulfur in thiosulfate ($S\text{-}S(O)_3^{2-}$) or as two sulfonates bound to a central approximately 2+ sulfur, in trithionate ($(O_3S\text{-}S\text{-}SO_3)^{2-}$). In this study we refer to the 2+ and 0 oxidation state sulfurs from trithionate and thiosulfate as 'reduced product' S, because they are grouped by our operational extraction (see Section *10*). For explicit definitions and nomenclature refer to the 'IUPAC Goldbook'(McNaught & Wilkinson 1997).

4.2.4 *A. fulgidus* DsrAB in vitro experiments

To extend our studies to a different taxonomic form of the enzyme, we used DsrAB from the thermophilic archaeon *A. fulgidus*. This enzyme operates at higher temperature and does not have DsrC present in the complex. Though these results are significantly limited compared to those with *D. vulgaris*, due to too few time points to apply the closed-system model (specifically due to significantly low sample sizes of reduced S for isotope measurements, note the effort made to correct the two data points on reduced *A. fulgidus* S, *see* Section 10.7), the results are comparable, when considering the measured $\delta^{34}S$. The values for these experiments are presented with *D. vulgaris* values in Extended Data Figure 4.S5.

Archeal (*Archaeoglobus fulgidus*) DsrAB experiments were conducted at one initial sulfite concentration and temperature (15mM and 65°C, respectively) and showed consistent loss of sulfite and accumulation of products between replicates. We selectively precipitate, separate, and directly measure the $^{32}S\text{-}^{33}S\text{-}^{34}S\text{-}^{36}S$ compositions (as described above) from the residual reactant ('sulfite S'), the 'sulfonate S' ($(SO_3)_x$), and only the $^{32}S\text{-}^{34}S/^{32}S$ compositions of the 'reduced product S' [$(S)_y$] reservoirs (again, due to significantly small reduced S samples). From these experiments were only able to get a complete set of samples (i.e. sulfite, sulfonate and

reduced S) from one-time point, and partial sets from another. We are unable to calculate the $^{34}\varepsilon_{DsrAB}$ directly using our model from the *A. fulgidus* DsrAB sulfite reduction experiments because of the dearth of time points (points of *f*), but highlight the values of the measured sulfite, sulfonate and few reduced S moieties are consistent with those by *D. vulgaris* (Extended Data Figure 4.S5) This general agreement between *D. vulgaris* and *A. fulgidus* DsrAB, independent of temperature or phylogenetic origin is perhaps unsurprising, given that previous theoretical predictions deemphasize the role of temperature in determining the magnitude of *kinetic* isotope effects (Bigeleisen & Wolfsberg 1958).

Section 4.3. In vitro fractionation experimental mass balance

Mass balance closes in all 33 individual reactions (grey squares) within a conservative window of +/-10% $[sulfite]_{t0}$ (lightest grey dashes), and 27 of 33 within +/-5% $[sulfite]_{t0}$ (darker grey dashes). Even so, the majority of this variance is due to noise in the sulfite quantification assay ('Fuschin'). In all instances when the mean mass balance is outside +/-10% of closure, it is less than $[sulfite]_{t0}$. Oxidative loss of sulfite during the Fuschin assay is commonly observed with standards let to sit over time (>1 hour following addition of reagents, or exposed to atmospheric oxygen during the assay), therefore we argue increased variance is due solely to the sulfite concentration determinations. Indeed, we only over-estimate mass balance in one replicate, and by < 5%.

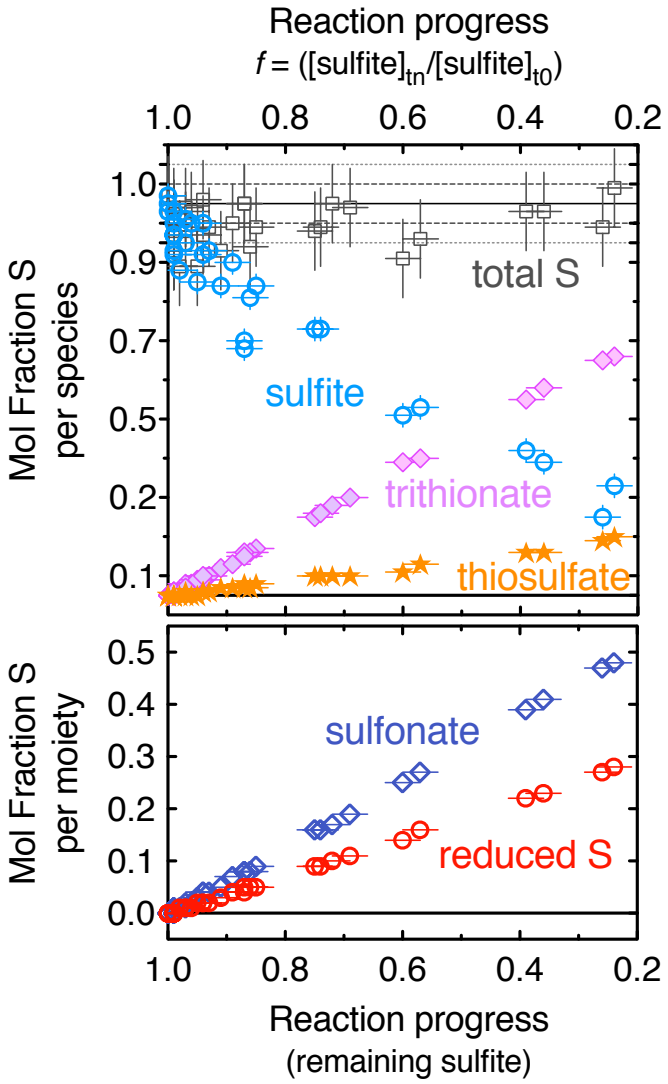

Extended Data Figure 4.S3. (Top) The mol fraction of S in each of the reactant (sulfite) or product (trithionate (mauve diamonds), thiosulfate (orange stars)) pools as a function of reaction progress (f), scaled to initial sulfite concentration ($[sulfite]_{t0}$). (Bottom) Product pools re-scaled by the more oxidized (sulfonate, diamonds) and more reduced S moieties (circles). The slopes of the product pool mol fractions over f are near constant. Data is compiled in Extended Dataframe S1, which is formatted to be directly input to the *R*-coded model.

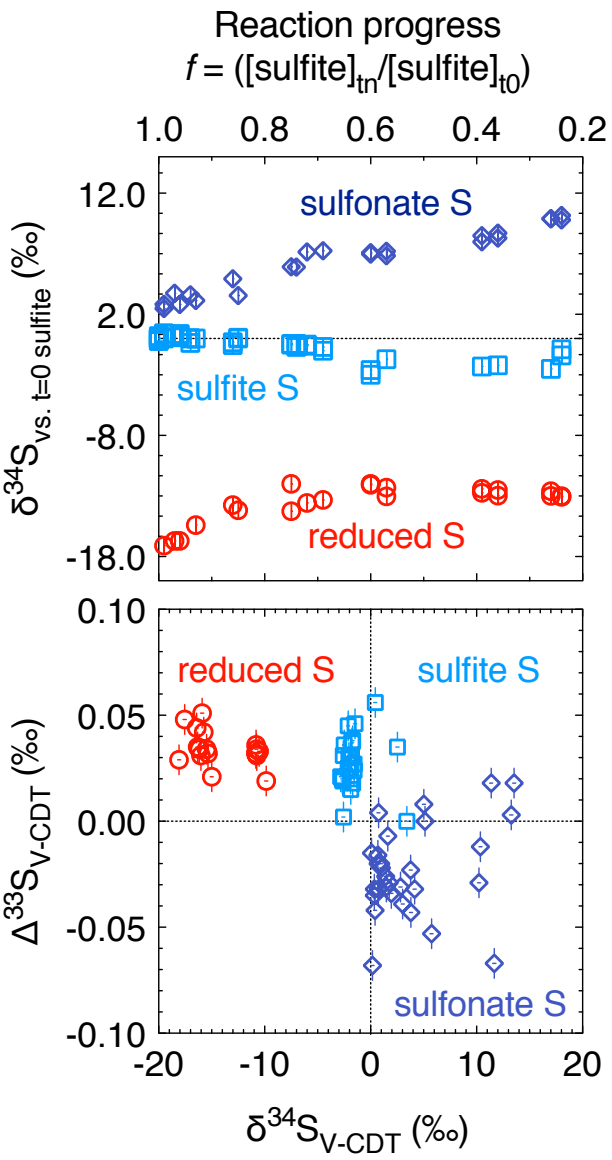

Extended Data Figure 4.S4. Major and minor isotope data from closed-system *D. vulgaris* DsrAB sulfite reduction experiments. (top) The fractionation between sulfite and sulfonate S or reduced S, as a function of *f* (with respect to initial sulfite). Analytical errors are the vertical bars, 1σ = 0.15‰ in $\delta^{34}S$. (bottom) Multiple sulfur isotopic compositions of the three operationally defined pools plotted as $\Delta^{33}S$ versus $\delta^{34}S$ scaled to the international scale V-CDT. Note: the same relation exists for $\Delta^{36}S$ vs. $\delta^{34}S$, with appropriate errors (data compiled in Extended Dataframe S1). Analytical errors are the horizontal bars: 1σ = 0.15 in $\delta^{34}S$ and vertical bars 1σ = 0.007 in $\Delta^{33}S$.

Section 4.4. Major and minor S isotope data from in vitro *D. vulgaris* experiments.

Sulfite reduction reactions were performed *in vitro* under strict anoxia with H_2, [NiFe] hydrogenase and methyl viologen as the electron donor system (see Section 2.2). DsrAB was purified following established protocols from *D. vulgaris* cells, and showed consistent activity over the range of sulfite conditions tested and a K_m well below the sulfite concentrations utilized (Extended Data Fig. 4.S2). The products are thiosulfate ($(S\text{-}SO_3)^{2-}$) and trithionate ($(O_3S\text{-}S\text{-}SO_3)^{2-}$) – with no detectable sulfide. This is consistent with previous reports, given the absence of active DsrC (Oliveira, Vonrhein, Matias, Venceslau, P. M. Pereira, et al. 2008b; Bradley et al. 2011), though under in vitro where DsrC is functional or sulfite concentrations are limiting, sulfide has been detected(H. E. Jones & Skyring 1975; H. E. Jones & Skyring 1974). In order to simplify the in vitro reactions occurring to focus on the DsrAB fractionation factors, we bias the system toward only the earliest parts of the sulfite reduction reaction sequence (i.e. the binding and reduction of sulfite, with concomitant thionate production due to scavenging of partially reduced sulfite from the DsrAB by free sulfite). We tracked the concentrations of reactants and products in each reaction vessel, closing mass balance within analytical error (Extended Data Figure 4.S3). The major sulfur isotopic composition ($\delta^{34}S$, $\delta^{33}S$) was measured at each time point on the residual sulfite as well as two operationally defined sulfur moieties, extracted from the pooled thionate products. Pooled products were grouped (physically extracted and isolated) and isotopically analyzed as (*i*) the bound unreduced sulfite ('sulfonate') moieties from thiosulfate and trithionate and (*ii*) the reduced S moieties of thiosulfate and trithionate, hereafter referred to as 'reduced S' (*see* Section 4.2.3). Products were generated at a constant ratio throughout the *in vitro* closed-system experiments, with 18±4% of the product sulfur forming thiosulfate and the remainder trithionate (Extended Data Figure 4.S4). These results are broadly consistent with additional experiments using DsrAB from the model hyperthermophilic Archeal sulfate reducer *Archaeoglobus fulgidus* (Extended Data Figure 4.S5 and Table 4.S1).

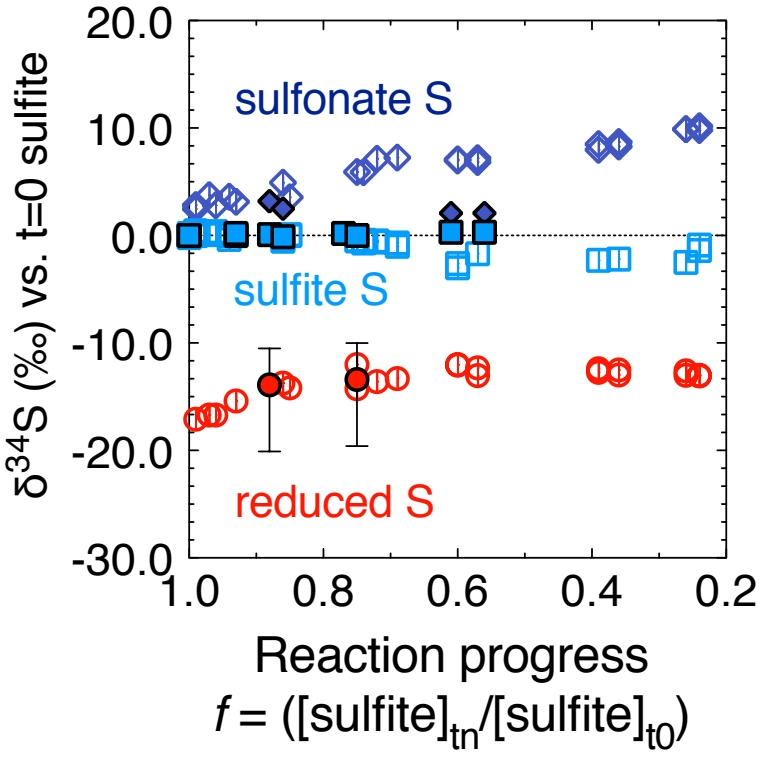

Extended Data Figure 4.S5. Major isotope ratios relative to the composition of sulfite at t_0, for the *A. fulgidus* (closed symbols) and *D. vulgaris* (open symbols) experiments both as a function of reaction progress. There is a clear consistency between the samples sets, particularaly at thre reduced sites, which is most important for tracking the fractionation during the reduction of sulfite by DsrAB. Note: the un-even error bars on reduced S moieties are a function of the non-linearity in correcting for the small sample sized from the isotope ratio measurements (explained in 4.10.6). Data compiled in Extended Data Table 4.S1

Extended Data Table 4.S1 (on following page). The final corrected *A. fulgidus* data on V-CDT and V-t_0_sulfite scales. We include samples measured at standard analytical masses (0.35 to 0.45mg), yielding the appropriate small standard errors, 1σ = 0.3‰.

Extended Data Table 4.S2 (from previous page).

ID	*f*	$\delta^{34}S_{V\text{-}CDT}$ sulfite V-CDT)	Std Err (‰)	$\delta^{34}S_{V\text{-}CDT}$ sulfonate	Std Err (‰)	$\delta^{34}S_{V\text{-}CDT}$ reduced S	CI_{95} Lower (‰)	CI_{95} Upper (‰)
0A	1	-2.7	0.3	n.d.	-	n.d.	-	-
1A	0.93	-2.7	0.3	n.d.	-	n.d.	-	-
2A	**0.88**	**-2.6**	**0.3**	**0.5**	**0.15**	**-16.57**	**-22.73**	**-13.22**
3A	0.77	-2.5	0.3	n.d.	0.15	n.d.	-	-
4A	0.61	-2.4	0.3	-0.6	0.15	n.d.	-	-
0B	1	-2.7	0.3	n.d.	-	n.d.	-	-
1B	0.93	-2.5	0.3	n.d.	-	n.d.	-	-
2B	0.86	-2.8	0.3	-0.18	0.15	n.d.	-	-
3B	**0.75**	**-2.7**	**0.3**	**n.d.**	**-**	**-16.05**	**-22.21**	**-12.66**
4B	0.56	-2.4	0.3	-0.57	0.15	n.d.	-	-

ID	*f*	$\delta^{34}S_{V\text{-}t0\_SO3}$ sulfite (V-t0 sulfite)	Std Err (‰)	$\delta^{34}S_{V\text{-}t0\_SO3}$ sulfonate	Std Err (‰)	$\delta^{34}S_{V\text{-}t0\_SO3}$ reduced S	CI_{95} Lower (‰)	CI_{95} Upper (‰)
0A	1	0	0.3	n.d.	-	n.d.	-	-
1A	0.93	0	0.3	n.d.	-	n.d.	-	-
2A	**0.88**	0.1	**0.3**	3.2	**0.15**	-13.9	-20.1	-10.5
3A	0.77	0.2	0.3	n.d.	0.15	n.d.	-	-
4A	0.61	0.3	0.3	2.1	0.15	n.d.	-	-
0B	1	0	0.3	n.d.	-	n.d.	-	-
1B	0.93	0.2	0.3	n.d.	-	n.d.	-	-
2B	0.86	-0.1	0.3	2.5	0.15	n.d.	-	-
3B	**0.75**	0	**0.3**	n.d.	**-**	-13.4	-19.6	-10
4B	0.56	0.3	0.3	2.1	0.15	n.d.	-	-

Section 4.5. Closed-system fractionation model development and implementation

4.5.1 Fractionation Factor Model Overview

Calculation of the isotopic fractionation imposed by the reduction of sulfite through DsrAB required measurement the consumption of the reactant, the accumulation of the products, and the isotopic composition of reactants and products as the reaction progressed. This allowed application of a closed-system model and calculation of a fractionation factor.

In the case of the reduction of sulfite by DsrAB, the standard closed-system (Rayleigh) isotope distillation model is complicated by the fact that DsrAB yields two major products: trithionate and thiosulfate, each of which contains sulfur moieties in more than one oxidation state. These products are likely to be minor products *in vivo* (L A Chambers & Trudinger 1975), but are the major products accumulated *in vitro*, as has been documented in previous studies (Kobayashi et al. 1974; Drake & Akagi 1977; Drake & Akagi 1978; Suh & Akagi 1969; Drake & Akagi 1976). Here, we outline the approach have taken to determine the sulfur isotope fractionation between sulfite and these products.

First, our *in vitro* reactions were terminated after various amounts of time, yielding a range of the fraction (f) of reactant sulfite remaining. The concentrations of sulfite, trithionate, and thiosulfate were measured at each time-point by the methods outlined above. For isotopic measurements, we were unable to preoperatively separate trithionate from thiosulfate with sufficient yield for independent determination of their isotopic compositions, due to lack of an established and reliable trithionate and thiosulfate separation protocol (a target for future work). Given this mixed product pool, we obtained quantitative separation of the oxidized (sulfonate) moieties deriving from trithionate and thiosulfate from the partially reduced (S^{2+} and S^0) moieties of both products. We then measured the isotopic compositions of the pooled oxidized and pooled reduced moieties. Information about the concentrations of trithionate and thiosulfate allowed calculation of how the isotope distribution must have occurred.

This was accomplished with a simple model described below. Scripts for the application of this model are available in a repository at:

https://github.com/bradleylab/DsrAB_enzyme_models.

4.5.2 Sulfur Pools

We track the three pools of sulfur that constitute the system:

Sulfite: reactant pool, molecule containing a single sulfur atom

Thiosulfate: product pool, molecule containing two sulfur atoms – a partially oxidized *sulfonate* moiety in the same redox state as sulfite (+4), and a partially reduced (S^{2+}) moiety

Thiosulfate: product pool, molecule containing three sulfur atoms – two oxidized *sulfonate* moieties in the same redox state as sulfite (+4), and a more reduced (S^{0}) moiety

We have assumed that the oxidized moieties in both thionates form through a side reaction between sulfite and the reduced (or partially reduced) sulfur atom at the active site of DsrAB. This reaction is predicted to occur *in vivo* under high intracellular sulfite concentrations(Bradley et al. 2011) and *in vitro* given high sulfite concentrations and the absence of DsrC(Oliveira, Vonrhein, Matias, Venceslau, P. M. Pereira, et al. 2008b). Conditions predicted to produce thionates are not essential to the isotopic model that follows, but allow a more intuitive understanding of the reactions involved.

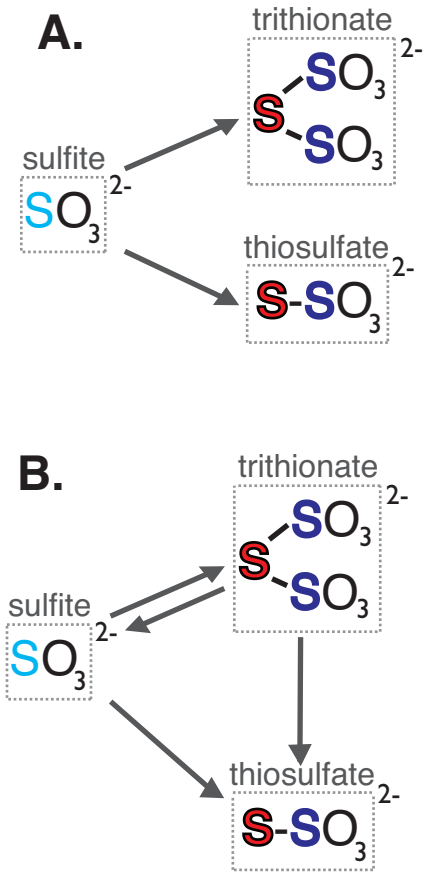

Extended Data Figure 4.S6. Reaction topology for closed-system models. (A) Section 5.4, the simple model for early in the experiments ($f > 0.85$). (B) Section 5.6 yields a more complex reaction model for later in the closed-system experiments ($f < 0.85$).

4.5.3 Data constraints that drive the model

We made direct measurements of concentrations and sulfur isotopes on the chemical species listed here:

Concentration measurements: sulfite, thiosulfate, trithionate

Isotopic measurements: sulfite, sulfonate (pooled from thiosulfate and trithionate), reduced S (pooled from thiosulfate and trithionate)

4.5.4 The simple model network topology ($f > 0.85$)

Our model assumes five pools of sulfur:

A: sulfite

B: thiosulfate S^0

C: thiosulfate sulfonate

D: trithionate S^{2+}

E: trithionate sufonyl.

That is, a reactant pool of sulfite (A) and two product pools: thiosulfate (B&C) and trithionate (D&E). Our isotopic measurements consist of sulfite (A), pooled reduced S (B+D), and pooled sulfonate (C+E).

In order to calculate the isotopic fractionation associated with each of these pools, our first approach is to define a total isotopic fractionation of the reaction (α_{total}). This *total fractionation* is the fractionation applied between reactant (sulfite) and the pooled products (both trithionate and thiosulfate; B&C+D&E).

4.5.5 Solving the model:

This reaction network makes several assumptions.

Assumption 1: There is no difference in the $\delta^{3x}S$ among SO_3 and the tautomers of bisulfite with which sulfite is in dynamic equilibrium (i.e. these are treated as a single pool)

Assumption 2: The proportion of thiosulfate to trithionate formed is invariant between the start of the reaction and the time at which we measure pools. This proportion is described in our model as the constant *j*, where *j* is equivalent to the total number of moles of sulfur in thiosulfate divided by the total number of moles of sulfur in

thiosulfate plus trithionate. The assumption that *j* is constant is consistent with estimates of *j* inferred from concentration measurements made throughout the course of the reactions.

Assumption 3: The $\delta^{3x}S$ of the two sulfonate groups of trithionate are identical.

Assumption 4: The $\delta^{3x}S$ of B is equal to that of D, and the $\delta^{3x}S$ of E is equal to that of C. The justification for this assumption is that B and D (and similarly, C and E) have undergone nearly identical chemical reactions. For the reduced pools (B&D), the reduction was via DsrAB at the same active site – the difference being only the number of electrons transferred. This is the most parsimonious assumption. It will be testable in the future when if we can separate trithionate and thiosulfate and then isolate their oxidized and reduced moieties.

For each experiment, we have collected data from which we make the following calculations:

1. Calculate *j*, the relative proportion of sulfur fluxing to thiosulfate:

Equation S5.1 $j = 2*(\text{mols thiosulfate}) / [2*(\text{mols thiosulfate}) + 3*(\text{mols trithionate})]$

2. Calculate *f*, the fraction of reactant remaining:

Equation S5.2 $f = [\text{sulfite concentration at time t}]/[\text{sulfite concentration at time 0}]$

3. Calculate *R*, the ratio of $^{3x}S/^{32}S$ for the isotope of interest (^{3x}S = ^{34}S, ^{33}S, or ^{36}S), based on the measured $\delta^{3x}S$ for:

R_{red} = the ratio of $^{3x}S/^{32}S$ in B+D

R_{ox} = the ratio of $^{3x}S/^{32}S$ in C+E

R_a = the ratio of $^{3x}S/^{32}S$ in A (i.e. in sulfite)

R_{ao} = the ratio of $^{3x}S/^{32}S$ in sulfite at the beginning of the experiment (time 0)

We can then calculate the ratio of $^{3x}S/^{32}S$ in the pooled product, R_p

Equation S5.3 $$R_p = \left[\frac{1}{2}j + \frac{1}{3}(1-j)\right]R_{red} + \left[\frac{1}{2}j + \frac{2}{3}(1-j)\right]R_{ox}$$

4. Calculate α_{total}. This can be calculated by one of two equations

First, using the residual sulfite pool

Equation S5.4 $$\alpha_{total} = \frac{\ln\left(\frac{R_a}{R_{a0}}\right)}{\ln(f)} + 1$$

Or second, using the pooled product and initial sulfite

Equation S5.5 $$\alpha_{total} = \frac{\ln\left(\frac{R_p}{R_{a0}}(f-1)+1\right)}{\ln(f)}$$

5. Calculate the fractionation between sulfite and the reduced & oxidized moieties of the products. The parameter α_{red} represents the fractionation between sulfite and the reduced sulfur moieties (B&D). The parameter α_{ox} represents the fractionation between sulfite and the oxidized sulfonate moieties (C&E). The form of the equation is similar for both α_{red} and α_{ox}:

Equation S5.6 $$\alpha_x = \frac{R_x}{R_{a0}} \frac{\alpha_{total}}{(f^{\alpha_{total}-1})}(f-1)$$

6. Fractionations are converted to fractionation factors by

Equation S5.7 $$\varepsilon_x = 10^3(\alpha_x - 1)$$

7. The minor isotope parameter λ is calculated as

Equation S5.8 $$^{3x}\lambda = \frac{ln(^{3x}\alpha)}{ln(^{34}\alpha)}$$

4.5.6 A more complex network ($f < 0.85$), i.e. mixing of multiple fractionation factors

The approach outlined above yielded results in which the observed fractionation factor between sulfite and reduced pools (B&D) appeared to change as a function of *f.* One explanation for this apparent behavior is that the reduced pool is not the product of a single set of reactions but of multiple reactions.

The most plausible explanation for this is that some fraction of the reduced pool (B&D) is derived from the sulfonate pool (C&E) rather than being derived solely from sulfite. Previous work (Parey et al. 2010; Drake & Akagi 1978; Drake & Akagi 1977) has demonstrated that DsrAB is capable of reducing trithionate to thiosulfate, and thiosulfate to sulfite and sulfide.

Reduced S pool

We can constrain the magnitudes of the fractionation factor related to the conversion of the sulfonate to reduced S through the following steps.

1. Utilize the framework given above to solve for α_{red} for the time points where f is nearest to 1. As these measurements are obtained at the lowest concentrations of product, we assume that this result gives an estimate α_{red} that reflects the production of reduced S from sulfite only, with minimal input of reduced S derived from sulfonate.

2. Write an equation for R_{red} as a function of α_{red}, R_{SO3}, and R_{ox}

Equation S5.9 $$R_{red} = X_{SO3}\alpha_{red}R_{SO3} + (1 - X_{SO3})\alpha_{unk}R_o$$

where X_{SO3} is the fraction of R_{red} generated directly from sulfite and α_{unk} is the unknown fractionation factor between R_{ox} and R_{red}. This equation is then rewritten and solved for α_{unk} as a function of the other parameters over a range of values of X_{SO3} $(0.01 – 0.99)$.

This does not yield a unique solution for the unknown fractionation, but constrains its value given the relative importance of the contribution to the reduced sulfur pool of both sulfonate and sulfite. We assume that the *relative* contribution of the secondary reaction is invariant over the course of the reaction, thereby manifesting as no change in *j*. Model outputs are presented in Extended Data Figure 4.S7, and re-scaled to epsilons in Figure 4.2.

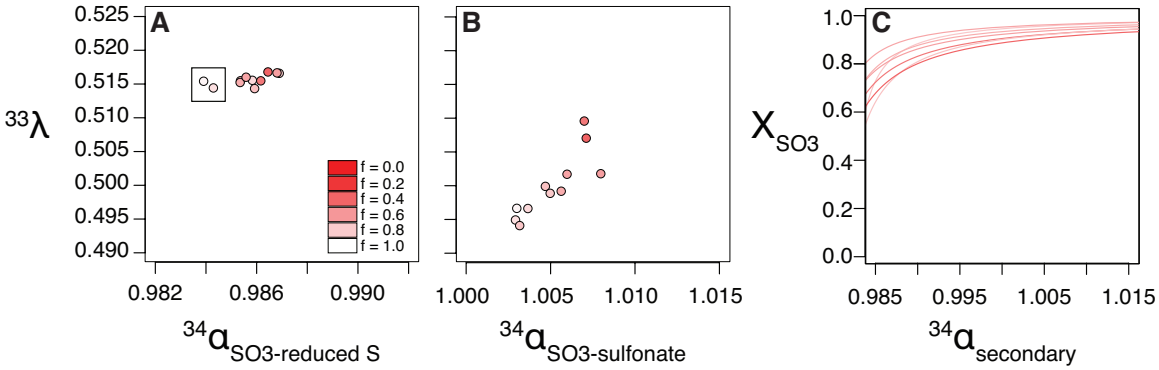

Extended Data Figure 4.S7. Sulfur isotope fractionation by bacterial DsrAB. (A) Fractionation between sulfite and the reduced sulfur moieties of trithionate and thiosulfate. Initial values of $^{34}\alpha$ are near 0.9847 ($^{34}\varepsilon$ = 15.3‰), and increase with decreasing *f* (*f* = fraction of reactant sulfite remaining). The exponent $^{33}\lambda$, relating ^{33}S and ^{34}S fractionation is stable near 0.5145, which can indicate kinetic breaking of an S-O bond, or equilibrium exchange, but is not mutually exclusive of one or the other**(Young et al. 2002)**. The box indicates the two points with highest *f*, selected to represent the fractionation of sulfite in the isotope-mixing model (panel C). (B) Fractionation between sulfite and the sulfonate moieties of trithionate and thiosulfate. Values of $^{34}\alpha$ range between 1.002 and 1.007, and all $^{33}\lambda$ values are < 0.510, suggesting a kinetic control on fractionation. (C) Relationship between the magnitude of a secondary fractionation ($^{34}\alpha_{secondary}$) and the proportion of reduced sulfur deriving directly from sulfite reduction (X_{SO3}). The balance (1- X_{SO3}) is from the parallel reduction of bound sulfonate.

4.5.7. Simple calculations to estimate the nature of DsrAB sulfite reduction reactions: kinetic *versus* equilibrium.

Triple isotope systems obey mass-dependent fractionation laws that differ for kinetic and equilibrium fractionation(Young et al. 2002). In the sulfur isotope system, this results in:

Equation S5.10 $$^{33}\alpha = {}^{33}\alpha^{\lambda}$$

where $^{33}\alpha$ is the fractionation factor that relates two ratios $^{33}S/^{32}S$ and $^{33}\alpha$ is the fractionation factor relating two ratios of $^{34}S/^{32}S$. The exponent λ is used to describe the relationship of these two fractionations. In equilibrium fractionations, the value for λ derives from the quantum part of the partition function, and depends only on the atomic masses, such that:

Equation S5.11 $$\lambda = \frac{\frac{1}{32} - \frac{1}{33}}{\frac{1}{32} - \frac{1}{34}} = 0.515$$

During kinetic fractionations, the value for λ derives from the classical part of the partition function, such that:

Equation S5.12 $$\lambda = \frac{\ln(M_1 / M_2)}{\ln(M_1 / M_3)}$$

where M1, M2, and M3 could represent the "reduced, molecular, or atomic masses" (states Young et al., 2002)(Young et al. 2002) depending on the nature of the reaction. If the reduction of sulfite is a kinetic process, the magnitude of its fractionation should be controlled by the

breaking of bonds between sulfur and oxygen, and from the formation of a bond between sulfur and iron (at the active site siroheme in Dsr). Making and breaking bonds requires the use of reduced mass in the partition function. In Extended Data Table S2 we show the predicted kinetic λ for each of these scenarios, using masses 32, 33, and 34 for sulphur, 16 for oxygen, and 56 for iron.

Extended Data Table 4.S3.

Relevant species	M1	M2	M3	lambda
S	32	33	34	0.507
SO_3^{2-}	80	81	82	0.503
S-Fe	20.36	20.76	21.16	0.510
S-S	16.00	16.25	16.48	0.511
S-O	10.67	10.78	10.88	0.513

This table of results shows that the value of λ during kinetic fractionation is not constant, and can have a wide range of values. Typically, the kinetic λ is assumed to be near 0.507, although this applies only to processes where the relevant mass is the atomic masses of the three isotopes of S. Transport processes applying to sulfite would be expected to have a value of λ near 0.503, while processes involving the making or breaking of S-O bonds should be expected to have a λ near 0.513, which approaches the equilibrium value. In light of this understanding, and the fact that sulfite reduction must necessarily involve the breaking of an S-O bond, we interpret the value of λ calculated from the reduction of sulfite to be unable to distinguish between a kinetic and equilibrium fractionation.

Section 4.6. Statistical re-analysis of laboratory and sedimentary fractionation data

To apply the compiled sedimentary sulfate reduction rates from Goldhaber & Kaplan(Goldhaber & Kaplan 1975) we re-plot their log-scale values to a linear scaling and apply the same non-linear regression one-phase decay model (Equn. S6.1) from our recent work on fractionation—rate relationships in MSR(Leavitt et al. n.d.), minimizing variance to arrive at the following parameters: Y_0 = 73‰, plateau = 12.3‰, and a decay-constant (K) of 6.4 (Extended Data Figure. 4.S8)

Equation S6.1 $$Y = (Y_0 - \text{Plateau}) \times e^{(-K \times X)} + \text{Plateau}.$$

For the chemostat (open-system) MSR data in the study where we derived this regression model(Leavitt et al. n.d.), we re-scale the cell-specific MSR rates to basic volumetric fluxes by multiplying out the number of cells at each sampling point, using the Database S1 values in Leavitt et al(Leavitt et al. n.d.). Applying the same one-phase decay model and minimize variance, we calculate the following parameters: Y_0 = 56.5‰, plateau = 17.2‰, and a decay-constant (K) of 0.054. All regressions were calculated using *Prism5c* (GraphPad, San Diego, CA).

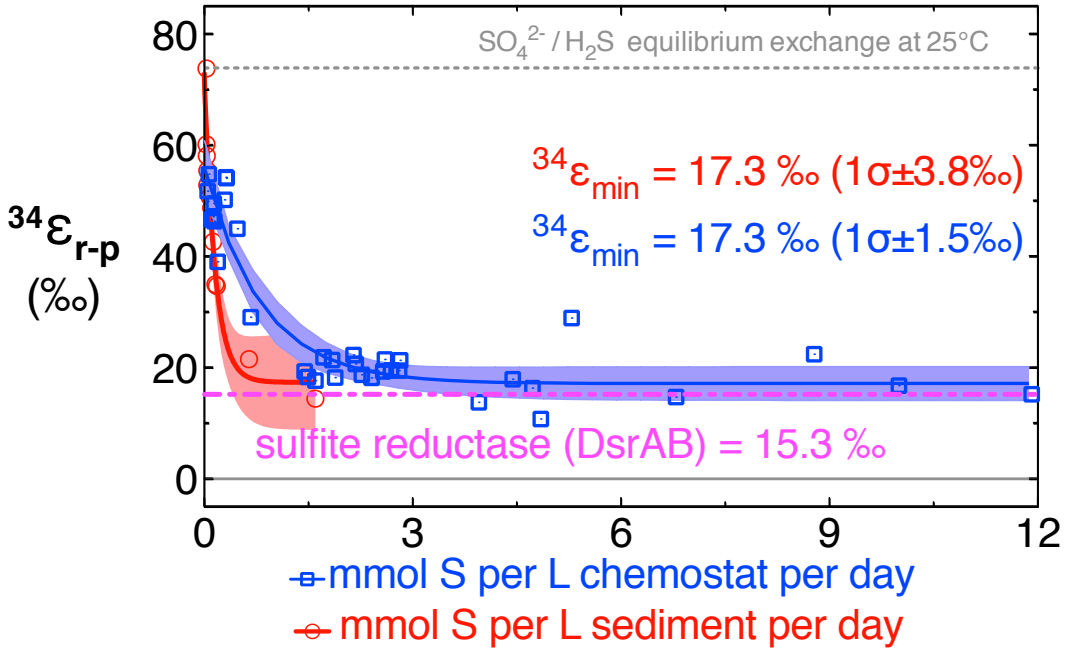

Extended Data Figure 4.S8. Non-linear regression model outputs (shaded areas) with chemostat (blue) and sediment (red) data recalculated as described in the text above. The regression-model estimates for the minimum fractionation factors in each system (inset values) are statistically indistinguishable from the sulfite reduction fractionation factor we measure from our in vitro experiments (pink dash). The Y-intercepts are not identical, likely due to the added complexity in natural sediments (e.g., oxidation and disproportionation reactions and slower MSR rates). The theoretical sulfate—sulfide equilibrium fractionation, calculated at 25°C(Tudge & Thode 1950), is provided for reference (grey dash).

Section 4.7. Compilation and statistical analysis of pure-culture MSR fractions

To place our DsrAB enzyme-specific fractionation factor in context with the previous 60+ years of pure-culture experimental work, we compile all available observations from studies using axenic cultures of MSR, in the following experimental systems: *batch* (closed-system, in vivo, whole-cell), *chemostat* (open-system, in vivo, whole-cell), *resting* (closed-system, in vivo, whole-cell, not growing), *cell-free* (closed-system, ex vivo crude cell extracts, not growing). From these four types of experiments we further subdivide experiments into where sulfate was reduced to sulfide or sulfite was reduced to sulfide. We count each experimental determination ($^{34}\varepsilon_{r\text{-}p}$) and compile them all in Extended Data Table 4.S4, from experiments where less than 10% of the reactant S-species was consumed. Herein we calculate and present column statistics (box-whisker plots in Extended Data Figure 4.S9, Extended Data 4.S1) using *Prism5c* (GraphPad, San Diego, CA). The key finding here is that the majority of the means from each set of experiments is significantly less than the previous estimates for the fractionation factor associated with Dsr (25-53‰, (Harrison & Thode 1957; Rees 1973; Brunner & Bernasconi 2005; J. Farquhar et al. 2003; Johnston et al. 2007)), and that the mean values from all 650+ experimental determinations, regardless of experiment type or whether it was a sulfate-sulfide or sulfite-sulfide experiments, the grand mean for $^{34}\varepsilon_{r\text{-}p}$ falls at 17.9‰, with the 95% confidence interval spanning 17‰ to 18.9‰, and the 25th and 75th percentile's falling at 10‰ and 22.5‰, respectively (Extended Data Figure 4.S8, Extended Data Table 4.S3) – these are all well within the maximum fractionation due to the sum of our DsrAB value (15.3‰), and our literature derived estimate for sulfate reduction to sulfite (~11±4‰), a total of ~26.3±4‰ (*see* Section 4.8) .

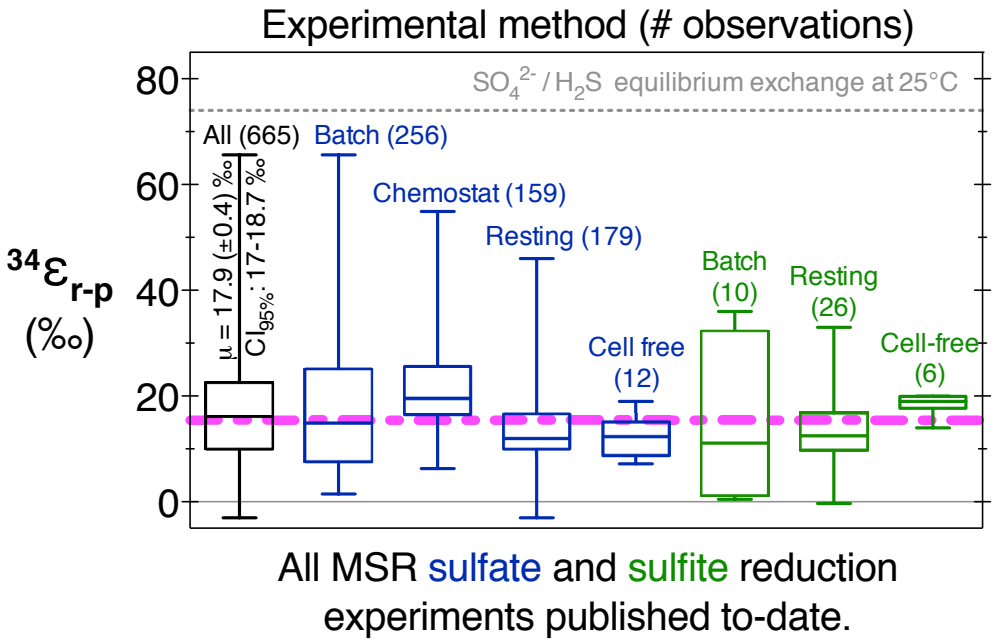

Extended Data Figure 4.S9. Box-whisker plots of the all published sulfate (blue) or sulfite (green) reduction experiments as of April 2014. All data are summarized in black (left-most box-whisker, with column statistics inset). The pink dash indicates the measured value for sulfite reduction by DsrAB we calculate in this study.

Extended Data Table 4.S4 (continued on next page). Column statistics on known literature compilation of MSR observed $^{34}\varepsilon_{r\text{-}p}$. Experimental method and reactant (*r*) pool (*r* = sulfate (SO_4^{2-}) or sulfite (HSO_3^-/SO_3^{2-})) are indicated in each column. In all experiments considered for this compilation the product (*p*) was sulfide ($H_2S/HS^-/S^{2-}$). References for the compilation used in the column statistical calculations for this table: (Harrison & Thode 1958; Harrison & Thode 1957; Krouse et al. 1968; MCCREADY et al. 1975; MCCREADY 1975; Sim et al. 2012; Sim et al. 2013; Sim, Ono, et al. 2011c; Sim, Bosak & Ono 2011a; Johnston et al. 2007; Johnston 2005; J. Farquhar et al. 2003; Thode et al. 1951; Bolliger et al. 2001; Knöller et al. 2006; Detmers et al. 2001; Galen E Jones 1957; Kleikemper et al. 2004; Mangalo et al. 2008; MANGALO et al. 2007; Canfield et al. 2006; HOEK et al. 2006; Pallud et al. 2007; Böttcher et al. 1999; Smock et al. 1998; Kemp & THODE 1968; Leavitt et al. n.d.; Ford 1957; Lyn A Chambers et al. 1975; Davidson et al. 2009; Habicht et al. 2005; Kaplan & Rittenberg 1964). Note: we define $^{34}\varepsilon$ with the reactant over the product, such that positive values represent an enrichment of the heavier isotope (^{34}S) in the residual reactant and concomitant depletion in the product. This keeps the majority of the values positive, simplifying the application of the statistical model.

Extended Data Table 4.S4 (Continued from previous page).

	All (r/p)	Abiotic (SO_4^{2-}/H_2S)	Batch (SO_3^{2-} /H_2S)	Batch (SO_4^{2-} /H_2S)	Cell-free (SO_3^{2-}/H_2S)	Cell-free (SO_4^{2-}/H_2S)	Chemostat (SO_4^{2-}/H_2S)	Resting (SO_3^{2-}/H_2S)	Resting (SO_4^{2-}/H_2S)
Observations *(n)*	*665*	*17*	*10*	*256*	*6*	*12*	*159*	*26*	*179*
Mean val. (‰)	17.9	21.6	14.9	18.3	18.5	12.4	22.6	13.7	13.9
Std. Deviation (‰)	11.2	1.1	14.8	13.6	2.2	3.7	9.7	7.9	7.3
Std. Error (‰)	0.4	0.3	4.7	0.9	0.9	1.1	0.8	1.5	0.5
Lower $CI_{95\%}$ (‰)	17	21	4.3	16.6	16.1	10.1	21.1	10.5	12.8
Upper $CI_{95\%}$ (‰)	18.7	22.1	25.5	20	20.8	14.8	24.1	16.9	14.9
Minimum val. (‰)	-3	20.1	0.5	1.5	14	7.2	6.3	-0.3	-3
25th percentile (‰)	10	20.6	1.3	7.6	17.7	8.8	16.5	9.9	10
Median val. (‰)	16.1	21.4	11.2	14.9	19	12.4	19.5	12.5	12
75th percentile (‰)	22.5	22.5	32.3	25.1	19.9	15	25.6	16.8	16.6
Maximum val. (‰)	65.6	23.5	36	65.6	20	19	54.9	33	46

Section 4.8. Literature estimates for the fractionations associated with enzyme-mediated sulfate/sulfite S-isotope exchange

To better interpret the full range of major S isotope fractionations compiled from biological (Extended Data Figure 4.S9), sedimentary (Extended Data Figure 4.S8) and geological data sources, in the context of our updated understanding of the MSR pathway (Oliveira, Vonrhein, Matias, Venceslau, P. M. Pereira, et al. 2008b; Parey et al. 2010; Bradley et al. 2011), and DsrAB constrains from this work, we incorporate the only attempts at measuring the enzymatically induced sulfate—sulfite S-isotope exchange (Ford 1957; Kemp & THODE 1968). We note that these values are not determined using purified enzymes (in vitro), nor over a range of reaction coordinate points ($f_{reactant}$, as in Fig. 4.2), nor were attempts made to quantify all the sulfur bearing pools and close mass balance. Still, these estimates from cell-free extracts ($^{34}\varepsilon_{SO4\text{-}SO3\_red}$ = 10.9 ± 3.9‰, CI_{95} ± 1.2‰, n = 37, Extended Data Table 4.S4) (Harrison & Thode 1958; Kaplan & Rittenberg 1964; Kemp & THODE 1968; Ford 1957) represent the only experimentally derived isotope fractionation measurements on the sum of the sulfate activation to APS followed its reduction to sulfite (Extended Data Figure 4.S1, steps *ii* + *iii*). Constraining this aggregated fractionation factor ($^{34}\varepsilon_{SO4\text{-}SO3}$) in vitro is a target for future pure enzyme experiments focusing on the constituent steps (Extended Data Figure 4.S1: step *i*. $^{34}\varepsilon_{SO4\text{-}uptake}$, step *ii*. $^{34}\varepsilon_{SO4\text{-}APS}$, step *iii*. $^{34}\varepsilon_{APS\text{-}SO3}$, and the reverse of each) as well as the minor isotope effects associate with each (*i.e.* the $^{33}\lambda$'s). Given our present understanding of the enzymes involved in this process (Bradley et al. 2011; I. A. C. Pereira et al. 2011), sulfate activation to APS and transport of sulfate into the cytoplasm are not likely to directly impact S-isotope compositions, whereas the reduction of APS by APSr is a strong target for such enzyme-isotope fractionation experiments.

Section 4.9. Relevance to Earth History and Sedimentary Records

Finally, there is a reasonable likelihood that intermediate valence S species reduction (e.g. thiosulfate, polythionates, and in particular sulfite) reducing metabolisms originated prior to complete sulfate reduction(Sousa et al. 2013). This is consistent with both the small range in major S isotope fractionation ($^{34}\varepsilon_{GEO}$) during the Achaean (Fig. 4.S7 (Canfield & J. Farquhar 2009; J. Farquhar et al. 2010)) which may be directly attributable to DsrAB (this study). Further, this hypothesis is supported by two independent lines of evidence: first, Halevy (Halevy 2013) calculates micromolar concentrations of thiosulfate and sulfite may well have been present in Achaean oceans in significant quantities; second, there is independent metagenomic evidence that intermediate-valence S metabolisms arose prior to sulfate reduction (David & Alm 2010). Why might sulfite or thiosulfate reduction originate prior to sulfate reduction? Consider that neither thiosulfate nor sulfite requires an energetically costly activation step prior to becoming a metabolically available terminal electron acceptor. Specifically, dissimilatory sulfate reduction requires Sat and ATP to convert sulfate to APS ($\Delta G^{0'}$ = +46 kJ/mol (R. K. Thauer et al. 1977)). In stark contrast, the metabolic machinery for coupling thiosulfate and sulfite reduction to the intracellular proton motive force and ultimately energy conservation is relatively simple and phylogenetically widely distributed (I. A. C. Pereira et al. 2011). Thus, dissimilatory intermediate S compound reduction may well have originated and evolved prior to complete dissimilatory sulfate reduction. This runs counter to the proposals that dissimilatory sulfate reduction or elemental sulfur disproportionation were responsible for the isotopic fractionations observed in Achaean meta-sedimentary rocks (Ford 1957; Shen et al. 2001; Harrison & Thode 1958; Kaplan & Rittenberg 1964; Kemp & THODE 1968; Habicht et al. 2002; Philippot et al. 2007). Whatever the case, DsrAB was involved, and it is clear that this is a very ancient enzyme that was present in LUCA. Moreover, further constraints on both biotic and abiotic S-cycling (Halevy 2013), mass independent fractionating processes (Masterson et al. 2011; Whitehill et al. 2013), and further metabolism specific major and minor S isotope fingerprinting (Johnston 2011) are needed before our 'best guess' for what S-based microbial energy metabolisms were present in the Archeal can be established. This study demonstrates the importance of direct measurements for interpreting the fractionations observed through a complex biochemical

network. These data inform both our biochemical understanding of the reaction mechanism and the geological interpretation of sulfur isotope records. References in the caption are: (Canfield & J. Farquhar 2009; Ford 1957; Kemp & THODE 1968; Kaplan & Rittenberg 1964; Sim, Bosak & Ono 2011a; Tudge & Thode 1950).

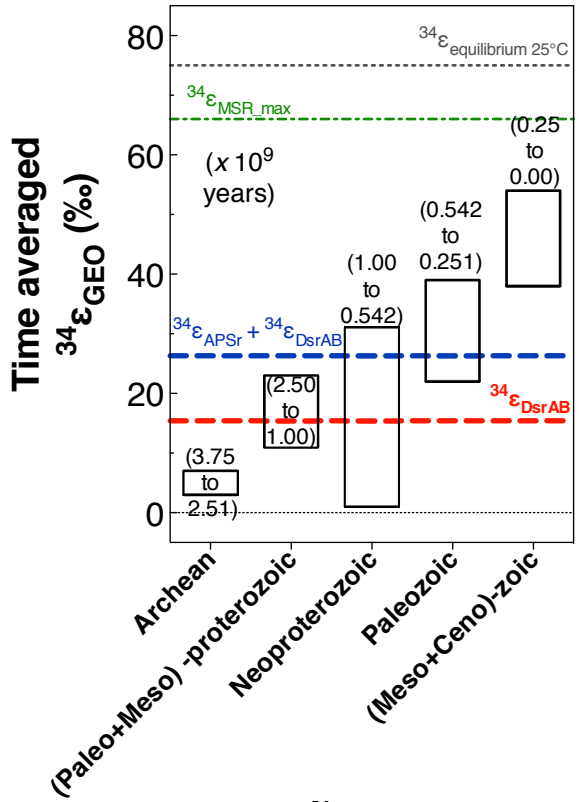

Extended Data Figure 4.S10. The range of $^{34}\varepsilon_{GEO}$ at different intervals in Earth history (compiled in supplement of1 Canfield & Farquhar (2009)1. The open bars are simple the range in mean fractionations from the age bins in Canfield & Farquhar (2009). No further processing was possible given the dearth of sedimentary sulfate values. The red line reperesets the *D. vulgaris* DsrAB measured in this study, the blue line is DsrAB added to our literature-derived estimate for ASPr, drawing from: Ford (1957), Kaplan & Rittenberg (1964), Kemp & Thode (1968). The green is the maximum MSR fractionation measured in Sim et al. (2011), and the equilibrium estimate is the same as in Figures 1 and 3, originating from Tudge & Thode (1950).

Section 4.10. Analytical procedures in detail

4.10.1 Sulfite (HSO_3^-/ HSO_3^{2-}) quantification method

This protocol is built on one developed by Grant (Grant 1947), but is specific to the in vitro DsrAB assay conditions. In short-hand we refer to it as the 'Fuschin' reaction, as originally derived from Grant (1947)(Grant 1947). Background (matrix) matching is critical in this assay. Trithionate, thiosulfate, sulfate, and zinc sulfide (precipitate) do not interact with this the color-reagent. This assay is useful over a range of 0-40 nanomoles of sulfite in the final assay volume, 1mL. Prepare Na_2SO_3 (anhydrous, analytical grade, recently purchased/opened and stored under argon) standards at 0, 31.125, 62.5, 125, and 250uM in 18.2MΩ H_2O, immediately before performing the assay. Work with pre-boiled nitrogen or argon degassed 18.2MΩ H_2O. *Reagents*: (step i) 0.04% w/v Pararosaniline HCl (analytical grade, Sigma-Aldrich) in 10% H_2SO_4 (analytical grade, Sigma-Aldrich) v/v, prepared in 18.2MΩ H_2O by first adding the acid, then the Pararosaniline. Store in an aluminum-foil wrapped tube or amber-glass bottle at 4°C (good for a few weeks, replace often, test against fresh standards often); you will need 0.1mL per 1mL reaction. (Step ii) 3.7% Formaldehyde (HCHO): prepare fresh by diluting 37% (stock, freshly opened/purchased) formaldehyde 1:10 in 18.2MΩ H_2O. Store on ice until used. (Step iii) 18.2MΩ H_2O for standards and dilutions, boiled and degassed with N_2. (Step iv) Prepare sulfite standards immediately before use and keep on ice: use recently acquired Na_2SO_3 (Sigma-Aldrich) that has been stored properly under N_2 and anoxic 18.2MΩ H_2O. First, prepare a 100mM standard by adding 0.1260g Na_2SO_3 to a 10mL volumetric flask, bring to 10mL with anoxic water. Dilute to 10 mM, then 1 mM using volumetric flasks, also in anoxic water. Dilute the 1 mM standard to 0.25 mM (250 micromolar) using P1000 pipette in a 1.5mL plastic tube. The 250mM standard is then diluted 1:1 with anoxic water, the 125 micromolar standard diluted 1:1, and so on until the lowest standard of 32.125 micromolar (or less) is achieved.

Reaction:

(Step 1) Either in the anaerobic chamber or on the bench, being careful to maintain a headspace of N_2 over all sulfite-containing solutions, prepare standards and sample dilutions. Dilute samples such that 0.1-0.8mL of

sample contains less than the highest sulfite standard. For example, if 0.5mL of sample contains a maximum of 50 micromolar sulfite, then you may use the entire 0.5mL in a 1mL Fuschin reaction.

(Step 2) Prepare 2x 1.5mL plastic tubes per sample or standard. All reactions are performed in duplicate, always. Prepare 1x plastic cuvette per reaction, carefully add 0.75mL anoxic water to each cuvette.

(Step 3) To each tube, add up to 0.8mL of anoxic 18.2MΩ H_2O, with the balance being sample. For standards, add 0.7mL anoxic water.

(Step 4) Add 0.1mL of each standard and up to 0.8mL of sample. Note, you will need to measure each sample 2x so it is best to use less than 0.4mL of sample, particularly when sample volumes are limiting (e.g. 1mL kinetic assays).

(Step 5) Rapidly add 0.1mL of the Fuschin reagent, cap the tubes and invert 3 times each, then store in the dark. Start a timer and incubate for 9min.

(Step 6) At 9minutes remove the tubes from the dark, add 0.1mL of 3.7% HCHO, cap and invert tubes. Place back in the dark for 9 min.

(Step 7) Remove the tubes from dark, quickly and carefully pipette 0.75mL of each sample into the cuvette's containing 0.75mL of water. Mix by pipetting up and down, being careful to avoid bubbles.

(Step 8) Read samples in a spectrophotometer (Shimadzu, UV-1603) at 570nm, blanked with 18.2MΩ H_2O. After the addition of the HCHO (step 6) you only have 10-15 minutes before the color of the product will being to fade. Read each sample 2-3 times and average, replacing to a dark place in-between reads. If the signal is degrading by the third read, you may correct for signal degradation using the in-run standards, assuming they are run at the same interval and order.

Cautionary note: this is a useful protocol when properly standardized to the reaction matrix, but is easily influenced by more complex solutions (e.g. microbial growth media containing redox indicators, or large amounts of yeast extract). It is ideally suited to our simple potassium phosphate buffer in vitro solution.

4.10.2 Trithionate and thiosulfate quantification method

Trithonate and thiosulfate were measured by a modified cyanolysis protocol (Don P Kelly & Wood 1994; Donovan P Kelly et al. 1969; Sörbo 1957). We primarily employed the method of Kelly and Wood (Don P Kelly & Wood 1994) modified in the following manner: the reaction volumes were reduced to 10 rather than 25 mL's (still in volumetric flasks) and we used nitric rather than perchloric acid. Nitric acid was used in the original version of this method (Sörbo 1957), allowing us to avoid the significant hazards of working with significant volumes of perchloric acid. Samples were added to the reaction buffer to fit within the range of ferric thiocyanate standards (prepared from potassium thiocyanate as a simple standard and thiosulfate as a reaction standard) from 5 to 25 micromolar (final concentration in the 10mL reaction), as well as 'blanks' prepared from the in vitro assay reaction buffer (50 millimolar potassium phosphate buffer at pH 7). This typically meant 400 microliters of in vitro solution was added to the 10 mL cyanolysis reaction, in duplicate per method (2x thiosulfate determinations and 2x trithionate determinations). We follow the original protocol closely though will happily provide a step-by-step protocol upon request.

4.10.3 Sulfide ($H_2S/HS^-/S^{2-}$) quantification method

For sulfide quantifications, we preserved samples in zinc acetate (2% w/v) from each closed system reaction, using a modified Cline (Cline 1969) method. In all samples no sulfide was detected above our standards determined detection limit of 6.25 μM. From the literature reports where membrane fractions were omitted (Drake & Akagi 1978), signifying a lack of DsrC re-cycling mechanism (Oliveira, Vonrhein, Matias, Venceslau, P. M. Pereira, et al. 2008b; Bradley et al. 2011), we expected little to no sulfide. This is further supported by the closure of S mass balance at each time-point (*see* below) from each experiment, within analytical error. Blanks were prepared identically to those in the cyanolysis protocol. Analytical grade sodium sulfide nonahydrate (>98.9% Na_2S*9H_2O, Sigma-Aldrich, St. Louis, MO) was used as the standard, and prepared in deoxygenated (boiled and N_2-sparged) in vitro reaction buffer, by precipitating the sulfide with excess zinc acetate (anhydrous), mimicking our sampling protocol (*see* 8.5).

Standards are prepared as follows: Measure out 10 mmol for a f/v (final volume) of 100 mL of Na_2S*9H_2O (0.24018 g). Dry out all Na_2S*9H_2O before weighing; measure 100 mL of anoxic H_2S-free media/reaction buffer; measure out 2x the amount of sulfide (mol) of zinc acetate (also accounting 3x for all PO_4^{3-} present, which will also precipitate with the Zn^{2+}), under N_2 flux or in an anaerobic chamber mix in the zinc acetate, then the Na_2S*9H_2O, once well mixed, seal and sonicate.

For the Cline reaction: Mix pre-chilled Cline reagents (LaMotte, Chestertown, MD). Only 'reagent A' (LaMotte 4458-G) and 'B' (LaMotte 4459-E) is necessary, mixed at a ratio of: 80 µL reagent A plus 20 µL reagent B, per reaction. Reactions are performed in 750 µL of anoxic (boiled, N_2-sparged18.2MΩ H_2O in 1.7mL tubes, where 250 µL of standard is used per 1.1 mL (f/v) reaction, each prepared in triplicate. Once the standard is added to the water, add 100 µL premixed LaMotte Cline reagents 'A+B', invert tubes 10x to mix, and place reactions in complete. Sit for 40 minutes, then pour reactions into 1mL plastic cuvettes and read absorbance at 670nm on a spectrophotometer (Shimadzu, UV-1603) quickly. Repeat at 50min to verify the reaction was complete upon first reading.

4.10.4 Sample preparation for isotope ratio analyses (isolation and purification)

All S-bearing samples for S-isotope analyses (ultimately as SF_6 and/or SO_2) were removed from the *in vitro* reaction solution (50mM potassium phosphate) following a sequential precipitation protocol, inspired by that of Smock and colleagues (Smock et al. 1998). Our protocol reflects our specific experimental setup and the pools we aimed to isolate and purify: sulfite, sulfonate, and reduced product S. All samples entering the elemental analyzer isotope ratio mass spectrometer (EA-IRMS), and combusted to and analyzed as SO_2, are prepared as dry $BaSO_{3(s)}$, $BaSO_{4(s)}$ or $Ag_2S_{(s)}$. All samples for quadruple S isotope analysis enter the fluorination line as pure dry $Ag_2S_{(s)}$.

Samples of the residual reactant (sulfite) and pooled products (reduced product S and sulfonate S) were removed from the in vitro reaction mixture by sequential precipitation and filtration or centrifugation to isolate solid-phases $Ag_2S_{(s)}$ (reduced product), $BaSO_{3(s)}$ (sulfite), $BaSO_{4(s)}$ (sulfonate).

Samples of residual reactant sulfite, sulfonate, or reduced product were extracted by the extraction scheme detailed here, and were captured as $BaSO_{3(s)}$, $BaSO_{4(s)}$ or $Ag_2S_{(s)}$, respectively. Sub-samples of the reduced product Ag_2S were directly fluorinated (after the below washing steps were carried out to ensure clean Ag_2S), or in the case of the sulfonate S-pool, collected from the AVS residue and converted from $BaSO_4$ to Ag_2S by the method of Thode (THODE et al. 1961), hence known as 'Thode-reduction'. Briefly: 5 to 8 mg of rinsed and dry barium sulfate (originally from sulfites or sulfonates) was converted to $H_2S_{(g)}$ in a distillation apparatus with a gently boiling 'Thode' solution (16% hypophosphorous acid, 32% hydriodic acid, and 52% hydrochloric acid) for three hours. Nitrogen carrier gas was bubbled through the solution to ensure no oxygen present, and to carry product $H_2S_{(g)}$ through a distilled water acid trap, then on into a trapping solution of 0.3 M zinc acetate buffered by acetic acid, where the $H_2S_{(g)}$ precipitates with Zn^{2+} to form a white $ZnS_{(s)}$ precipitate. $ZnS_{(s)}$ is then converted to silver sulfide by cation exchange by 1mL addition of 0.3M $AgNO_3$ solution, allowed to sit overnight in the dark. All silver sulfides are then collected and cleaned by filtration onto 0.22um cellulose nitrate filters, washed with 3 or 4 volumes (15 mL each) of 18.2MΩ H_2O to remove excess silver and acetate ions, then 3 or 4 volumes of each of the following, always in this order (all stock solutions are prepared and diluted in 18.2MΩ H_2O to avoid trace sulfate contamination): 1M acetic acid, rinses in 18.2MΩ H_2O, 1M ammonium hydroxide, rinses in 18.2MΩ H_2O. Samples are then scraped off the filter gently onto clean dry Al-foil, so as to avoid any contamination of the sample with cellulose nitrate (never allowing samples to dry on or be scraped dry from the filter), followed by drying at 70°C for two days (in the dark), then stored in Al-foil packets (in a dark dry locale) prior to weighing and fluorination (in addition to re-analysis of some of the peroxide oxidized, Thode reduced sulfites, via CF-IRMS, to ensure isotope fractionation did not occur and yields were quantitative through these steps). All sulfite samples (reacted as $BaSO_{3(s)}$) were oxidized prior to 'Thode'-reduction. For sulfite samples (as $BaSO_{3(s)}$), oxidation to sulfate (collected as $BaSO_{4(s)}$) is required before the thermochemical conversion to sulfide by the Thode-reagent/protocol. If the oxidation is not performed, sulfite rapidly evolves to $SO_{2(g)}$ upon the initial injection of the Thode-reduction reagent (reagent is pH ~ -2, pK_{a1} = 1.81 for H_2SO_3/HSO_3^-, where $H_2SO_{3(aq)}$ rapidly dissociates to $SO_{2(aq)}$ and is carried away by the N_2 stream in the reduction-distillation line as $SO_{2(g)}$), and

would be lost. Subsequently the native isotopic composition of the sulfite intended to be determined my CF- or DI-RIMS would be altered and no longer be reflective of the enzymatic process we aim to characterize. To avoid this unfortunate scenario we were able to oxidize $BaSO_{3(s)}$ to $BaSO_{4(s)}$ by placing up to 80mg of the reactant in 15mL conical plastic tubes, adding 10mL of 30% v/v fresh hydrogen peroxide, sonicating vigorously for 30-45 minutes, then incubating in vacuum at ~90°C until the peroxide has completely dried. The tubes then removed from the vacuum oven, filled with 18.2MΩ H_2O, sealed and sonicated at maximum for another 30min, and the drying process repeated. This protocol was determined using lab-standard $BaSO_{3(s)}$ precipitate from Na_2SO_3, and the two washing-drying cycles determined idea for destroying residual H_2O_2 prior to Thode-reduction. The last step (destroying residual H_2O_2) is critical to not oxidizing the reducing capacity of the Thode-reagent prior to it acting on the $BaSO_4$ during reduction-distillation.

4.10.5 Major S-isotope ($^{34}S/^{32}S$) ratios measurements

Continuous flow isotope ratio mass spectrometric (CF-IRMS) measurements of the three S-bearing pools of interest, sulfite, sulfonate and reduced product S, were performed as follows: 0.4mg (+/- 0.05mg) $BaSO_3$, $BaSO_4$ or Ag_2S were converted to SO_2 by combustion at 1040°C in the presence of excess V_2O_5 (Elemental Analyzer, Costech ECS 4010) and analyzed by continuous flow isotope ratio mass spectrometry (1σ of ±0.3‰; Thermo-Finnegan DELTA V Plus). All samples yielded clean chromatography and most m/z 66 amplitudes (corresponding primarily to the $(^{16}O^{34}S^{16}O)^+$ ionization product) within the range of in-run standards (IAEA: S1, S2, and S3 for Ag_2S or SO5, SO6, and NBS-127 for $BaSO_4$ and $BaSO_3$). Some sulfite precipitates ($BaSO_{3\_sulfite}$) though not any of the sulfate or sulfide precipitates ($BaSO_{4\_sulfonate}$ or $Ag_2S_{\_reduced\ product}$) produced atypical weight to m/z 66 response we see with lab standards of $BaSO_3$ or $BaSO_4$—specifically the signal was less than predicted, likely due to occlusion of phosphates (from the in vitro reaction buffer) in the barium sulfite matrix. As a result, we use the m/z 66 to $BaSO_3$ weight ratio (mg of $BaSO_3$ per unit area of the m/z 66 peak) to calculate the desired sample weight to achieve standard signal size, re-weighed and re-combusted/measured the requisite samples, and in all cases achieved m/z 66 peak areas in the range of our IAEA $BaSO_4$ and in-house $BaSO_3$ standards. Each

standards is measured at least 4x in-run and each sample 2-3x (when sufficient sample is available). This simplifies the scale-conversion calculation for taking samples referenced in-run to in-house standard tank gas ($HAR1_{SO2}$) and ultimately to the international reference frame (V-CDT).

4.10.6 Multiple S-isotope ($^{33}S/^{32}S$, $^{34}S/^{32}S$, $^{36}S/^{32}S$) ratio measurements

Duel-inlet (DI-IRMS) measurements of all four stable S isotopes (^{32}S, ^{33}S, ^{34}S, ^{36}S) from the three S-bearing pools of interest, sulfite, sulfonate and reduced product S, were performed as previously described (Leavitt et al. n.d.). Briefly, all samples for quadruple S-isotope analysis, prepared dry and clean Ag_2S (described above), were fluorinated under 10X excess F_2 to produce SF_6, which is then purified cryogenically (distilled at -107°C) and chromatographically (on a 6' molecular sieve 5Å inline with a 6' HayeSep Q 1/8"-stainless steel column, detected by TCD). Purified SF_6 was measured as SF_5^+ (*m/z* of 127, 128, 129, and 131) on a Thermo-Finnegan Scientific MAT 253 (1σ: $\delta^{34}S$ ±0.2, $\Delta^{33}S$ ±0.006‰, $\Delta^{36}S$ ±0.15‰). All isotope ratios are reported in parts per thousand (‰) as experimentally paired sulfates and sulfides measured. Long-term running averages and standard deviations for IAEA standards: S1, S2, S3 for sulfides, or NBS-127, SO5, SO6 for sulfates. Isotope calculations and notation are detailed below. Standard errors for each value is estimated as reported previously (Johnston et al. 2007).

4.10.7 Scale-compression correction calculations for con-flow IRMS measurement of small S samples (0.35 to 0.01 mg) from *A. fulgidus* in vitro experiment samples

Experiments with *A. fulgidus* yielded small amounts of product, which required additional data handling during isotope analysis. Given the small size of these samples, we ran each sample only once and bracketed the samples (n = 2) with a series of standards: IAEA S1, S2 and S3 (n = 16, 14, and 14, respectively) run over a size series that captured the sample sizes. As expected, we observed that the measured isotopic composition of the standards varied non-linearly as a function of signal intensity (monitored as peak integrated areas and peak intensities on m/z 64 and 66 for SO_2^+ and 48 and 50 for SO^+). The size dependence on the isotopic composition

(handled as ^{50}R and ^{66}R, which are the 50/48 and 66/64, respectively) scale compression is calculated as a proportional change. For SO (*correction factor* in Extended Data Figure 4.S11):

Equation S10 $$\left|\frac{^{50}R_{predicted} - {}^{50}R_{\boldsymbol{measured}}}{^{50}R_{predicted}}\right|.$$

We focus on SO here as these samples yielded sharper chromatography on slightly different sized signals (due to resistor differences between SO and SO_2 cups – 3 x 10^{10} Ω and 1 x 10^{10} Ω respectively). Thus, using the three IAEA standards, we developed a correction whereby we solve (in the standards) for the non-linear features of the data as it relates to signal intensity (here monitored as the peak integrated area on mass 48 – ^{32}SO). This is shown in Extended Data Figure 4.S11. After this correction is applied to $^{50}R_{measured}$, SO data is converted to an SO_2 scale (see Extended Data Figure 4.S12), which is linear transfer function again derived from IAEA standard data. The final correction places all the data (now on a SO_2 scale against in-house reference SO_2 tank gas) to the V-CDT scale. To review, we perform the following steps 1) correcting the ^{50}R on SO for sample size, 2) convert ^{50}R to ^{64}R (against tank gas), and finally 3) convert all data to a VCDT scale.

The largest source of error in this treatment is associated with the sample size correction. As such, we propagate the error associated with the fit in Extended Data Figure 4.S11 to determine the uncertainty in the final isotope value. As expected, for small samples this error is quite large (Extended Data Table 4.S1), with the value decreasing in absolute magnitude as signal intensity (peak integrated area) increases. We also compare these error estimates to the calculated shot noise for this measurement (pink line in Extended Data Figure 4.S13). As is presented below, our regressed error is in excess of the shot noise limit. Similarly, the error on the population of standards that were used in deriving this fit is ~1‰ (n = 44).

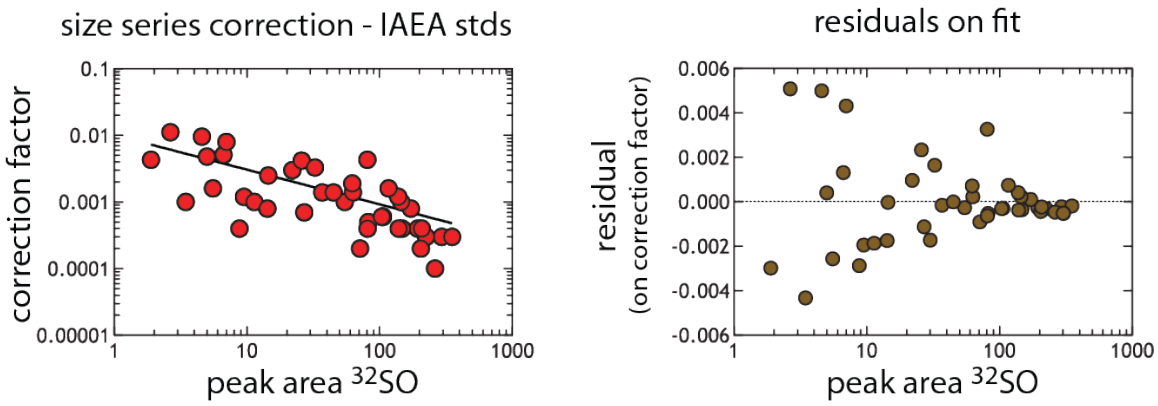

Extended Data Figure 4.S11. The size series correction calculated from (n = 44) IAEA standards. At left is the correction (value from eq. 1 against peak integrated area). At right is the calculated residual around that fit, demonstrating a symmetric distribution that scales with peak area. This is an illustration of the goodness of the fit.

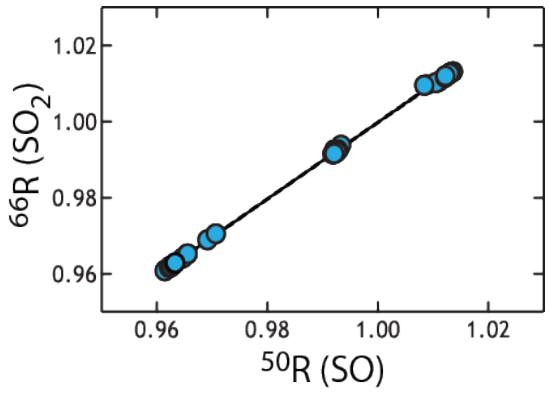

Extended Data Figure 4.S12 (left). The regression used to convert SO data to an SO_2 scale.

Extended Data Figure 4.S13 (right). The calculated shot noise for SO as a function of signal intensity (peak height in mV). This precision limit is below that which we propagate through the correction, and is provided for reference here.

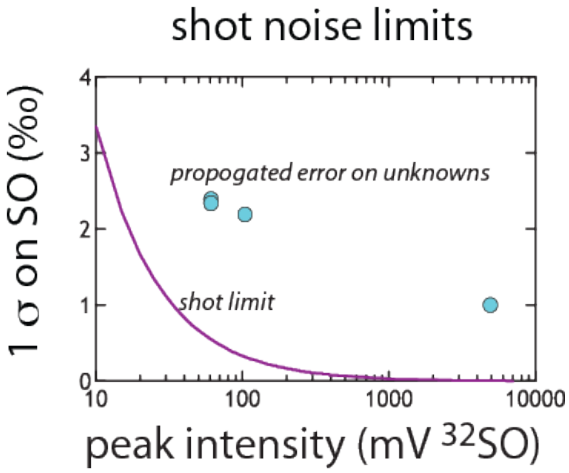

Acknowledgements:

Thanks to Sofia Venceslau and Fabian Grein for discussions on MSR biochemistry and DsrC cycling. Isabelle Pacheco for the hydrogenase; to Erin Beirne and Andy Masterson for expert assistance in measurements and separation chemistry. Thanks to Ann Pearson, John Hayes and David Fike for comments, which greatly improved earlier drafts. Funding was provided by the NSF-GRFP (WDL), NSF Geobiology and Low-Temperature Geochemistry (DTJ, IAPC), Sloan Foundation (DTJ), PTDC/QUI-BIQ/100591/2008 (IACP), Pest-OE/EQB/LA0004/2011 (to ITQB) funded by Fundação para a Ciência e Tecnologia (FCT, Portugal), and Washington University in St. Louis (ASB). Many thanks to the reviewers.

CHAPTER 5

DSRC AVAILABILITY INFLUENCES SULFATE REDUCER S ISOTOPE FRACTIONATION

This chapter will be submitted to *Frontiers in Microbial Chemistry* or *PLOS ONE* in summer 2014 with co-authors:

S. Venceslau, F, Grien, I.A.C Pereria, and D. Johnston

Abstract

The global biogeochemical sulfur cycle is set in motion and maintained by the microbiological reduction of marine sulfate to sulfide. The enzymatic cascade of reactions induces a distinct range of sulfur and oxygen isotope fractionations between reactant sulfate and product sulfide. The biochemical machinery of microbial sulfate reducers controls fractionation, where the magnitude of discrimination is a microbial response to their environment. To better understand how the net fractionation is produced we utilize recent advances in sulfate reducer genetics and enzymology to determine the influence of the terminal step in microbial sulfate reduction, the production of hydrogen sulfide by a sulfur transfer protein, DsrC. DsrC couples the soluble cytoplasmic reduction of sulfite by DsrAB to the membrane potential that ultimately allows these cells to generate ATP. Here we utilize recently generated mutants in the model sulfate reducer *Desulfovibrio vulgaris*, which impair the function of DsrC. We compare disrupted strains to the wildtype in terms of growth rate, specific sulfate reduction rate, and biomass yield as well as the magnitude of S and O isotope fractionation. One site-specific mutation in *dsrC* at the penultimate cysteine (Cys93) disrupts growth rate, specific sulfate reduction rate and the magnitude of S isotope fractionation, though not O isotope fractionation. The sulfur isotope fractionation for this mutant results in closed system fractionation behavior that does not look like a traditional 'Rayleigh' profile, whereas wildtype and other mutants show no distinct phenotype, other than variable growth and specific sulfate reduction rates. Implications for intra-cytoplasmic S cycling and dissimilatory sulfate reduction metabolism are discussed.

Introduction

Microbiological sulfate reduction is the dissimilatory energy metabolism to directly couple organic matter and hydrogen oxidation to the reduction of sulfate (Rabus et al. 2006). Microbial sulfate reduction (MSR) is an enzymatic process, performed by both Archaea and Bacteria, which accounts for up to half of the organic matter remineralization in modern marine sediments (JORGENSEN 1982). MSR is critical in coupling the biogeochemical S and C cycles (Szabo et al. 1950; Thode et al. 1953) and redox-active metal cycles, such as iron

and manganese. Moreover, the major MSR product sulfide is a strong reductant, dictating the redox potential in a diverse array of marine and freshwater habitats (Stumm & Morgan 2012). Further, MSR has played a dramatic role in the marine realm throughout the history of life on Earth. Indeed, the activity of MSR, in conjunction with oxygenic phototrophs, aerobic heterotrophs, and abiotic weathering reactions (GARRELS & LERMAN 1981) dictates the redox state of Earths oceans and atmosphere (Holland 1973; Canfield 2004a). Through its role in environmental redox chemistry and the toxicity of major by-product sulfide, MSR influences the function of more complex organisms in modern environments and has prejudiced the timing of major origination and extinction events in the geologic past (Sperling et al. 2013). Therefore, tracking the activity of MSR in modern and ancient environments is priority in geobiology

Unlike tracking MSR activity in modern environments, which is accomplished through direct rate measurements and functional gene quantification (Canfield, Stewart, et al. 2010b), identifying the activity of S-cycle metabolisms in ancient environments is only possible through stable isotope analysis of sedimentary S-bearing minerals coupled with paleo-environmental reconstructions. Sulfurs four stable isotopes (^{32}S, ^{33}S, ^{34}S, ^{36}S) are distributed amongst geologically stable S reservoirs (e.g. gypsum and pyrite) in distinct ratios that reflect the integrated effects of all biotic and abiotic S-cycle processes (Lyons & Gill 2010). Processes that lead to the temporal isotope patterns observed in these ancient sedimentary and modern marine and pore-waters are thought to be predominately biological (Szabo et al. 1950; Canfield 2001a), and thus are due to the metabolic networks of the constituent microbial metabolisms at play. Their constituent enzymes in turn underpin their mechanisms of energy conservation. Of these, MSR dominates sulfur isotope fractionations, with oxidative and disproportionation metabolisms contributing some signal, but to the best of our understanding, significantly less (Johnston 2011). To understand and interpret the commonalities and differences between biochemical fractionation mechanisms in MSR (and later in other metabolisms) we require a mechanistic understanding for how fractionation occurs at the intracellular (Harrison & Thode 1958; Kaplan & Rittenberg 1964; Lyn A Chambers et al. 1975; Kemp & THODE 1968), indeed enzymatic (Chapter 4) level. Such constraints feed into our understanding for how the component enzymatic steps influence the metabolic network as a whole. This

'bottom up' approach informs biochemically constrained S and O isotope fractionation models (Brunner et al. 2005; Bradley et al. 2011; Wankel et al. 2014). The small gains in our understanding will ultimately improve interpretations of fractionation in modern (Jorgensen 1979; Druhan et al. 2014; Goldhaber & Kaplan 1975) and ancient (Wu et al. 2010; D. S. Jones & Fike 2013; Leavitt et al. n.d.) isotopic records.

To understand the range and environmental controls on the magnitude of MSR fractionations (Goldhaber & Kaplan 1975; Leavitt et al. n.d.), we turn to understand the constituent enzymatic steps responsible for the reductive transformation of sulfate to sulfide inside microbial cells (Figure 5.1). Before sulfate is reduced in the Bacterial or Archeal cytoplasm, it enters the cell by active transport, and in the Gram-negative proteobacteria must further pass through the periplasm and inner-membrane (Piłsyk & Paszewski 2009). Due to its stability at Earths surface conditions (e.g. pH, T, E_h), microbes must 'activate' sulfate prior to any reductive transformations. This is accomplished enzymatically through the addition of sulfate to adenosine triphosphate (ATP) to generate adenosine-5′-phosphosulfate (APS) by the combined action of ATP sulfurylase (AtpS) and pyrophosphatase (Figure 5.1) (Harry D Peck 1960; Peck 1962). As with sulfate transport enzymes, AtpS binds the sulfate at the oxygen atoms (Ullrich et al. 2001; PFLUGRATH & QUIOCHO 1988). Secondary kinetic isotope effects are quite small in light-stable isotope systems other than hydrogen (Kohen & Limbach 2005), and so the non-S binding steps are unlikely to induce measurable S isotope fractionation, for example between external/internal sulfate and sulfate/APS. On the other hand there may be oxygen isotope fractionations, but this remains to be clearly tested (Kohl et al. 2012; Wankel et al. 2014). Following activation of sulfate, APS is reduced to bisulfite/sulfite (HSO_3^-/SO_3^{2-}, pK_a = 6.97) by APS reductase (APSr) (Peck 1962), the first redox reaction in the MSR pathway. This is also the first central catabolic enzyme to directly bind at the S atom (Fritz 2002). APSr is a highly reversible enzyme and able to catalyze either the formation of APS from sulfite and ATP (reverse) or reduce APS to sulfite (forward) (Peck 1962; Harry D Peck 1960). As such the reactants and products are likely close to equilibrium inside the cell, presuming downstream steps are slower (Rees 1973). Reaction reversibility has dramatic consequences on the net isotope effect between an initial reactant and terminal product, particularly if multiple steps in a pathway fractionate upstream of the slowest (rate-determining) step (Mariotti et al. 1981), as

is likely the case for MSR (Harrison & Thode 1958; Kaplan & Rittenberg 1964; Rees 1973; Brunner & Bernasconi 2005; Johnston et al. 2007; J. Farquhar, Johnston, et al. 2007a; J. Farquhar et al. 2008; Bradley et al. 2011). At sulfite, the MSR metabolic network may branch and operate in one of two modes: (*i*) a strictly linear reaction pathway (Figure 5.1a), where sulfite is reduced to sulfide, with four electrons sourcing from DsrAB, and the terminal two from DsrC, or (*ii*) a branched reaction network (Figure 5.1b) where mode (*i*) occurs in parallel to the production and reduction of thionates (e.g. trithionate and thiosulfate), formed from the scavenging of DsrAB reaction intermediates by a backlog of sulfite. Mode (*i*) is likely to occur when MSR cells are under no electron limitation and DsrC is efficiently re-reduced at the inner membrane, while mode (*ii*) will occur when DsrC re-cycling is slowed relative to the production of sulfite by APSr. Thus toggling between modes (*i*) and (*ii*) is strongly a function of reduced DsrC availability, as proposed previously (Oliveira, Vonrhein, Matias, Venceslau, P. M. Pereira, et al. 2008b) with potentially dramatic consequences for the net fractionation between sulfate and sulfide during MSR (Bradley et al. 2011). Moreover, the potential for branched rather than strictly linear material flow allows for the fractionation factors at individual steps to combine in generating a net fractionation (Bradley et al. 2011; Hayes 2001; Johnston et al. 2007) between reactant (sulfate) and product (sulfide).

In order to test the role of DsrC in the efficiency of net sulfate reduction to sulfide and associated isotope fractionations, we take advantage of recent advances in the genetic manipulation of sulfate reducing bacteria. By genetically altering intracellular DsrC activity we are, in principle, able to interfere with the ability of the MSR metabolic network to operate efficiently, inducing a buildup of partially reduced S-compounds in the cytoplasm (notably sulfite and perhaps thionates), slowing net sulfate reduction rates. Here we compare the growth rate, yield, specific sulfate reduction rate and net sulfur ($^{34}\varepsilon_{SO4\text{-}H2S}$) and oxygen ($^{18}\varepsilon_{H2O\text{-}SO4}$) isotope fractionations incurred during MSR during closed system ('batch') experiments with a model sulfate reducing bacterial strain and three mutant strains where *dsrC* specifically is targeted. In this study we directly test the importance of DsrC expression and functionality on the sulfate reduction rates and consequences in sulfur and oxygen isotope fractionation during MSR. Implications for intra- and extracellular sulfur cycling are discussed as well as a way

forward in designing experiments to better investigate the inner lives of sulfate reducing cells and their impact on the global S and C cycles.

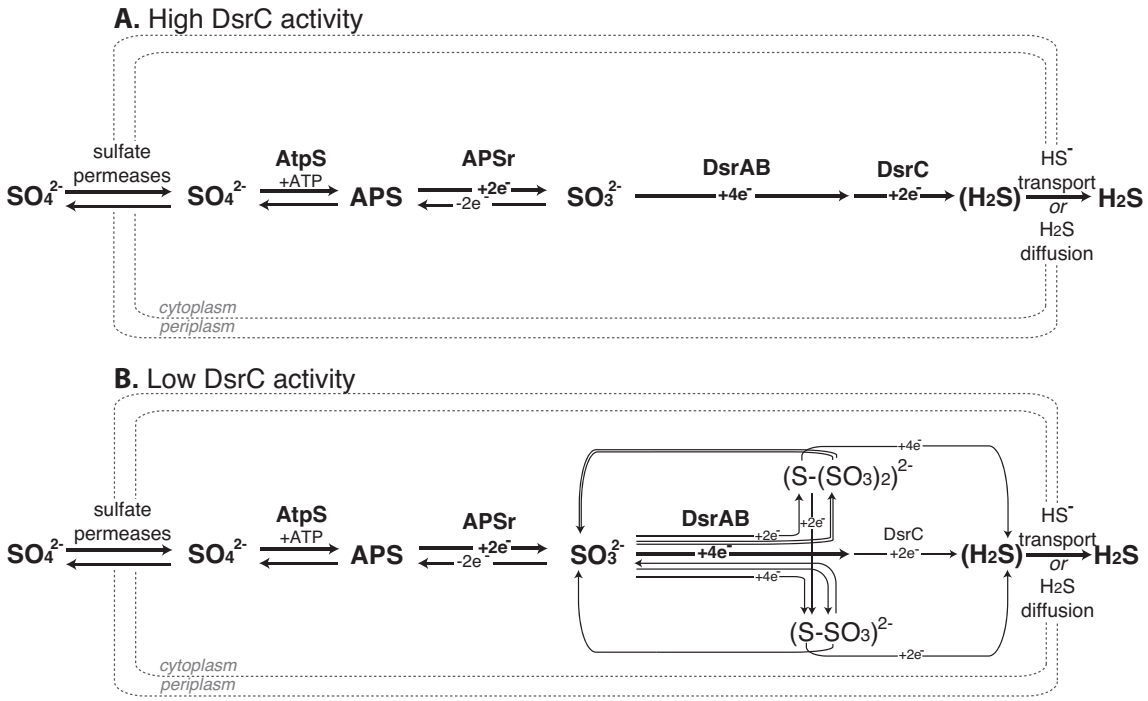

Figure 5.1. A simplified cartoon of the dissimilatory sulfate reduction pathway in MSR organisms. **(A**) The MSR pathway in mode *i*, when DsrC is recycled efficiently and sulfide is rapidly produced from intracellular sulfite. (**B)** The MSR pathway in mode *ii*, when DsrC activity is low and recycled slowly relative to the production flux if intracellular sulfite. In mode *ii* material flow branches to produce trithionate or thiosulfate. These thionates may then be further reduced to re-release sulfite and sulfide. For a complete description of the pathway refer to the main text as well as (Bradley et al. 2011; I. A. C. Pereira et al. 2011).

MATERIALS & METHODS

Experimental design, setup, and sampling

All experiments were conducted at 37°C in complete darkness. All strains were cultivated in MOY medium (Venceslau et al. 2013), containing 0.1% yeast extract, rather than 1% (w/v). Medium for mutant strains is dosed with filter-sterilized antibiotics following the autoclave sterilization, once the medium bottles cool to room temperature. Medium for mutant strains was supplemented with antibiotics as described below.

D. vulgaris mutant strains derive from a background in the wildtype (WT), where IPFG06, IPFG07, and IPFG09 were constructed as previously described (Venceslau et al. n.d.). The *dsrC* gene from *Desulfovibrio vulgaris* Hildenborough was amplified from chromosomal DNA and was fused to a 6xHis-tag tail at the N-terminus of the protein. The resulting plasmid is denoted pMOIPHisDsrC. This plasmid was electroporated giving DvH strain IPFG06. As a first approach we aimed to create a mutant strain lacking the *dsrC* gene completely. For that, a plasmid was created to delete the chromosomal copy of *dsrC* (pMOIP6). Using the sequence ligation independent cloning (SLIC) technique (Li & Elledge 2007), three different fragments were fused together containing namely the upstream and the downstream of the *dsrC* gene and the kanamycin resistance gene and then added into pMO719 background. Products from the amplifications were transformed into *E. coli* α-select Silver Efficiency (Bioline®) and successful transformants were isolated on LB medium containing 50μg/ml of kanamicyn. Correct isolates were identified by the expected PCR amplicons from the plasmids constructs and also by plasmid sequencing. The plasmid was electroporated (1500V, 250 W, and 25 mF, according to (Keller et al. 2011) into *D. vulgaris* cells grown on either lactate/sulfate or pyruvate/sulfate medium. Although repeated several times, clones could never be obtained from the respective plates containing geneticin (a kanamycin analogue). Negative and positive controls were also done to exclude problems with the electroporation itself. The fact that no clones were obtained may lead to the conclusion that DsrC is an essential protein in DvH. It was already reported that a Δ*dsrC* deletion strain from *Allochromatium vinosum* was genetically not stable (Cort et al. 2008). A second approach was started to reduce the expression level of *dsrC* in DvH. Therefore strain IPFG06 (which contains a plasmid encoding a His-tagged DsrC) was electroporated with the

deletion plasmid pMOIP6. Colonies were picked from lactate/sulfate and pyruvate plates containing geneticin and spectinomycin. The resulting strain is IPFG07. We then used pMOIPHisDsrC to introduce point mutation on DsrC, substituting the cysteine residue for an alanine. Plasmids pMOIPHisDsrCC26AC93A and pMOIPHisDsrCC26AC104A were created, and these were electroporated into DvH giving strains IPFG08 and IPFG10, respectively. Subsequently, deletion plasmid pMOIP6 was successfully introduced in IPFG08 and IPFG10 by electroporation (Li & Elledge 2007), selecting with pyruvate medium containing 400 μg/ml of geneticin and 100 μg/ml of spectinomycin, generating a chromosomal deletion of *dsrC* in DvH strains. Only the strain containing the pMOIPHisDsrCC26AC93A (IPFG08) give raise to a *dsrC* chromosomal deletion strain (IPFG09). Although the same approach was used for IPFG10 to originate a *dsrC* chromosomal deletion strain (IPFG11), clones could never be obtained, showing the importance of Cys104. The deletion of *dsrC* gene in strains IPFG07 and IPFG09 was confirmed by Southern blot using as probe an upstream fragment of *dsrC* gene. The cell stocks of DvH WT, IPFG06, IPFG07 and IPFG09 strains were kept in pyruvate medium with 10% glycerol at -80ºC. The pre-inoculums were grown in pyruvate as well, while only the phenotypic growth curves were in lactate/sulfate medium.

Table 5.1.Summary of strains, with those used in this study in bold (Venceslau et al. n.d.)

***D. vulgaris* strains**	**Strain characteristics**
Wildtype (WT)	***D. vulgaris* Hildenborough ATCC 29579**
IPFG06	**WT + pMOIPHisDsrC**
IPFG07	**DvH Δ *dsrC*::Km^R + pMOIPHisDsrC**
IPFG08	WT + pMOIPHisDsrCC26AC93A
IPFG09	**DvH Δ *dsrC*::Km^R + pMOIPHisDsrCC26AC93A**
IPFG10	WT + pMOIPHisDsrCC26AC104A

DsrC plays a significant role in the efficiency of the biochemical MSR pathway, and is most likely a requisite protein in regulating cytoplasmic reduction potential. This is evidenced in growth rates of the Hildenborough wild type relative to the three mutants targeting DsrC functionality. Moreover, no mutants completely lacking *dsrC* have been yet, despite numerous attempts. Genetic manipulation has only been successful when simultaneous complementation of *dsrC* on a plasmid is provided (Venceslau et al. n.d.). In this

study we work with the wildtype *Desulfovibrio vulgaris* strain as IPFG06 has two copies of *dsrC*, one chromosomal and one plasmid born, and is the pre-complementation background from which subsequent strains were derived (Venceslau et al. n.d.). Mutant IPFG07 possess only the plasmid copy of *dsrC*, is therefore the deletion/complementation strain. Mutant IPFG09 possesses only the plasmid copy of *dsrC*, with the penultimate Cys93 mutated to an alanine – the second of two critical cysteine's for terminal sulfide production (Oliveira, Vonrhein, Matias, Venceslau, P. M. Pereira, et al. 2008b). Despite concerted efforts, mutants in cys104 or complete deletions of *dsrC* from the chromosome and plasmid have been unsuccessful (Venceslau et al. n.d.), further supporting the criticality of DsrC to sulfate reducer viability. The S isotope fractionation experiments are conducted in duplicate (per strain), in an initial volume of 0.8L in 1L borosilicate media bottles, sealed with 2.5cm thick #6.5 butyl rubber stoppers held in place by bored media bottle screw-caps. All wetted components are acid washed (10% HCl) and autoclave sterilized. Sulfate is always provided in stoichiometric (>2*x*) excess of lactate to prevent complete distillation of sulfate S isotopes to product sulfide.

Each experimental bottle (two per strain) is sub-sampled through the septa aseptically and anaerobically at the indicated time intervals (Table 5.4) for the following parameters: optical density (absorbance at 600nm); concentration data (sulfate, sulfide, acetate, lactate and any possible thionates); isotopic composition of sulfate and sulfide; as well as unfixed cell/biomass samples for protein quantification and DsrC/B Western Blot quantifications. When sampling more often only for A600 measures (optical densities), 1mL deoxygenated sterile syringes are used to push in 1mL deoxygenated sterile Ar, and 0.7 mL culture removes and read, blanked by deionized water. To sample for the full suite, sterile and equivalent volume as that removed of deoxygenated Ar is pushed into the 1L vessel through the septa via 20 mL syringes fitted with 18-gauge needles, followed by the removal of 20 mL's of well-mixed culture. The tip of the needle is then placed below the surface of the preservative (0.8 mL's 20% w/v zinc nitrate solution in a 50 mL conical centrifuge tube) and the sample rapidly dispensed so as to immediately zinc sulfide (ZnS) and arrest microbial activity. Samples are stored at 4°C in the dark until analysis (within 48 hours) and further extraction (within 1 week). Samples for protein quantification (1.8 mL's, no additives) are flash frozen at each time point and stored at -20°C until analysis.

Analytical methods

Duplicate 0.7mL samples are removed from each bottle at all time-points for absorbance/optical density (A600nm) measurement, immediately dispensed into 1mL plastic cuvettes and read against the same deionized water blank on a UV/visible spectrophotometer (Shimadzu UV-1603). Samples frozen for protein quantification were thawed on ice and total protein quantified by the Bradford assay (Bradford 1976). Western Blot analyses on DsrB and DsrC are also performed on these fractions, utilizing the recently developed antibodies and method (Venceslau et al. 2013) (Venceslau et al. n.d.)

Sulfate, lactate, and acetate concentrations in the zinc nitrate fixed samples are determined on centrifuged samples (18,000x*g*, 10min) by suppressed anion chromatography with conductivity detection (Dionex ICS-2000, AS11 column). Matrix-matched standards – i.e. standards of each anion prepared in the same MOY medium background with the same concentration of zinc nitrate, as this influences chromatographic separation timing, and background/blank stability – over a concentration range of 30 to 300 μM, in backgrounds of the MOY and fixative of appropriate dilution, with samples diluted into this range (typically a 200-fold dilution, carried out through multiple lower dilutions). An eluent gradient method was employed: running first 1mM KOH isocratically for 6 minutes, followed by a linear ramp to 30mM KOH over 8 minutes, then a linear ramp to 60mM KOH over 4 minutes, followed by 5 minutes re-equilibration at 1mM KOH between samples (standards and sample replicate 1σ S.D. ±5%; detection limit 1μM). Sulfide concentrations were measured by a modified methylene blue 'Cline' method (Cline 1969), as described in detail elsewhere (Leavitt et al. n.d.)(duplicate S.D. ±6%; detection limit 5μM). We also measure for thiosulfate ($S_2O_3^{2-}$) and trithionate ($S_3O_6^{2-}$) in all samples by cyanolysis, following our adaptation (Leavitt et al. n.d.) of the older protocols (Sörbo 1957; Don P Kelly & Wood 1994). All samples exhibit no detectable thionates (less than 50 μM).

Sulfate or product sulfide samples were first prepared for major isotope analysis ($\delta^{34}S$) as $BaSO_4$ or Ag_2S, respectively. All samples for sulfur isotope analysis are first centrifuged to remove the sulfide (as ZnS) and biomass bound S. These fractions are then quickly transferred to 2.0 mL centrifuge tubes and maintained on ice

until freeze dried (FreeZone Plus 4.5L Cascade Freezer Dry System, Labconco). Freeze-dried samples are kept in the dark, dry, for shipping from ITQB to Harvard (within 1 month of the experiment). Sulfide and biomass S samples are then subject to distillation by sequential acid-volatile sulfur (AVS, referred to as the sulfide fraction) and chromium reducible sulfide (CRS) extractions as described previously (Johnston 2005), captured in separate zinc acetate traps, converted to silver sulfide and washed as though preparing for multiple S isotope analyses (Leavitt et al. n.d.). Sulfate is precipitated from the supernatant medium with excess barium chloride, following removal of the zinc sulfide and biomass S, and removed from the supernatant by centrifugation (18,000xg, 30min, 4°C). Sulfate precipitates (as $BaSO_4$) are then freeze-dried and stored in the dark, as for the zinc sulfides. No further washing is performed on the sulfates, as the precipitates displayed clean chromatography upon combustion on an elemental analyzer.

For S isotope analysis, 0.4 mg precipitated dry Ag_2S (pooled product H_2S (PP) sulfides or chromium reducible sulfur in the biomass pellet (CRS)) or $BaSO_4$ (initial reactant (IR) and residual reactant (RR) sulfates) were converted to SO_2 by combustion at 1040°C in the presence of excess V_2O_5 (Elemental Analyzer, Costech ECS 4010) and analyzed by continuous flow isotope ratio mass spectrometry (Thermo-Finnegan DELTA V Plus). All isotope ratios are reported in parts per thousand (‰) against the international atomic energy agency standards (IAEA) V-CDT (Table 5.4, Figure 5.2d) or recalculated in reference to the composition of initial sulfate S (Figure 5.3). Long-term running averages and standard deviations for IAEA standards: S1, S2, S3 for sulfides, or NBS-127, SO5, SO6 for sulfates are conservatively reported as 1σ of ±0.3‰. We report all values in standard stable isotope notation. Isotope ratios (${}^{3x}R = {}^{3x}r/{}^{32}r = [({}^{3x}S/{}^{32}S)_A/({}^{3x}S/{}^{32}S)_B]$) are used to determine the fractionation factor (α) between two pools (A and B), where A is a sample and B is either a standards or t_0 sulfate (${}^{34}R_{SO4\_t0}$): ${}^{3x}\alpha_{A-B} = \left[\left({}^{3x}S/{}^{32}S\right)_A/\left({}^{3x}S/{}^{32}S\right)_B\right]$. These values are then converted to the standard delta-notation scale by: ${}^{3x}\delta_{A-B} = \left({}^{3x}\alpha - 1\right)\times 1000$. All initial and residual reactant sulfates are analyzed for oxygen ${}^{18}O/{}^{16}O$ compositions by pyrolysis of precipitated and dried $BaSO_4$ in the presence of powdered glassy carbon to generate CO in helium-flushed thermal conductivity elemental analyzer (1450°C, TC/EA) coupled directly to a

DeltaV continuous flow isotope ratio mass spectrometer (ThermoFinnegan). Samples are analyzed at minimum twice and in many up to four times. Long-term running averages and standard deviations for IAEA standards NBS-127, SO5, SO6 are reported as 1σ of ±0.4‰ on the V-SMOW scale (Fig. 5.2) or relative to initial sulfate ($\delta^{18}O_{SO4\_t0}$, ‰). Delta notation is the same as for sulfur, substituting $^{18}O/^{16}O$ for $^{34}S/^{32}S$ in the *R*, α and δ expressions.

For some CRS and t_0 sulfide isotope analyses, small sample quantities required an additional a peak area correction in order to place these samples on the same isotope scale. To do so we measured a set of standards (S1, S2, S3) over the same size range as the samples. From the standards, we fit a non-linear correction for $\delta^{34}S$ as a function of peak integrated area on major masses (48 for SO and 64 for SO_2). The error associated with this correction also scales to signal intensity. Importantly, these analyses and errors are above the shot noise limit for the instrument (Chapter 4).

Basic calculations

Growth parameters.

Equations 5.1 through 5.5 are applicable during the log-phase of microbial growth (Rabus et al. 2006; Detmers et al. 2001).

Specific growth rate:

Equn. 5.1. $$\mu\ (\text{per hour}) = \frac{\ln(A600_{t=n+1}) - \ln(A600_{t=n})}{(t_{n+1} - t_n)},$$

Specific sulfate reduction rate:

Equn. 5.2. $$\mu SRR = \frac{[sulfate]_{t=n} - [sulfate]_{t=n}}{\frac{A600_{t=n+1} - A600_{t=n}}{2} \times (t_{n+1} - t_n)},$$

Biomass yield:

Equn. 5. 3. $$Yield = \frac{A600_{t=n+1} - A600_{t=n}}{([lactate]_{t=n} - [lactate]_{t=n}) \times vol},$$

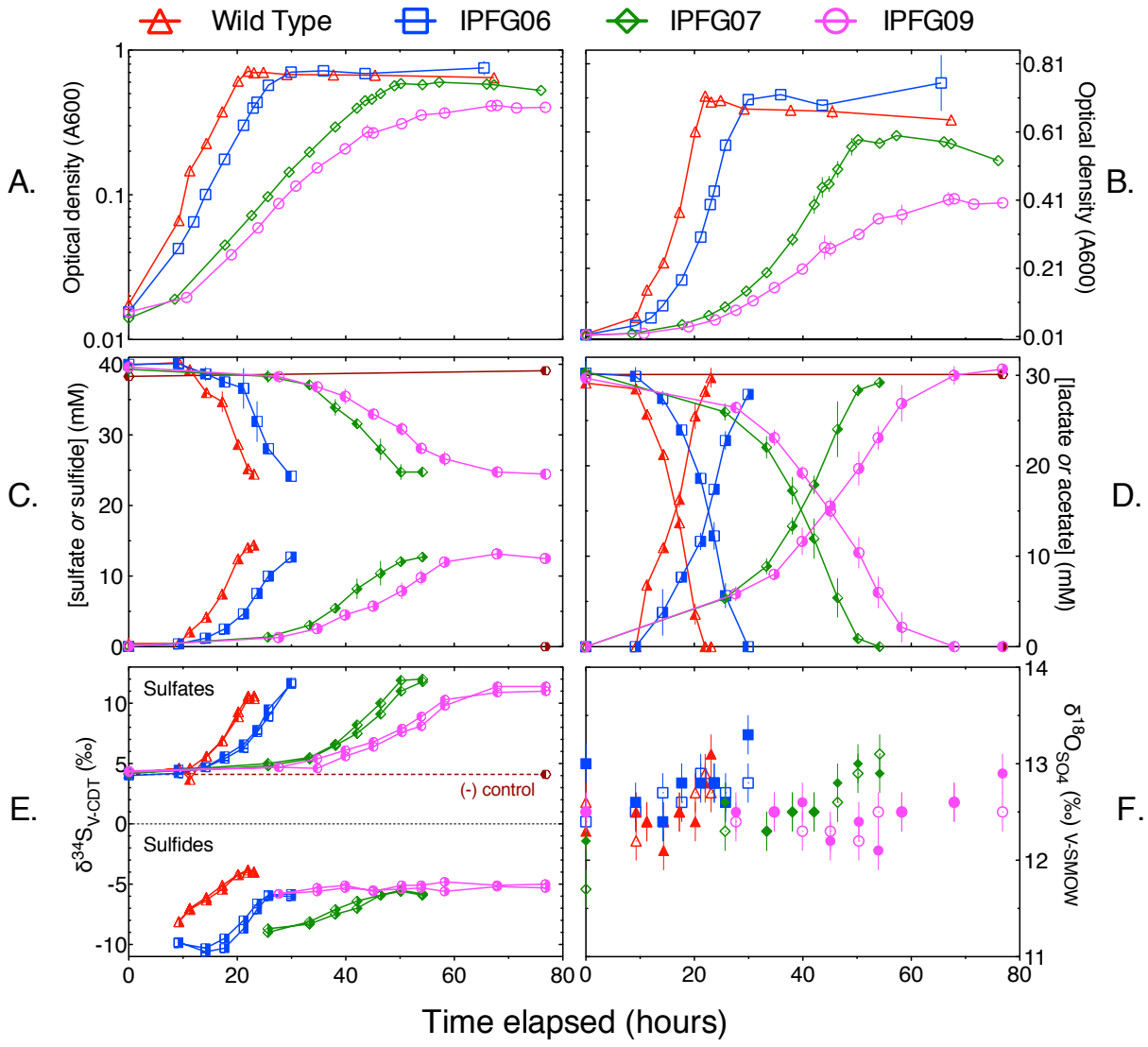

Figure 5.2 Batch experiments with WT and three Δ*dsrC* mutant strains. Replicate average cell densities (A600) over time for WT and the three mutant strains grown at 37°C plotted on (A) a log and (B) linear y-axis. Samples for concentrations (C and D) and isotopic analyses (E and F) were taken at a subset of these time-points. In (C-E) the left half-filled symbols are sulfates, right half-filled are sulfides, where (F) is only sulfates. Standard errors are present, if not smaller than the symbols (*see* Methods).

Product production (PPR) and reductant partitioning (RPR) ratios:

Equn. 5.4. $$PPR = \frac{[acetate]_{t=n+1} - [acetate]_{t=n}}{[sulfide]_{t=n+1} - [sulfide]_{t=n}},$$

Equn. 5.5. $$RPR = \frac{[lactate]_{t=n+1} - [lactate]_{t=n}}{[sulfide]_{t=n+1} - [sulfide]_{t=n}}.$$

Equations 5.4 and 5.5 allow us to determine the MSR reaction stoichiometry over the course of log-phase. We normalize the consumption or production of the electron donor or its measurable product acetate, respectively, to sulfide production. These equations may just as easily be re-written to track the change in sulfate, using the data in Fig. 5.2, with no discernable difference (calculations not shown).

Mass balance

Mass balance and isotope mass balance are calculated from the standards equations for a closed system. Isotope mass balance closes as all points. Mass balance estimates from concentration data alone (Equation 5.6) closes at almost all points, with exception of final and second to last time points in a few cases (Table 5.3) and over estimates early in the experiment. Overestimates are likely due to the error in the quantification method. Underestimates from Equation 5.6 at latest time points are due to the partitioning of some sulfide into the headspace, which is un-sampled by the method of removing liquid at each time point. That is, the 1L experimental vessels started at 0.824 to 0.820 L of liquid volume and then sub-sampled at each time-point, increasing the ratio of headspace to liquid, allowing more aqueous sulfide to partition into the headspace as the experiment progressed. Therefore, the concentration measurements of aqueous sulfide underestimate the total mass of sulfide in the system, which is only noticeable later in the experiments when sulfide accounts for a more significant fraction of total S (Table 5.3). To account for this pool we simply test whether isotope and mass balance are accounted for by summing the aqueous sulfate, aqueous sulfide, and headspace sulfide pools. To do so we must calculate the mass of the headspace sulfide and do so as follows: assume that the errors output by Equation 6 are accounted for by the head-space sulfide or over-estimates due to sulfate concentrations errors, and assume that the isotopic composition of headspace sulfide is identical to that of aqueous sulfide. The latter is a fair

assumption considering the bottles were homogenized (e.g. vigorously shaken for 3-4 minutes, exchanging aqueous and gaseous sulfide) prior to sample extraction at any given time point, and is cross-checked by comparing the outputs of mass-balance and isotope mass-balance calculations (Table 5.3). This exercise demonstrates the importance of calculating isotope mass balance at all sampling points, particularly as experimental designs become more and more complex (e.g. chemostats (Leavitt et al. n.d.) or semi-closed systems (Davidson et al. 2009)).

A simple method of calculating mass balance from concentration or mass measurements:

Equn. 5.6. $$\sum_{j=1}^{m} X_j = 1,$$

are the mole fractions of *m* components, and should sum to 1 if all mass/concentration estimates are accurate.

While isotope mass balance is calculated from:

Equn. 5.7. $$R_{system} = \sum_{j=1}^{m}\left(X_j R_j\right) = 1,$$

is the whole system isotope ratio such that:

Equn. 5.8. $$\delta_{system} = \sum_{j=1}^{m}\left(X_j \delta_j\right),$$

which is only approximate.

Equation 5.7 must be applied for exact calculation of isotope mass balance, then converted to delta values.

We define the reaction coordinate from the residual reactant with respect to the initial reactant sulfate as:

Equn. 5.9. $$f_{SO4,t} = \frac{\left[SO_4^{2-}\right]_{t=n}}{\left[SO_4^{2-}\right]_{t=0}}$$

Or with respect to the pooled product sulfide relative to the initial reactant:

Equn. 5.10. $$f_n{}^{*} = \frac{\left[SO_4^{2-}\right]_{t=0} - \left[H_2S\right]_{t=n}}{\left[SO_4^{2-}\right]_{t=0}}$$

To determine mole ratio of head-space sulfide using isotope constraints:

Equn. 5.11. $$f_{headspace,t=n} = \frac{\left({}^{34}R_{SO4,t=0} \times f_{SO4,t=0}\right) + \left({}^{34}R_{SO4,t=n} \times f_{SO4,t=n}\right) + \left({}^{34}R_{H2S,t=n} \times f_{SO4,t=n}\right)}{\left\{{}^{34}R_{headspace,t=n} = {}^{34}R_{H2S,t=n}\right\}}$$

Summing the mol ratios calculated in Equations 5.6 and 5.11 should reflect the initial, if the assumption that dissolved sulfide and headspace sulfide maintain identical sulfur isotopic compositions holds. To test this

approach, we compare Equation 5.11 estimates to the simple difference between f_{SO4} and 1-f^*. The approaches are indeed consistent (Table 5.3), validating this approach.

Fractionation factors are calculated using a standard derivation of the Rayleigh equation for a closed system, using our more conservative estimates of f_{SO4} as inputs, and all measured ${}^{34}R_{V\text{-}t0\_SO4}$.

Equn. 5.12. $$ {}^{34}\varepsilon_{t=n}(‰) = \frac{\ln\left(\frac{{}^{34}R_{SO4,t=n}}{(1-f_{SO4,t=n})\times f_{H2S,t=n}+f_{SO4,t=n}\times f_{H2S,t=n}}\right)}{\ln(f_{SO4,t=n})}\times 1000. $$

All calculations are performed with isotope ratios (${}^{34}R$) and not delta-values ($\delta^{34}S$), in order to minimize error (Hayes 2001). Strain and replicate-specific averages are presented in Table 5.2.

RESULTS & DISCUSSION

Growth experiments

Dynamics in the closed system are tracked for each strain. Sulfate reduction is coupled to lactate oxidation with the stoichiometric production of acetate and sulfide and concomitant increases in cell density (Figure 5.2a-c). From changes in optical density and concentration measures we approximate: log-phase doubling time (μ), biomass specific sulfate reduction rate (μSRR), and biomass yield (Y) of each strain (Table 5.1). The doubling times from log-phase WT and IPFG06 are nearly equivalent, offset by a longer lag-phase for IPFG06, whereas μ for IPFG07 and IPFG09 were significantly less (e.g. fewer doubling per hour), at factors of approximately 0.5 and a 0.25 the WT, respectively (Table 5.1). While the lack of chromosomally encoded *dsrC* did increase the length of lag-phase (IPFG06 vs. IPFG07), it reduced μSRR in IPFG07 and IPFG09 to approximately have that of the WT and IPFG06, the strains with chromosomally encoded *dsrC*. Interestingly, the production ratio of acetate:sulfide (PPR) and lactate:sulfide (RPR) are statistically indistinguishable between all strains (Table 5.1). Biomass yield is consistent between WT, IPFG06 and IPFG07, but significantly less in the mutant lacking a fully functional DsrC, IPFG09 (Y, Table 5.1), and terminal cell densities for this mutant are consistently half that of the other strains (Figure 5.2, Table 5.1).

Oxygen isotope measurements

The oxygen isotopic composition of sulfate does not significantly vary outside the analytical error of the measurement (0.4‰). The composition of the starting water ($\delta^{18}O_{H2O}$) is still being determined, and will then allow us to calculate the fractionation factor between sulfate and oxygen – nonetheless, it is near invariant (Figure 5.3). Previous studies of closed-system MSR experiments have yielded conflicting results. In some cases there is no change in the composition of the sulfate, until very late on a ration coordinate (Turchyn et al. 2010). In other cases, the $\delta^{18}O_{SO4}$ shifts earlier. The best example of experiments where the $\delta^{18}O_{SO4}$ shifts significantly are MSR experiments where the medium water is labeled with a -40 or +700‰ $^{18}O_{H2O}$ spike, and the organisms inhibited with increasing concentrations of nitrite (MANGALO et al. 2007; Mangalo et al. 2008; Einsiedl 2009). Insignificant isotopic enrichment occurs in the $\delta^{18}O_{SO4}$ in cultures with no nitrite, and given the small isotopic shift these authors observe under the huge $^{18}O_{H2O}$ spike, we would expect little to no measureable shift in the $\delta^{18}O_{SO4}$ in our un-spiked system. Performing similar experiments as to those herein, incorporating the isotopically labeled water, is certainly a future direction for targeted experimental work with these mutants. We hypothesize that the sulfate will indeed become detectably enriched if the reversibility of APSr and AtpS enzymes holds (Harry D Peck 1960; J. Farquhar et al. 2008; Rees 1973), and downstream DsrAB or DsrC steps are slower, allowing for the exchange of sulfite-O with the labeled water, followed by sulfite backflow/reoxidation to sulfate, and exchange with the extracellular sulfate pool (Wankel et al. 2014; Müller et al. 2013).

Sulfur isotope measurements

The major S isotopic compositions ($\delta^{34}S_{V\text{-}CDT}$) of reactant sulfate, product sulfide, and where available, biomass sulfur (CRS), are presented from each experiment, from each replicate bottle, for each strain (Figure 5.2D). Classic closed-system fractionation behavior is observed in the WT, IPFG06 and IPFG07 bottles (Figure 5.2D). In stark contrast, IPFG09 sulfide compositions ($\delta^{34}S_{H2S}$) show no compositional change, despite increasing sulfate S isotopic compositions. The concentration behavior as a function of *f*, sulfide increasing with decreasing sulfate,

are consistent between all strains (Figure 5.2B, 5.2D, 5.3) – further highlighting the odd behavior of $\delta^{34}S_{H2S}$ in IPFG09 replicates.

While mass balance closes within analytical error in all time point samples from all strains (Table 5.3), we were able to extract enough chromium reducible sulfur (CRS) from the biomass pellet (known as 'biomass S' here forward) in a number of later time points from each strain, and a few from earlier time points from IPFG09. From these few biomass $\delta^{34}S_{CRS}$ measurements it is clear that this pool sits consistently between sulfate and sulfide compositions (Table 5.5), though the error range (95% confidence intervals) is large due to the small sample sizes, and incorporates the range of $\delta^{34}S_{H2S}$. This is consistent with previous measurements of biomass sulfur during MSR experiments (Kaplan & Rittenberg 1964).

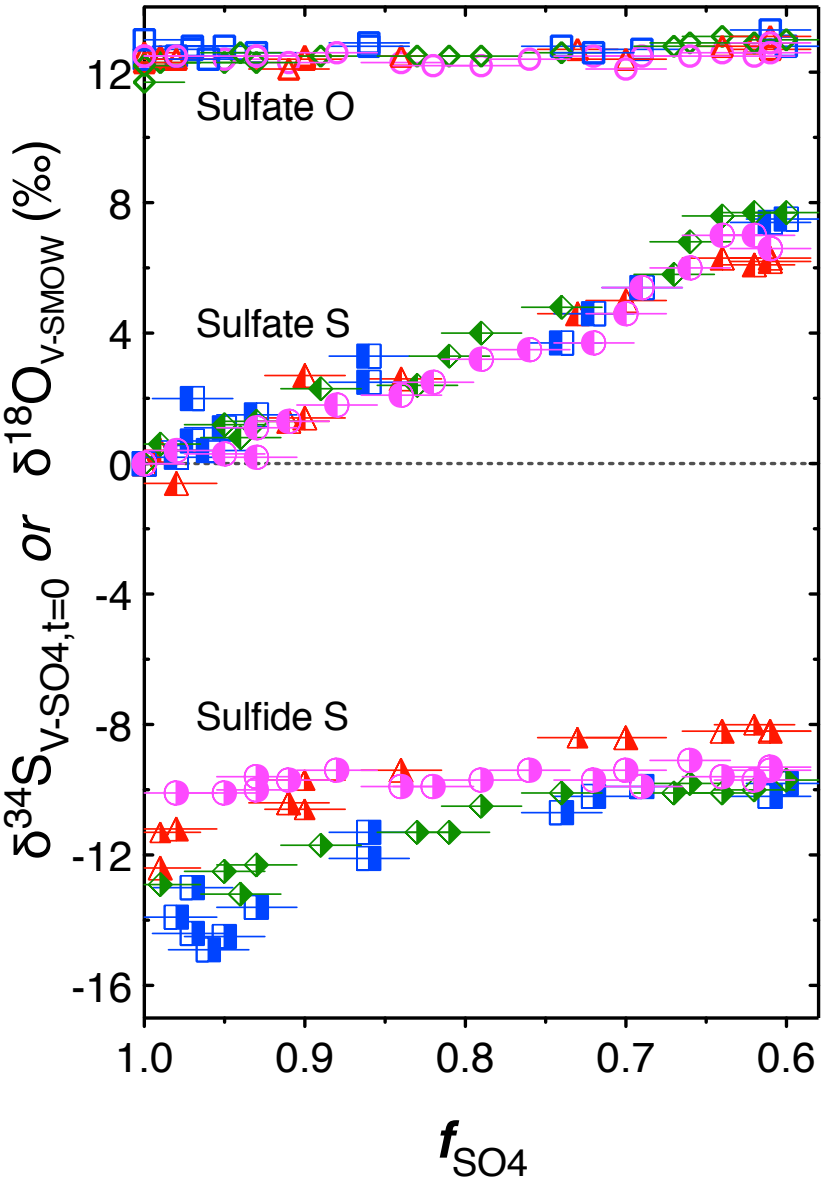

Figure 5.3. Isotope ratios over the reaction coordinate. Reactant sulfate S and product sulfide S relative to the initial composition of sulfate. Sulfate O relative to international standards V-SMOW. The x-axis is the reaction coordinate ($f_{SO4} = [SO_4^{2-}]_{tn}/[SO_4^{2-}]_{t0}$). Long-term isotopic composition measurement errors (1σ) are smaller than the symbols, at 0.3‰ and 0.4‰ for $\delta^{34}S$ and $\delta^{18}O$, respectively.

Sulfur isotope fractionation ($^{34}\varepsilon$)

We evaluate the classic derivation of the closed-system Rayleigh distillation model to estimate the fractionation factors ($^{34}\varepsilon$) for each strain (Equation 5.12). There is no clear trend between $^{34}\varepsilon$ and μSRR (Figure 5.4) when comparing the wild-type to the three mutants. This may run counter to observations in other batch experimental studies (Kaplan & Rittenberg 1964; Sim, Ono, et al. 2011c), including recent work with hydrogenase mutants (Sim et al. 2013). That is, the observation that the magnitude of fractionation correlates negatively with specific sulfate reduction rate holds in pure culture experiments (closed- and open-system) and modern marine sediments (Harrison & Thode 1958; Kaplan & Rittenberg 1964; Kemp & THODE 1968; Lyn A Chambers et al. 1975; Sim, Ono, et al. 2011c; Sim, Bosak & Ono 2011b; Leavitt et al. n.d.; Sim et al. 2013; Sim et al. 2012; Goldhaber & Kaplan 1975). The fact that IPFG06 grows as fast as the WT, but fractionates S more (Figure 5.4), is not clearly explained by the previous working theory. It is possible that the rate limiting step within the IPFG06 MSR pathway is shifted to a step that fractionates more strongly than in the other strains – particularly IPFG07 and WT. For example, if DsrAB is the rate-limiting step in IPFG06 and has a fractionation of approximately 15‰ (Chapter 4), whereas APSr is the slowest step in IPFG07 and IPFG07 with a fractionation of about 11‰ , this pattern may be accounted for. This prediction requires further experimental validation.

Perhaps most intriguing is the decoupled behavior of the sulfate and sulfide S isotope trajectories in the IPFG09 experiments. While the growth parameters suggest a significant decrease in net metabolic efficiency relative to the other strains, the depressed fractionation early in the experiments ($^{34}\varepsilon_{SO4\text{-}H2S}$ < 10‰ at f > 0.9), also less than the other strains, is inconsistent with the rate—fractionation relationship common in the literature, and indeed our previous work (Chapter 2, Appendix B, (Leavitt et al. n.d.)). The depressed μ, μSRR, and lower Y suggest a suppressed DsrC cycle in the cytoplasm of IPFG09 cells. Moreover, the lack of response in IPFG09 $\delta^{34}S_{sulfide}$ indicates the MSR biochemical network operates uniquely in IPFG09, and influences the net fractionation between sulfate and sulfide ($^{34}\varepsilon_{SO4\text{-}H2S}$). Semi-quantitative Western blot analysis of DsrC and DsrB are underway, and will be included in this study prior to manuscript submission. We predict an increased expression of the enzyme DsrC relative to DsrAB in this strain, such that the cells might compensate for the

significant loss of metabolic efficiency in the IPFG09 mutant, where DsrC is hobbled at the penultimate cysteine. What insulates the $\delta^{34}S_{H2S}$ composition from shifts in response to $\delta^{34}S_{SO4}$ enrichment remains a mystery at present. In the absence of further evidence, we suggest it is the result non-steady state conditions at the intracellular level, yielding varying combinations of fractionation factors at different times in the experiment. This then manifests as a changing $^{34}\varepsilon_{SO4\text{-}H2S}$ over f (Figure 5.3).

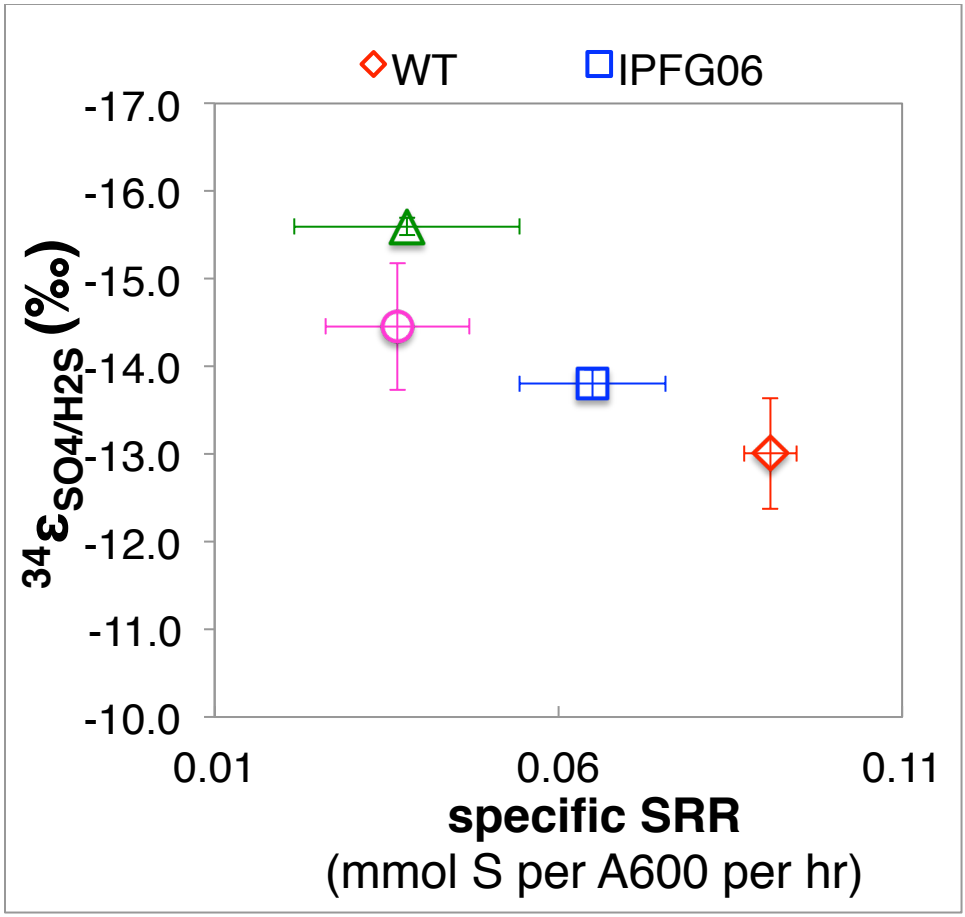

Figure 5.4. Strain-specific fractionation factors versus specific sulfate reduction rate. The fractionation factors ($^{34}\varepsilon$) are calculated for each time point and each replicate experiment separately, the means of individual bottles plotted as the symbol. The y-error bars are the range of fractionation factors calculated for each replicate, while the x-error bars are the range of values calculated for each replicate during log-phase, the only time calculating μSRR is meaningful in a batch experiment. Symbols are the same as for earlier figures.

CONCLUSIONS

In this study we demonstrate that the role of DsrC at high and low intracellular efficiencies influence the closed-system dynamics of MSR metabolism and S isotope fractionation. We observe a de-coupling in the standard fractionation metric $^{34}\varepsilon_{SO4\text{-}H2S}$ in response to different specific growth rates, between mutants and WT. Furthermore, we observe the decoupling of isotopic responses in the reactant and product pools during MSR with the strain IPFG09. This mutant strain contains only one of two terminal cysteines critical to the terminal production of sulfide in the MSR pathways – the first time a point mutation has been used to investigate isotope fractionation.

To peel these apart the fractionation response in each of these mutants, and in particular the non-traditional closed-system behavior of IPFG09, open system work is necessary. In a chemostat we may fix the μSRR between strains (e.g. Chapter 3) and observe strain-specific responses in fractionation. In such future works, we also aim to simultaneously track intracellular parameters, such as DsrC:AB expression ratios, intracellular redox state, and the relative concentrations of key MSR intermediates. In conjunction with the standard growth and fractionation parameters measured herein, such data will allow us to better parameterize the metabolic isotope models of MSR (Johnston et al. 2007; J. Farquhar, Johnston, et al. 2007a; Bradley et al. 2011). Coupling the work here with the concentration and isotopic compositional measurements of intracellular MSR intermediates is a clear next step.

ACKNOWLEDGEMENTS

We thank Erin Beirne for expert analytical assistance with oxygen and sulfur isotope analyses. Many thanks to the Colleen Hansel for access to the ion chromatograph, and Emily Estes and Adiari Rodriguez-Vasquez assistance in running it.

Table 5.2 (continued on next page). Final reaction coordinate ($f_{t=final}$), growth rate (μ), specific sulfate reduction rate (μSRR), growth yield (Y), product partitioning ratio (PPR), reductant partitioning ratio (RPR), and average fractionation factors ($^{34}\varepsilon$) for each experimental replicate (*a*, *b*) from each strain (*see* Methods for equations).

Table 5.2. (continued from previous page)

	WT a	WT b	IPFG06 a	IPFG06 b	IPFG07 a	IPFG07 b	IPFG09 a	IPFG09b
$f_{t=final}$	0.61	0.61	0.6	0.61	0.64	0.62	0.62	0.61
μ	0.15 ± 0.03	0.17 ± 0.00	0.15 ± 0.02	0.15 ± 0.03	0.07 ± 0.02	0.07 ± 0.02	0.04 ± 0.03	0.04 ± 0.03
μSRR	0.09 ± 0.00	0.09 ± 0.00	0.06 ± 0.01	0.07 ± 0.01	0.04 ± 0.01	0.04 ± 0.01	0.04 ± 0.01	0.04 ± 0.01
Yield	0.013 ± 0.002	0.015 ± 0.003	0.013 ± 0.002	0.015 ± 0.003	0.013 ± 0.004	0.014 ± 0.004	0.007 ± 0.001	0.007 ± 0.003
PPR	1.7 ± 0.3	1.9 ± 0.2	2.2 ± 0.6	1.9 ± 0.4	2.1 ± 0.2	2.5 ± 1.0	2.1 ± 0.9	2.2 ± 0.5
RPR	2.1 ± 0.2	2.3 ± 0.4	2.7 ± 0.4	2.3 ± 0.2	2.4 ± 0.4	2.2 ± 0.5	2.3 ± 0.5	2.4 ± 0.7
$^{34}\varepsilon$ (‰)	-11.6 ± 0.6	-11.4 ± 0.7	-13.7 ± 0.9	-14.2 ± 0.9	-13.4 ± 0.4	-13.2 ± 0.5	-11.5 ±1.3	-11.4 ±0.9

Units: $f_{t=final}$, mol fraction; μ (per hour); μSRR (change in mM sulfate per change in A600 per hour);
yield (unit change A600 per mmol lactate per hour);
PPR and PRP(acetate: sulfide production or lactate:sulfite balance ratios), and 34ε in standard per mil (‰) notation.

Table 5.3. Mass Balance.

strain t_n	$f_{SO4} + (1\text{-}f^*)$ Equn.: 5.9 + (1 - 5.10)		$f_{H2S\_headspace}$ 1 – Equn 5.9		$f_{H2S\_headspace}$ Equn. 5.11		mass balance Equn. 5.9 + 5.11	
WT	**a**	**b**	**a**	**b**	**a**	**b**	**a**	**b**
1	100%	102%	n.a.	n.a.	0%	-4%	n.a.	n.a.
2	103%	101%	-3%	-3%	-3%	-3%	100%	98%
3	104%	103%	-4%	-5%	-4%	-5%	100%	98%
4	100%	102%	0%	-4%	0%	-4%	100%	98%
4	108%	103%	-9%	-5%	-8%	-5%	100%	98%
5	104%	102%	-4%	-4%	-4%	-4%	100%	98%
6	98%	98%	1%	0%	1%	0%	100%	98%
7	98%	97%	2%	1%	2%	1%	100%	98%
IPFG06	**a**	**b**	**a**	**b**	**a**	**b**	**a**	**b**
1	100%	100%	n.a.	n.a.	0%	0%	n.a.	n.a.
2	99%	103%	0%	-3%	0%	-3%	100%	100%
3	100%	99%	0%	1%	0%	1%	100%	100%
4	99%	101%	0%	-1%	0%	-1%	100%	100%
4	98%	108%	2%	-9%	2%	-9%	100%	100%
5	94%	103%	6%	-3%	6%	-3%	100%	100%
6	94%	96%	6%	4%	6%	4%	100%	100%
7	92%	92%	8%	8%	8%	8%	100%	100%
IPFG07	**a**	**b**	**a**	**b**	**a**	**b**	**a**	**b**
1	100%	100%	n.a.	n.a.	0%	0%	n.a.	n.a.
2	102%	98%	-2%	2%	-2%	2%	100%	100%
3	102%	101%	-2%	-2%	-2%	-2%	100%	100%
4	102%	97%	-2%	2%	-2%	2%	100%	100%
4	100%	102%	0%	-2%	0%	-2%	100%	100%
5	98%	96%	2%	4%	2%	4%	100%	100%
6	96%	91%	4%	9%	4%	9%	100%	100%
7	95%	94%	4%	5%	4%	6%	100%	100%
IPFG09	**a**	**b**	**a**	**b**	**a**	**b**	**a**	**b**
1	100%	100%	n.a.	n.a.	0%	0%	n.a.	n.a.
2	98%	101%	2%	-1%	2%	-1%	100%	100%
3	98%	100%	2%	0%	1%	0%	100%	100%
4	101%	100%	-2%	-1%	-2%	0%	100%	100%
4	98%	98%	2%	2%	2%	2%	100%	100%
5	97%	99%	3%	1%	3%	1%	100%	100%
6	95%	96%	5%	3%	5%	3%	100%	100%
7	98%	97%	2%	2%	2%	3%	100%	100%
8	96%	95%	3%	4%	3%	5%	100%	100%
9	93%	93%	6%	7%	6%	7%	100%	100%

Table 5.4. Sulfide blank and biomass (CRS) sulfur isotopic compositions, corrected from small EA-IRMS measurements. The 95% confidence intervals are asymmetric (*see* Methods for size correction method).

Strain	Time Point	Replicate	Pool	$\delta^{34}S$ (‰) VCDT	95% confidence interval	
					Upper	Lower
WT	t0	A	H2S	-10.5	-8.9	-22.2
FG06	t0	A	H2S	-6.9	-6.4	-12.7
FG07	t0	B	H2S	-7.2	-3.7	-24.5
FG09	t0	B	H2S	-9.5	-2.7	-34.1
FG06	t7	A	H2S	0.0	0.7	-6.9
WT	t5	B	CRS	-2.1	-0.6	-13.4
WT	t6	B	CRS	0.6	1.0	-4.8
WT	t6	A	CRS	0.8	1.1	-3.6
WT	t7	B	CRS	0.5	0.7	-3.3
WT	t7	A	CRS	0.4	0.8	-4.5
FG06	t5	B	CRS	-10.4	-3.0	-36.1
FG06	t6	B	CRS	-3.9	-0.3	-21.4
FG06	t7	B	CRS	-1.5	-1.0	-7.4
FG07	t4	B	CRS	-2.2	-0.5	-13.9
FG07	t5	A	CRS	-3.8	-0.4	-21.1
FG07	t6	A	CRS	-4.8	-4.2	-11.4
FG07	t6	A	CRS	-4.4	-4.1	-8.7
FG07	t6	B	CRS	0.4	0.7	-4.0
FG07	t7	B	CRS	0.1	0.5	-4.6
FG07	t7	A	CRS	-0.9	-0.6	-5.5
FG09	t2	B	CRS	-3.6	-2.4	-13.5
FG09	t7	A	CRS	-0.8	0.3	-10.4
FG09	t8	A	CRS	1.0	1.9	-7.4
FG09	t8	B	CRS	0.7	1.6	-7.2
FG09	t9	B	CRS	0.6	1.1	-5.8
FG09	t9	A	CRS	0.7	1.4	-6.8

CHAPTER 6

CONCLUSIONS

Conclusions

The global sulfur cycle has evolved to include and eventually be driven by the operation of MSR. Over the duration of Earth's history, MSR has played a role of varying importance to global carbon, oxygen, and metal cycles (notably iron and manganese). Critically, MSR may have dominated the reductive sulfur cycle since its origination.

The overarching goal of this dissertation is to determine the primary environmental and biochemical constraints on the magnitude of MSR sulfur isotope fractionation. Herein we demonstrate the enzyme-specific fractionation factor for the key enzyme in the MSR metabolic network, DsrAB. Furthermore, we place quantitative constraints on the influence of organic matter versus sulfate limitation on net fractionation during dissimilatory sulfate reduction. These observations make predictions for isotopic patterns in modern marine and freshwater systems, as well as facies testable predictions for sedimentary-rock hosted sulfur isotope records.

In Chapter 2 we test the hypothesis that the availability of electron donor drives specific sulfate reduction rates, and moreover, that both major and minor sulfur isotope fractionations scale negatively and inversely with rate. We accept this hypothesis and then apply this relationship to an example in the Phanerozoic geological sulfur isotope records and shallow-water depositional environment reconstructions. From this work we propose that concomitant expansions in the magnitude of major and minor sulfur isotope fractionation (between sedimentary sulfate and sulfide minerals) represents a deceleration of globally integrated sulfate reductions rates. This slowing is likely driven by changes in the delivery of organic matter quantity and quality to MSR, and puts in place predictions for the redox structure of water column or sediments overlying the zone of sulfate reduction.

In Chapter 3, the influence of sulfate concentration on the magnitude of sulfur isotope fractionation is revisited. Using two strains of differing natural histories (e.g. one freshwater, one from a brine well) and also under steady-state growth regimes in a chemostat, we test the importance of oxidant availability over a range of concentrations complimentary to those in the original study of Habicht and colleagues (2002). We observe two distinct relationships between the magnitude of fractionation and concentrations of sulfate. One strain exhibits no response in fractionation from 0.1 to 6 mM sulfate, with fractionation nearly constant and greater than 20‰,

whereas the strain isolated from the brine shows a tight linear relationship between the magnitude of fractionation and the available sulfate over the same concentration range. In this section we highlight the necessity to revisit the application of previous work (Habicht et al. 2002) as a means of placing concentration constraints on Archean seawater sulfate. On-going work will aid in determining a mechanistically constrained relationship between fractionation and the physiological demand for sulfate by MSRs. Ultimately, reconstructing the evolutionary trajectory of this relationship using genomic and physiological data from extant MSRs hailing from a diversity of natural settings will bolster our ability to re-read the isotope records, and taken in conjunction with facies constrained sequence stratigraphic records, shed new light on the state of ancient environments.

In Chapter 4, we constrain, for the first time in the sulfur isotope literature, the magnitude of a specific enzyme fractionation factor ($^{34}\varepsilon_{DsrAB}$) – better still, we also constrain minor sulfur isotope fractionation ($^{33}\lambda_{DsrAB}$). Doing so with the keystone enzyme in MSR, DsrAB, we are able to better interpret MSR isotope effects from the last sixty years of experimental work, and as the rest of the MSR metabolic system – as well as those in oxidative and disproportionative metabolisms become constrained at this level – we look to cleanly interpret isotopic observations from modern natural systems and ultimately, the geological record.

In Chapter 5 the influence of metabolic network efficiency on the magnitude of isotope fractionation is tested. We employed recently developed mutants in *dsrC*, traditional closed-system fractionation experiments, coupling these old and new techniques to determine the influence of single point mutation on the global biochemical network of MSR, and in response, growth and sulfate reduction rates, with intriguing and somewhat unexpected outcomes in the magnitude of major isotope fractionations. On-going work will couple the fractionation and growth rate profiles of three mutant strains and the wildtype to DsrB:DsrC protein expression profiles. This will be the first study to directly link both the functionality and expression of a single enzyme to the efficiency of the MSR pathway and the magnitude of fractionation.

Many of the ideas for this dissertation originated from a reading group between Dave Johnston, Alex Bradley, Renata Cummins and myself back in the summer of 2010, when I was desperately seeking a project that did not involve the Archean – as things so old terrify me. The outcome was my dissertation proposal and shortly

thereafter a publication in *Geobiology* detailing our revision of the MSR metabolic network model (Appendix A), incorporating the latest biochemical observations from Ines Pereira's group (Oliveira, Vonrhein, Matias, Venceslau, P. M. Pereira, et al. 2008b). As a brief retrospective on this publication, I highlight updates to the ongoing revision of the MSR metabolic fractionation model. This publication and the novel mathematical derivation of a metabolic MSR model, updating the often cumbersome algebraic formulation to a more elegant matrix (linear algebraic) formulation, as well as the coding into an open source ***R***-based format (freely available: github.com/bradleylab/SRBmodel), were spearheaded by Alex Bradley, with text sourced from my dissertation proposal. While the revision of the MSR model featured in Appendix A is the most up-to-date in the literature, both with regard to the MSR biochemistry and our knowledge of intracellular fractionations at that time in late 2010. It can now be updated further following the chapters herein. Most notable are constraint to the magnitude of DsrAB fractionation and the dredging up of limited sulfate reduction to sulfite fractionations found by Ford (Ford 1957), both in Chapter 4. Further, the relative control of reductant (Chapter 2) or oxidant (Chapter 3) availability on net $^{34}\varepsilon_{MSR}$ and $^{33}\lambda_{MSR}$, as well as the potential for intracellular thionate production in response to high sulfite concentrations/ residence times (Appendix B; (Bertran et al. 2013)), can be included.

In sum, it is clear from the chemostat work in Chapter 2 that as the rate of sulfate reduction approaches zero, the sum of all biochemical and cellular effects heads toward those equilibrium fractionations originally predicted more than sixty years ago (Figure 6.1) (Tudge & Thode 1950). On the other end of the spectrum, as the rate of MSR increases toward a biochemically limited maxima, but electron donor availability is still ultimately limiting reaction rate (e.g. chemostat versus batch experiments), a minimum fractionation is approached, statistically identical to that of DsrAB at 15.3‰ (Figure 4.2, Figure 6.1). Under all of these regimes, the influence of closed versus open system ('reservoir') effects may be felt, and will ultimately limit the absolute magnitude of fractionation the MSR system may reach when in play (Chapter 3). Finally, the situation of co-limited oxidant and reductant is perhaps the most confounding. The situations where both biochemical (e.g. K_S, K_M) and physical (e.g. [sulfate], [organic matter]) factors control the observed fractionation are likely more common throughout the geological and modern isotope records, and as such, experimental traction is necessary. Further investigations

employing similar simple experimental approaches as those above will lead us to a better understanding of stable isotope distributions in modern and ancient natural and their relevance to Earths biogeochemical cycles.

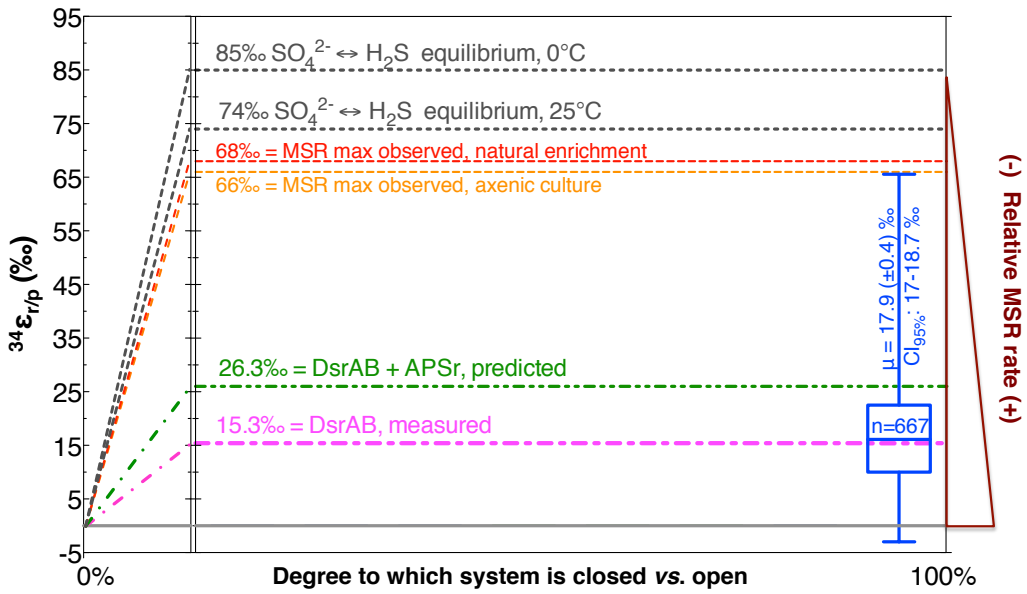

Figure 6.2. The predicted relationship between sulfate—sulfide fractionation in response to (*x-axis*) the degree to which the system is open vs. closed and the degree to which the isotopic exchange reaction is in equilibrium vs. dis-equilibrium (kinetic). The closer to equilibrium the slower the reaction, such that in the case of MSR, this relates directly to relative reaction rates of the net forward vs. net backward reaction (reduction relative to oxidation). For reference, the compilation from Chapter 4 (blue box-whisker plot), showing all literature reported sulfate or sulfite reduction experimental fractionations (n = 667). The most common MSR fractionation (is very near our measured value for DsrAB (15.3‰). The whiskers reflect the entire range, the box holds the 95% confidence interval (17.0 to 18.7‰), and the most frequent falls at 17.9 ± 0.4‰.

ON-GOING AND FUTURE WORK

Enzyme fractionation factors from other enzymes in the MSR network

Determining the magnitude of multiple sulfur and oxygen enzyme isotope fractionation factors from other MSR network enzymes is necessary to completely constrain metabolic fractionation models (Rees 1973; L A Chambers & Trudinger 1979; Brunner & Bernasconi 2005; Johnston et al. 2007; J. Farquhar, Johnston, et al. 2007a; Bradley et al. 2011). The enzyme noted even in the earliest works on MSR fractionation networks, other than DsrAB, is adenosine-5'-phosphosulfate (APS) reductase (APR) (Rees 1973). Determining the fractionations factors the in vitro during both forward and reverse APR-catalyzed reactions, along with determining the forward and reverse oxygen isotope fractionations associated with APS formation or degradation to sulfate and ATP by the enzyme sulfate adynlate transferase (SAT). SAT sulfur isotope fractionation are most likely negligible, as SAT binds the sulfate on the oxygen's (Ullrich et al. 2001), meaning that any kinetic effect is secondary, and these are likely small for sulfur (Kohen & Limbach 2005). Analytical and experimental approaches to determine the APR and SAT fractionation factors are currently underway, spearheaded by A. Bradley (Washington University in St. Louis) and colleagues. As highlighted in Chapter 4, the only approximations for the sum of the sulfate reduction to sulfite sulfur isotope fractionations (i.e. the sum of SAT and APR) stem from the unpublished PhD thesis of R.W. Ford (1957) in the lab of H. G. Thode. The only experimental attempt to determine the oxygen isotope fractionation across the SAT step (Kohl et al. 2012) is deeply flawed – though the modeling component in the same study is sound. In addition to APR and SAT, enzymes involved in the reduction of intermediate valence sulfur compounds that may participate significantly in the MSR network under certain growth regimes, are future targets for enzyme-specific fractionation work, including DsrAB itself (Chapter 4). Examples include the putative trithionate-reducing enzyme (TR-1) from *D. vulgaris* (Kim & Akagi 1985), and known enzymes such as thiosulfate/polysulfide reductase (Phs/Psr) commonly found in sulfate, sulfite, and thiosulfate reducers (Jormakka et al. 2002; Burns & Dichristina 2009; Shirodkar et al. 2010). These experiments can be performed in the manner pioneered in this work (Chapter 4) or in a more crude, though potentially higher throughput method, utilizing partially purified cell extracts and ex vivo experimental approaches (Drake & Akagi 1978), with

appropriate mass balance and isotope ratio analyses. Adapting either purified enzyme or crude-extracts to a stopped-flow or fully open-system experimental approach is also a crucial goal in on-going and future works.

Testing the ecology of sulfite reductase isotope fractionation factors

Determining the fractionation factors of DsrAB homologs and paralogs from microorganisms isolated from diverse environments will deepen our understanding for the fractionations determined in Chapter 5. Much like the work targeting isoforms of RuBisCO (Roeske & O'Leary 1984; G. D. Farquhar et al. 1982; Scott et al. 2004; Guy et al. 1993), the values presented in this work will only stand the test of time if others workers test other sulfite reductases as well as that of *D. vulgaris.* Targeting functional DsrAB homologs with the highest divergence in active site structure are ideal first targets. For example, the thioredoxin-dependent F_{420}-dependent sulfite reductase (Fsr) in methanogen *Methanocaldococcus jannaschii* is a sound target (Johnson 2005; Susanti et al. 2014). Furthermore, we will need to compare the fractionation factors from sulfite reductases containing non-siroheme active sites. For example, *Shewnanella oneidensis* MR-1 does not contain the standard DsrAB or C genes in known sulfate/sulfite/thiosulfate reducers (I. A. C. Pereira et al. 2011), and instead utilizes the non-siroheme containing sulfite reductase (Sir) (Burns & Dichristina 2009; Shirodkar et al. 2010). As mentioned above, MR-1 does not reduce sulfate for energy metabolism, and may thus provide and interesting highly divergent intermediate valence sulfur-cycling organism. The Sir and Fsr are ideal targets for future work in both open-system in vivo experiments, like those conducted in this Chapters 2 and 3; and perhaps semi-open experiments like those attempted previously with MR-1, but with a more constrained approach (*see* Appendix C). More important will be performing in vitro experiments similar to those in Chapter 5. Determining fractionation factors from these homologs to the *D. vulgaris* and *A. fulgidus* sulfite reductases (Chapter 4) will greatly expand our understanding for intracellular multiple sulfur isotope fractionation factors, the MSR network more broadly, and ultimately the sulfur cycle by a wider array of the organisms and greater number of natural environments.

Coupling theoretical models to empirical constraints

Moving to couple *ab initio* models, enzyme and co-factor structural information, and empirical fractionation data to provide a predictive framework for enzyme-induced kinetic isotope effects is daunting, but if successful, a powerful exercise. A possible workflow would include determining experimental kinetic isotope fractionations during sulfite reduction using the simplest sulfite reduction system possible – the siroheme reaction center in isolation (Soriano & Cowan 1995), determining the multiple S-isotope fractionation factors in response to different kinetic regimes (*e.g.* above/below the V_{max}, $K_{m\_Sulfite}$, or with/without competitive inhibition), as well as structural information of the siroheme-Fe~S complex during reaction (Fujii & Albarède 2012). Finally, using structural data of sulfite S and reaction products bound to the siroheme Fe-ligand, and extracting parameters (e.g. bond distances) relevant to kinetic isotope fractionation in the organo-metallic complex (c.f. (Fujii & Albarède 2012; Fujii et al. 2011)), *ab initio* model results for KIEs can be compared with empirical results, such as those obtained in Chapter 4. Such an approach may significantly expand our ability to predict enzymatic fractionation factors from structural information. Simpler theoretical approaches have been taken in related light-stable isotope systems, namely with nitrate reductase (Guo et al. 2010), in an effort to fit experimental observations (Karsh et al. 2012). This is an exciting new overlap in the fields of isotope geochemistry and biochemistry, with applications wide-ranging from earth history to medical biochemistry.

Intracellular response to extracellular reduction potential

Determining the direction and magnitude of isotopic response to environmental redox is a key challenge in future works. By determining the relationship between of S isotope fractionation, expression profiles of the central MSR enzymes (e.g. DsrAB/C/MKJOP, APSr, SAT, QmoABC), and intracellular redox indicators, a better coupling of geochemical and –*omic* datasets in lab (c.f Chapter 5) and field studies (c.f. (Canfield, Stewart, et al. 2010b)) will be possible. Moreover, determining the intracellular redox state of DsrC (Venceslau et al. 2013), expression profiles of MSR enzymes, and measuring the concentration and isotopic composition of intracellular MSR intermediates (APS, sulfite, thiosulfate), will better constrain our metabolic network models, as has been

proposed previously (Johnston et al. 2007; Bradley et al. 2011). Combining methods for streamlining intracellular concentration measurements (Newton & Fahey 1995), maintaining cells at steady state (Leavitt et al. n.d.), and adapting measurement of concentration and isotopic compositions measurements at ultralow concentrations (Paris et al. 2013) to intracellular metabolites, remain significant challenges.

Threshold effects on fractionation: when does sulfate become limiting?

Brought to the forefront in Chapter 3, the relationship between a MSRs organismal (cellular) K_S for sulfate and the magnitude of sulfur isotope fractionation possible between sulfate and sulfide ($^{34}\varepsilon_{MSR}$) is an active vein of inquiry. In part, this stems from recent challenges (Nakagawa et al. 2012; Gomes & Hurtgen 2013) to the original supposition that the magnitude of fractionation observed in sedimentary sulfur mineral proxies offers a metric as the mass of sulfate in the Earths oceans (Habicht et al. 2002; Canfield 2004a), due to observations in those challenges that sulfur isotope fractionations greater than 10‰ may occur at sulfate concentrations less than the 200 μM. In Chapter 3 we raise broader challenges to understanding this question, and in on-going work we aim to derive a more sound understanding for the evolutionary and physiological nature of the $K_{S\_Sulfate}$ – $^{34}\varepsilon_{MSR}$ relationship. The outcome of this work may well derive novel predictions and interpretations for modern and ancient sedimentary isotope signatures and their host environments. This is likely to be the case in light of the magnificently high $K_{S\_Sulfate}$ estimated for MSRs in hypersaline environments with high (> 100 mM) sulfate concentrations (Roychoudhury & Porter 2013). Implications for the original prescriptions of Archean and Paleoproterozoic oceans (Habicht et al. 2002), freshwater systems (Nakagawa et al. 2012; Gomes & Hurtgen 2013), and reservoir effects (Wortmann & Paytan 2012), will come to light.

Equilibrium isotope effects in MSR and the sulfur cycle

Ames and Willard (Ames & Willard 1951) observed that sulfite and the outer sulfonate sulfur in thiosulfate are freely exchangeable in buffered solutions of pH, temperature and concentration relevant to the MSR system. Moreover, preliminary calculations estimate equilibrium isotope effects between sulfite and the

sulfonate S (in thiosulfate) of greater than 16‰ at 30°C (Guo 2013). Together, these observations demand further experimental and theoretical investigations and will inform our observations from systems where sulfite and thiosulfate comingle in solution (Chapter 4, Appendix B, and (Bertran et al. 2013)). Preliminary abiotic work is underway to determine if such equilibrium isotope fractionation is observable under geobiologically relevant conditions.

Final Remarks

To render the types of studies herein broadly applicable and accessible a thermodynamically consistent kinetic theory is necessary. Specifically, combining the recent developments in geomicrobial kinetic theory (Bethke et al. 2011; Jin et al. 2013) with practical transient kinetic fractionation models (Maggi & Riley 2009; Maggi & Riley 2010), will allow the highly specific in vivo and in vitro experimental determinations of isotope fractionation factors, like those herein and in related biogeochemical cycles (Karsh et al. 2012; Karsh et al. 2013), to be interpreted and applied more broadly (c.f. (Druhan et al. 2014)). Extending the empirical approaches in this dissertation, and the theoretical yet to be devised, to other microbial sulfur metabolisms is absolutely necessary before a full understanding of the global sulfur cycle on any time scale is possible.

In the epilogue to his now prolific book chapter (Hayes 2001), John Hayes writes:

"It often seems that isotopic fractionations provide *too much* information about *too many* processes, combining it all in a package that is unmanageably intricate. In response, investigators keep increasing the complexity of the available data by providing more and more detailed analyses. … Does it increase the information-carrying capacity of the isotopic channel or is it another case of the triumph of entropy? To obtain the preferred result, we will have to understand biosynthetic fractionations …". I would extend this to include both catabolic and anabolic (*i.e.* all metabolic) reactions carried out by microorganisms important to the global geochemical cycles of light stable isotopes. My investigations into the organismal and enzymatic stable isotope fractionation factors of microbial sulfate reducers test Prof. Hayes prediction and hopefully lend some support toward further investigations of this and related subjects.

APPENDIX A

REVISITING THE DISSIMILATORY SULFATE REDUCTION PATHWAY

A version of this chapter is published as:

Bradley, A.S., Leavitt, W.D. & Johnston, D.T., 2011. Revisiting the dissimilatory sulfate reduction pathway. *Geobiology*, 9(5), pp.446–457.

Abstract

Sulfur isotopes in the geological record integrate a combination of biological and diagenetic influences, but a key control on the ratio of sulfur isotopes in sedimentary materials is the magnitude of isotope fractionation imparted during dissimilatory sulfate reduction. This fractionation is controlled by the flux of sulfur through the network of chemical reactions involved in sulfate reduction, and by the isotope effect associated with each of these chemical reactions. Despite its importance, the network of reactions constituting sulfate reduction is not fully understood, with two principle networks underpinning most isotope models.

In this study we build on biochemical data and recently solved crystal structures of enzymes to propose a revised network topology for the flow of sulfur through the sulfate reduction metabolism. This network is highly branched and under certain conditions produces results consistent with the observations that motivated previous sulfate reduction models. Our revised network suggests that there are two main paths to sulfide production: one strictly through Dsr, and a second that involves both Dsr and thionate intermediates. We suggest that a key factor in determining sulfur isotope fractionation associated with sulfate reduction is the ratio of the rate at which electrons are supplied to subunits of Dsr versus the rate of sulfite delivery to the active site of Dsr. This network of reactions may help geochemists to better understand the relationship between the physiology of sulfate reduction and the isotopic record it produces.

Introduction

The sedimentary sulfur isotope record is of fundamental importance for reconstructing the history of Earth surface oxidation (Canfield 2001a; Canfield 2004b; R. A. Berner & Canfield 1989). For instance, models for Phanerozoic oxygen concentrations (e.g. Geocarb and COPSE) rely on estimates of pyrite burial that are derived from mass-balance arguments involving the sulfur isotope record (Bergman & Lenton 2004; R. A. Berner & Canfield 1989). An assumption of these studies is a fixed isotopic offset between seawater sulfate and

contemporaneous sedimentary sulfide; a net fractionation that is dominated by dissimilatory sulfate reduction (DSR) with added contributions from oxidative cycling. Reconstructions of Earth surface environments therefore rely on an understanding of isotope fractionation associated with DSR. The precision of these reconstructions will improve as we come to better understand the fractionations associated with DSR.

Attempts to understand DSR date back to a suite of biochemical observations from which two simple models for the step-wise reduction of sulfate to sulfide were proposed (Peck 1959; Peck 1962; Kobayashi et al. 1969; Bandurski et al. 1956; Harrison & Thode 1958). The simplest model was a linear sequence of reactions, where sulfate was imported to the cell, activated to adenosine phosphosulfate (APS), and reduced to sulfite before the terminal (and unidirectional) reduction to sulfide. Rees (1973) formalized this pathway as an isotope model. In this model the key step is a direct six-electron reduction of sulfite to sulfide by dissimilatory sulfite reductase (Dsr). A second model incorporated the observations that enzyme preparations from sulfate reducers produced trithionate and thiosulfate *in vitro*, suggesting that intermediate sulfur species were produced between sulfite and sulfide (Kobayashi et al. 1969). The trithionate pathway, as it would come to be called, was translated into an isotope model more recently (Brunner & Bernasconi 2005). In the trithionate model, Dsr catalyzes only a two-electron reduction of sulfite. The uncertainty regarding the function of Dsr and the basic biochemical network of sulfate reduction has hampered our ability to determine the key factors controlling isotope fractionation. Although both the Rees and trithionate models help to explain the range of fractionation measured in culture and environmental sulfate reduction experiments (where depletions in $\delta^{34}S$ typically range from as 0‰ to -46‰), understanding the details of the physiological controls on the magnitude of fractionation remains under-developed. Further, with the recent observation of even larger fractionations (Canfield, Farquhar, et al. 2010a; Wortmann et al. 2001) -- fractionations that approach theoretical predictions (J. Farquhar et al. 2003; Tudge & Thode 1950; Szabo et al. 1950; Johnston et al. 2007) – understanding the metabolic network for DSR is even more critical. We suggest that recent biochemical observations provide the next generation of predictions (Oliveira, Vonrhein, Matias, Venceslau, P. M. Pereira, et al. 2008b; Parey et al. 2010; Schiffer et al. 2008). Our

biochemically informed DSR network suggests that both the *Rees* and *trithionate* models are partially correct, yet incomplete in important and testable ways.

The goal of this paper is to outline a revised network for dissimilatory sulfate reduction that draws from recent biochemical work. Central to this model is an updated understanding of how sulfite is reduced to sulfide, which can proceed through parallel processes. Our incomplete knowledge of the fractionation factors associated with each discrete step in this revised model precludes specific predictions about matching environmental records. However, the DSR network outlined below provides a framework for future experiments and for the quantification of those discrete fractionation factors.

Previous models for the sulfate reduction network

At the most fundamental level, the isotopic composition of the products of any biosynthetic process depends on the network of chemical reactions involved in that process and the isotope effects associated with each constituent reaction (Rees 1973; J. Farquhar, Johnston, et al. 2007a; Hayes 2001). In the case of dissimilatory sulfate reduction, the influence of network topology on isotope fractionation has long been of interest (Rees 1973; Brunner & Bernasconi 2005; Johnston et al. 2007; J. Farquhar, Johnston, et al. 2007a). The leading models (*Rees* and *trithionate* pathways) share many features, most of which are derived from early biochemical studies of the sulfate reduction pathway (Bandurski et al. 1956; Peck 1959; Peck 1961; H D Peck 1962; Helmuth Hilz 1955; Robbins & Lipmann 1956; Robbins & Lipmann 1958; Michaels et al. 1970). There is wide agreement that sulfate is actively transported into the cell via sulfate permease (Piłsyk & Paszewski 2009). ATP sulfurylase then activates intracellular sulfate to the reactive intermediate adenosine phosphosulfate (APS) (Robbins & Lipmann 1958; Helmuth Hilz 1955; Robbins & Lipmann 1956), which – unlike sulfate – can be readily reduced to sulfite. APS reductase (Michaels et al. 1970) catalyzes the latter reaction and is responsible for sulfite production. APS is also generally the branch point for catabolic reactions involving sulfur (Gregory & Robbins 1960). Based on experimental data available at the time Rees's model was published (1973), kinetic isotope effects were assigned to these upstream reactions, including the transport of sulfate into the cell ($^{34}\varepsilon$ =

+3‰; (Harrison & Thode 1958)) and to the reduction of APS to sulfite ($^{34}\varepsilon$ = -25‰). This is where the commonality between models ends, as each carries a specific prediction for the reduction of sulfite to sulfide and associated fractionations.

The Rees pathway

The sulfur isotope fractionation model presented by Rees (1973) suggests that Dsr catalyzes a six-electron transformation of sulfite to sulfide (Figure A1.1a). In the *Rees* model, the three reactions upstream of sulfite reduction are reversible, while sulfite reduction is a terminal and unidirectional step that carries a significant fractionation ($^{34}\varepsilon$ = -25‰). The choice of fractionation factors was guided by experimental data predating the Rees model. Incorporating these, the *Rees* model yields a maximum fractionation of -47‰. Maximum fractionation in the *Rees* model occurs when reactions between external sulfate and sulfite are fully reversible.

All the experimental data forming the basis of the *Rees* model were derived from measurements of metabolic sulfur isotope fractionation associated with reduction of sulfate or sulfite by live cultures of bacteria (Kaplan & Rittenberg 1964; Ford 1957). There were no data from purified enzymes; therefore the fractionations assigned to particular enzymatic steps in the network are inferences, not direct measurements. Furthermore, the calculations critically rely on the assumed linear network structure. The magnitude of the fractionation assigned to the *Rees* pathway was derived from experimental results in which observed isotope fractionation could approach -47‰, but rarely exceeded -25‰. This suggested that the isotope effect associated with the reduction of sulfite was rarely expressed, which could be explained if this reaction was very rapid relative to the upstream steps. This is consistent with the suggestion that the APS to sulfite reduction is the rate-limiting step in sulfate reduction (Harrison & Thode 1958). Under these conditions, the reduction of APS to sulfite would effectively be irreversible, and no downstream isotope effects could be expressed. The few cases at that time in which fractionations up to -47‰ had been observed were considered exceptional, in which this rapid processing of sulfite did not apply, and reversibility of sulfite reduction allowed expression of the upstream fractionation. These

interpretations, and the material fluxes that they suggest, are also consistent with later modeling studies targeting the *Rees* network (J. Farquhar, Johnston, et al. 2007a; Johnston et al. 2007).

The trithionate pathway

The six-electron reduction of sulfite to sulfide by Dsr, as outlined in Rees, has been controversial because numerous studies have detected the production of sulfur redox intermediates. For example, enzyme preparations from the sulfate-reducing bacterium *Desulfovibrio vulgaris* produced thiosulfate and trithionate when provided with sulfite (Kobayashi et al. 1969; Kobayashi et al. 1972; Findley & Akagi 1969; Findley & Akagi 1970). On the basis of these presumed intermediates, Kobayashi et al., (1969) proposed the *trithionate* pathway for sulfate reduction, in which trithionate and thiosulfate were intermediate steps in sulfite reduction to sulfide. In this model, Dsr reduces sulfite via a two-electron transfer, producing trithionate. A trithionate reductase catalyzes another two-electron transfer, reducing trithionate to thiosulfate. Finally, thiosulfate is reduced to sulfide by a third enzyme (Figure A1.1b). This model has been supported by some *in vitro* studies (Lee & Peck 1971; Jin-Po Lee 1973) and the predicted intermediates are produced under variable conditions of electron donor and sulfite availability (Akagi et al. 1994; Broco et al. 2005; Fitz & Cypionka 1990; Sass et al. 1992). Despite the measured presence of these intermediates, the authors of these studies questioned the overall significance of the *trithionate* pathway to net DSR. Consistent with this, recent genetic work suggests that while thiosulfate does form as an intermediate of sulfite reduction, thiosulfate reductase is not required for sulfate reduction (Broco et al. 2005). These studies suggest that sulfate-reducers are capable of processing thionates, but the conditions under which this is physiologically important remains unclear.

In detail, the *trithionate* pathway seemingly requires two reactions that are not required by *Rees:* the reductions of trithionate and thiosulfate. These reactions require enzymes (trithionate reductase and thiosulfate reductase), which have been partially characterized in some sulfate reducing bacteria (Akagi et al. 1994; Drake & Akagi 1977; Hatchikian 1975; Ishimoto et al. 1955; Haschke & Campbell 1971). An important disclaimer, and as noted by Akagi et al. (1984) however, is that presence of these enzymes does not confer their participation or

importance in DSR. In addition to the presence of dedicated enzymes to catalyze these reactions, a complicating factor is that Dsr itself may be capable of catalyzing the reduction of both trithionate and thiosulfate, at least in *Archaeoglobus* (Parey et al. 2010).

The trithionate pathway has been controversial in the four decades since it was proposed. Chambers and Trudinger (1975) argued against its presence on the basis of ^{35}S labeling studies. Peck and Legall (1982) also argued against a functional trithionate pathway because the reduction of trithionate and thiosulfate did not appear to be coupled to proton translocation. These authors suggest that the main benefit of thionate reduction is the regeneration of sulfite, which can then be reduced (coupled to energy conservation) by DsrAB and DsrC. They also point out that the relevant enzymes are not universal in sulfate reducers. For example, Drake and Akagi (Drake & Akagi 1977) describe an enzyme from *Desulfovibrio vulgaris* that forms thiosulfate from sulfite and trithionate. Peck and Legall state that while present in *D. vulgaris*, this enzyme is absent in *D. gigas*. The absence this enzyme in some sulfate reducers was argued to be evidence against the presence of this pathway. Even if this enzyme is not central to sulfate reduction, its observed irregular presence in sulfate reducers suggests that even closely related sulfate reducing bacteria may differ in their DSR network structure.

Brunner and Bernasconi (2005) (hereafter, *BB05*) revised *Rees* to mathematically incorporate the trithionate pathway. This revision includes two principle changes from the previous model. The first of these is that in *BB05* sulfite reduction to sulfide occurs via the trithionate pathway, and all of these reactions are assumed to be highly reversible. This followed in the tradition of some of the earliest estimates of sulfur isotope fractionation between sulfate and sulfide (Tudge & Thode 1950; Szabo et al. 1950). *BB05* add considerable detail to the pathway between sulfate and sulfide, but arrive at a similar conclusion. The *BB05* model proposes that reversibility extends to all of the sulfur atoms in trithionate and thiosulfate, and that each of these could back-react to form sulfite. They point out that the assumption of reversibility should extend from sulfate all the way to sulfide.

The second major change proposed by *BB05* is that they assign a very large isotope effect to the reduction of sulfite. *Rees* assigns this reaction a kinetic isotope effect of -25‰, while *BB05* assign a -53‰

fractionation to this step, yielding a -70‰ fractionation to the whole pathway. *BB05* predict that large fractionations will occur under high sulfide concentrations, when reversibility of the pathway will be maximized. The basis for the prediction of a larger fractionation rests on thermodynamic predictions of equilibrium isotope effects between sulfite and sulfide (J. Farquhar et al. 2003). The -70‰ estimated is similar in magnitude that arrived at by Tudge and Thode (1950) and Szabo et al. (1950). *BB05* use this equilibrium, and the kinetic isotope effect associated with the aerobic oxidation of sulfide to sulfite (Gest & Hayes 1984; FRY et al. 1985) to estimate the kinetic isotope effect associated with sulfite reduction through trithionate to sulfide. Similarly, thermodynamic data were used in Johnston et al. (2007), where minor sulfur isotope data (^{33}S and ^{36}S) was employed in an unsuccessful attempt to differentiate between *Rees* and *BB05*. The application of thermodynamic calculations is in many ways well-supported given its grounding in chemistry, however it clearly does not fully describe the biochemistry of a cell. The mechanistic aspects of sulfite reduction must also be considered, including the formation of an enzyme-substrate complex and the equilibrium between this complex and sulfite in solution. A kinetic model might be more appropriate for many aspects of this process. In the absence of any direct isotope fractionation measurements from purified Dsr, a thermodynamic approach provides fractionation estimates that are enticing to geochemists, as the predicted magnitude of fractionation during DSR is large (~70‰), consistent with some recent observations (Canfield, Farquhar, et al. 2010a). The advantage of a more detailed understanding is that it has the potential to relate the magnitude of sulfur isotope fractionation to the physiology of sulfate-reducing microorganisms.

A REVISED MODEL FOR THE SULFATE REDUCTION NETWORK

A recent, and significant advance in our understanding of sulfate reduction comes in the form of new protein crystal structures that elucidate the biochemistry of Dsr. Combined with explicit consideration of older biochemical data, these data allow a reexamination of the network of reactions involved in sulfate reduction, specifically the reduction of sulfite to sulfide. These data lead us to suggest that sulfate reduction proceeds via a branching network that incorporates aspects of both the *Rees* and *trithionate* pathways (Table A1.1).

The crystal structures of dissimilatory sulfite reductases (Oliveira, Vonrhein, Matias, Venceslau, P. M. Pereira, et al. 2008b; Parey et al. 2010) show that it consists of two subunits, DsrA and DsrB, in a symmetrical $\alpha_2\beta_2$ arrangement. Each αβ unit contains a siroheme in the active site, which binds sulfite prior to its reduction. Each siroheme is bound to an $[Fe_4S_4]$ iron-sulfur cluster that mediates electron transfer to sulfite. A second $[Fe_4S_4]$ cluster assists in this electron transfer from an (as yet unidentified) external electron donor, lending to the net capacity of DsrAB to reduce sulfite to zero valent sulfur (after transferring four electrons). Sulfite in the active site is likely reduced by a series of two-electron transfers (Parey et al. 2010; LUI et al. 1993). This observation is critical in understanding the production of sulfur species with intermediate oxidation states. Each αβ unit also contains an additional pair of $[Fe_4S_4]$ clusters associated with a sirohydrochlorin (demetallated siroheme) – these are likely peripheral to sulfite reduction.

A key insight derived from the Dsr crystal structure was the recognition of a second protein, DsrC, in association with the DsrAB dimer (Oliveira, Vonrhein, Matias, Venceslau, P. M. Pereira, et al. 2008b). The association of DsrC with DsrAB is very close, and initially DsrC was mistakenly believed to be a third subunit of Dsr (PIERIK et al. 1992). The crystal structure reveals that the C terminus of the DsrC protein inserts into a cleft in the DsrAB dimer, and contains a terminal cysteine (Cys104) in close proximity to the siroheme in the DsrAB active site. Oliveira et al. (2008) suggest that DsrC plays a key role in the terminal reduction of the zero valent S produced by DsrAB. They propose that the zero valent S forms a persulfide bond with the Cys104 of DsrC (formally, Cys104 transfers the fifth electron to the bonded sulfur atom). The DsrC protein, now with a persulfide at Cys104, decouples from the DsrAB dimer. The persulfide is reduced by a highly conserved cysteine (Cys93) in close proximity to it, releasing H_2S and forming a disulfide bond within the C terminus of the DsrC protein. The crystal structure of isolated DsrC from *Archaeoglobus* also indicates the presence of this redox-active disulfide bond between highly conserved cysteines (Mander et al., 2005). Thus, the sixth electron in the reduction of sulfite to sulfide is derived from Cys93. The DsrC containing the disulfide bond then likely acts as a shuttle carrying oxidizing capacity to the membrane, where a DsrMKJOP complex reduces it back to Cys93 and Cys104 (Oliveira, Vonrhein, Matias, Venceslau, P. M. Pereira, et al. 2008b). This membrane complex includes

the enzyme DsrK, which is a probable heterodisulfide reductase, and is homologous to the energy-conserving heterodisulfide reductase of methanogens (Grein et al. 2010; R. Thauer et al. 2008). The reduction catalyzed by the DsrMKJOP complex is likely coupled to proton translocation and energy conservation (Figure A1.2) (Oliveira, Vonrhein, Matias, Venceslau, P. M. Pereira, et al. 2008b).

This scheme provides solutions to several previously outstanding problems in the biochemistry of sulfate reduction. It sheds light on our understanding of the relationship between sulfite reduction and proton translocation, suggesting a mechanism by which oxidizing capacity can be transported from cytoplasmic DsrAB to the membrane. These studies also suggest that rather than mediating a direct six-electron transfer, DsrAB transfers only four electrons to sulfite, and may do so in a step-wise fashion. The two conserved cysteine residues of DsrC donate the fifth and sixth electron involved in sulfite reduction. This framework then suggests that the source of trithionate and thiosulfate within DSR may likely be derived from nucleophilic attack of aqueous sulfite on the partially reduced intermediates bound to the DsrAB siroheme (Oliveira, Vonrhein, Matias, Venceslau, P. M. Pereira, et al. 2008b; Parey et al. 2010). Further work supports this proposal: structures of the DsrAB from *Archaeoglobus* crystallized with analogues of partially reduced intermediates demonstrated that sulfite is capable of entering the enzyme pocket to facilitate the production of intermediate species (Parey et al. 2010). For instance, two sulfite molecules can bind with S^{2+} in the active site to form trithionate. Similarly, reaction of sulfite with an intermediate in the zero valent state could produce thiosulfate (Figure A1.2).

It has not been established whether trithionate or thiosulfate formed in these reactions can be linked to energy conservation. It is possible that the enzymes that reduce trithionate and thiosulfate serve as a salvage pathway. That is, in addition to generating reduced products these reactions regenerate sulfite from thionate intermediates, thereby recycling the sulfite for later reduction by DsrAB in the energy-conserving pathway. It is also possible that these reductases modulate any potential toxicity of the thionate side products or intercellular sulfite. Finally, there is the potential that thionate reductases are directly coupled to energy conservation by an unknown mechanism. It is possible that in some organisms other steps (such as APS reduction) may also be coupled to energy conservation (I. A. C. Pereira et al. 2011).

On the basis of this information, we suggest a revised network for the reactions controlling the isotopic fractionation of sulfide produced during DSR (Figure A1.3). This network is based our improved knowledge of the biochemistry of each enzyme in the network. While it is a revision of previous models, it is in many respects similar to its predecessors, and it adopts the reaction sequence from sulfate uptake to the production of sulfite from *Rees*. Our network differs in the predicted fate of sulfite, as we suggest that the network branches at sulfite with three possible outcomes. Each of these reactions may be catalyzed by more than one enzyme.

The primary means of reducing sulfite first involves binding to the active site in DsrAB, where it is sequentially reduced in two-electron transfers to a zero valent intermediate. The subsequent reduction of the zero valent intermediate to sulfide is catalyzed by DsrC (Oliveira, Vonrhein, Matias, Venceslau, P. M. Pereira, et al. 2008b). When these enzymes unidirectionally reduce sulfite to sulfide, the *Rees* pathway is realized. This pathway is probably responsible for most sulfite reduction during DSR, and is the only pathway positively coupled to energy conservation. However, the reaction of the zero valent intermediate to sulfide may also be catalyzed by DsrAB (Parey et al. 2010). This sulfide probably represents wasted effort by the cell, since it does not cycle through DsrC it is unlikely to be coupled to energy conservation and therefore may not contribute a large proportion of sulfide production. It is worth noting that Dsr is not the only enzyme capable of dissimilatory sulfite reduction: another dissimilatory sulfite reductase enzyme (SirA) has been identified in *Shewanella oneidensis* (Shirodkar et al. 2010). *Shewanella* is capable of growth on sulfite, but the SirA enzyme does not appear in the genome of any currently sequenced sulfate-reducing microbe.

Sulfite may pass through two other pathways to sulfide, although evidence for these is incomplete. First, sulfite can be partially reduced and react to form trithionate, which may – at least in some organisms – be subsequently reduced to thiosulfate and finally to sulfide. Another option is that sulfite can be reduced to form thiosulfate directly, which is then partially reduced to sulfide. In each case, site-specific oxidation states should be considered in the production and consumption of these species. For example, the reductions of trithionate and/or thiosulfate result in stoichiometric productions of intracellular sulfite from their sulfonyl moieties, while the reduced moieties are further reduced to sulfide (Table A1.1, Figure A1.4). For trithionate, at least two

reduction enzymes have been reported from *Desulfovibrio* (Akagi et al. 1994). The first enzyme, referred to as thiosulfate-forming enzyme, or TF (Drake & Akagi 1977), catalyzes the reaction of trithionate with a sulfite molecule, forming thiosulfate and two molecules of sulfite (Figure A1.4, Table A1.1). The second enzyme, trithionate reducing enzyme (TR) (Kim & Akagi 1985), does not rely on sulfite but splits trithionate, forming sulfite and (via a two-electron transfer) thiosulfate. While each of these enzymes has reportedly been purified, the genes encoding these enzymes are unknown and the genomes of sulfate-reducers contain no independent evidence of a capability for trithionate reduction (I. A. C. Pereira et al. 2011). Thiosulfate reductase, on the other hand, has been characterized physiologically and genetically (Aketagawa et al. 1985; Haschke & Campbell 1971), and cleaves the sulfonyl moiety of thiosulfate into sulfite while reducing the sulfanyl moiety to sulfide (Findley & Akagi 1970) (Figure A1.4, Table A1.1). DsrAB is also capable of catalyzing the reductions of trithionate and thiosulfate (Parey et al. 2010), and may impart an isotope effect during this reaction that is different than the one imposed by enzymes dedicated to these reactions. Together, all these reactions constitute a 'thionate loop' that recycles sulfite while generating sulfide.

Given the network of reactions involved in the transformation of sulfite to sulfide, we can evaluate the potential causes of thionate production. Thionate production is the likely consequence of the provision of sulfite to DsrAB in excess of the capacity of DsrC to remove reduced intermediates. In this circumstance, DsrAB would produce partially reduced sulfur intermediates, which would then react with the excess sulfite. This circumstance might arise as a consequence of elevated intercellular sulfite concentrations, of low DsrC expression, or of rate-limitation in electron transfer to DsrC by the membrane complex. It has been established that DsrC and DsrAB expression are independently regulated, and that DsrC expression varies through the cell cycle with a maximum in stationary phase (KARKHOFF-SCHWEIZER et al. 1993). If the capacity of DsrC to remove intermediate valence sulfur species lags the rate of sulfite reduction by DsrAB, then production of intermediates might be expected.

This biochemical information provided by crystal structures allows for construction of a more detailed network for sulfate reduction than has previously been possible. We suggest several changes from previous

models. First, the nature of the transformation of sulfite to sulfide involves distinct steps (in DsrAB and then DsrC), each of which could potentially involve isotope fractionation, and each of which is potentially reversible. A multi-step process was considered in Rees (1973), and is now confirmed. Second, we suggest that the key bond-forming step in sulfite reduction is the formation of a bond between sulfite sulfur and siroheme iron. If the formation of this Fe-S bond carries a kinetic isotope effect, then the fractionation expressed by this process may be very different than that predicted by equilibrium models. Similarly, the equilibrium of interest is between bound and free sulfite. Third, unlike previous networks, our revised model suggests that it is important to explicitly account for the distinct source and fate of each sulfur atom on trithionate and thiosulfate. This has important consequences for the fractionation calculated between sulfate and sulfide, since the reduced atoms in thionates do not reoxidize to sulfite. Finally, the branching nature of the network and the presence of numerous sub-cycles suggests a mechanism for the expression of isotope effects in downstream parts of the reaction network, and for additive effects that may be important in generating large fractionations.

CONSEQUENCES OF A REVISED NETWORK STRUCTURE

The network shown in Figure A1.3 is complex, with multiple branch points. For simplicity and clarity we have drawn each reaction as unidirectional, but *in vivo* each reaction may be reversible under some circumstances. Experiments conducted with oxygen isotope labels in water, which will exchange readily with intercellular sulfite, have demonstrated that reactions between sulfate and sulfite are highly reversible (J. Farquhar et al. 2008). Early work on Dsr suggested it produced thionates irreversibly, at least *in vitro* (Akagi & Adams 1973); however cultures of *D. desulfuricans* grown in the presence of ^{35}S-labeled sulfide produced ^{35}S-sulfate under anoxic conditions (Trudinger & Lynette A Chambers 1973), suggesting the full reversibility of the DSR pathway. Consistent with this hypothesis, recent work with *Desulfobacter latus* points the capacity for to sulfide reoxidation within the DSR scheme (Eckert et al. 2011). Evidence from phototrophic-sulfide oxidizing bacteria provides even further evidence. Here, proteins closely related to DsrAB and DsrC play an important role in the oxidation of intracellular sulfur globules in phototrophic sulfide oxidizing bacteria (Dahl et al. 2005; Pott & Dahl 1998),

suggesting that these enzymes can catalyze the oxidation of reduced sulfur. The prospect of reversibility of these enzymes offers a potential pathway for the return flow of sulfur from sulfide to more oxidized compounds (Trudinger & Lynette A Chambers 1973; Eckert et al. 2011). With a newfound, and biochemically calibrated picture of the DSR network, it is clear that there are multiple opportunities for sulfur isotope fractionation, three models of which we consider below.

A Rees-like model

In its simplest form, the *Rees* model may still describe most sulfate reduction in experimental systems, although we now understand that the 6-electron conversion of sulfite to sulfide is a multi-step process. This model is likely to be relevant where electron donors are abundant relative to intracellular sulfite production, and all sulfite is fully reduced. In this version of the network, there is no production of trithionate or thiosulfate, and fractionation of sulfur isotopes downstream of sulfite is imposed wholly by the reactions involving the enzymes DsrAB and DsrC. The magnitude of these fractionations, however, has not been directly quantified. Rees (1973) assigned the transformation of sulfite to sulfide a fractionation factor $^{34}\alpha = 0.975$ on the basis of experimental results. The transformation of sulfite to sulfide involves several steps of bond formation and breakage, and it is not yet clear which of these imposes discrimination against the heavier isotopes of sulfur. As suggested above, the key step may be the binding and equilibration of the sulfite - siroheme iron complex. Formation of the persulfide in DsrC may also carry an isotope effect. Each of these steps may play a role in determining the isotopic composition of the terminal sulfide. Determination of the isotopic fractionation at each step is probably best resolved through *in vitro* experiments with purified enzyme fractions under conditions of replete electron donation. Such experiments (in the absence of DsrC) will probably generate thiosulfate and thiosulfate, and it could be instructive to measure the isotopic content of the sulfane moieties of these products as proxies for partially reduced sulfite. Fractionation of sulfur isotopes during persulfide bond formation should also be targeted in the future.

Incorporation of the thionate loop

If the sulfate reduction network is expanded to include trithionate and thiosulfate, this is expected to alter isotopic composition of sulfide. Isotope fractionation is likely to occur both in the production of these intermediates, and in downstream reactions. Equally as important, the complex series of forward and reverse reactions and independent cycles will undoubtedly influence the observed net fractionation.

Even given the complexity of the thionate loops, additional constraints/predictions can be placed. It is critical to appreciate that thiosulfate and trithionate are likely to have intramolecular differences in their isotopic compositions, as a result of the differing source and fate of each sulfur moiety. Trithionate is formed enzymatically by the reaction of a partially reduced S (in the S^{2+} state) in the DsrAB complex with sulfite. If a kinetic fractionation is imposed during the binding of sulfite with the iron in siroheme, then the reduced sulfur atom in trithionate is likely to be depleted in the heavy isotopes of sulfur relative to the oxidized atoms, which are derived from the sulfite pool. Similarly, during the formation of thiosulfate in Dsr, the more reduced sulfur atom is likely sourced from zero valent S derived from DsrAB, while the more oxidized S is from the sulfite pool. Thiosulfate may also be produced from trithionate via one of the enzymes described by Drake and Akagi (Drake & Akagi 1977), in which case thiosulfate inherits the intramolecular isotopic composition of trithionate, plus any fractionation associated with this reaction. Under neutral to mildly alkaline conditions, the formation of thiosulfate may also proceed abiotically, by the reaction of sulfite with sulfide (Siu & Jia 1999). In this case, the sulfane moiety of thiosulfate is likely substantially depleted in heavy isotopes relative to sulfite, and intramolecular differences in isotopic content may be large.

Studies of the mechanisms of thionate reduction suggest that the oxidized moieties of thionates are quantitatively returned to the sulfite pool, while only the reduced moiety is further reduced to sulfide (Haschke & Campbell 1971; Aketagawa et al. 1985; Smock et al. 1998; Akagi et al. 1994; Drake & Akagi 1977; Kim & Akagi 1985). This implies that any discrimination upon the oxidized atom in thionates has (in the absence of thionate leaks from the cell) little impact in the final isotopic composition of sulfide. The sulfonyl moieties may be depleted in heavy isotopes, but at steady state are continually returned to the sulfite pool. This is not the case for

the reduced moieties of thionates, which have been processed, to varying degrees via DsrAB. Further reduction may occur in DsrAB/C or via thionate reduction. These reactions may have associated isotope effects of unknown magnitude, although initial work by Smock et al. (1998) suggests that they may be small. Critical experiments to be performed include the isolation of the thionate reductases and the examination of the isotope fractionation they produce. It may also be important to understand whether Dsr produces a different isotope fractionation during thionate reduction, as well as measuring the isotope fractionation imposed during the abiotic formation of thiosulfate.

Incorporation of the cellular leaks

A complete isotope model should also consider exchange reactions with the extracellular environment. During sulfate reduction, intermediates such as sulfite, trithionate, or thiosulfate may leak out of the cell. Accumulation of extracellular thionate intermediates has been observed during growth on sulfite (Sass et al. 1992; Broco et al. 2005). At equilibrium, loss of intermediates from the cell will carry an isotopic signature that must be accounted for in satisfying overall isotopic mass balance. Careful measurements of extracellular pools of trithionate and thiosulfate under various growth conditions, and examination of the sulfur isotopic contents of these species (at the oxidized and reduced positions) will inform our understanding of the importance of these intermediates.

DISCUSSION AND CONCLUSIONS

We propose a revised network of chemical reactions that control the isotopic composition of sulfide produced by dissimilatory sulfate reducing bacteria and archaea. Recent crystal structure work has indicated that the biochemical route of sulfate reduction does not occur via the canonical *Rees* scenario, in which sulfite is directly reduced to sulfide, nor via the *trithionate* pathway. Instead, the complex interaction between the DsrAB and DsrC structures suggests that sulfite is mainly reduced in a two-step process involving a zero-valent sulfur intermediate. This series of two-electron transfers was originally proposed, although not accepted, by Peck

(1962). Trithionate and thiosulfate are the likely products of side reactions between sulfite and partially reduced sulfur in the DsrAB complex. These side reactions may be more likely when the supply rate of sulfite via APS exceeds the rate at which DsrC can be cycled to the membrane and back to the cytoplasmic DsrAB complex. These rates, in turn, may depend on the nature and concentration of electron donors and would relate back to ambient organic carbon as well as environmental oxidative stresses that consume cellular reducing equivalents (Zheng & Storz 2000).

The degree to which this network alters the isotopic composition of sulfide depends on the relative magnitudes of fractionations involved in the reduction of sulfite, trithionate, thiosulfate, and the disulfide bond in DsrC. Understanding the nature of sulfur isotope fractionation, and our ability to make predictions about physiology or environment on the basis of the isotopic composition of sulfide, rests on the identification and quantification of these unknown isotopic fractionations and the fluxes between these species. As such, we deem it inappropriate to present mathematical solutions to the proposed pathway, since without properly calibrated fractionation factors this exercise will be fruitless. However, in anticipation of these fractionation factors being determined in the future, many of the mathematical solutions to network structures presented here are described in supplemental material. It also remains possible that there are additional, unrecognized enzymes that allow for other redox reactions, such as the oxidation of sulfide, and posses isotopic consequences.

Many of these predictions and prescriptions are testable through careful experimentation. For example, the importance of the thionate loop could be resolved through *in vitro* studies of fractionation factors associated with trithionate and thiosulfate formation and reduction. Whereas the reaction mechanism for the thiosulfate forming enzyme has been determined (Akagi et al. 1994), the mechanics underpinning trithionate and thiosulfate reduction by DsrAB (Parey et al. 2010) or otherwise are underdetermined. It is very likely that the mechanism of thionate reduction by DsrAB is similar to thionate reductases, all the while regenerating sulfite from the thionate cycling (Parey et al. 2010). These reaction mechanisms and their sulfur isotope fractionations remain a target for future investigations.

The most direct means of addressing the details of isotope fractionation during DSR is via *in vitro* enzyme-specific studies. Measuring the concentration and isotopic composition of key intermediates could also inform our understanding of the network pathway. Isotope measurements on intracellular sulfite might be useful in ascertaining the degree of reversibility of the sulfate reduction pathway, and in constraining the fractionation factor of the step immediately downstream of sulfite reduction (cf. (Johnston et al. 2007)). If there is little or no division in the flow of sulfur after the production of sulfite (i.e. a pseudo-*Rees* pathway dominates), then a large isotope fractionation during sulfite reduction requires a significant accumulation of the heavy sulfur isotopes in sulfite (Hayes 2001).

As focused work on the DSR metabolism proceeds, the details and assumptions associated with any network become important. For instance, quantitative models applied to this network will initially assume that each intermediate, with its various sources and sinks, will reside within a single well-mixed pool in the cell. This may be a reasonable assumption, as the species of interest are largely quite soluble and are interacting with cytoplasmic enzymes (Hansen 1994). Conversely, if key species were found to be periplasmic, the physical separation would need to be included. Another missing feature from our cellular mass-balance is sulfur assimilation, which may account for as little as ~ 0.1% of biomass (Canfield 2001a), and can probably be neglected. This assumption remains untested. Additionally, we assume that other than trithionate, higher order polythionates ($S_nO_6^{2-}$, n>3) do not play a major role in intracellular sulfur cycling.

The goal of these isotopic studies will be to understand the relationship between the metabolism of sulfate reducing microorganisms, and their isotopic signature. This will require understanding the fractionation imposed by each enzyme in the chemical network and what controls the flux through each node of the network. As outlined throughout, this broad goal can be approached through a number of more targeted experiments. At a cellular level, directly investigating the isotopic composition of intracellular metabolites or placing novel constraints on flux through the DSR metabolism (Zhou et al. 2011) would provide critical information. Isotopic fractionation through DSR networks perturbed by genetic manipulation might yield complementary information. A more direct approach would involve investigations of enzyme-specific fractionations *in vitro*. Finally,

underpinning these proposed experiments is a more basic understanding; one which articulates the regulation of enzyme expression and controls of electron delivery to certain key reactions within the cell. There may be physiological differences between sulfate-reducing microorganisms (I. A. C. Pereira et al. 2011; Zhou et al. 2011) that manifest in the isotopic content of sulfur products. As should be clear from the above discussion, unraveling this metabolism will require a multidisciplinary approach involving microbiology, biochemistry, isotope geochemistry, and mathematical modeling. The convergence of these fields and future experiments should yield a quantitatively calibrated understanding of isotope fractionation during dissimilatory sulfate reduction, and promote a more precise articulation of Precambrian and Phanerozoic oxidant budgets.

Acknowledgements

We thank A. Pearson, P. Girguis A. Knoll, D. Fike, and R. Cummins for productive and insightful comments on drafts of this manuscript. DTJ thanks NASA Exobiology, the Microbial Sciences Initiative, and Harvard University for funding. J. Farquhar and anonymous reviewers are thanked for detailed comments.

Figure A1.1: The *Rees* pathway (a) and a generalized *trithionate* pathway (b) for dissimilatory sulfate reduction. The dotted lines indicate the cell boundary. Each pathway is more fully described in the text.

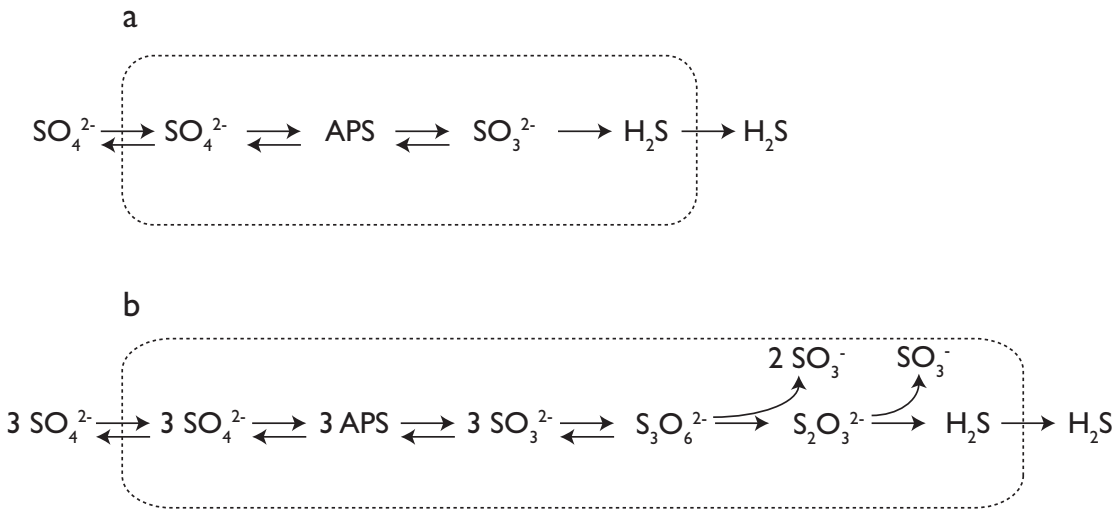

Figure 1

Figure A1.2: The proposed DsrC cycle and mechanism of sulfite reduction. Sulfite is reduced in the DsrAB-C complex in sequential two-electron transfers. DsrAB is represented as blue/purple ovals, DsrC as orange (note: for simplicity, only half of the dimer is shown). Sulfite is reduced first to S^{2+}, then to S^{0}. Each intermediate may bind to sulfite in the siroheme-containing enzyme pocket forming trithionate or thiosulfate. The zero valent stage may be directly reduced to sulfide as a side reaction (not shown) or bind to DsrC, which then forms a disulfide bond between cysteines, losing sulfide as a product. DsrC carries oxidizing power to the membrane, probably to the DsrMKJOP complex (green), where the heterodisulfide is reduced and then recycled back to DsrAB.

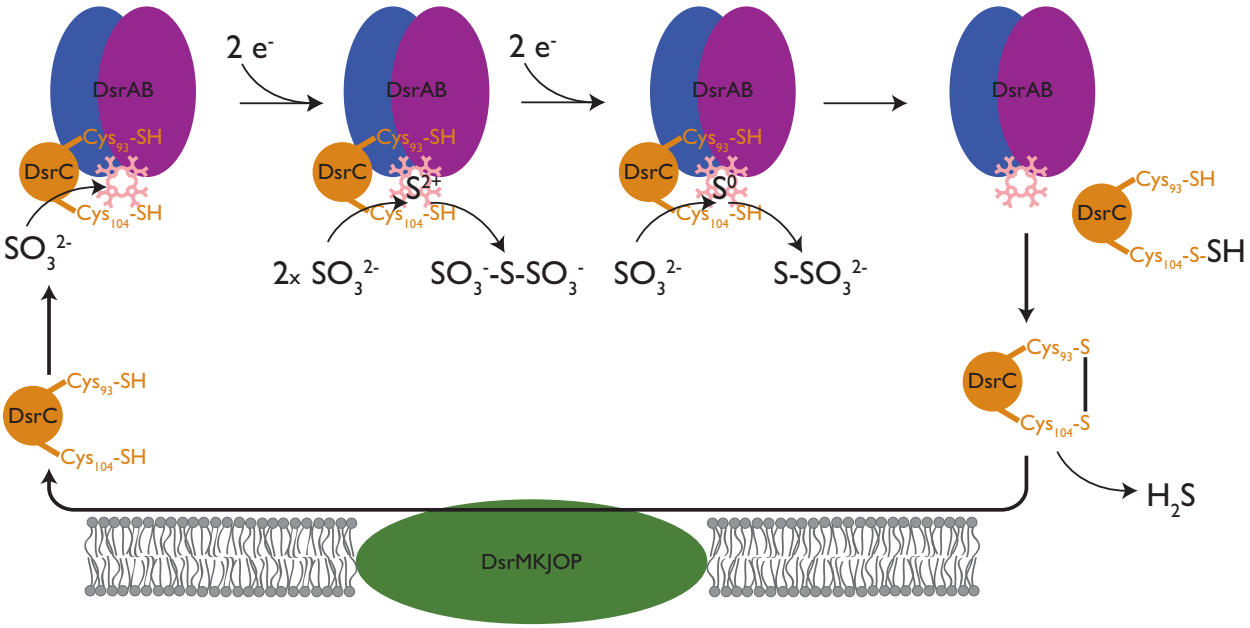

Figure 2

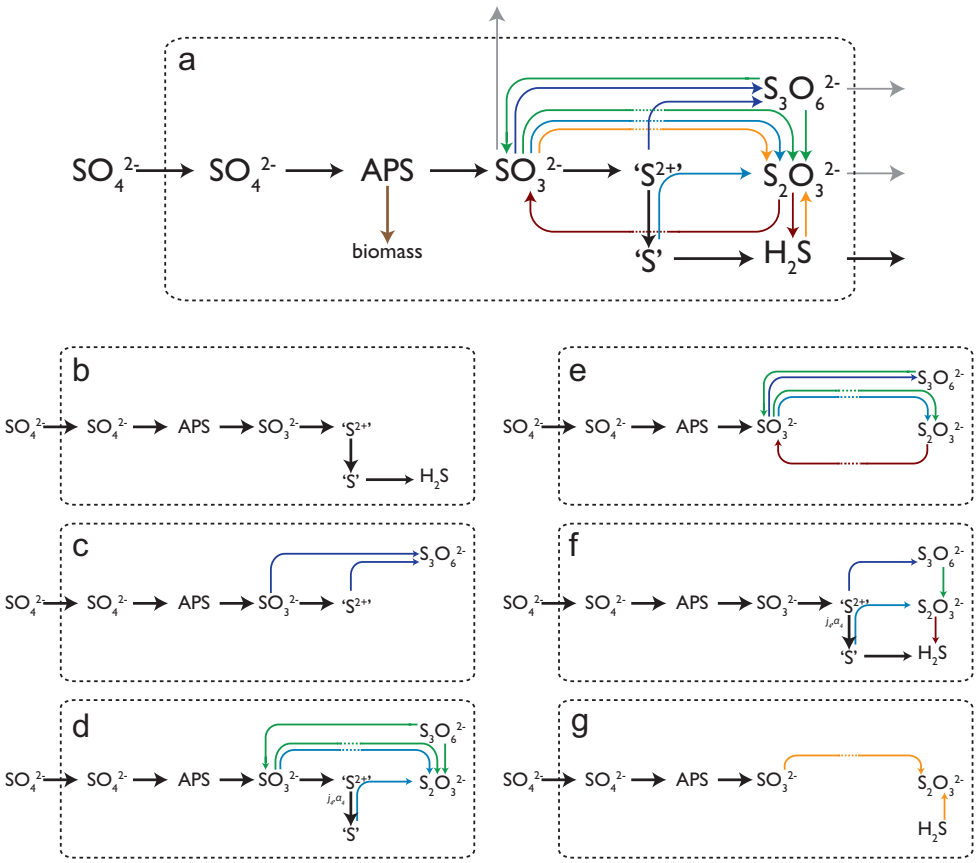

Figure A1.3: Proposed metabolic network for the reduction of sulfate to sulfide. For simplicity and to call attention to the reaction pools involved, we have not included back reactions. a) A branching network of reactions for dissimilatory sulfate reduction. Dark black arrows indicate the central '*Rees*-like' pathway. Colors indicate specific reactions within the thionate loop: *dark blue* = trithionate formation, *light blue* = thiosulfate formation, *green* = trithionate reduction, *crimson* = thiosulfate reduction, *orange* = nonenzymatic reactions. Each of the reductions in the thionate loop regenerates sulfite. b) The central '*Rees*-like' part of the pathway, c) the trithionate generating reaction, consuming sulfite and partially reduced (S^{2+}) sulfur. d) the thiosulfate forming reactions, *green*: from trithionate and sulfite via the enzyme described by Drake and Akagi (1977); *light blue*: from partially reduced (S^0) sulfur in Dsr and sulfite. e) reactions involving the oxidized moieties of trithionate and thiosulfate. The oxidized moieties are returned to the sulfite pool, and not directly reduced to sulfide. f) reactions generating sulfide. Sulfide derives from Dsr, and form the sulfane moiety of thiosulfate. This sulfane may derive from Dsr or from the reduced sulfur atom in trithionate. g) abiotic reaction, forming thiosulfate from sulfite and sulfide.

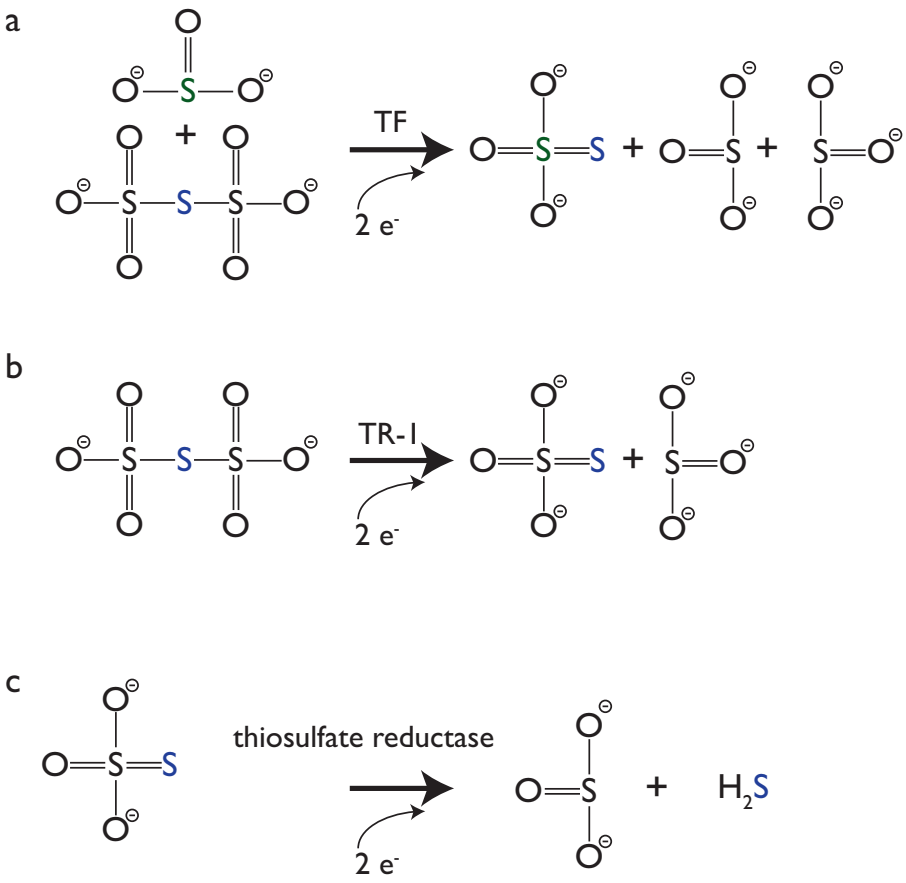

Figure 4

Figure A1.4: Probable reactions with fate of each sulfur moiety in trithionate and thiosulfate reducing enzymes. a) The putative reaction catalyzed by TF (thiosulfate forming enzyme). This reaction mechanism has been determined via isotope labeling, and involves the reaction of trithionate with sulfite, producing thiosulfate and two sulfites (Drake & Akagi 1977). b) The putative reaction catalyzed by TR (trithionate-reducing enzyme.) This reaction mechanism has not been absolutely determined, but likely involves the cleavage of sulfite, and further reduction of the reduced sulfur moiety. c) The putative reaction catalyzed by thiosulfate reductase, which likely produces sulfide from the sulfanyl moiety of thiosulfate, releasing sulfite.

Table A1.1: Main reactions involved in dissimilatory sulfate reduction and the associated enzyme.

Reaction	Enzyme	flux parameters
SO_4^{2-} (external) → SO_4^{2-} (internal)	sulfate permease	j_0 j_{0r}
SO_4^{2-} + ATP → APS + pyrophosphate	ATP sulfurylase	j_1 j_{1r}
APS + $(e^-$ carrier$)_{red}$ → SO_3^{2-} + AMP + $(e^-$ carrier$)_{ox}$	APS reductase	j_2 j_{2r}
SO_3^{2-} + DsrC + $(e^-$ carrier$)_{red}$ → DsrC-S + $(e^-$ carrier$)_{ox}$	Dissimilatory sulfite reductase $\alpha_2\beta_2$	j_3 j_4
SO_3^{2-} + $(e^-$ carrier$)_{red}$ → $S_3O_6^{2-}$ + $(e^-$ carrier$)_{ox}$	Dissimilatory sulfite reductase $\alpha_2\beta_2$	j_3 j_6 j_7
SO_3^{2-} + $(e^-$ carrier$)_{red}$ → $S_2O_3^{2-}$ + $(e^-$ carrier$)_{ox}$	Dissimilatory sulfite reductase $\alpha_2\beta_2$	j_3 j_4 j_8 j_9
SO_3^{2-} + $(e^-$ carrier$)_{red}$ → H_2S + $(e^-$ carrier$)_{ox}$	Dissimilatory sulfite reductase $\alpha_2\beta_2$	j_3 j_4 j_5
$S_3O_6^{2-}$ → $S_2O_3^{2-}$ + SO_3^{2-}	trithionate reducing enzyme	j_{10} j_{12}
$S_3O_6^{2-}$ + SO_3^{2-} → $S_2O_3^{2-}$ + 2 SO_3^{2-}	thiosulfate forming enzyme	j_{10} j_{11} j_{12}
DsrC-S → $DsrC_{ox}$	Dissimilatory sulfite reductase γ	j_5
$S_2O_3^{2-}$ Cyt*c3*$_{red}$ → H_2S + SO_3^{2-} + Cyt*c3*$_{ox}$	thiosulfate reductase	j_{13} j_{14}

APPENDIX B

MULTIPLE SULFUR ISOTOPE SIGNATURES OF SULFITE AND THIOSULFATE REDUCTION BY A COMMON SULFATE-REDUCING BACTERIUM

This appendix will be submitted to *Geobiology* in 2014 with co-authors:

R. Cummins, M. Schmidt, A. Bradley, and D. Johnston

ABSTRACT

Dissimilatory sulfate reduction serves as a key metabolic remineralization process in anoxic marine environments. As sulfate reducers impart large, mass-dependent isotopic fractionation, the presence and activity of these organisms is preserved within geological materials. By extension, sulfur isotope records are used to infer the redox character (e.g., oxygen content) of Earth's atmosphere and oceans. However, recent work suggests that our understanding of microbial sulfate reduction (MSR) may be missing complexity associated with the presence and role of key chemical intermediates in the reductive process. This study provides a test of proposed metabolic models by growing an axenic culture of the sulfate-reducing bacterium *Desulfovibrio alaskensis* strain G20 under a matrix of experimental conditions, and tracking the multiple S isotopic consequences of each condition set. This includes variability in electron donors (lactate and formate with sulfate) and, more importantly, electron acceptors (sulfate, sulfite and thiosulfate). Using growth on sulfate as a reference to previous work, the dissimilatory reduction of thiosulfate and sulfite each produced unique results that shed light on the metabolic (and isotopic) capacity of MSR. These experiments reveal a complex biochemistry associated with sulfite reduction while thiosulfate simply generates sulfide. That is, under high sulfite, sulfur is shuttled to an intermediate pool of thiosulfate. Curiously, site-specific isotope effects (within the thiosulfate) are large ($^{34}\varepsilon$ ~ 30‰) while product sulfide carries only a small isotopic signature: a signature similar in magnitude to sulfate and thiosulfate reduction. Together these findings point to a MSR network (and associated isotope effect) that is highly sensitive to environmental conditions.

INTRODUCTION

The geological record preserves only select snapshots of paleo-environments. One of the more robust, continuous records of paleo-redox state is stored in sedimentary sulfide and sulfate minerals (Canfield 2004b; Canfield & Raiswell 1999; Strauss 1997). The isotopic composition of these phases serves as a prominent proxy for the oxidation state of Earth surface environments (R. A. Berner & Canfield 1989; HALEVY et al. 2012). For

instance, the partial pressure of oxygen in Earth's atmosphere is thought to control concentrations of dissolved sulfate and oxygen in the oceans, which in turn may be recorded by the difference in isotopic composition between sulfate and sulfide (Canfield 2001b; Canfield 2001a; Habicht et al. 2002). At the core of these interpretations is an understanding of the isotope effects associated with the numerous redox reactions that characterize the modern sulfur cycle. Among the biological catalysts of sulfur redox reactions is microbial sulfate reduction (MSR): a dissimilatory metabolic pathway coupling the oxidation of organic matter or hydrogen to the reduction of sulfate (Bradley et al. 2011; Peck 1959; Harry D Peck 1960). MSR is responsible for a majority of the organic matter remineralization in anoxic environments (JORGENSEN 1982), making it a key environmental process and an important link between the cycles of sulfur, carbon and oxygen. Notably, this metabolism is also capable of producing a wide range of mass-dependent sulfur isotope fractionations (Johnston 2011; Canfield 2001a; Leavitt et al. 2013; Sim, Bosak & Ono 2011a). In order to interpret the sulfur isotope variability within geological records as it relates to environmental conditions, we first need to understand the controls on the fractionation of sulfur isotopes by MSR.

Studies of the sulfate reduction metabolism often converge on the idea that sulfate and electron donor concentrations control the rates of reduction, and in turn, the expressed isotopic fractionation (Bradley et al. 2011; Canfield 2001b; Habicht et al. 2002; Habicht et al. 2005; Leavitt et al. 2013). Simply, these variables determine the capacity to deliver reductant to the respiratory reaction network and the relative rates at which electrons and S-bearing oxidants are supplied to catabolic enzymes. The isotopic fractionation associated with MSR is visualized through a schematic depiction of the central metabolism (Bradley et al. 2011; Brunner & Bernasconi 2005; Rees 1973; J. Farquhar, Johnston, et al. 2007a). This schematic has evolved as our understanding of the metabolism has become more true to the biochemistry, beginning with a simple three step process (Harrison & Thode 1958), through to a revised reaction series with the first thorough mathematic derivation (Rees, 1973), and finally to the most recent update that incorporates a variety of biochemical and protein crystal structure information (see Fig. 1; (Bradley et al. 2011)).

Much is gained through a close and quite literal reading of the MSR network as presented in Fig. 1. For example, the fractionations classically prescribed to this pathway are associated with sulfate uptake by the cell, the reduction of activated sulfate (APS: 3'-phosphoadenosine-5'-phosphosulfate) to sulfite, and the terminal reduction of sulfite to sulfide. Given empirical limits from lab experiments, the maximum fractionation capacity was inferred as the sum of these three steps (with fractionation factors of 3, -25 and -25‰, respectively and 47‰ in total)(Harrison & Thode 1958; Rees 1973). More recently however, work with pure and enrichment cultures demonstrated an increased fractionation capacity of MSR (Canfield et al., 2010; Leavitt et al., in press; Sub Sim et al., 2011a), approaching theoretical predictions (~ 70‰) from low temperature equilibrium (Tudge & Thode 1950; J. Farquhar et al. 2003; Johnston et al. 2007). These observations require a careful reevaluation of how isotopic fractionation is manifested within MSR.

Determining fractionation factors within the MSR metabolism necessitates a multi-faceted approach. Classic isotope theory states that the kinetic isotope effects of a particular step are only expressed if that step is rate limiting within the reaction scheme (Hayes 2001). Each reaction that outpaces the rate-limiting step will quantitatively transform its particular substrate to its product, precluding any isotopic discrimination. In reality, reaction chains (particularly in biological systems) do not behave so simply, as multiple steps may compete for rate limitation. The expressed fractionation associated with a particular reaction may instead be a function of how material is transported through a system (e.g., a linear versus branched pathway, (Hayes 2001; Johnston et al. 2007; Brunner & Bernasconi 2005; Bradley et al. 2011)). Given these considerations, the network topology in Figure 1 provides a roadmap for identifying the significant reactions within MSR, highlighting where experimental work is most needed. As is also clear from this topology, sulfite serves as the major hub in determining both the reversibility of the MSR reaction network and whether intermediates (such as $S_2O_3^{2-}$) factor into the reaction scheme during net sulfide production. Fortunately, the physiology of most cultured sulfate reducers carries some plasticity, allowing them to utilize MSR intermediates as terminal electron acceptors in place of sulfate. For instance, *Desulfovibrio alaskensis* strain G20 will reduce sulfite or thiosulfate, in lieu of or in addition to sulfate. Here we present and discuss the results from a matrix of closed-system (batch) experiments with an axenic culture

of strain G20. For each experiment we successfully tracked sulfur isotope mass balance, and measured the major and minor S-isotope fractionation factors during the dissimilatory reduction of three different electron acceptors: sulfate, thiosulfate, and sulfite. These data shed new light on the inner workings of the sulfate reduction metabolism, illustrate the range of isotopic potential intrinsic to these reactions, and capture a complex chemistry that blurs the lines between the classic picture of MSR and sulfur disproportionation reactions.

METHODS

A pure culture of the sulfate-reducing bacterium *Desulfovibrio alaskensis* strain G20 was grown in airtight glass Balsch tubes sealed with butyl rubber septa under a gas headspace of 90% nitrogen and 10% carbon dioxide. Media was sparged with this mix prior to inoculation. The medium consisted of (per liter) NaCl, 20 g; $MgCL_2 \bullet 6H_2O$, 3 g; $CaCl_2 \bullet 2H_2O$, 0.15 g; NH_4Cl, 0.25 g; KH_2PO_4, 0.2 g; KCl, 0.5 g; $Na_2SeO_4 \bullet 10H_2O$, 370 mg, as well as a vitamins and amino acids solution and a trace metals solution (Widdel and Bak, 1992). Sulfate and sulfite were provided at concentrations of 20 mM, while thiosulfate was provided at 10 mM. Lactate and formate were both provided at concentrations of 10 mM. Experiments were conducted in all cases to test the isotopic consequences of G20 growth on sulfate, sulfite and thiosulfate, as well as to constrain growth rates. In addition, sulfate reduction experiments were conducted with both lactate or formate as the sole electron donor, whereas sulfite and thiosulfate reduction experiments paired solely with lactate. In each experiment uninoculated controls were monitored for contamination, and a killed control to quantify any inoculum sulfur. All cultures were grown in their respective media for >10 transfers prior to the inoculation of the experiments reported here. Bacteria were transferred (1:100 dilution) into a prepared Balsch tube with correct media solutions and headspace compositions. At this transfer ratio, the quantity of reduced sulfur carried over with the inoculum was below detection. Each tube was sampled at roughly five time points spread throughout each experiment to ensure capture of exponential phase growth.

At each sampling, including at the start of the experiment ('time zero'), optical density and chemistry measurements were performed. The optical density of each tube was measured at 600nm. These measurements

were calibrated to absolute cell counts through a standard staining protocol (Chisholm et al. 1998). In parallel, concentrations of relevant chemical species were measured throughout. Sulfide was quantified colorimetrically (Cline 1969) whereas sulfate, thiosulfate and sulfite were all measured via ion chromatography. Sulfate concentrations were measured using an isocratic method, while sulfite and thiosulfate were measured using gradient elution. Trithionate was measured independently via cyanolysis (Don P Kelly & Wood 1994). In all cases, reduced species were captured as zinc sulfide, whereas oxidized species were captured with $BaCl_2$. A flow chart of sample handling was adopted from (Smock et al. 1998).

Sulfur isotope measurements of sulfate, sulfide and thiosulfate sulfur were performed first on a Thermo-Finnigan Delta V mass spectrometer, configured in continuous flow mode and connected to an Elemental Analyzer (measuring SO_2). Given the above chemical methods, sulfate and sulfonate were measured as $BaSO_4$ whereas sulfide and sulfane were measured as Ag_2S (data are reported in Tables 1-3), always with an excess of V_2O_5. From this, select data were chosen for high precision analyses via dual inlet on a Thermo Finnigan MAT 253 (as SF_5^+). Samples already as silver sulfide were fluorinated directly with an excess of pure F_2, cleaned cryogenically and via gas chromatography before introduction to the mass spectrometer. Samples as $BaSO_4$ precipitates were chemically reduced to Ag_2S (Forrest & Newman 1977) prior to high precision analyses.

All isotope data presented herein is in standard delta notation, where the composition of a given sample is normalized (in our case) back to the original composition of the sulfoxy anion in the experiment. In the case of thiosulfate experiments, samples are normalized to the bulk composition of the bulk $S_2O_3^{2-}$. This results in two distinct delta values – $\delta^{33}S$ and $\delta^{34}S$ (the ratios of $^{34}S/^{32}S$ in a standard relative to that of a reference). Values for $\delta^{34}S$ are from both SO_2 and SF_6 measurements, whereas $\delta^{33}S$ data are exclusively from SF_6 measurements. When the composition of two reservoirs is being related, we define $^{34}\varepsilon$ ($(= {}^{34}\alpha - 1)*1000$) and where $^{34}\alpha$ between reservoirs A and B is $(\delta^{34}S_A/1000 + 1)/ (\delta^{34}S_B/1000 + 1)$. The triple isotope composition of a given reservoir can be related through:

$$\Delta^{33}S = \delta^{33}S - 1000\times[(1 + (\delta^{34}S/1000)^{0.515}) - 1].$$

When two pools are being related in triple isotope space, we can use the slope of the line on a $\delta^{33}S$ vs. $\delta^{34}S$ plot, or:

$$^{33}\lambda = ln(^{33}\alpha)/ln(^{34}\alpha).$$

For further information about the meaning and specific controls on mass-dependent fractionations, readers are referred to published discussions (J. Farquhar & Wing 2003; Young et al. 2002; Miller 2002; Johnston 2011).

Propagating error when calculating minor isotope fractionation relationships, especially $^{33}\lambda$, is critical given that s is nonlinearly dependent on $\delta^{34}S$. Here we use an error propagation equation derived previously (Johnston et al. 2007), where:

$$\sigma_\lambda = \sqrt{\sigma^2_{\Delta^{33}S} * \left(\frac{\partial\lambda_{obs}}{\partial\Delta^{33}S}\right)^2 + \sigma^2_{\delta^{34}S} * \left(\frac{\partial\lambda_{obs}}{\partial\delta^{34}S}\right)^2}, \qquad \text{(eqn. B1)}$$

which can be broken down into

$$\frac{\partial\lambda_{obs}}{\partial\Delta^{33}S} = \frac{1}{\ln\left[\frac{\delta^{34}S}{1000}+1\right]} \times \frac{1}{\frac{\Delta^{33}S}{1000} + \left[\frac{\delta^{34}S}{1000}+1\right]^{\lambda_{RFL}}} \times \frac{1}{1000} \qquad \text{(eqn. B2)}$$

and

$$\frac{\partial\lambda_{obs}}{\partial\delta^{34}S} = \frac{1}{\ln\left[\frac{\delta^{34}S}{1000}+1\right]} \times \frac{1}{\frac{\Delta^{33}S}{1000} + \left[\frac{\delta^{34}S}{1000}+1\right]^{\lambda_{RFL}}} \times {}^{33}\lambda_{RFL} \times \left[\frac{\delta^{34}S}{1000}+1\right]^{{}^{33}\lambda_{RFL}-1} \times \frac{1}{1000}$$

$$+ \ln\left[\frac{\Delta^{33}S}{1000} + \left[\frac{\delta^{34}S}{1000}+1\right]^{\lambda_{RFL}}\right] \times \frac{-1}{\left(\ln\left[\frac{\delta^{34}S}{1000}+1\right]\right)^2} \times \frac{1}{\left[\frac{\delta^{34}S}{1000}+1\right]} \times \frac{1}{1000} \qquad \text{(eqn. B3)}$$

.

All compiled data and new data presented in this study were treated with the same formulation.

RESULTS & DISCUSSION

Four discrete experiments were performed in this study. In each case, the dominant electron acceptor in the system was consumed with time as one or more reduced S-products accumulated. This study includes two experiments where G20 was grown with sulfate as the sole terminal electron acceptor and either lactate or formate as the sole electron donor. In the two additional experiments only lactate was provided as the electron donor with either sulfite or thiosulfate as the sole terminal electron acceptor. For each, we directly measure the quantitative loss of reactant and generation of product(s) to explicitly track elemental and isotopic mass balance at each time point. Given the complex chemistry involved in sulfite and thiosulfate reduction in particular, we emphasize the requirement to explicitly measure each S pool at each time-point to close mass-balance. When coupled with optical densities and cell count data, cell specific reduction rates are attained (Detmers et al. 2001).

The closed system (batch) nature of the experiments requires an additional framework in order to ascertain a fractionation factor ($^{3x}\alpha$). Fortunately, our experimental methods circumvented an inoculum sulfide blank, streamlining previous mathematical treatments (Johnston et al. 2007). In the simplest case, the loss of a reactant and generation of a single product pool is then determined through a Rayleigh fractionation model (Hayes 2001). Here, the fractionation factor of a given step or reaction is calculated with respect to the reactant:

$$\delta^{34}S_{R,t} = \left[\left(\left(\delta^{34}S_{R,t=0}\right) + 1000\right) \times f_t^{\left(^{3x}\alpha - 1\right)}\right] - 1000 \qquad \text{Eqn 1.}$$

where $\delta^{34}S_{R,t}$ is the isotopic composition (x = 3 or 4) of the reactant (R) though time (0, t). For this expression, the reaction coordinate is tracked with f, which represents the mole fraction of reactant remaining at time t. Additionally, the composition of a given product is calculated:

$$\delta^{34}S_{P,t} = \left[\left([R]_0 \times \delta^{34}S_{R,t=0}\right) - \left(f_t \times \delta^{34}S_{R,t}\right) + \left([P]_0 \times \delta^{34}S_{P,t=0}\right)\right]/[R]_t \qquad \text{Eqn. 2.}$$

where the sulfur isotope composition of the reactant (R) or product (P) are related to their concentrations ([R] and [P]) at a given time point (t). It is through the use of these two expressions that we come to understand isotope fractionation effects in our experiments.

SULFATE REDUCTION

Sulfate reduction experiments with both lactate and formate generated sulfide as the lone S-bearing product. Near the end of exponential phase growth, 28.1% and 18.9% of the available sulfate had been consumed by formate and lactate oxidation, respectively (Fig. 2a). This results in exponential phase cell specific reduction rate (csSRR) ranging up to 142 and 494 *f*mol per cell per day for formate and lactate, respectively. These rates are calculated from the change in sulfate concentrations between adjacent time points, divided by the difference in average cell count during that interval (Detmers et al. 2001). The same calculation can be performed with the product sulfide concentrations. These results are consistent with csSRR for related strains (cf. (Harrison & Thode 1958)).

The fractionation associated with sulfate reduction was calculated using a modified Rayleigh model, described above. For the formate experiments, the net $^{34}\varepsilon$ fractionation associated with sulfate reduction averaged -4.25 ± 0.44‰, whereas growth on lactate resulted in slightly larger fractionation of -5.93 ± 0.61‰ (Fig. 2c). Both observations are consistent with previous work on related strains where csSRR was compared to the magnitude of fractionation (Harrison & Thode 1958). At higher rates, like those here, fractionation approaches a minimum near 4‰ and ranges up to > 50‰ as rates slow. For the purposes of this study, we take these fractionations as a representative baseline for the growth of G20 on sulfate, which is then directly comparable to growth on the other terminal electron acceptors tested here.

These experiments also serve to extend the catalog of minor sulfur isotopic data for sulfate reduction. From earlier works, it is clear that the MSR process is broadly characterized as having highly variable $^{34}\varepsilon$ effects with $^{33}\lambda$ that is exclusively less than equilibrium predictions of 0.515. Minor isotope fractionations range down to less than 0.510 with a mean near 0.512 (Canfield, Farquhar, et al. 2010a; Johnston 2005; Johnston et al. 2007; J. Farquhar et al. 2008; Sim, Bosak & Ono 2011a; Sim, Ono, et al. 2011c; Leavitt et al. 2013). Consistent with these findings, the sulfate reduction experiments from this work yield calculated $^{33}\lambda$ of 0.508 ± 0.002 and 0.511 ± 0.001 for lactate and formate, respectively (Table A2.1). It is important to note that the error on $^{33}\lambda$ is heavily (and non-

linearly) dependent on $^{34}\varepsilon$, meaning that at low $^{34}\varepsilon$, the error is larger and the $^{33}\lambda$ less uniquely resolvable. Here we use the error propagation equations derived previously (Johnston et al. 2007).

Along with our new data, we recalculated (i.e. normalized) and compiled all published pure culture results from both open- and closed-system sulfate reduction experiments (Fig. A2.3b). The compilation highlights a number of key observations. Foremost among these is the resolvable triple isotope trend where elevated $^{33}\lambda$ corresponds to larger $^{34}\varepsilon$ fractionation. Despite this trajectory toward low temperature thermodynamic equilibrium, such theoretical values have not yet been observed in a microbial experiment (Leavitt et al. 2013). In light of this clear triple isotope relationship, it is important to note that this compilation represents numerous different strains of sulfate reducing bacteria grown over a range of conditions. For a deeper understanding and real physiological insight, further continuous culture (open-system) work is necessary (Leavitt et al. 2013; Lyn A Chambers et al. 1975; Sim, Bosak & Ono 2011a). Still, a great deal of isotopic behavior is shared among the different experimental approaches.

THIOSULFATE REDUCTION

The thiosulfate reduction experiment with G20 carried straightforward geochemical results, where thiosulfate was stoichiometrically reduced to hydrogen sulfide (Fig. A2.4a). This is consistent with previous reports for three other strains of sulfate reducers (*D. desulfuricans*, *D. sulfoexigens*, and *D. multivorans*) grown on thiosulfate (Smock et al. 1998; Habicht et al. 1998). Over the course of our experiment, 15% of the thiosulfate sulfur was reduced to sulfide, leading to cell specific thiosulfate reduction rates of up to 265 *f*mol per cell per day during exponential phase (Fig. A2.4b). However, predictions from earlier work on MSR suggest that sulfite serves as an intermediate between thiosulfate and sulfide (essentially the liberation and subsequent reduction of the sulfonate S) (Smock et al. 1998). Although methods for quantifying sulfite were employed in these experiments, sulfite was never above the detection limit. This means that if present, sulfite has an exceedingly short residence time and is quickly reduced to sulfide. Given this short lifetime, the isotopic consequences of a sulfite intermediate should not be expressed.

Calculating an accurate fractionation factor is more challenging, however, as there are multiple possible reaction pathways to generate sulfide from thiosulfate. There are two unique S sites within thiosulfate, the potential for intermediates, and the possibility that not only one pathway operates at a time. The three simplest scenarios are:

$$(a)\, S_2O_3^{2-} \rightarrow SO_3^{2-} + S^0 \rightarrow SO_3^{2-} + HS^-$$
$$(b)\, S_2O_3^{2-} \rightarrow SO_3^{2-} + S^0 \rightarrow HS^- + S^0$$
$$(c)\, S_2O_3^{2-} \rightarrow SO_3^{2-} + S^0 \rightarrow 2HS^- \qquad \text{Eqn. 3}$$

Beginning with the most simplistic approach, it is possible that thiosulfate reduction is not site-specific, which is the same as having a wholesale reduction of thiosulfate to sulfide (Eqn. 3c). This would generate sulfide fractionated away from the bulk isotopic composition of thiosulfate. If true, then the fractionation effect is calculated (using a typical Rayleigh fractionation expression and yields a $^{34}\varepsilon$ of -7.12 ± 0.18‰. In evaluating the possibility that the sulfane or sulfonate S is preferentially reduced (Eqn. 3a, 3b), we first note a small mass-imbalance (never exceeding 10%) in these experiments (see Fig. A2.4a). We presume that this imbalance relates in part to a small elemental S pool that was in fact measurable from the later time. This may suggest preferential sulfonate reduction (Eqn. 3b), leaving the sulfane S behind, which contribute to residual S^0. Using the same mathematical treatment as above, a calculated sulfonate reduction fractionation -8.06 ± 0.80‰ is extracted. This solution is within one standard deviation of the fractionation factor extracted from wholesale thiosulfate reduction, and is thus indistinguishable. For completeness, we calculate the predicted fractionation if sulfane reduction (Eqn. 3a) alone is responsible for sulfide production, resulting in an estimate of -5.17 ± 0.68‰. Given the lack of measurable sulfite, the modest in-growth of S^0, and the similarity between the sulfonate and full thiosulfate fractionation factors, we again take sulfide production as predominately indiscriminate, wholesale thiosulfate reduction with the potential for modest contributions from preferential sulfonate reduction (the role of intermediate sulfite remains unclear).

This study presents the first minor sulfur isotope data for thiosulfate reduction (Fig. A2.5). In a similar fashion to that observed elsewhere (Habicht et al. 1998), relative to the starting sulfur, the sulfonate S sites become isotopically enriched in ^{34}S whereas the sulfane becomes more depleted. During mid- and late-exponential phase growth (the samples analyzed for ^{33}S), ^{34}S enrichment is accompanied by a modest increase in the $\Delta^{33}S$ of sulfonate S and the decrease in $\Delta^{33}S$ of sulfane S. In complement to the isotopic evolution of the thiosulfate, product sulfide is isotopically depleted in ^{34}S and preserves a slightly increased $\Delta^{33}S$. Under the assumption of wholesale thiosulfate reduction, we can extract a $^{33}\lambda$ between the bulk composition of thiosulfate and product sulfide of ~0.512 (0.5119 and 0.5124) for both time points presented in Fig. A2.5. Interestingly, this value is remarkably similar to that extracted from sulfate reduction experiments (Fig. A2.3b). This is interpreted as suggesting either a shared biochemical pathway or a commonality in the physical chemistry of both bacterial sulfate and thiosulfate reduction. Regardless, the fact that sulfane and sulfonate isotopically balance one another throughout the experiment further suggests wholesale thiosulfate reduction, rather than a site-specific reaction.

SULFITE REDUCTION

The mechanism(s) of sulfite reduction to sulfide is at the core of the MSR metabolism and the topic of much discussion (see (Bradley et al. 2011)). For this reason, experiments growing sulfate reducers on sulfite are relatively common (Drake & Akagi 1978; Fitz & Cypionka 1990; Habicht et al. 1998; Harrison & Thode 1958; Smock et al. 1998) and capture two very different manifestations of the MSR reaction network. In the most straightforward experiments, sulfite reduction only produces sulfide (cf. (Habicht et al. 1998)). Estimated fractionation factors for sulfite reduction suggested a small (~6‰) $^{34}\varepsilon$ between residual sulfite and sole product sulfide (Habicht et al. 1998). Conversely, other studies demonstrate the production of other sulfoxy anions (thionates: thiosulfate, trithionate and tetrathionate) during sulfite reduction that are either intermediate or terminal reaction products (cf. (Fitz & Cypionka 1990; Kobayashi et al. 1969)). One such reaction pathway involving intermediates is summarized as three reactions:

$$(a)\ 3SO_3^{2-} \leftrightarrow S_3O_6^{2-}$$
$$(b)\ S_3O_6^{2-} \leftrightarrow S_2O_3^{2-} + SO_3^{2-}$$
$$(c)\ S_2O_3^{2-} \leftrightarrow HS^- + SO_3^{2-}$$

Eqn. 4

and results in the net stoichiometry of $SO_3^{2-} \rightarrow HS^-$. In this case, trithionate is always the first intermediate produced (Fitz & Cypionka 1990; Kobayashi et al. 1969), and during the step-wise reduction, sulfite is continually regenerated (Fitz & Cypionka 1990). It is presumed (and testable) that the sulfonate S is simply shuttled between sulfoxy anions and would, as a result, not change in isotopic composition. If true, the only isotopic consequences would be the result of sulfide production: a consequence isotopically distributed within the sulfite pool. What is unclear however is the relative rates of these reactions, whether they are truly linked, and what shared (or unique) proteins are responsible for catalysis.

This cascade of reactions was classically investigated through enzyme studies (Haschke & Campbell 1971; Hatchikian 1975; Findley & Akagi 1969), tracking the balance of electron acceptors and donors (Sass et al. 1992), as well as interrogating the subcellular localization of the component proteins involved in the reduction (Drake & Akagi 1978; Venceslau et al. 2010). Despite the simplified overall stoichiometry and general reaction outline (Fig. A2.1), the potential for myriad unique overall pathways (each with differing reaction rates and residence times in each intermediate phase) could carry significant isotopic consequences. This is all in an attempt to locate the machinery and drivers behind thionate production, and in the end, better understand the reduction of sulfite to sulfide.

In these experiments *D. alaskensis* strain G20 grew on sulfite while producing a mixture of products. That is, rather than simply producing sulfide, G20 follows a net stoichiometry similar to equation 4. We arrive at this conclusion given that the detectable products include both thiosulfate and sulfide in a fixed 2:1 stoichiometry (Fig. A2.6). Notably, trithionate was below detection (2.5 mM) for each experiment – this is not unexpected (Fitz & Cypionka 1990). What is measureable is sulfite loss in parallel to sulfide and thiosulfate generation (at rates approaching 100 and 250 *f*mol per cell per day), respectively: Fig A2.6b). These rates are similar to, but slightly

lower than that for sulfate and thiosulfate reduction experiments. The isotopic behavior in these experiments is similarly complex (Fig. A2.6c). The residual sulfite pool only changes composition slightly, becoming more enriched. As expected, product sulfide is isotopically depleted relative to residual reactant sulfite (by up to 10‰ in ^{34}S), whereas sulfonate and sulfane in thiosulfate carry much more enriched and depleted values, respectively. Diverging from the prediction of equation 4, thiosulfate here is produced in excess of sulfide (a 2:1 rather than 1:1 concentration ratio: Fig. A2.6a). That is, sulfide and thiosulfate concentrations should track in concert if the only loss mechanism for thiosulfate is to sulfide and sulfite according to equation 4.

At first pass, we may posit from this data that thiosulfate reduction is the rate limiting reaction and if true, would predict that the isotopic signature of thiosulfate reduction would be recorded in sulfide and reflect that observed in our thiosulfate reduction experiment. Alternatively, thiosulfate production may suggest the possibility of numerous reactions occurring in parallel, rather than all reactions happening in sequence, as in equation 4. De-convolution of the overall reaction sequence is aided by multiple S isotope measurements. Importantly, despite this complex mixture of products, isotopic mass balance is closed (Fig. A2.6a, A2.7b). It is critical to demonstrate the closure of isotopic mass balance. Relative proportions are noted as:

$f_{sulfide} = [sulfide]_{t=n}/[sulfite]_{t=0}$ and $f_{thiosulfate} = [thiosulfate]_{t=n}/[sulfite]_{t=0}$. We note that two-component mixing is nonlinear in $\delta^{34}S$ - $\Delta^{33}S$ (see Fig A2.7b). We therefore convert compositions back to ^{3x}R and solve for both ^{33}R and ^{34}R independently (where R is the ratio of the target pool normalized to the initial sulfite), such that for any given time point (t = n):

$$^{3x}R_{sulfite,t=0} = \left(\left[1 - f_{sulfide,} - f_{thiosulfate,}\right] \times {}^{3x}R_{sulfite,t=n}\right) + \left(f_{sulfide,} \times {}^{3x}R_{sulfide,t=n}\right) + \left(0.5 f_{thiosulfate,} \times {}^{3x}R_{sulfonate-S,t=n}\right) + \left(0.5 f_{thiosulfate,} \times {}^{3x}R_{sulfane-S,t=n}\right).$$

The difference between the bulk composition of the experiment at time zero (constituting total S in the experiment) and our summed pools of directly quantified S at any given time point is within 1σ of one another, once analytical errors (for *f* and δ) are propagated. This harkens back to the essential nature of measuring the concentration of intermediate species and closure of overall mass balance. Given this tight constraint, we feel confident interpreting the data presented in Figure A2.7.

Herein sulfite reduction has three distinct products: sulfide, thiosulfate sulfane sulfur and sulfonate sulfur, each of which we measured for $\delta^{34}S$ and $\Delta^{33}S$. Mass and isotopic evolution of residual reactant sulfite is balanced by sulfide and thiosulfate sulfurs at each time point. For the later, we note that sulfonate sulfur is an approximate redox equivalent of aqueous sulfite (S^{4+}) (Vairavamurthy et al. 1994). What is immediately clear form these results are the large fractionations associated with the production of thiosulfate, with the sulfane and sulfonate S separated by nearly 30‰ (both $\Delta^{33}S$ are slightly positive: Fig A2.6c, A2.7a). This is striking given that, over the course of sulfite reduction, the isotopic composition of sulfite becomes only modestly enriched in both $\delta^{34}S$ and $\Delta^{33}S$ (Fig. A2.7). The sulfide reservoir does preserve a more significant isotope fractionation, with depletion in $\delta^{34}S$ approaching 10‰ and a small but resolvable enrichment in $\Delta^{33}S$.

There are numerous different approaches to solve the overall reaction sequence occurring in the sulfite experiment. The first clear possibility is for a 'stepwise reduction', where trithionate and thiosulfate are the necessary intermediates in sulfide production (see above). If trithionate is transiently produced, for every sulfide produced, two sulfites would be cycled through the thionate (Eqn. 4a). For simplicity here we assume the two sulfonate moieties in trithionate carry identical $\delta^{34}S$ and $\Delta^{33}S$, given the symmetry of the molecule and identical bonding environment for the oxidized sulfur. If trithionate and thiosulfate formation are similar, the sulfonate sulfurs would be significantly enriched in $\delta^{34}S$ and the sulfane sulfur significantly depleted (perhaps near the respective 15‰ and -15‰, observed here, from thiosulfate in sulfite reduction experiments). It is difficult to uniquely predict the composition of the residual sulfite at the time of trithionate production, given the evolving isotopic buffering capacity provided by the size of the extracellular sulfite reservoir. However, the eventual recycling of two of three S atoms would predict a residual reactant sulfite value slightly enriched in $\delta^{34}S$ and depleted in and $\Delta^{33}S$ relative to the starting composition, as the only terminal loss (i.e. that not recycled back to sulfite) is the production of sulfide. Put differently, the sulfite should essentially close mass balance with the sulfide. This does not appear to fit the data well (see Fig A2.7b) and stumbles further when the sulfane S is considered. If the 'step-wise reduction' model is correct, the fate of the sulfane S from trithionate is sulfide. For this to be the case, and if we presume that trithionate production would carry a similar isotopic consequences to

thiosulfate production, there would have to exist a more than 10‰ inverse isotope effect associated with S^0 reduction to sulfide; a process understood as carrying little to no isotope effect in other systems (FRY et al. 1985). Thus, sulfite reduction in G20 does not appear to be shuttled through a site-specific reduction of trithionate.

Given that trithionate was not detected in our experiments, we now consider the case where thiosulfate is the only reaction intermediate. Thiosulfate production would commence with four electron transfers onto sulfite, generating an S^0 equivalent, which can then form a S-S bond with another sulfite molecule, (Eqn 4c) (Heunisch 1977). From there, two possibilities exist. The first would predict that the sulfane S is preferentially reduced to sulfide ($S_2O_3^{2-} \Rightarrow SO_3^{2-} + HS^-$), while sulfonate S is recycled back to the residual sulfite reservoir. However, we observe the residual sulfite pool remains quite isotopically depleted in $\delta^{34}S$ relative to the sulfonate S (near 0 and +15‰ respectively, Fig. A2.6c). In fact, if this were the mechanism, the stoichiometry of sulfonate S shuttling to sulfite would equal that of sulfide production, such that at minimum, ~50% of the residual sulfite would cycle through thiosulfate by the end of the experiment. Assuming a sulfonate S composition of 15‰, this recycling would pull the residual sulfite composition toward much more enriched values than are observed. Furthermore, the thiosulfate reduction experiment (Fig. A2.4) supports a wholesale and not site-specific reduction pathway. As such, if a step-wise reduction scheme for sulfite is correct, we expect product sulfide to be offset from the bulk thiosulfate composition by approximately 7‰ and along a $^{33}\lambda$ vector of 0.512 (Fig. A2.5). Early in the experiment sulfide is in fact offset by roughly -7‰ from net thiosulfate (Fig. A2.7), but contracts to -3‰ depleted by the end of the experiment (^{33}S data is only available for the later two time points, the associated $^{33}\lambda$ is ~ 0.5135). These isotopic data suggest that sulfide generation in sulfite reduction experiments may in fact be recording thiosulfate reduction.

For completeness, we also consider that sulfite reduction could follow two *parallel and independent reductions*: $SO_3^{2-} \Rightarrow HS^-$ and $SO_3^{2-} \Rightarrow S_2O_3^{2-}$. In the case of parallel and independent reductions, sulfite reduction to sulfide would proceed as a single six-electron reduction step. A small fractionation between sulfite and sulfide ($^{34}\varepsilon$ < 8‰) has been demonstrated in sulfite reduction experiments where only sulfide is produced

(Habicht et al., 1998). Like all solely reductive kinetic processes measured to date, the expectation is for a $^{33}\lambda$ less than 0.515. This overall scheme appears inconsistent with the data at the later time points, however, as the $\delta^{34}S$ fractionation between sulfite and sulfide is quite small (<5‰) with an apparent $^{33}\lambda$ of ~ 0.519. We specifically term this an apparent $^{33}\lambda$ given that there may not be a single process relating these pools, and as such, it may not be a process-specific value.

We acknowledge that a unique solution to how sulfur is transferred and fractionated during sulfite reduction is difficult to ascertain through these experiments alone. We propose, however, that trithionate is not a critical intermediate in these reactions, and if present, is short-lived. It is also difficult to directly account for any reactions between sulfide and sulfite in generating some of the thiosulfate (Heunisch 1977). We suggest however that the primary metabolic reaction fractionating isotopes is the wholesale reduction of thiosulfate to sulfide, like that seen in the direct thiosulfate experiments. The source of that thiosulfate certainly involves reduced products and perhaps some scavenging of S^0 from DsrAB, which in turn reacts with sulfite. Shuttling sulfur to a thiosulfate intermediate pool makes some biochemical sense, given the environmental conditions at the beginning of these experiments may not be overly hospitable to a microbial sulfate reducer. The presence of a large ambient sulfite pool, as is the case here, imposes significant redox stress on the cell, even though a sulfite is a thermodynamically favorable electron acceptor. If the organism is capable of generating a more stable reservoir of electron acceptor, such as in the form of thiosulfate, this may be optimal. Indeed this is what we propose here: sulfite is shuttled to thiosulfate and then reduced to sulfide. Revisiting the role of sulfite during sulfate reduction, intra-cellular concentrations of sulfite likely never approach those of our media (10 mM), leaving our experiments as an informative, yet imperfect, analogue to sulfate reduction.

CONCLUSIONS

Our overall motivation and emphasis rests with characterizing the isotopic consequences of sulfite reduction within microbial sulfate reduction network. This is grounded in the central role that SO_3^{2-} plays in the branching and reduction within that process (Bradley et al., 2011). Understanding what then controls the

shuttling of sulfite to particular intermediates (possibilities including trithionate, thiosulfate, zero valent S, or sulfide) and the isotopic consequences of that shunt (both the intrinsic fractionation of that reaction and the mass balance consequences at the cellular scale) are tractable through the types of experiments presented here. Importantly, we note that we are not the first to engage in such a pursuit and our experimental protocol is adopted from earlier works. Harrison and Thode (1958), for instance, found that *Desulfovibrio desulfuricans* reduced sulfite at the same rate and associated isotope effect as during sulfate reduction. Other studies since that time have targeted sulfite reduction, some of which suggest the direct production of sulfide while others illustrate the importance of intermediates (Fitz and Cypionka, 1990; Habicht et al., 1998; Harrison and Thode, 1958; Kaplan et al., 1963; Krouse et al., 1968; Sass et al., 1992a; Smock et al., 1998). In an ideal case, the reduction of sulfoxy anion intermediates in experiments where they are the lone electron acceptor would perfectly mimic the *in situ* biochemical reactions present when grown on sulfite. For example, direct sulfite reduction experiments would behave the same was as sulfite reduction during sulfate reduction experiments. Here, we extend the insights gleaned from our experiments from major isotope information by including ^{33}S and, where necessary, site-specific isotope measurements.

It is important to appreciate that performing sulfite reduction experiments with whole cells and live cultures is not a perfectly analogous system to the operation of DsrAB/C within a fully constituted sulfate reducer. Thus, we discuss below the range of possibilities to help us hone in on the particular reactions and fractionation factors that are expressed, and are aware of the limits of this approach. We began with the characterization of sulfate reduction by our model organism (G20), using two different electron donors. Consistent with previous works, our data demonstrate that G20 produces small $^{34}\varepsilon$ fractionations while operating at high (relative) rates of reduction. The inverse rate versus fractionation relationship is well established (Harrison and Thode, 1958; Leavitt et al., in press) and further supported here. Finally, these data extend our picture of ^{33}S fractionation from sulfate reduction at small $\delta^{34}S$, and are consistent with the composite $^{33}\lambda$ vs. $\delta^{34}S$ relation from previous works (Fig. A2.3).

Thiosulfate reduction presented a number of possible reduction schemes, however our results suggest a simple, wholesale reduction to sulfide. There are interesting implications at the enzyme level if this is true. Specifically, once the thiosulfate is bound to the active site, both sulfurs are reduced completely to sulfide or to the valence where DsrC can bind and reduce each to sulfide before it escapes the active site pocket. That is, they must remain bound to or closely associated with the active site of the host enzyme such that loss of either S back to the bulk intracellular solution is minimized.. Differentiating reaction pathways at such spatial and temporal scales will require knowledge of the enzymes involved, the electron delivery scheme, and enzyme-substrate geometry throughout the reduction process.

The reduction of sulfite proved to be quite complex in G20. Although the measured products are thiosulfate and sulfide (in a fixed ratio), it is possible that trithionate is the first intermediate, but below analytical detection due to a very short residence time. The most parsimonious interpretation of the sulfite-thiosulfate-sulfide system is the transformation of sulfite to thiosulfate, which is then quantitatively reduced to sulfide. The largest fractionation here is associated with the reductive formation of thiosulfate from sulfite, however this isotope effect is largely lost upon the ensuing reduction to sulfide. We reach this interpretation based on the parallel thiosulfate reduction experiments with the same organism. Further, the role of DsrAB/C in this system is also unclear. The enzyme system may be acting independently or in parallel with separate thiosulfate forming and reducing enzymes or performing all reactions independently (see discussion in (Bradley et al., 2011). The difference in fractionations we observed between sulfate versus thiosulfate reduction experiments may simply relate to differences in net metabolic rate with the same enzymatic machinery (c.f. (Leavitt et al., in press), or may indicate the operation of different enzymes. Differentiating between these scenarios is beyond the scope of this study, but critical to ultimately understanding these reactions.

The collection of these experimental results has clear implications for how we interpret MSR, however the lessons extend beyond that. Equally as important is that cycling of sulfur intermediates like sulfite and thiosulfate is complex and can carry significant isotope effects. This is especially true during thiosulfate production. A careful revisiting of the enzymes involved in these reactions is a target for future research. As the

key proteins come to be better understood, the similarities and differences with companion processes like sulfur disproportionation will also become more clear. As presented above, the production of thiosulfate from sulfite can induce an apparent 30‰ fractionation, before reduction (or disproportionation) begins. How we view net isotope effects in modern or ancient environments, where a broader suite of chemistry is possible, must now consider a suite of S intermediates. Future microbiological work will help to define how and when certain reactions are catalyzed and by which enzymes. Once MSR reactions are understood at that level, and with complementary data from disproportionation reactions, more detailed and precise environmental interpretations will be possible.

Acknowledgements: Thanks to Colleen Hansel and her group generosity in sharing lab space and equipment. Funding was provided by NASA-Exobiology (DTJ and AB), NSF CAREER (DTJ), NSF Instrument and facilities (DTJ), and NSF GRFP (WDL). Many thanks to Andy and Erin for lab support and safety meetings!

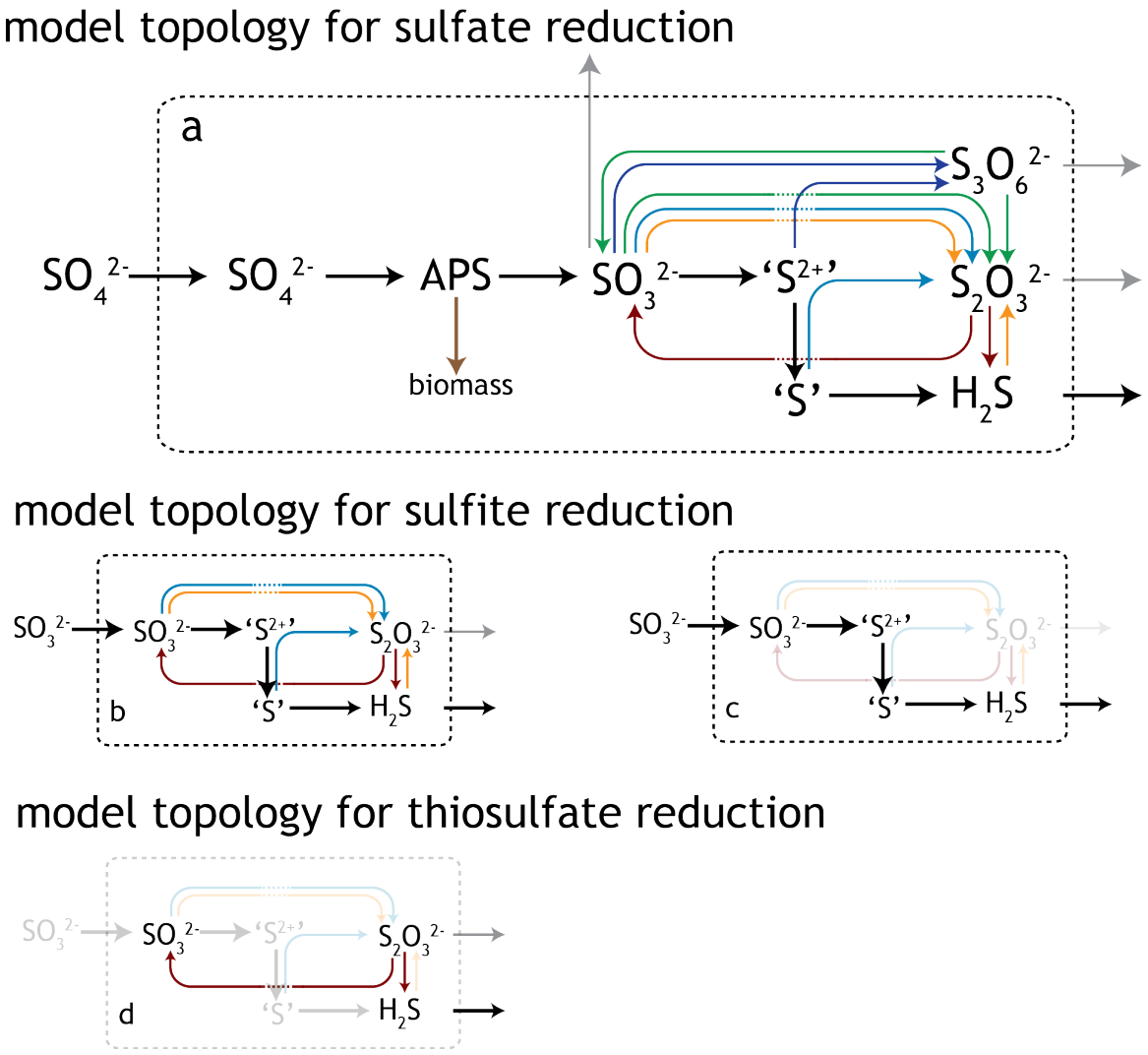

Figure A2.1: The model of dissimilatory sulfate reduction from Bradley et al. 2011. As it relates to this study, the schematic outlines the potential for numerous reactions between sulfite and sulfide (insets b-d). As the isotopic consequences of most of these potential reactions are unknown or under-constrained, this work aims to better assay both the isotope effects and conditions that favor the production of some of these intermediates. What is outlined for sulfite and thiosulfate reduction are the potential reactions given the standard model of the biochemistry associated with sulfate reduction. Trithionate is included here, however not seen in this study. This is not exhaustive network, and is a topological prediction that is testable and would be informed with future biochemical inquiry.

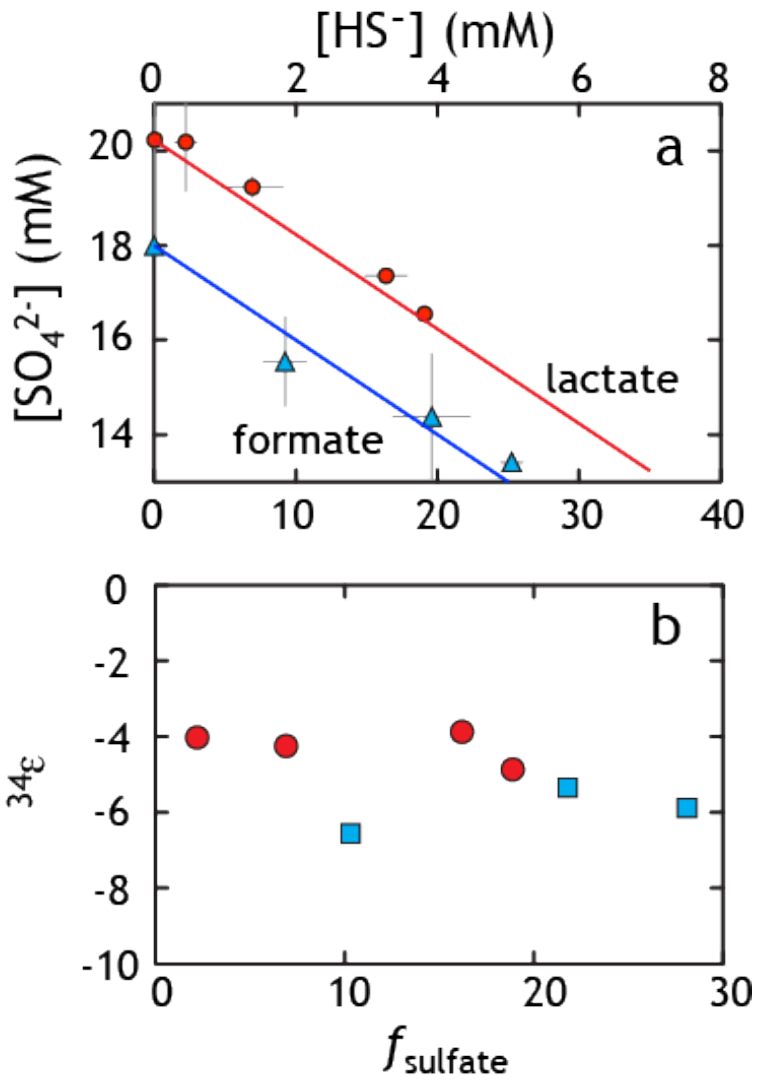

Figure A2.2: Data from two sulfate reduction experiments, one with lactate (red) and one with formate (blue). In frame **A**, the loss of sulfate is accounted for with the ingrowth of sulfide. Data reflect various time points throughout the experiment and the line corresponds to perfect closure of elemental mass balance (theory). Frame **B** catalogs the calculated fractionation factor relating sulfate and sulfide. The isotopic residuals (to satisfy the calculated mass-imbalance) on the sulfate experiments are 0.18‰ and 0.42‰ in $\delta^{34}S$ and 0.007‰ and 0.017‰ in $\Delta^{33}S$ for formate and lactate, respectively.

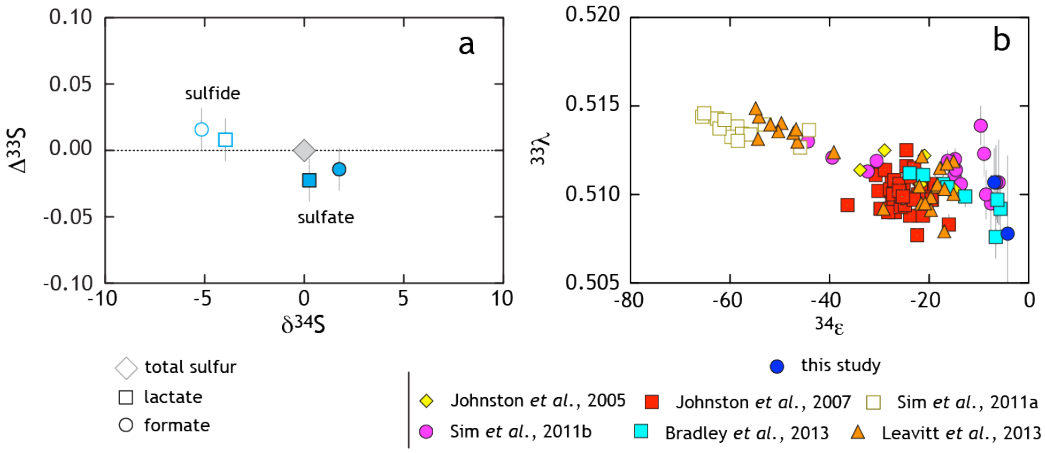

Figure A2.3: The triple isotope consequences of sulfate reduction are presented in two complementary frames (**A**-**B**). In frame **A**, data from lactate and formate experiments are presented relative to the starting composition (gray diamond). White symbols with colored outlines are sulfide data whereas filled symbols are sulfates (see key for further description). Here, sulfides become characteristically depleted in $\delta^{34}S$ and enriched in $\Delta^{33}S$, whereas sulfate preserves the opposite behavior. Frame **B** presents a compilation of pure culture sulfate reduction experiments (references in legend).

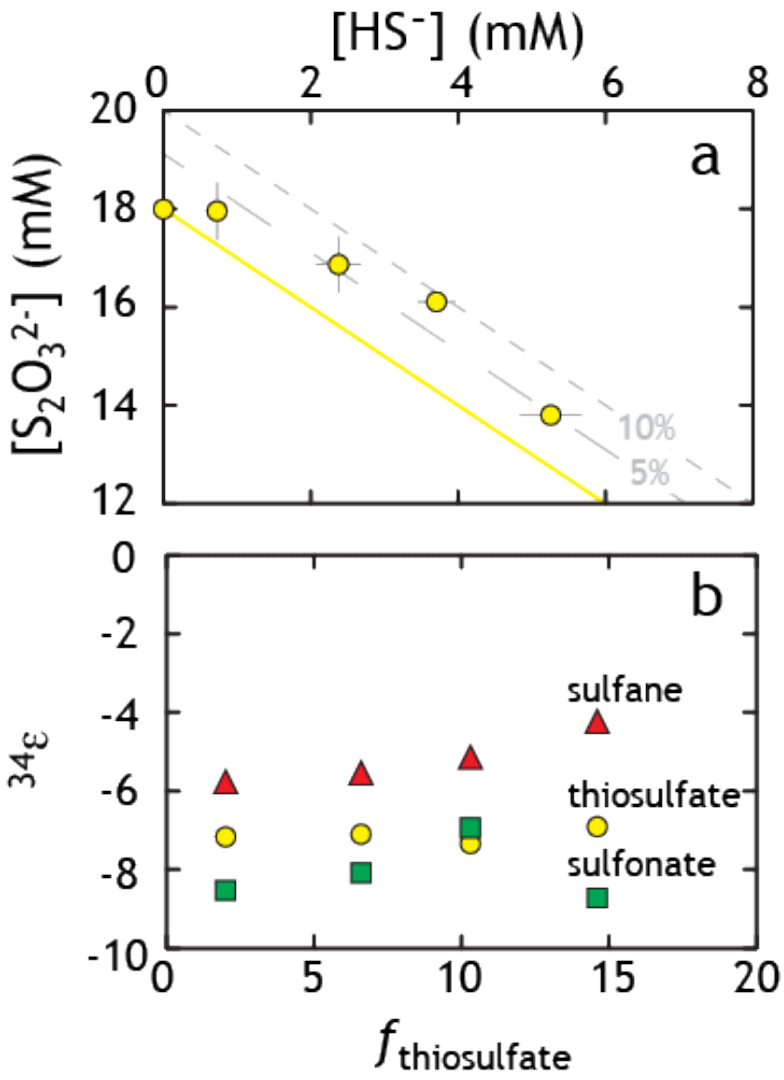

Figure A2.4: Geochemical and isotopic data from experiments with G20 as a thiosulfate reducer. As seen in frame **A**, thiosulfate was lost to the production of sulfide. The yellow line represents ideal closure of mass-balance, with the two gray lines representing 5% and 10% excess of total S. Frame **B** demonstrates three different methods for calculating the fractionation associated with thiosulfate reduction (thiosulfate total, sulfane and sulfonate: see text for discussion). The isotopic residuals (calculated mass-imbalance) on the thiosulfate experiments are 0.28‰ and 0.35‰ in $\delta^{34}S$ and 0.005‰ and 0.003‰ in $\Delta^{33}S$.

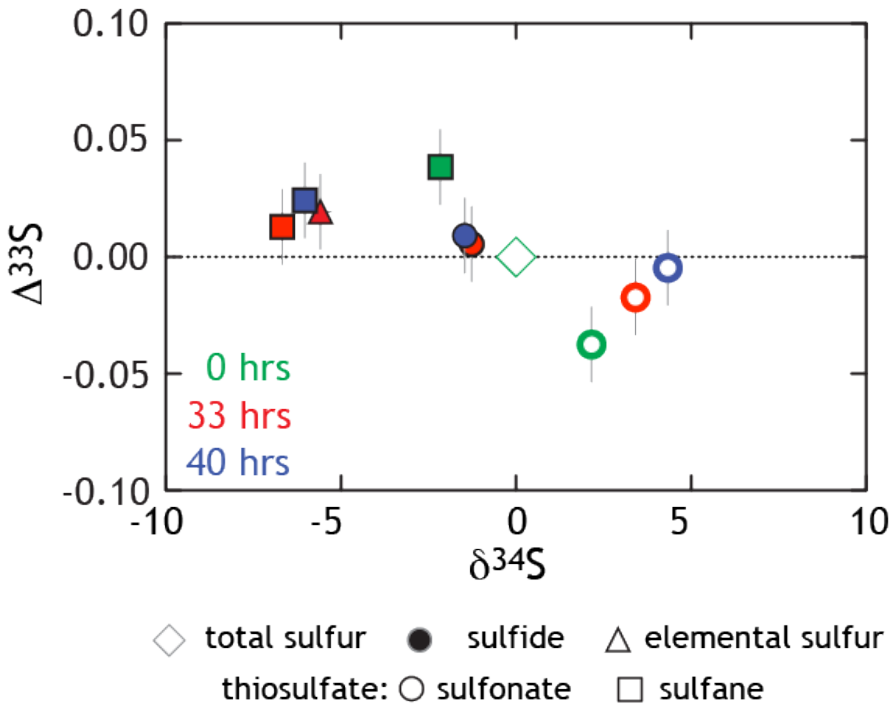

Figure A2.5: Triple isotope data for thiosulfate reduction experiments. As opposed to Figure A2.4b, here all isotope data is normalized to the bulk composition of the starting thiosulfate (green diamond at origin). Also in green are the site-specific compositions of the sulfane and sulfonate S (square and circle, respectively). Those same S sites at times 33 hrs (red) and 40 hrs (blue) hours are also included.

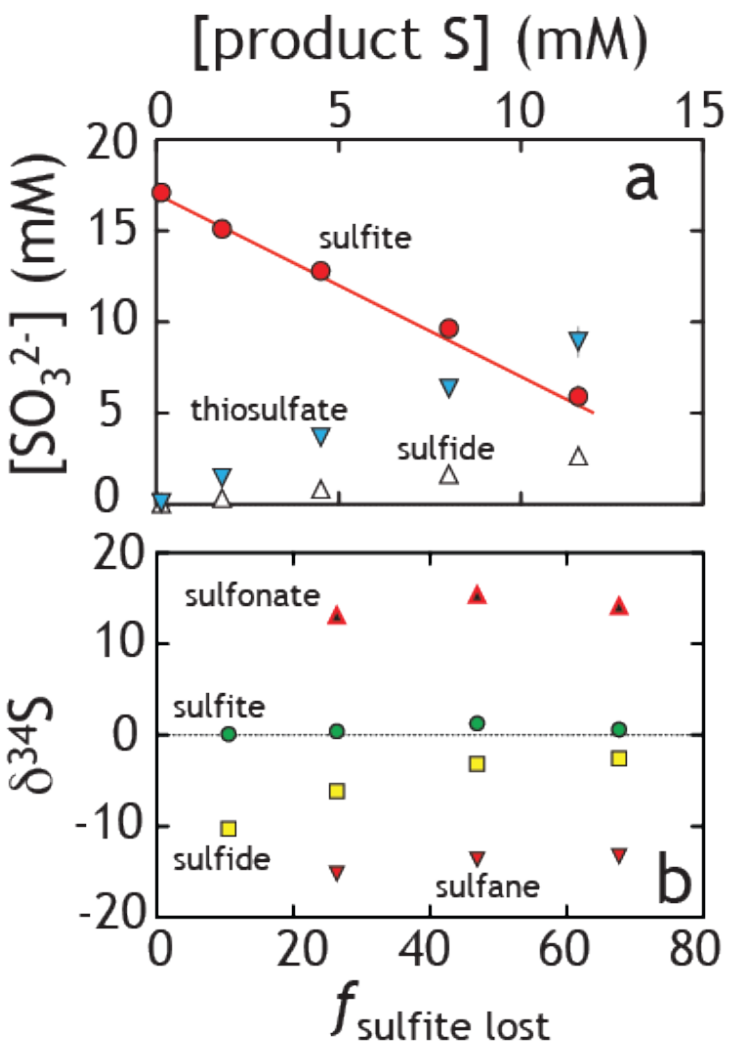

Figure A2.6: Sulfite reduction experiments, where both thiosulfate and sulfide were produced. In the upper frame, the line represents closure of mass balance (the overlap of the red dots and line). In Frame B, the isotopic compositions of the various products and residual reactants over the course of the experiment are presented. Unlike the sulfate and thiosulfate reduction experiments (figures A2.2 and A2.4), simple a values cannot uniquely be calculated. Thus here we present the isotopic composition of various pools ($\delta^{34}S$) relative to the total S in the system rather than a derived $^{34}\varepsilon$ value. See text for more discussion.

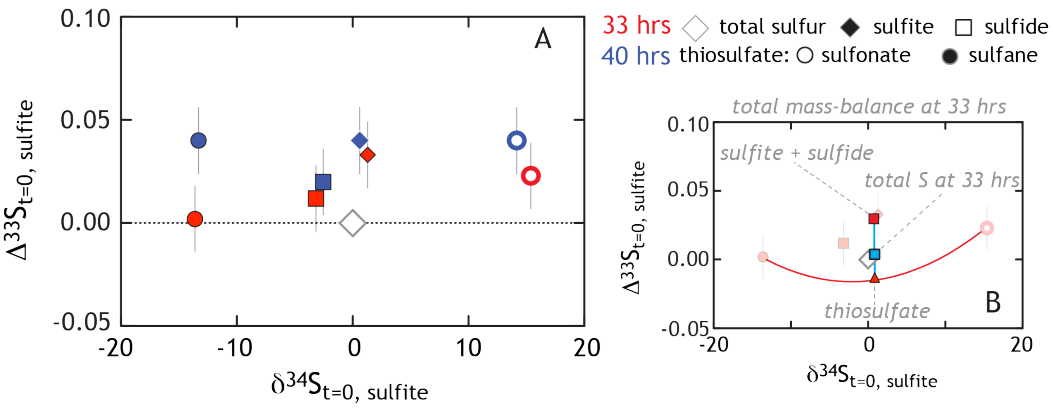

Figure A2.7: Here we present the triple isotope consequences for sulfite reduction by G20. In Frame A, all data is plotted relative to the total sulfur at the initiation of the experiment. From there, sulfite gains a modest $^{34}\varepsilon$ and $\Delta^{33}S$ enrichment, while sulfide tracks toward depleted $\delta^{34}S$ with an enriched $\Delta^{33}S$. Thiosulfate is also generated with sulfane and sulfonate falling compositionally very far outside the residual sulfite and product sulfide (see text for further discussion). In frame B, we use the 26.5 hrs data (fraction of sulfite lost is 49%) to demonstrate the degree to which mass-balance is closed. For instance, the red triangle is the 'total thiosulfate' composition, falling at the 50% mark of a mixing line between sulfane and sulfonate. Note that in this coordinate system, mixing is non-linear. Similarly, the red square is the mixture of sulfite and sulfide. The blue square is the calculated total S at 26.5 hrs. This value is then directly comparable to the total S at the initiation of the experiment (gray diamond). The isotopic residual (calculated mass-imbalance) on the sulfite experiments are 0.7‰ and 0.02‰ in $\delta^{34}S$ and 0.013‰ and 0.024‰ in $\Delta^{33}S$ for the 26.5 hrs and 30 hrs experiments, respectively.

APPENDIX C

Things to do better the next time around; if you are about to try experiments like those in this dissertation, please read!

"It never got weird enough for me."

Hunter S. Thompson

Methodological improvements for analytical and experimental design(s)

Batch (closed-system) isotope fractionation experimental methodologies

Batch experiments sub-sampled with time, such as those in Chapter 5, where a head-space/liquid partitioning may occur in product sulfide, is a non-deal experimental approach. The small mass imbalance later in the experiment, where we track the concentrations of aqueous species only, is most likely due to $H_2S_{(liq)}/H_2S_{(g)}$ partitioning within the reaction vessels. While in our experiment we can easily estimate the mass and composition of this pool, it leaves open a parameter that may be simple constrained. A revised experimental approach in future works can either: (*a*) perform the same experiments in head-space free collapsible gas-tight bags, or by (*b*) preparing as many replicate volumes of culture as time point, multiplied by number of replicates. In either case, but particularly the second, I strongly recommend pre-mixing the inoculum with the medium (aseptically and anaerobically) before the distributing to the individual reaction vessels in order to homogenize initial cell densities. Each approach has its drawbacks. In the latter case, a significant amount of glassware is required and there may still be significant differences between vessels, rendering time point replicates non-uniform. For examples, if partial flow-through systems are required, as in the MR-1 experiments I note above, many individual vessels for each time points adds up and renders an impractical experimental setup. This highlights the utility of larger volumes systems that may be sub-sampled. The main drawback to sub-sampling large vessels is indeed highlighted from our work with the DsrC mutants. Otherwise, if deformable gas-tight vessels are available, and batch (closed) system approach is desired, then the subsampling method is recommended over separate bottle sacrifices. Controls, both un-inoculated and inoculated lacking key reactant, are absolutely required in any case, and at bare minimum duplicate, though preferably triplicate vessels under each experimental condition, should be used. It must not be forgotten that each bottle is a separate experiment, and must be treated as such.

Semi-closed/open experiments with a static liquid volume and continuous gas flux

Early in my dissertation work I attempted batch experiments designed to determine the magnitude of sulfur isotope fractionation between sulfite or thiosulfate and product sulfide using the model γ-Proterobacteria

Shewanella oneidensis strain MR-1 (MR1). MR-1 is commonly studied as an iron reducer, but is also known to couple the oxidation of organic acids to the reduction of sulfite, thiosulfate and even elemental sulfur (Myers & Nealson 1988; Burns & Dichristina 2009). Intriguingly, MR-1 is unable to utilize sulfate as its sole terminal electron acceptor (Myers & Nealson 1988). As I quickly realized, MR-1 is strongly inhibited by the sulfide it produces during sulfite or thiosulfate reduction, coupled to either lactate or formate reduction – controls fermenting fumarate were unaffected by the experimental design and grew rapidly in the fully closed system. To work around the sulfide inhibition I developed a simple method to flux N_2 or mixed N_2:CO_2 through the rubber septum seal via a stainless steel needle, into the bottom of each anaerobic culturing tubes (24 mL Balch), forcing sulfide out of the medium and into a separate zinc acetate trapping solution, in >40 individual tubes simultaneously. This allows for quantitation and isotope analysis of each culture tube efficiently upon sacrifice. While this approach effectively relives sulfide stress and induces rapid MR-1 growth and reduction of sulfite or thiosulfate in, this approach also introduces significant challenges in maintaining a balanced gas flux through each replicate, and will require precision gas flow control if it is to be executed successfully (e.g. one mass flow controller per tube, at ~$1000 each, this is impractical). Moreover, maintaining constant liquid levels in each experimental volume and subsequent zinc trap is critical to accurately accounting for reactant and product S-compound concentration (mass balance) accounting, and due to gas-flow induced drying and blowouts, this was not possible. I recommend moving to a completely continuous flow system, similar to the chemostats in Chapters 2 and 3. If a semi-closed/open system is desired, employing a chemostat-like setup, where a larger reactor volume and only gas flow is allowed, may be a viable option. This would further allow for volume level and pH control.

Improvements to chemostat design and expanding the testable MSR parameter-space

In two of the projects presented in this dissertation (Chapters 2 and 3) we employed an open system microbial cultivation and experimental approach. In each experimental run the liquid level in the chemostat must be maintained at a constant value. In the first run an automated LED-actuated liquid-level controller was designed and constructed in-house by Andy Masterson and myself. The controller consisted of an 'Electro-Optic Point-

Level Sensors' (Cole-Parmer #68964-00) and the optical sensor controller (#S-32772-50), mounted on the end of a stainless tube introduced through a dedicated port, wired through a second peristaltic pump (4-channel Ismatech, Reglo). For a more complete picture, refer to the chemostat schematic and description in Chapter 2. For the experiments that were run over a range of dilution rates with constant sulfate concentrations (Chapter 2), the automated liquid level controller was used. At times the 'normally closed' circuit became stuck in the 'open' position, meaning the secondary effluent pump was engaged constantly and decreased the volume in the reactor to the level of the outlet tubing. In these instances we rapidly refilled the reactor to the previous medium level with sterile anaerobic medium and allowed the organisms to achieve the prior steady-state biomass density and specific sulfate reduction rate before continuing to collect samples from the experiment. The level controller likely became fouled by biomass growth around the optical sensor. Devising a method for controlling growth on the sensor is a goal for future chemostat experiments, as this degree of control allows for greater confidence in a chemostat of near constant volume. Finally, integrating an externally referenced redox probe and sensor into the reactor vessel, and controlling the growth medium flux through this, is a goal for future experimental work with both wildtype and mutant strains of MSR (e.g. Chapter 5), and in column flow-through experiments utilizing natural sediments or synthetic minerals.

Depending on the question at hand, continuous flow systems are strongly recommended for most biochemical and geomicrobial kinetic experimental work that necessitates steady-state observations. The open-system experimental approach allows the experimenter to control for physiological variance normally left to the whim of the metabolism or enzyme under investigation. Numerous excellent resources are available for the practical and mathematical approaches to building, performing and understanding chemostat experiments (Herbert et al. 1956; Smith 1995).

Quantitation and separation of individual thionates for site-specific S and O isotope analyses

In determining the multiple sulfur isotope fractionation factors of the DsrAB enzyme (Chapter 4), the need to carefully quantitate and separate the multiple intermediate valence S-phases, particularly thiosulfate and

trithionate, was a necessity. Regarding quantitation, more sensitive (down to nM concentrations) and rapid methods to uniquely identify and quantify sulfide, thiosulfate, trithionate, sulfite and sulfate simultaneously from in vitro reaction buffer or in vivo culture medium, are desirable. Such methods exist in part (Newton & Fahey 1995), but must first be tested thoroughly in our matrix solutions and compared with our standard methodologies (Sörbo 1957; Cline 1969; Don P Kelly & Wood 1994; Leavitt et al. n.d.). In future mixed S-species work we also aim to separate the thionates from one another before degrading and separating the intra-molecular sulfur's of differing redox state, and is fully necessary for future experiments involving sulfur isotope fractionations between thionates and other intermediate valence compounds. Examples include enzymatic trithionate reduction to thiosulfate (Akagi et al. 1994) or trithionate–thiosulfate—sulfite equilibrium exchange/fractionation experiments (Ames & Willard 1951). In Chapter 4 the method employed to extract the more reduced from more oxidized ('sulfonate') sulfur moieties from mixtures of trithionate and thiosulfate, and purifying these operational pools for subsequent sulfur isotope analysis, is viable for the purpose of that investigation. However, a more elegant solution is to isolate each individual sulfur moiety in each compound class – a goal in future works. This may be accomplished by a combination of preparative anion chromatography – to separate each compound from others, protecting compounds like sulfite from degradation (Kiryushov & Skvortsova 2010), assuming appropriate chromatographic conditions may be determined – followed by selective degradation and distillation separation of the different valence pools (Chapter 4, Appendix B, (Smock et al. 1998)). Where applicable and of interest, the oxygen isotopic composition may be determined, primarily in order to address knowledge-gaps in our understanding for intracellular equilibrium and kinetic oxygen isotope effects, recently the subject of intensified interest (Müller et al. 2013; Wankel et al. 2014; Antler et al. 2013).

BIBLIOGRAPHY

Aharon, P. & Fu, B., 2000. Microbial sulfate reduction rates and sulfur and oxygen isotope fractionations at oil and gas seeps in deepwater Gulf of Mexico. *Geochimica Et Cosmochimica Acta*, 64(2), pp.233–246.

Akagi, J.M. & Adams, V., 1973. Isolation of a bisulfite reductase activity from Desulfotomaculum nigrificans and its identification as the carbon monoxide-binding pigment P582. *Journal Of Bacteriology*, 116(1), pp.392–396.

Akagi, J.M. et al., 1994. [17] Thiosulfate and trithionate reductases. *Methods in enzymology*, 243, pp.260–270.

Aketagawa, J., Kobayashi, K. & Ishimoto, M., 1985. Purification and properties of thiosulfate reductase from Desulfovibrio vulgaris, Miyazaki F. *Journal of biochemistry*, 97(4), pp.1025–1032.

Ames, D.P. & Willard, J.E., 1951. The Kinetics of the Exchange of Sulfur between Thiosulfate and Sulfite1. *Journal of the American Chemical Society*.

Antler, G. et al., 2013. Coupled sulfur and oxygen isotope insight into bacterial sulfate reduction in the natural environment. *Geochimica Et Cosmochimica Acta*, 118, pp.98–117.

Bak, F. & Cypionka, H., 1987. A novel type of energy metabolism involving fermentation of inorganic sulphur compounds. *Nature*, 326(6116), pp.891–892.

Bak, F. & Pfennig, N., 1987. Chemolithotrophic growth of Desulfovibrio sulfodismutans sp. nov. by disproportionation of inorganic sulfur compounds. *Archives of Microbiology*, 147(2), pp.184–189.

Bak, F. & Pfennig, N., 1991. Microbial sulfate reduction in littoral sediment of Lake Constance. *FEMS Microbiology Letters*.

Bandurski, R.S., Wilson, L.G. & Squires, C.L., 1956. The Mechanism of "Active Sulfate" Formation. *Journal of the American Chemical Society*, 78(24), pp.6408–6409.

Bergman, N.M. & Lenton, T.M., 2004. A New Biogeochemical Earth System Model for the Phanerozoic Eon. *Scientists Debate Gaia: ...* .

Berner, R., 2001. Modeling atmospheric O-2 over Phanerozoic time. *Geochimica Et Cosmochimica Acta*, 65(5), pp.685–694.

Berner, R.A., 2004. A model for calcium, magnesium and sulfate in seawater over Phanerozoic time. *American Journal Of Science*, 304(5), pp.438–453.

Berner, R.A., 2006. GEOCARBSULF: A combined model for Phanerozoic atmospheric O 2 and CO 2. *Geochimica Et Cosmochimica Acta*, 70(23), pp.5653–5664.

Berner, R.A., 2009. Phanerozoic Oxygen: new results of the GEOCARBSULF Model. *American Journal Of Science*, 309(7), pp.603–606.

Berner, R.A. & Canfield, D.E., 1989. A new model for atmospheric oxygen over Phanerozoic time. *Am. J. Sci*, 289(4), pp.333–361.

Bertran, E. et al., 2013. Deconstructing the dissimilatory sulfate reduction pathway: Isotope fractionation of a mutant unable to grow on sulfate. *Mineralogical Magazine*, 77(5), pp.636–804.

Bethke, C.M. et al., 2011. The thermodynamic ladder in geomicrobiology. *American Journal Of Science*, 311(3), pp.183–210.

Bigeleisen, J. & Wolfsberg, M., 1958. Theoretical and experimental aspects of isotope effects in chemical kinetics. *Advances in Chemical Physics, Volume 1*, pp.15–76.

Bolliger, C., Schroth, M.H. & Bernasconi, S.M., 2001. Sulfur isotope fractionation during microbial sulfate reduction by toluene-degrading bacteria. *... et Cosmochimica Acta*.

Boudreau, B.P. & Westrich, J.T., 1984. The dependence of bacterial sulfate reduction on sulfate concentration in marine sediments. *Geochimica Et Cosmochimica Acta*.

Böttcher, M.E., Sievert, S.M. & Kuever, J., 1999. Fractionation of sulfur isotopes during dissimilatory reduction of sulfate by a thermophilic gram-negative bacterium at 60 C. *Archives of Microbiology*, 172(2), pp.125–128.

Bradford, M.M., 1976. A rapid and sensitive method for the quantitation of microgram quantities of protein utilizing the principle of protein-dye binding. *Analytical Biochemistry*, 72(1-2), pp.248–254.

Bradley, A.S., Leavitt, W.D. & Johnston, D.T., 2011. Revisiting the dissimilatory sulfate reduction pathway. *Geobiology*, 9(5), pp.446–457.

Broco, M. et al., 2005. Deletion of flavoredoxin gene in Desulfovibrio gigas reveals its participation in thiosulfate reduction. *FEBS letters*, 579(21), pp.4803–4807.

Brunner, B. & Bernasconi, S.M., 2005. A revised isotope fractionation model for dissimilatory sulfate reduction in sulfate reducing bacteria. *Geochimica Et Cosmochimica Acta*, 69(20), pp.4759–4771.

Brunner, B. et al., 2005. A model for oxygen and sulfur isotope fractionation in sulfate during bacterial sulfate reduction processes. *Geochimica Et Cosmochimica Acta*, 69(20), pp.4773–4785.

Brüchert, V., Knoblauch, C. & Jorgensen, B.B., 2001. Controls on stable sulfur isotope fractionation during bacterial sulfate reduction in Arctic sediments. *Geochimica Et Cosmochimica Acta*, 65(5), pp.763–776.

Buchner, P., 2004. Plant sulphate transporters: co-ordination of uptake, intracellular and long-distance transport. *Journal of Experimental Botany*, 55(404), pp.1765–1773.

Burns, J.L. & Dichristina, T.J., 2009. Anaerobic Respiration of Elemental Sulfur and Thiosulfate by Shewanella oneidensis MR-1 Requires psrA, a Homolog of the phsA Gene of Salmonella enterica Serovar Typhimurium LT2. *Applied and Environmental Microbiology*, 75(16), pp.5209–5217.

Canfield, D.E., 2001a. Biogeochemistry of Sulfur Isotopes. *Reviews in Mineralogy and Geochemistry*.

Canfield, D.E., 1994. Factors influencing organic carbon preservation in marine sediments. *Chemical Geology*, 114(3), pp.315–329.

Canfield, D.E., 2001b. Isotope fractionation by natural populations of sulfate-reducing bacteria. *Geochimica Et Cosmochimica Acta*, 65(7), pp.1117–1124.

Canfield, D.E., 2006. Models of oxic respiration, denitrification and sulfate reduction in zones of coastal upwelling. *Geochimica Et Cosmochimica Acta*, 70(23), pp.5753–5765.

Canfield, D.E., 1989. Reactive iron in marine sediments. *Geochimica Et Cosmochimica Acta*, 53(3), pp.619–632.

Canfield, D.E., 2004a. THE EARLY HISTORY OF ATMOSPHERIC OXYGEN: Homage to Robert M. Garrels. *Annual Reviews*.

Canfield, D.E., 2004b. THE EVOLUTION OF THE EARTH SURFACE SULFUR RESERVOIR. *EVOLUTION*.

Canfield, D.E. & Farquhar, J., 2009. Animal evolution, bioturbation, and the sulfate concentration of the oceans. *Proceedings of the National Academy of Sciences*, 106(20), pp.8123–8127.

Canfield, D.E. & Raiswell, R., 1999. The evolution of the sulfur cycle. *American Journal Of Science*, 299(7-9), pp.697–723.

Canfield, D.E. & Thamdrup, B., 2005. Aquatic Geomicrobiology - Donald E. Canfield, Bo Thamdrup - Google Books.

Canfield, D.E. et al., 1993. Pathways of organic carbon oxidation in three continental margin sediments. *Marine Geology*, 113(1-2), pp.27–40.

Canfield, D.E., Farquhar, J. & Zerkle, A.L., 2010a. High isotope fractionations during sulfate reduction in a low-sulfate euxinic ocean analog. *Geology*, 38(5), pp.415–418.

Canfield, D.E., Olesen, C. & Cox, R., 2006. Temperature and its control of isotope fractionation by a sulfate-reducing bacterium. *Geochimica Et Cosmochimica Acta*.

Canfield, D.E., Stewart, F.J., et al., 2010b. A Cryptic Sulfur Cycle in Oxygen-Minimum-Zone Waters off the Chilean Coast. *Science*, 330(6009), pp.1375–1378.

Casciotti, K.L., McIlvin, M. & Buchwald, C., 2010. Oxygen isotopic exchange and fractionation during bacterial ammonia oxidation (vol 55, pg 753, 2010). *Limnology And Oceanography*, 55(4), pp.1805–1805.

Cárdenas, A.L. & Harries, P.J., 2010. Effect of nutrient availability on marine origination rates throughout the Phanerozoic eon. *Nature Geoscience*, 3(6), pp.430–434.

Chambers, L A & Trudinger, P.A., 1975. Are thiosulfate and trithionate intermediates in dissimilatory sulfate reduction? *Journal Of Bacteriology*, 123(1), pp.36–40.

Chambers, L A & Trudinger, P.A., 1979. Microbiological fractionation of stable sulfur isotopes: a review and critique. *Geomicrobiology Journal*, 1(3), pp.249–293.

Chambers, Lyn A et al., 1975. Fractionation of sulfur isotopes by continuous cultures of Desulfovibrio desulfuricans. *Canadian Journal Of Microbiology*, 21(10), pp.1602–1607.

Chisholm, S.W., Moore, L.R. & Rocap, G., 1998. Physiology and molecular phylogeny of coexisting : Prochlorococcus: ecotypes : Abstract : Nature. *Nature*, 393(6684), pp.464–467.

Cline, J.D., 1969. Spectrophotometric determination of hydrogen sulfide in natural waters. *Limnology And Oceanography*, 14, pp.454–458.

Coplen, T.B. et al., 2002. Isotope-abundance variations of selected elements (IUPAC Technical Report). *Pure and Applied Chemistry*, 74(10), pp.1987–2017.

Cort, J.R. et al., 2008. Allochromatium vinosum DsrC: Solution-State NMR Structure, Redox Properties, and Interaction with DsrEFH, a Protein Essential for Purple Sulfur Bacterial Sulfur Oxidation. *Journal of Molecular Biology*, 382(3), pp.692–707.

Czyzewski, B.K. & Wang, D.-N., 2012. Identification and characterization of a bacterial hydrosulphide ion channel. *Nature*, 483(7390), pp.494–497.

Dahl, C. et al., 2005. Novel Genes of the dsr Gene Cluster and Evidence for Close Interaction of Dsr Proteins during Sulfur Oxidation in the Phototrophic Sulfur Bacterium Allochromatium vinosum. *Journal Of Bacteriology*, 187(4), pp.1392–1404.

Dalsgaard, T. & Bak, F., 1994. Nitrate reduction in a sulfate-reducing bacterium, Desulfovibrio desulfuricans, isolated from rice paddy soil: sulfide inhibition, kinetics, and regulation. *Applied and Environmental Microbiology*, 60(1), pp.291–297.

David, L.A. & Alm, E.J., 2010. Rapid evolutionary innovation during an Archaean genetic expansion. *Nature*, 469(7328), pp.93–96.

Davidson, M.M. et al., 2009. Sulfur Isotope Enrichment during Maintenance Metabolism in the Thermophilic Sulfate-Reducing Bacterium Desulfotomaculum putei. *Applied and Environmental Microbiology*, 75(17), pp.5621–5630.

DE, C., 1991. Sulfate reduction in deep-sea sediments. *American Journal Of Science*, 291(2), pp.177–188.

Detmers, J. et al., 2001. Diversity of sulfur isotope fractionations by sulfate-reducing prokaryotes. *Applied and Environmental Microbiology*, 67(2), pp.888–894.

Drake, H.L. & Akagi, J.M., 1977. Characterization of a novel thiosulfate-forming enzyme isolated from Desulfovibrio vulgaris. *Journal Of Bacteriology*.

Drake, H.L. & Akagi, J.M., 1978. Dissimilatory reduction of bisulfite by Desulfovibrio vulgaris. *Journal Of Bacteriology*.

Drake, H.L. & Akagi, J.M., 1976. Product analysis of bisulfite reductase activity isolated from Desulfovibrio vulgaris. *Journal Of Bacteriology*.

Druhan, J.L. et al., 2014. A large column analog experiment of stable isotope variations during reactive transport: I.A comprehensive modelof sulfur cycling and d. *Geochimica Et Cosmochimica Acta*, 124(C), pp.366–393.

Eckert, T. et al., 2011. Microbially mediated re-oxidation of sulfide during dissimilatory sulfate reduction by Desulfobacter latus. *Geochimica Et Cosmochimica Acta*, 75(12), pp.3469–3485.

Einsiedl, F., 2009. Effect of NO 2−on Stable Isotope Fractionation during Bacterial Sulfate Reduction. *Environmental Science & Technology*, 43(1), pp.82–87.

Farquhar, G.D., O'leary, M.H. & Berry, J.A., 1982. On the relationship between carbon isotope discrimination and the intercellular carbon dioxide concentration in leaves. *Functional Plant Biology*, 9(2), pp.121–137.

Farquhar, J. & Wing, B.A., 2003. Multiple sulfur isotopes and the evolution of the atmosphere. *Earth And Planetary Science Letters*.

Farquhar, J. et al., 2010. Connections between Sulfur Cycle Evolution, Sulfur Isotopes, Sediments, and Base Metal Sulfide Deposits. *Economic Geology*, 105(3), pp.509–533.

Farquhar, J. et al., 2003. Multiple sulphur isotopic interpretations of biosynthetic pathways: implications for biological signatures in the sulphur isotope record. *Geobiology*, 1(1), pp.27–36.

Farquhar, J. et al., 2013. Pathways for Neoarchean pyrite formation constrained by mass-independent sulfur isotopes. *Proceedings of the ...* .

Farquhar, J. et al., 2008. Sulfur and oxygen isotope study of sulfate reduction in experiments with natural populations from Faellestrand, Denmark. *Geochimica Et Cosmochimica Acta*, 72(12), pp.2805–2821.

Farquhar, J., Bao, H. & Thiemens, M., 2000. Atmospheric influence of Earth's earliest sulfur cycle. *Science*, 289(5480), pp.756–758.

Farquhar, J., Johnston, D.T. & Wing, B.A., 2007a. Implications of conservation of mass effects on mass-dependent isotope fractionations: Influence of network structure on sulfur isotope phase space of dissimilatory sulfate reduction. *Geochimica Et Cosmochimica Acta*, 71(24), pp.5862–5875.

Farquhar, J., Peters, M., et al., 2007b. Isotopic evidence for Mesoarchaean anoxia and changing atmospheric sulphur chemistry. *Nature*, 449(7163), pp.706–709.

Findley, J.E. & Akagi, J.M., 1969. Evidence for thiosulfate formation during sulfite reduction by Desulfovibrio vulgaris. *Biochemical and Biophysical Research Communications*, 36(2), pp.266–271.

Findley, J.E. & Akagi, J.M., 1970. Role of thiosulfate in bisulfite reduction as catalyzed by Desulfovibrio vulgaris. *Journal Of Bacteriology*, 103(3), pp.741–744.

Fitz, R. & Cypionka, H., 1990. Formation of thiosulfate and trithionate during sulfite reduction by washed cells of Desulfovibrio desulfuricans. *Archives of Microbiology*, 154(4).

Ford, R.W., 1957. Sulphur isotope effects in chemical and biological processes. *PhD Thesis. McMaster University*.

Forrest, J. & Newman, L., 1977. Silver-110 microgram sulfate analysis for the short time resolution of ambient levels of sulfur aerosol. *Analytical Chemistry*, 49(11), pp.1579–1584.

Frigaard, N.-U. & Dahl, C., 2009. Sulfur Metabolism in Phototrophic Sulfur Bacteria. *Advances in Microbial Physiology, Vol 54*, 54, pp.103–200.

Fritz, G., 2002. Structure of adenylylsulfate reductase from the hyperthermophilic Archaeoglobus fulgidus at 1.6-A resolution. *Proceedings of the National Academy of Sciences*, 99(4), pp.1836–1841.

FRY, B., GEST, H. & Hayes, J., 1985. Isotope Effects Associated with the Anaerobic Oxidation of Sulfite and

Thiosulfate by the Photosynthetic Bacterium, Chromatium-Vinosum. *FEMS Microbiology Letters*, 27(2), pp.227–232.

Fujii, T. & Albarède, F., 2012. Ab Initio Calculation of the Zn Isotope Effect in Phosphates, Citrates, and Malates and Applications to Plants and Soil. *Plos One*, 7(2), p.e30726.

Fujii, T. et al., 2011. Theoretical and experimental investigation of nickel isotopic fractionation in species relevant to modern and ancient oceans. *Geochimica Et Cosmochimica Acta*, 75(2), pp.469–482.

Fukui, M. & Takii, S., 1994. Kinetics of sulfate respiration by free-living and particle-associated sulfate-reducing bacteria. *FEMS Microbiology Ecology*, 13(4), pp.241–247.

Furusaka, C., 1961. Sulphate Transport and Metabolism Desulphovibrio Desulphuricans. *Nature*, 192, pp.427–429.

Galen E Jones, R.L.S., 1957. Fractionation of Stable Isotopes of Sulfur by Microorganisms and Their Role in Deposition of Native Sulfur. *Applied Microbiology*, 5(2), p.111.

GARRELS, R. & LERMAN, A., 1981. PHANEROZOIC CYCLES OF SEDIMENTARY CARBON AND SULFUR. *Proceedings Of The National Academy Of Sciences Of The United States Of America*, 78(8), pp.4652–4656.

Gest, B.F.H. & Hayes, J.M., 1984. Isotope effects associated with the anaerobic oxidation of sulfide by the purple photosynthetic bacterium, Chromatium vinosum. *FEMS Microbiology Letters*, 22(3), pp.283–287.

Goldhaber, M.B. & Kaplan, I.R., 1975. Controls and consequences of sulfate reduction rates in recent marine sediments. *Soil Science*, 119(1), pp.42–55.

Goldhaber, M.B. et al., 1977. Sulfate reduction, diffusion, and bioturbation in Long Island Sound sediments; report of the FOAM Group. *American Journal Of Science*, 277(3), pp.193–237.

Gomes, M.L. & Hurtgen, M.T., 2013. Sulfur isotope systematics of a euxinic, low-sulfate lake: Evaluating the importance of the reservoir effect in modern and ancient oceans. *Geology*, 41(6), pp.663–666.

Grant, W.M., 1947. Colorimetric determination of sulfur dioxide. *Analytical Chemistry*, 19(5), pp.345–346.

Gregory, J.D. & Robbins, P.W., 1960. Metabolism of sulfur compounds (sulfate metabolism). *Annual review of biochemistry*, 29(1), pp.347–364.

Grein, F. et al., 2010. DsrJ, an essential part of the DsrMKJOP transmembrane complex in the purple sulfur bacterium Allochromatium vinosum, is an unusual triheme cytochrome c. *Biochemistry*, 49(38), pp.8290–8299.

Guo, W., 2013. personal communication W. Guo, ed.

Guo, W., Granger, J. & Sigman, D.M., 2010. Nitrate isotope fractionations during biological nitrate reduction: Insights from first principles theoretical modeling. *AGU Fall Meeting Abstracts*, -1, p.08.

Guy, R.D., Fogel, M.L. & Berry, J.A., 1993. Photosynthetic fractionation of the stable isotopes of oxygen and carbon. *Plant Physiology*, 101(1), pp.37–47.

H D Peck, J., 1962. Comparative metabolism of inorganic sulfur compounds in microorganisms. *Bacteriological reviews*, 26(1), p.67.

Habicht, K. & Canfield, D.E., 1997. Sulfur isotope fractionation during bacterial sulfate reduction in organic-rich sediments. *Geochimica Et Cosmochimica Acta*.

Habicht, K. et al., 2002. Calibration of sulfate levels in the Archean Ocean. *Science*, 298(5602), pp.2372–2374.

Habicht, K., Canfield, D.E. & Rethmeier, J., 1998. Sulfur isotope fractionation during bacterial reduction and disproportionation of thiosulfate and …. *Geochimica Et Cosmochimica Acta*.

Habicht, K.S. et al., 2005. Effect of Low Sulfate Concentrations on Lactate Oxidation and Isotope Fractionation during Sulfate Reduction by Archaeoglobus fulgidus Strain Z. *Applied and Environmental Microbiology*, 71(7), pp.3770–3777.

Halevy, I., 2013. Production, preservation, and biological processing of mass-independent sulfur isotope fractionation in the Archean surface environment. *Proceedings of the National Academy of Sciences*.

HALEVY, I., Peters, S.E. & Fischer, W.W., 2012. Sulfate Burial Constraints on the Phanerozoic Sulfur Cycle. *Science*, 337(6092), pp.331–334.

Hannisdal, B. & Peters, S.E., 2011. Phanerozoic Earth System Evolution and Marine Biodiversity. *Science*, 334(6059), pp.1121–1124.

Hansen, T.A., 1994. Metabolism of sulfate-reducing prokaryotes. *Antonie van Leeuwenhoek*, 66(1-3), pp.165–185.

Harrison, A.G. & Thode, H.G., 1958. Mechanism of the bacterial reduction of sulphate from isotope fractionation studies. *Transactions of the Faraday Society*, 54, pp.84–92.

Harrison, A.G. & Thode, H.G., 1957. The kinetic isotope effect in the chemical reduction of sulphate. *Transactions of the Faraday Society*, 53, pp.1648–1651.

Harry D Peck, J., 1960. Adenosine 5′-Phosphosulphate as an intermediate in the oxidation of thiosulfate by Thiobacillus thioparus. *Proceedings Of The National Academy Of Sciences Of The United States Of America*, 46(8), p.1053.

Hartnett, H.E. et al., 1998. Influence of oxygen exposure time on organic carbon preservation in continental margin sediments : Abstract : Nature. *Nature*, 391(6667), pp.572–575.

Haschke, R.H. & Campbell, L.L., 1971. Thiosulfate reductase of Desulfovibrio vulgaris. *Journal Of Bacteriology*, 106(2), pp.603–607.

Hatchikian, E.C., 1975. Purification and properties of thiosulfate reductase from Desulfovibrio gigas. *Archives of Microbiology*, 105(1), pp.249–256.

Hauser, L.J. et al., 2011. Complete Genome Sequence and Updated Annotation of Desulfovibrio alaskensis G20. *Journal of …*.

Hayes, J.M., 1993. Factors controlling 13 C contents of sedimentary organic compounds: Principles and evidence.

Marine Geology, 113(1), pp.111–125.

Hayes, J.M., 2001. Fractionation of carbon and hydrogen isotopes in biosynthetic processes. *Reviews in Mineralogy and Geochemistry*, 43(1), pp.225–277.

Hayes, J.M. & Waldbauer, J.R., 2006. The carbon cycle and associated redox processes through time. *Philosophical Transactions of the Royal Society B: Biological Sciences*, 361(1470), pp.931–950.

Hayes, J.M., STRAUSS, H. & Kaufman, A.J., 1999. The abundance of 13C in marine organic matter and isotopic fractionation in the global biogeochemical cycle of carbon during the past 800 Ma. *Chemical Geology*.

Heidelberg, J.F. et al., 2004. The genome sequence of the anaerobic, sulfate-reducing bacterium Desulfovibrio vulgaris Hildenborough. *Nature Biotechnology*, 22(5), pp.554–559.

Helmuth Hilz, F.L., 1955. The enzymatic activation of sulfate. *Proceedings Of The National Academy Of Sciences Of The United States Of America*, 41(11), p.880.

Herbert, D., Elsworth, R. & Telling, R.C., 1956. The Continuous Culture of Bacteria; a Theoretical and Experimental Study. *Microbiology*, 14(3), pp.601–622.

Heunisch, G.W., 1977. Stoichiometry of the reaction of sulfites with hydrogen sulfide ion. *Inorganic Chemistry*, 16(6), pp.1411–1413.

Higgins, M.B. et al., 2012. Dominant eukaryotic export production during ocean anoxic events reflects the importance of recycled NH4. *Proceedings of the National Academy of Sciences*, 109(7), pp.2269–2274.

HOEK, J. et al., 2006. Effect of hydrogen limitation and temperature on the fractionation of sulfur isotopes by a deep-sea hydrothermal vent sulfate-reducing bacterium. *Geochimica Et Cosmochimica Acta*, 70(23), pp.5831–5841.

Holland, H.D., 1973. Systematics of the isotopic composition of sulfur in the oceans during the Phanerozoic and its implications for atmospheric oxygen. *Geochimica Et Cosmochimica Acta*, 37(12), pp.2605–2616.

Holland, H.D., 2006. The oxygenation of the atmosphere and oceans. *Philosophical Transactions of the Royal Society B: Biological Sciences*, 361(1470), pp.903–915.

Holland, H.D., 2009. Why the atmosphere became oxygenated: a proposal. *Geochimica Et Cosmochimica Acta*, 73(18), pp.5241–5255.

Holmer, M. & Storkholm, P., 2001. Sulphate reduction and sulphur cycling in lake sediments: a review. *Freshwater Biology*, 46(4), pp.431–451.

Horita, J., Zimmermann, H. & Holland, H.D., 2002. Chemical evolution of seawater during the Phanerozoic:: Implications from the record of marine evaporites. *Geochimica Et Cosmochimica Acta*, 66(21), pp.3733–3756.

Ingvorsen, K., Zehnder, A.J.B. & Jørgensen, B.B., 1984. Kinetics of Sulfate and Acetate Uptake by Desulfobacter postgatei. *Applied and ...* .

Ishimoto, M., KOYAMA, J. & NAGAI, Y., 1955. Biochemical studies of sulfate reducing bacteria IV. Reduction of

thiosulfate by cell-free extract. *Journal of biochemistry*, 42(1), pp.41–53.

Jin, Q., Roden, E.E. & Giska, J.R., 2013. Geomicrobial Kinetics: Extrapolating Laboratory Studies to Natural Environments. *Geomicrobiology Journal*, 30(2), pp.173–185.

Jin-Po Lee, C.-S.Y.J.L.H.D.P.J., 1973. Isolation of a New Pigment, Desulforubidin, from Desulfovibrio desulfuricans (Norway Strain) and Its Role in Sulfite Reduction. *Journal Of Bacteriology*, 115(1), p.453.

Johnson, E.F., 2005. A New Type of Sulfite Reductase, a Novel Coenzyme F420-dependent Enzyme, from the Methanarchaeon Methanocaldococcus jannaschii. *The Journal of biological chemistry*, 280(46), pp.38776–38786.

Johnston, D.T., 2005. Multiple sulfur isotope fractionations in biological systems: A case study with sulfate reducers and sulfur disproportionators. *American Journal Of Science*, 305(6-8), pp.645–660.

Johnston, D.T., 2011. Multiple sulfur isotopes and the evolution of Earth's surface sulfur cycle. *Earth Science Reviews*, pp.1–23.

Johnston, D.T., 2010. Touring the Biogeochemical Landscape of a Sulfur-Fueled World. *Elements*, 6(2), pp.101–106.

Johnston, D.T. et al., 2005. Active microbial sulfur disproportionation in the Mesoproterozoic. *Science*, 310(5753), pp.1477–1479.

Johnston, D.T., Farquhar, J. & Canfield, D.E., 2007. Sulfur isotope insights into microbial sulfate reduction: When microbes meet models. *Geochimica Et Cosmochimica Acta*, 71(16), pp.3929–3947.

Jones, D.S. & Fike, D.A., 2013. Dynamic sulfur and carbon cycling through the end-Ordovician extinction revealed by paired sulfate–pyrite δ34S. *Earth And Planetary Science Letters*, 363(C), pp.144–155.

Jones, H.E. & Skyring, G.W., 1974. Reduction of Sulphite to Sulphide Catalysed by Desulfoviridin From Desulfovibrio gigas. *Australian Journal of Biological Sciences*, 27(1), pp.7–14.

Jones, H.E. & Skyring, G.W., 1975. Effect of enzymic assay conditions on sulfite reduction catalysed by desulfoviridin from Desulfovibrio gigas. *Biochimica et Biophysica Acta (BBA)-Enzymology*, 377(1), pp.52–60.

JORGENSEN, B., 1982. Mineralization of organic matterin the sea bed - the role of sulfate reduction. *Nature*, 296(5858), pp.643–645.

Jorgensen, B.B., 1979. A theoretical model of the stable sulfur isotope distribution in marine sediments. *Geochimica Et Cosmochimica Acta*, 43(3), pp.363–374.

Jorgensen, B.B., 1990. A thiosulfate shunt in the sulfur cycle of marine sediments. *Science*, 249(4965), pp.152–154.

Jormakka, M. et al., 2002. Molecular basis of proton motive force generation: Structure of formate dehydrogenase-N. *Science*, 295(5561), pp.1863–1868.

Jørgensen, B.B., 1978. Comparison of methods for the quantification of bacterial sulfate reduction in coastal

marine-sediments. 2. Calculation from mathematical-models. *Geomicrobiology Journal*, 1(1), pp.29–47.

Kaplan, I.R., 1975. Stable isotopes as a guide to biogeochemical processes. *Proceedings of the Royal Society of London. Series B. Biological Sciences*, 189(1095), pp.183–211.

Kaplan, I.R. & Rittenberg, S.C., 1964. Microbiological fractionation of sulphur isotopes. *Journal of General Microbiology*, 34(2), pp.195–212.

Kaplan, I.R., Emery, K.O. & Rittenbebg, S.C., 1963. The distribution and isotopic abundance of sulphur in recent marine sediments off southern California. *Geochimica Et Cosmochimica Acta*, 27(4), pp.297–331.

KARKHOFF-SCHWEIZER, R.R., BRUSCHI, M. & Voordouw, G., 1993. Expression of the gamma-subunit gene of desulfoviridin-type dissimilatory sulfite reductase and of the alpha- and beta-subunit genes is not coordinately regulated. *European Journal of Biochemistry*, 211(3), pp.501–507.

Karsh, K.L. et al., 2013. Accepted Manuscript. *Geochimica Et Cosmochimica Acta*, pp.1–71.

Karsh, K.L. et al., 2012. Eukaryotic Assimilatory Nitrate Reductase Fractionates N and O Isotopes with a Ratio near Unity. *Environmental Science & Technology*, 46(11), pp.5727–5735.

Keller, K.L. & Wall, J.D., 2011. Genetics and Molecular Biology of the Electron Flow for Sulfate Respiration in Desulfovibrio. *Frontiers in Microbiology*, 2.

Keller, K.L., Wall, J.D. & Chhabra, S., 2011. *Methods for Engineering Sulfate Reducing Bacteria of the Genus Desulfovibrio* 1st ed., Elsevier Inc.

Kelly, Don P & Wood, A.P., 1994. [35] Synthesis and determination of thiosulfate and polythionates. *Methods in enzymology*, 243, pp.475–501.

Kelly, Donovan P, Chambers, L.A. & Trudinger, P.A., 1969. Cyanolysis and spectrophotometric estimation of trithionate in mixture with thiosulfate and tetrathionate. *Analytical Chemistry*, 41(7), pp.898–901.

Kemp, A. & THODE, H., 1968. The mechanism of the bacterial reduction of sulphate and of sulphite from isotope fractionation studies. *Geochimica Et Cosmochimica Acta*, 32(1), pp.71–91.

Kim, J.H. & Akagi, J.M., 1985. Characterization of a trithionate reductase system from Desulfovibrio vulgaris. *Journal Of Bacteriology*, 163(2), pp.472–475.

Kiryushov, V.N. & Skvortsova, L.I., 2010. Advantages of masking sulfite ions with dilute formaldehyde solutions in the iodometric analysis of sulfur-containing mixtures. *Journal of Analytical Chemistry*, 65(3), pp.305–307.

Kleikemper, J. et al., 2004. Sulfur isotope fractionation during growth of sulfate-reducing bacteria on various carbon sources. *Geochimica Et Cosmochimica Acta*, 68(23), pp.4891–4904.

Knöller, K. et al., 2006. Sulfur and Oxygen Isotope Fractionation during Benzene, Toluene, Ethyl Benzene, and Xylene Degradation by Sulfate-Reducing Bacteria. *Environmental Science & Technology*, 40(12), pp.3879–3885.

Kobayashi, K., Tachibana, S. & Ishimoto, M., 1969. Intermediary formation of trithionate in sulfite reduction by a

sulfate-reducing bacterium. *Journal of biochemistry*, 65(1), pp.155–157.

Kobayashi, K., TAKAHASHI, E. & Ishimoto, M., 1972. Biochemical studies on sulfate-reducing bacteria XI. Purification and some properties of sulfite reductase, desulfoviridin. *Journal of biochemistry*, 72(4), pp.879–887.

Kobayashi, K., Yasuhide, S. & Ishimoto, M., 1974. Biochemical Studies on Sulfate-reducing Bacteria XIII. Sulfite Reductase fromDesulfovibrio vulgaris-Mechanism of Trithionafe, Thiosulfate, and Sulfide Formation and Enzymatic Properties. *Journal of biochemistry*, 75(3), pp.519–529.

Kohen, A. & Limbach, H.H., 2005. Isotope Effects In Chemistry and Biology - Google Books.

Kohl, I.E., Asatryan, R. & Bao, H., 2012. No oxygen isotope exchange between water and APS–sulfate at surface temperature: Evidence from quantumchemical modeling and triple-oxygen isotope experiments. *Geochimica Et Cosmochimica Acta*, 95(C), pp.106–118.

Krouse, H.R. et al., 1968. Sulfur Isotope Fractionation and Kinetic Studies of Sulfite Reduction in Growing Cells of Salmonella heidelberg. *Biophysical Journal*, 8(1), pp.109–124.

Kump, L.R., 2008. The rise of atmospheric oxygen. *Nature*, 451(7176), pp.277–278.

LaRowe, D.E. & Van Cappellen, P., 2011. Degradation of natural organic matter: A thermodynamic analysis. *Geochimica Et Cosmochimica Acta*, 75(8), pp.2030–2042.

Laws, E.A. et al., 1995. Dependence of phytoplankton carbon isotopic composition on growth rate and [CO 2) aq: Theoretical considerations and experimental results. *Geochimica Et Cosmochimica Acta*, 59(6), pp.1131–1138.

Le Gall, J. et al., 1994. Localization and specificity of cytochromes and other electron transfer proteins from sulfate-reducing bacteria. *Biochimie*, 76(7), pp.655–665.

Leavitt, W.D. et al., 2013. Influence of sulfate reduction rates on the Phanerozoic sulfur isotope record. *Proceedings Of The National Academy Of Sciences Of The United States Of America*, 110(28), pp.11244–11249.

Leavitt, W.D. et al., Influence of sulfate reduction rates on the Phanerozoic sulfur isotope record M. H. Thiemens, ed. *Proceedings of the National Academy of Sciences*.

Lee, J.P. & Peck, H.D., 1971. Purification of the enzyme reducing bisulfite to trithionate from Desulfovibrio gigas and its identification as desulfoviridin. *Biochemical and Biophysical Research Communications*, 45(3), pp.583–589.

Li, M.Z. & Elledge, S.J., 2007. Harnessing homologous recombination in vitro to generate recombinant DNA via SLIC. *Nature Methods*, 4(3), pp.251–256.

LUI, S.M., Soriano, A. & Cowan, J.A., 1993. Enzymic reduction of inorganic anions. Pre-steady-state kinetic analysis of the dissimilatory sulfite reductase (desulfoviridin) from Desulfovibrio vulgaris (Hildenborough). Mechanistic implications. *Journal of the American Chemical Society*, 115(23), pp.10483–10486.

Lyons, T.W. & Gill, B.C., 2010. Ancient Sulfur Cycling and Oxygenation of the Early Biosphere. *Elements*, 6(2),

pp.93–99.

Lyons, T.W., Reinhard, C.T. & Planavsky, N.J., 2014. The rise of oxygen in Earth's earlyocean and atmosphere. *Nature*, 506(7488), pp.307–315.

Maggi, F. & Riley, W.J., 2010. Mathematical treatment of isotopologue and isotopomer speciation and fractionation in biochemical kinetics. *Geochimica Et Cosmochimica Acta*, 74(6), pp.1823–1835.

Maggi, F. & Riley, W.J., 2009. Transient competitive complexation in biological kinetic isotope fractionation explains nonsteady isotopic effects: Theory and application to denitrification in soils. *Journal of Geophysical Research*, 114(G4), p.G04012.

MANGALO, M. et al., 2007. Stable isotope fractionation during bacterial sulfate reduction is controlled by reoxidation of intermediates. *Geochimica Et Cosmochimica Acta*, 71(17), pp.4161–4171.

Mangalo, M. et al., 2008. Influence of the enzyme dissimilatory sulfite reductase on stable isotope fractionation during sulfate reduction. *Geochimica Et Cosmochimica Acta*, 72(6), pp.1513–1520.

Mariotti, A. et al., 1981. Experimental determination of nitrogen kinetic isotope fractionation: Some principles; illustration for the denitrification and nitrification processes. *Plant and Soil*, 62(3), pp.413–430.

Marritt, S.J. & Hagen, W.R., 1996. Dissimilatory Sulfite Reductase Revisited. The Desulfoviridin Molecule does Contain 20 Iron Ions, Extensively Demetallated Sirohaem, and an S= 9/2 Iron-Sulfur Cluster. *European Journal of Biochemistry*, 238(3), pp.724–727.

Martinez-Ruiz, F. & Eagle, M., 2004. Using sulfur isotopes to elucidate the origin ofbarite associated with high organic matter accumulation events in marine sediments. *Sulfur Biogeochemistry: Past And Present*, 379, p.151.

Masterson, A.L., Farquhar, J. & Wing, B.A., 2011. Sulfur mass-independent fractionation patterns in the broadband UV photolysis of sulfur dioxide: Pressure and third body effects. *Earth And Planetary Science Letters*, 306, pp.253–260.

MCCREADY, R., 1975. SULFUR ISOTOPE FRACTIONATION BY DESULFOVIBRIO AND DESULFOTOMACULUM SPECIES. *Geochimica Et Cosmochimica Acta*, 39(10), pp.1395–1401.

MCCREADY, R., LAISHLEY, E. & KROUSE, H., 1975. STABLE ISOTOPE FRACTIONATION BY CLOSTRIDIUM-PASTEURIANUM .1. S-34/S-32 - INVERSE ISOTOPE-EFFECTS DURING SO42- AND SO32- REDUCTION. *Canadian Journal Of Microbiology*, 21(3), pp.235–244.

McNaught, A.D. & Wilkinson, A., 1997. International Union of Pure and Applied Chemistry.

Michaels, G.B., Davidson, J.T. & Peck, H.D., Jr., 1970. A flavin-sulfite adduct as an intermediate in the reaction catalyzed by adenylyl sulfate reductase from. *Biochemical and Biophysical Research Communications*, 39(3), pp.321–328.

Middelburg, J.J., 1989. A simple rate model for organic matter decomposition in marine sediments. *Geochimica Et Cosmochimica Acta*, 53(7), pp.1577–1581.

Miller, M.F., 2002. Isotopic fractionation and the quantification of 17 O anomalies in the oxygen three-isotope

system: an appraisal and geochemical significance. *Geochimica Et Cosmochimica Acta*, 66(11), pp.1881–1889.

Monod, J., 1950. La Technique de Culture Continue Theorie et Applications. *Annales de L Institue Pasteur*, p.390.

Monod, J., 1949. The growth of bacterial cultures. *Annual Reviews in Microbiology*, 3(1), pp.371–394.

Motulsky, H.J. & Ransnas, L.A., 1987. Fitting curves to data using nonlinear regression: a practical and nonmathematical review. *The FASEB journal*, 1(5), pp.365–374.

Müller, I.A. et al., 2013. Accepted Manuscript. *Geochimica Et Cosmochimica Acta*, pp.1–57.

Myers, C. & Nealson, K., 1988. Bacterial manganese reduction and growth with manganese oxide as the sole electron acceptor. *Science*, 240(4857), pp.1319–1321.

Nakagawa, M. et al., 2012. Seasonal change in microbial sulfur cycling in monomictic Lake Fukami-ike, Japan. *Limnology And Oceanography*, 57(4), pp.974–988.

Nakai, N. & Jensen, M.L., 1964. The kinetic isotope effect in the bacterial reduction and oxidation of sulfur. *Geochimica Et Cosmochimica Acta*, 28(12), pp.1893–1912.

Newton, G.L. & Fahey, R.C., 1995. *Methods in Enzymology*, Elsevier.

Newton, G.L., Dorian, R. & Fahey, R.C., 1981. Analysis of biological thiols: derivatization with monobromobimane and separation by reverse-phase high-performance liquid chromatography. *Analytical Biochemistry*, 114(2), pp.383–387.

Nikaido, H. & Saier, M.H., 1992. Transport proteins in bacteria: common themes in their design. *Science*, 258(5084), pp.936–942.

Ohmoto, H. & Lasaga, A.C., 1982. Kinetics of reactions between aqueous sulfates and sulfides in hydrothermal systems. *Geochimica Et Cosmochimica Acta*, 46(10), pp.1727–1745.

Okabe, S., Nielsen, P.H. & Characklis, W.G., 2004. Factors affecting microbial sulfate reduction by Desulfovibrio desulfuricansin continuous culture: Limiting nutrients and sulfide concentration. *Biotechnology and Bioengineering*, 40(6), pp.725–734.

Oliveira, T.F., Vonrhein, C., Matias, P.M., Venceslau, S.S., Pereira, I.A.C., et al., 2008a. Purification, crystallization and preliminary crystallographic analysis of a dissimilatory DsrAB sulfite reductase in complex with DsrC. *Journal Of Structural Biology*, 164(2), pp.236–239.

Oliveira, T.F., Vonrhein, C., Matias, P.M., Venceslau, S.S., Pereira, P.M., et al., 2008b. The crystal structure of Desulfovibrio vulgaris dissimilatory sulfite reductase bound to DsrC provides novel insights into the mechanism of sulfate respiration. *The Journal of biological chemistry*, 283(49), pp.34141–34149.

Pallud, C. & Van Cappellen, P., 2006. Kinetics of microbial sulfate reduction in estuarine sediments. *Geochimica Et Cosmochimica Acta*, 70(5), pp.1148–1162.

Pallud, C. et al., 2007. ScienceDirect.com - Marine Chemistry - The use of flow-through sediment reactors in

biogeochemical kinetics: Methodology and examples of applications. *Marine Chemistry*.

Parey, K. et al., 2010. Reaction cycle of the dissimilatory sulfite reductase from Archaeoglobus fulgidus. *Biochemistry*, 49(41), pp.8912–8921.

Paris, G. et al., 2013. Chemical Geology. *Chemical Geology*, 345(C), pp.50–61.

Park, R. & Epstein, S., 1960. Carbon isotope fractionation during photosynthesis. *Geochimica Et Cosmochimica Acta*, 21(1), pp.110–126.

Peck, H.D., 1961. Enzymatic basis for assimilatory and dissimilatory sulfate reduction. *Journal Of Bacteriology*, 82(6), pp.933–939.

Peck, H.D., 1962. The role of adenosine-5'-phosphosulfate in the reduction of sulfate to sulfite by Desulfovibrio desulfuricans. *The Journal of biological chemistry*, 237(1), pp.198–203.

Peck, H.D., Beeumen, J.V. & LeGall, J., 1982. Biochemistry of Dissimilatory Sulphate Reduction [and Discussion]. *Philosophical Transactions of the Royal Society B: Biological Sciences*, 298(1093), pp.443–466.

Peck, H.D., Jr, 1959. The ATP-dependent reduction of sulfate with hydrogen in extracts of Desulfovibrio desulfuricans. *Proceedings Of The National Academy Of Sciences Of The United States Of America*, 45(5), p.701.

Pereira, I.A.C. et al., 2011. A comparative genomic analysis of energy metabolism in sulfate reducing bacteria and archaea. *Frontiers in Microbiology*, 2.

PFLUGRATH, J. & QUIOCHO, F., 1988. The 2-a Resolution Structure of the Sulfate-Binding Protein Involved in Active-Transport in Salmonella-Typhimurium. *Journal of Molecular Biology*, 200(1), pp.163–180.

Philippot, P. et al., 2007. Early Archaean microorganisms preferred elemental sulfur, not sulfate. *Science*, 317(5844), pp.1534–1537.

PIERIK, A.J. et al., 1992. The third subunit of desulfoviridin-type dissimilatory sulfite reductases. *European Journal of Biochemistry*, 205(1), pp.111–115.

Pires, R. et al., 2003. A novel membrane-bound respiratory complex from Desulfovibrio desulfuricans ATCC 27774. *Biochimica Et Biophysica Acta-Bioenergetics*, 1605(1-3), pp.67–82.

Pires, R.H. et al., 2006. Characterization of the Desulfovibrio desulfuricansATCC 27774 DsrMKJOP ComplexA Membrane-Bound Redox Complex Involved in the Sulfate Respiratory Pathway. *Biochemistry*, 45(1), pp.249–262.

Piłsyk, S. & Paszewski, A., 2009. Sulfate permeases — phylogenetic diversity of sulfate transport. *Acta Biocimica Polonica*, 56(3), pp.375–384. Available at: http://www.actabp.pl/pdf/3_2009/375.pdf.

Pott, A.S. & Dahl, C., 1998. Sirohaem sulfite reductase and other proteins encoded by genes at the dsr locus of Chromatium vinosum are involved in the oxidation of intracellular sulfur. *Microbiology*, 144(7), pp.1881–1894.

Poulton, S.W. & Canfield, D.E., 2011. Ferruginous Conditions: A Dominant Feature of the Ocean through Earth's History. *Elements*, 7(2), pp.107–112.

Prokoph, A., Shields, G.A. & Veizer, J., 2008. Compilation and time-series analysis of a marine carbonate δ18O, δ13C, 87Sr/86Sr and δ34S database through Earth history. *Earth Science Reviews*, 87(3-4), pp.113–133.

Rabus, R., Hansen, T.A. & Widdel, F., 2006. *Dissimilatory Sulfate- and Sulfur-Reducing Prokaryotes* M. Dworkin et al., eds., New York, NY: Springer New York.

Raiswell, R., 2011. Iron Transport from the Continents to the Open Ocean: The Aging-Rejuvenation Cycle. *Elements*, 7(2), pp.101–106.

Rees, C., 1973. A steady-state model for sulphur isotope fractionation in bacterial reduction processes. *Geochimica Et Cosmochimica Acta*, 37(5), pp.1141–1162.

Robbins, P.W. & Lipmann, F., 1958. Enzymatic synthesis of adenosine-5'-phosphosulfate. *The Journal of biological chemistry*, 233(3), pp.686–690.

Robbins, P.W. & Lipmann, F., 1956. The Enzymatic Sequence in the Biosynthesis of Active Sulfate. *Journal of the American Chemical Society*, 78(24), pp.6409–6410.

Roeske, C.A. & O'Leary, M.H., 1984. Carbon isotope effects on enzyme-catalyzed carboxylation of ribulose bisphosphate. *Biochemistry*, 23(25), pp.6275–6284.

Romão, C.V. et al., 1997. Characterization of the [NiFe] Hydrogenase from the Sulfate ReducerDesulfovibrio vulgarisHildenborough. *Biochemical and Biophysical Research Communications*, 240(1), pp.75–79.

Roychoudhury, A.N. & Porter, D., 2013. Dissimilatory Sulfate Reduction in Hypersaline Environments: What is regulating sulfate uptake? *Mineralogical Magazine*, 77(5), pp.2015–2107.

Saito, M.A., Goepfert, T.J. & Ritt, J.T., 2008. Some thoughts on the concept of colimitation: Three definitions and the importance of bioavailability. *Limnology And Oceanography*, 53(1), p.276.

Santoro, A.E. et al., 2011. Isotopic Signature of N2O Produced by Marine Ammonia-Oxidizing Archaea. *Science*, 333(6047), pp.1282–1285.

Sass, H. et al., 1992. Formation of thionates by freshwater and marine strains of sulfate-reducing bacteria. *Archives of Microbiology*, 158(6), pp.418–421.

Schiffer, A. et al., 2008. Structure of the Dissimilatory Sulfite Reductase from the Hyperthermophilic Archaeon Archaeoglobus fulgidus. *Journal of Molecular Biology*, 379(5), pp.1063–1074.

Scott, K.M. et al., 2004. Influence of form IA RubisCO and environmental dissolved inorganic carbon on the delta13C of the clam-chemoautotroph symbiosis Solemya velum. *Environmental Microbiology*, 6(12), pp.1210–1219.

Shen, Y., Buick, R. & Canfield, D.E., 2001. Isotopic evidence for microbial sulphate reduction in the early Archaean era. *Nature*, 410(6824), pp.77–81.

Shirodkar, S. et al., 2010. The octahaem SirA catalyses dissimilatory sulfite reduction in Shewanella oneidensis

MR-1. *Environmental Microbiology*, 13(1), pp.108–115.

Sim, M.S. et al., 2013. Fractionation of sulfur isotopes by Desulfovibrio vulgaris mutants lacking hydrogenases or type I tetraheme cytochrome c3. *... in Microbiology*, pp.1–10.

Sim, M.S., Bosak, T. & Ono, S., 2011a. Large Sulfur Isotope Fractionation Does Not Require Disproportionation. *Science*, 333(6038), pp.74–77.

Sim, M.S., Bosak, T. & Ono, S., 2011b. Large Sulfur Isotope Fractionation Does Not Require Disproportionation. *Science*, 333(6038), pp.74–77. Available at: http://link.springer.com/article/10.1007%2FBF01820726.

Sim, M.S., Ono, S. & Bosak, T., 2012. Effects of Iron and Nitrogen Limitation on Sulfur Isotope Fractionation during Microbial Sulfate Reduction. *Applied and Environmental Microbiology*, 78(23), pp.8368–8376.

Sim, M.S., Ono, S., et al., 2011c. Effect of electron donors on the fractionation of sulfur isotopes by a marine Desulfovibrio sp. *Geochimica Et Cosmochimica Acta*, pp.1–16.

Siu, T. & Jia, C.Q., 1999. Kinetic and Mechanistic Study of Reaction between Sulfide and Sulfite in Aqueous Solution. *Industrial & Engineering Chemistry Research*, 38(10), pp.3812–3816.

Smith, H.L., 1995. The Theory of the Chemostat: Dynamics of Microbial Competition.

Smock, A., Bottcher, M. & Cypionka, H., 1998. Fractionation of sulfur isotopes during thiosulfate reduction by Desulfovibrio desulfuricans. *Archives of Microbiology*, 169(5), pp.460–463.

Soriano, A. & Cowan, J.A., 1995. Sulfite Reductase: Active Site Residues are "Noncatalytic." Comparison of Reaction Energetics for Enzyme- and Siroheme-Catalyzed Reduction of Inorganic Substrates. *Journal of the American Chemical Society*, 117(16), pp.4724–4725.

Sousa, F.L. et al., 2013. Early bioenergetic evolution. *Philosophical Transactions of the Royal Society B: Biological Sciences*, 368(1622), pp.20130088–20130088.

Sörbo, B.O., 1957. A colorimetric method for the determination of thiosulfate. *Biochimica et Biophysica acta*, 23, pp.412–416.

Sperling, E.A. et al., 2013. Oxygen, ecology, and the Cambrian radiation of animals. *Proceedings of the National Academy of Sciences*, 110(33), pp.13446–13451.

Stam, M.C. et al., 2011. 34S/32S fractionation by sulfate-reducing microbial communities in estuarine sediments. *Geochimica Et Cosmochimica Acta*, 75(14), pp.3903–3914. Available at: http://www.sciencedirect.com/science/article/pii/S0016703711002511.

Stam, M.C. et al., 2010. Sulfate reducing activity and sulfur isotope fractionation by natural microbial communities in sediments of a hypersaline soda lake (Mono Lake, California). *Chemical Geology*, 278(1-2), pp.23–30.

Strauss, H., 1997. The isotopic composition of sedimentary sulfur through time. *Palaeogeography, Palaeoclimatology, Palaeoecology*, 132(1), pp.97–118.

Stumm, W. & Morgan, J.J., 2012. Aquatic Chemistry: Chemical Equilibria and Rates in Natural Waters - Werner

Stumm, James J. Morgan - Google Books.

Suh, B. & Akagi, J.M., 1969. Formation of Thiosulfate from Sulfite by Desulfovibrio vulgaris. *Journal Of Bacteriology*.

Susanti, D. et al., 2014. Thioredoxin targets fundamental processes in a methane-producing archaeon, Methanocaldococcus jannaschii. *Proceedings Of The National Academy Of Sciences Of The United States Of America*, 111(7), pp.2608–2613.

Szabo, A. et al., 1950. The distribution of S34 in nature and the sulfur cycle. *Science*, 111(2887), pp.464–465.

Tarpgaard, I.H., Røy, H. & Jorgensen, B.B., 2011. Concurrent low- and high-affinity sulfate reduction kinetics in marine sediment. *Geochimica Et Cosmochimica Acta*, 75(11), pp.2997–3010.

Tcherkez, G.G.B., Farquhar, G.D. & Andrews, T.J., 2006. Despite slow catalysis and confused substrate specificity, all ribulose bisphosphate carboxylases may be nearly perfectly optimized. *Proceedings Of The National Academy Of Sciences Of The United States Of America*, 103(19), pp.7246–7251.

Thamdrup, B. et al., 1993. Bacterial Disproportionation of Elemental Sulfur Coupled to Chemical Reduction of Iron or Manganese. *Applied and Environmental Microbiology*.

Thauer, R. et al., 2008. Methanogenic archaea: ecologically relevant differences in energy conservation. *Nature Reviews Microbiology*, 6(8), p.579.

Thauer, R.K., Jungermann, K. & Decker, K., 1977. Energy conservation in chemotrophic anaerobic bacteria. *Bacteriological reviews*, 41(1), p.100.

THODE, H., MONSTER, J. & DUNFORD, H., 1961. Sulphur Isotope Geochemistry. *Geochimica Et Cosmochimica Acta*, 25(3), pp.159–174.

Thode, H.G., Kleerekoper, H. & McElcheran, D., 1951. Isotope fractionation in the bacteria reduction of sulfate. *Research (London)*, 4, pp.581–582.

Thode, H.G., Macnamara, J. & Fleming, W.H., 1953. ScienceDirect.com - Geochimica et Cosmochimica Acta - Sulphur isotope fractionation in nature and geological and biological time scales. *Geochimica Et Cosmochimica Acta*.

Torsvik, T.H. & Voo, R.V.D., 2002. Refining Gondwana and Pangea Palaeogeography: Estimates of Phanerozoic non-dipole (octupole) fields. *Geophysical Journal International*, 151(3), pp.771–794.

Trudinger, P.A. & Chambers, Lynette A, 1973. Reversibility of bacterial sulfate redaction and its relevance to isotope fractionation. *Geochimica Et Cosmochimica Acta*, 37(7), pp.1775–1778.

Tsandev, I., Slomp, C.P. & Van Cappellen, P., 2008. Glacial-interglacial variations in marine phosphorus cycling: Implications for ocean productivity. *Global Biogeochemical Cycles*, 22(4), pp.n/a–n/a.

Tudge, A.P. & Thode, H.G., 1950. Thermodynamic properties of isotopic compounds of sulphur. *Canadian Journal of Research*, 28(9), pp.567–578.

Turchyn, A.V. et al., 2010. Kinetic oxygen isotope effects during dissimilatory sulfate reduction: a combined

theoretical and experimental approach. *Geochimica Et Cosmochimica Acta*, 74(7), pp.2011–2024.

Ullrich, T.C., Blaesse, M. & Huber, R., 2001. Crystal structure of ATP sulfurylase from Saccharomyces cerevisiae, a key enzyme in sulfate activation. *The EMBO journal*, 20(3), pp.316–329.

Vairavamurthy, A. et al., 1994. Sulfonates: a novel class of organic sulfur compounds in marine sediments. *Geochimica Et Cosmochimica Acta*, 58(21), pp.4681–4687.

Venceslau, S.S. et al., DsrC-bound sulfane sulfur is the product of DsrAB dissimilatory sulfite reductase. *in preparation*.

Venceslau, S.S. et al., 2013. Redox states of Desulfovibrio vulgaris DsrC, a key protein in dissimilatory sulfite reduction. *Biochemical and …* .

Venceslau, S.S., (null) & Pereira, P.M., 2010. The Qrc membrane complex, related to the alternative complex III, is a menaquinone reductase involved in sulfate respiration. *The Journal of biological chemistry*, 285(30), pp.22774–22783.

Wall, J.D., Rapp-Giles, B.J. & Rousset, M., 1993. Characterization of a small plasmid from Desulfovibrio desulfuricans and its use for shuttle vector construction. *Journal Of Bacteriology*, 175(13), pp.4121–4128.

Wankel, S.D. et al., 2014. Determination and application of the equilibrium oxygen isotope effect between water and sulfite. *Geochimica Et Cosmochimica Acta*, 125, pp.694–711.

Westrich, J.T. & Berner, R.A., 1984. The role of sedimentary organic matter in bacterial sulfate reduction: The G model tested. *Limnology And Oceanography*, pp.236–249.

Whitehill, A.R. et al., 2013. Vibronic origin of sulfur mass-independent isotope effect in photoexcitation of SO2 and the implications to the early earth's atmosphere. *Proceedings Of The National Academy Of Sciences Of The United States Of America*, 110(44), pp.17697–17702.

WOLFE, B.M., LUI, S.M. & COWAN, J.A., 1994. Desulfoviridin, a multimeric-dissimilatory sulfite reductase from Desulfovibrio vulgaris (Hildenborough) Purification, characterization, kinetics and EPR studies. *European Journal of Biochemistry*, 223(1), pp.79–89.

Wortmann, U.G. & Paytan, A., 2012. Rapid Variability of Seawater Chemistry Over the Past 130 Million Years. *Science*, 337(6092), pp.334–336.

Wortmann, U.G., Bernasconi, S.M. & Böttcher, M.E., 2001. Hypersulfidic deep biosphere indicates extreme sulfur isotope fractionation during single-step microbial sulfate reduction. *Geology*, 29(7), pp.647–650.

Wu, N. et al., 2010. Evaluating the S-isotope fractionation associated with Phanerozoic pyrite burial. *Geochimica Et Cosmochimica Acta*, 74(7), pp.2053–2071.

Young, E.D., Galy, A. & Nagahara, H., 2002. Kinetic and equilibrium mass-dependent isotope fractionation laws in nature and their geochemical and cosmochemical significance. *Geochimica Et Cosmochimica Acta*, 66(6), pp.1095–1104.

Zerkle, A.L. et al., 2009. Fractionation of multiple sulfur isotopes during phototrophic oxidation of sulfide and elemental sulfur by a green sulfur bacterium. *Geochimica Et Cosmochimica Acta*, 73(2), pp.291–306.

Zheng, M. & Storz, G., 2000. Redox sensing by prokaryotic transcription factors. *Biochemical pharmacology*, 59(1), pp.1–6.

Zhou, J. et al., 2011. How sulphate-reducing microorganisms cope with stress: lessons from systems biology. *Nature Reviews Microbiology*, 9(6), pp.452–466. Available at: http://www.nature.com/nrmicro/journal/v9/n6/abs/nrmicro2575.html.